INVESTIGATION OF THE BIOLOGICAL ROLE OF THE POLYCYSTIC KIDNEY

DISEASE PROTEIN BICAUDAL C (BICC1) USING COMPARATIVE ANIMAL

MODELS

_____

A Dissertation

presented to

the Faculty of the Graduate School

at the University of Missouri-Columbia

_____

In Partial Fulfillment

of the Requirements for the Degree

Doctor of Philosophy

_____

by

DENISE J. BOUVRETTE

Dr. Elizabeth Bryda, Dissertation Advisor

DECEMBER, 2009

The undersigned, appointed by the dean of the Graduate School, have examined the dissertation entitled

INVESTIGATION OF THE BIOLOGICAL ROLE OF THE POLYCYSTIC KIDNEY DISEASE PROTEIN BICAUDAL C (BICC1) USING COMPARATIVE ANIMAL MODELS

presented by Denise J. Bouvrette,

a candidate for the degree of doctor of philosophy and hereby certify that, in their opinion, it is worthy of acceptance.

Elizabeth Bryda, Ph.D.

Anand Chandrasekhar, Ph.D.

John Cannon, Ph.D.

Lela Riley, Ph.D.

Frank Schmidt, Ph.D.

DEDICATION

I would like to dedicate this dissertation to my parents, Jean and Greg Bouvrette and to Chet McKinney, whose love, patience and understanding truly made the completion of this work possible. Thank you for all of your support.

ACKNOWLEDGEMENTS

TABLE OF CONTENTS

LIST OF TABLES

LIST OF FIGURES

INVESTIGATION OF THE BIOLOGICAL ROLE OF THE POLYCYSTIC KIDNEY DISEASE PROTEIN BICAUDAL C (BICC1) USING COMPARATIVE ANIMAL MODELS

Denise J. Bouvrette

Dr. Elizabeth C. Bryda, Dissertation Advisor

ABSTRACT

Polycystic kidney disease (PKD) is a common inherited disorder affecting 600,000 Americans and more than 12 million people worldwide. Clinical manifestations include renal enlargement, abnormal tubular development and accumulative cyst formation. PKD is the leading cause of end stage renal disease in adults and children. Currently, there is no cure for PKD and treatment is limited to dialysis and transplantation. The molecular mechanisms involved in cystogenesis remain unclear. *Bicaudal C* (*Bicc1*) is the disease-causing gene in the *j*uvenile *c*ongenital *p*olycystic *k*idney (*jcpk*) mouse model for PKD. The function of *Bicc1* is unknown; however the Bicc1 protein contains two conserved functional domains, three K-homology (KH) domains which are known to bind RNA and a sterile alpha motif (SAM) domain which are predicted to participate in protein-protein interactions. We hypothesize that *Bicc1* plays an integral role in normal kidney development. In this study, we investigated in vitro RNA and protein interactions of the Bicc1 protein and generated an alternative, comparative zebrafish model to further study the function of *Bicc1* in vivo.

CHAPTER I

Introduction

Polycystic kidney disease (PKD) is the most common life-threatening genetic disorder in humans, affecting 600,000 Americans and more than 12 million people worldwide (1). PKD is more common than cystic fibrosis, muscular dystrophy, Down's syndrome, sickle cell anemia, and hemophilia *combined* (www.pkdcure.org). PKD is characterized by bilateral renal cysts that grow and multiply over time, impeding kidney function and ultimately leading to renal failure. PKD is the principal cause of end-stage renal disease in adults and children (2). Currently there is no cure for PKD and treatment is limited to costly dialysis and organ transplantation. Although many rodent models have been established that mimic certain aspects of human PKD and have been useful in the identification of disease-causing genes, the specific molecular functions of these genes and their protein products are still largely unknown. Studies involving one such model, the *j*uvenile *c*ongenital *p*olycystic *k*idney (*jcpk*) mouse model, identified the PKD causal gene as *bicaudal C* (*Bicc1*) (3). *Bicaudal C* was first described in *Drosophila* (*BicC*), and encodes a putative RNA binding protein that is required for many aspects of oogenesis and proper anterior-posterior patterning of the embryo (4). The *Xenopus Bicc1* homolog was observed to have similar functions, as well as involvement in germ layer specification (5).

However, the specific role of mammalian *Bicc1* in cystogenesis remains unknown.

Purpose of the research

The objective of the following body of research is to investigate the biological role of mammalian *bicaudal C* (*Bicc1*) in the kidney as it relates to the pathogenesis of polycystic kidney disease (PKD) through the utilization of comparative animal models. Animal models are often needed to understand the complexity of human diseases and to find treatments for these diseases. Despite advances in PKD research, the molecular mechanisms leading to cystogenesis remain unclear. The use of a comparative approach is based on the observation that the basic molecular processes involved in many diseases are conserved in multiple species. Therefore, we can use animal models such as the zebrafish, mouse and rat, to gain a better understanding of PKD disease processes, and eventually transfer what we learn back to humans.

Significance of the research

The rationale for the research is that once we uncover the molecular pathways involved in the making of a cyst, we can identify potential therapeutic targets and develop better therapies focused on the delay or prevention of cyst formation. Delaying the formation of cysts would also delay the need for dialysis and allow more time for patients and doctors to find an appropriate organ donor.

If cyst initiation and progression can be stopped in its tracks, we may be able to provide a cure for the disease. The use of comparative animal models to gain a better understanding of the molecular mechanisms involved in cyst formation may help to accelerate the discovery process. This research is significant in that a new animal model was established to study the role of *Bicc1* in an accelerated fashion. In addition, this work establishes a direct link between Bicc1 and other PKD-related genes and proteins, thus beginning to piece together one of the pathways leading to cystogenesis. This dissertation contributes to the current knowledge of PKD pathogenesis in that it begins to outline the interactions of key molecular players involved in cyst formation and provides the first evidence of a link between *Bicc1* and the Wnt signaling pathway. Further examination of these interactions will lead to an increased understanding of the underlying molecular mechanisms involved in cystogenesis and hopefully bring us closer to a cure.

Organization of the dissertation

This dissertation is divided into five chapters. Chapter I describes the purpose of the dissertation and provides a basis for understanding the following research. Chapter II provides a review of the relevant literature related to polycystic kidney disease, rodent animal models for PKD, and the utility of using zebrafish as a model for human disease. Chapter III consists of a detailed description of the materials, methods, and experimental design for the research. Chapter IV describes the results of the research. Chapter V provides a summary

of the previous chapters, discusses the conclusions that can be drawn from the results of the research, and relates the significance of this work in the context of the current field of PKD research.

CHAPTER II

REVIEW OF THE LITERATURE

Polycystic kidney disease

Polycystic kidney disease (PKD) is a clinically important heritable disorder characterized by progressive cyst formation, abnormal tubular morphology and various extrarenal effects. Clinical symptoms of PKD include bilateral renal cysts, hematuria, chronic urinary tract infections, hypertension, kidney stones, abdominal pain and discomfort, and renal insufficiency (6). Renal cysts are fluid-filled sacs that originate from nephrons, which are the filtering units within the kidney (Figure 2.1). The cysts are lined by a single layer of renal epithelial cells, which are less differentiated in PKD than normal epithelial cells (7). These cells also exhibit changes in extracellular matrix (ECM) composition, cell polarity defects, and improper apoptosis and proliferation (7, 8) (Figure 2.2). PKD pathogenesis is complex and several molecular mechanisms and signaling pathways have been proposed to play a role in the initiation and progression of cyst formation.

Figure 2.1. Renal cyst formation in PKD
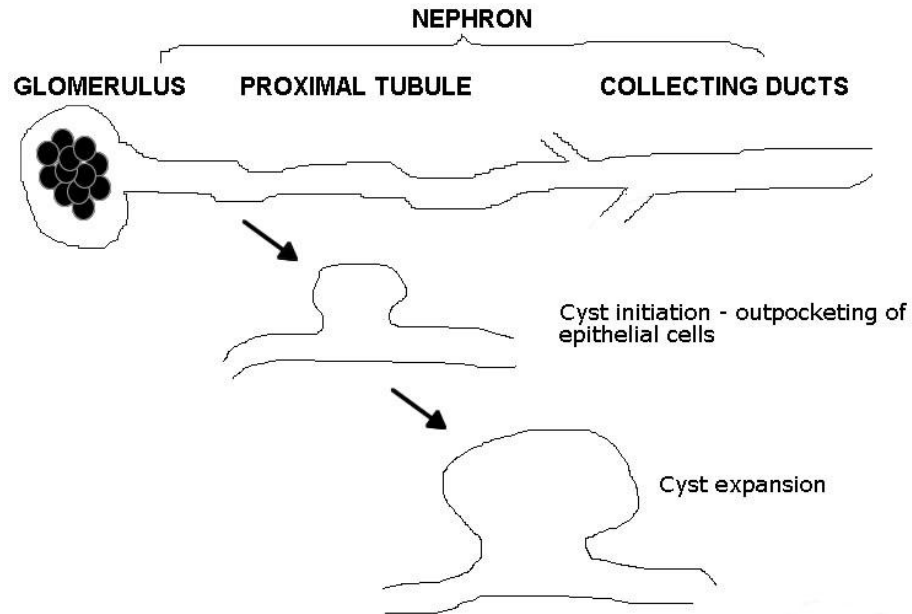
Figure 2.1. An illustration of cyst formation in PKD. Renal cysts initiate as an outpocketing of the epithelial cells within the nephrons, which are the filtering units of the kidney. Each nephron consists of a glomerulus, proximal tubule and collecting duct. After cyst initiation, the cysts continue to grow and expand, impeding kidney function and leading to renal failure.

Normal mature kidney cells are relatively quiescent, neither dividing nor undergoing apoptosis; however, during development there exists a critical balance between cellular differentiation, which leads to tubular heterogeneity and proliferation, which is required for kidney growth. In cystic cells, this balance is disrupted. Alterations in ECM make PKD epithelia more adherent to the matrix and less migratory, affecting tubulomorphogenesis during development.

Figure 2.2. Hallmarks of PKD
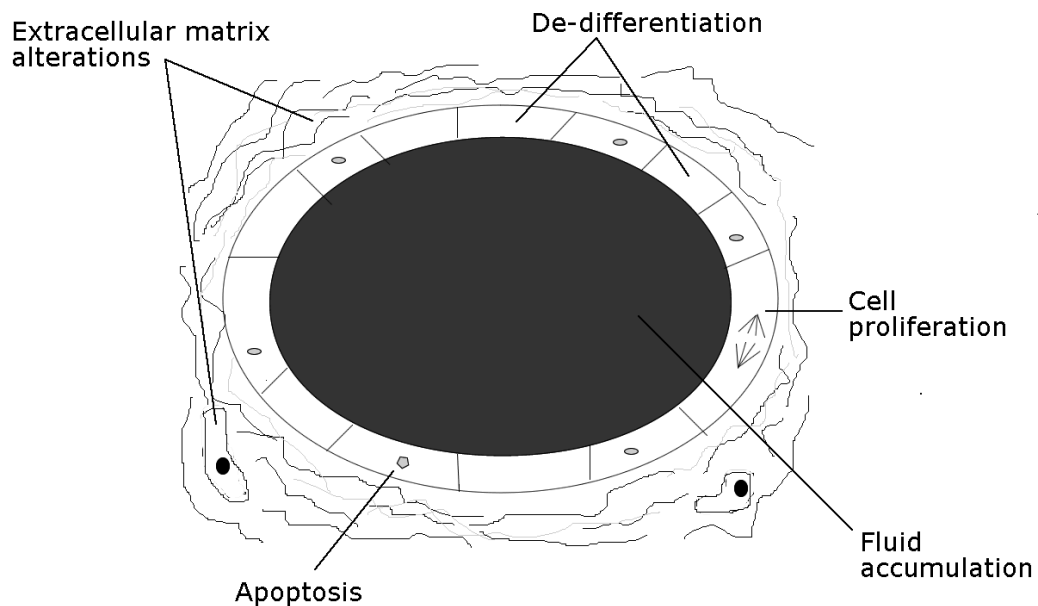
Figure 2.2. Illustration summarizing the hallmarks of PKD. Renal epithelial cells in PKD exhibit changes in the extracellular matrix (ECM) composition, defects in cell polarity, fluid accumulation, and changes in apoptosis and cell proliferation. The epithelial cells are also less differentiated than normal epithelial cells (7).

Renal epithelial cells develop a distinct polarity that is imperative for their function in the tubules and collecting ducts. This polarity is partly established by the localization of specific proteins to particular areas of the cell. Apical mislocalization of membrane proteins such as epidermal growth factor receptor (EGFR) and Na$^+$K$^+$ATPase leads to increased cell proliferation and fluid secretion in cystic areas of the nephron, contributing to cystic growth. Defects in planar cell polarity are predicted to allow cells to divide at asymmetric angles, leading to cystic dilations during tubular morphogenesis (Figure 2.3) (9-12).

Figure 2.3. Planar cell polarity and cyst formation

Planar
asymmetry

Normal

Directional cell division
Orientation along longitudinal axis

PKD

Asymmetric cell division
Disruption planar orientation
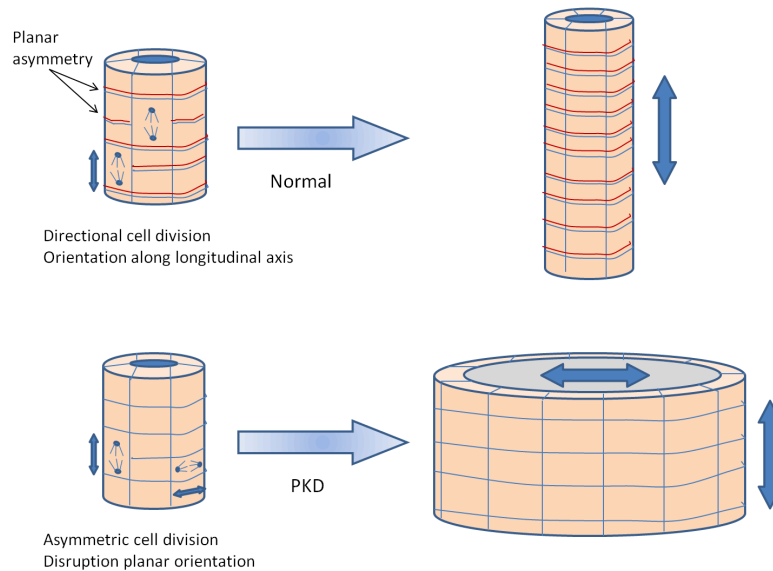
Figure 2.3. Planar cell polarity theory of cyst formation in PKD. (Top panel) As the tubule is forming, it is important for renal epithelia to orient along the longitudinal axis of the tubule. This is facilitated by an inherent planar asymmetry (red vs. blue line), which is established by the apical/baso-lateral distribution of specific molecules within the cell. (Bottom panel) This polarity is disrupted in PKD cells. It is predicted that defects in planar cell polarity result in asymmetric cell division and the formation of cystic dilations during development. Figure adapted from Germino, 2005 (12).

In addition to accumulative renal cysts, PKD also exerts systemic effects, including liver, biliary and pancreatic cysts, cerebral and aortic aneurysms, cardiac valve abnormalities, and diverticulitis of the colon (13). There is no current cure for PKD. Currently, as patients realize renal failure, they undergo dialysis until they are able to receive a kidney transplant. According to the Organ Procurement and Transplantation Network (http://optn.translant.hrsa.gov), the current waiting list for a kidney consists of 102,996 individuals, while the number of donors is limited to approximately 6,000.

8

Human polycystic kidney disease (PKD) occurs in two forms, a common autosomal dominant (ADPKD) form, affecting 1 in 500 individuals and a rarer autosomal recessive (ARPKD) form, with an incidence of 1 in 20,000 individuals.

Mutations in the *PKD1* gene account for 85% of human ADPKD cases, while 15% are caused by mutations in *PKD2* (14). More than 300 different mutations have been reported along the entire sequence of *PKD1*, located on human chromosome 16, most of which are unique to single ADPKD families (15). All types of mutations have been detected, but the consequence of most (70%) is a truncated protein product (15). Like *PKD1*, mutations in *PKD2*, located on chromosome 4, occur all along the sequence of the gene with the majority resulting in the truncation of the encoded protein (16, 17).

PKD1 and *PKD2* encode two large transmembrane proteins, Polycystin 1 (PC1) and Polycystin 2 (PC2), respectively (18, 19). PC1 contains an extracellular domain that facilitates cell-cell and cell-matrix interactions (6) and an intracellular domain that is involved in the activation of downstream signaling cascades, protein-protein interactions, and G-protein activation (20-22). Based on its structure and location, PC1 is predicted to function as a membrane receptor that receives and transduces extracellular signals to the cell (8). PC2 contains several transmembrane domains and intracellular N- and C-termini, which are predicted to be involved in protein-protein interactions and calcium-binding. PC2 also contains multiple phosphorylation sites and has been shown to interact with PC1 and components of the actin cytoskeleton (23-25). The structure and cellular localization of PC2 indicates that its primary function is as a non-selective cation

channel with the ability to conduct calcium in both the cell and endoplasmic reticulum membranes (26-28).

In normal kidney epithelial cells, these proteins co-localize at the apical primary cilia, basolateral cell-matrix focal adhesions, and lateral cell-cell adherens junctions, functioning together to detect and respond to extracellular signals (14). While PC1 and PC2 seem to promote normal kidney development and proper renal tubular maintenance, defects in either of these proteins, as seen in PKD, result in the formation of cysts and abnormalities in renal epithelia cell morphology.

ADPKD is typically a slowly progressive disease with most individuals entering renal insufficiency during middle age. One hallmark of the disease is numerous bilateral renal cysts which grow and multiply over time, progressively replacing normal kidney tissue, and eventually leading to renal failure. Cysts develop in all parts of the nephron, including the glomeruli, tubules, and collecting ducts. Although ADPKD is 100% penetrant with all affected individuals developing renal cysts, the age of onset of end-stage renal disease and rate of cystic growth can vary dramatically, even in individuals with the same mutation. This observation suggests that genetic modifiers and/or other factors may play a role in the pathogenesis of the disease.

ARPKD results from mutations in the *PKHD1* gene located on chromosome 6. Most of the 300 plus identified mutations in this gene are missense; however, other types have also been noted (29, 30). As in *PKD1* and *PKD2*, most of the disease-correlated mutations result in the truncation of the

protein product, but unlike *PKD1* and *PKD2*, several unrelated families with ARPKD have been shown to share common mutations in the *PKHD1* gene (31-33).

PKHD1 encodes a receptor-like membrane bound protein, designated Fibrocystin-1 (FC-1) (34). FC-1 contains a long extracellular N-terminal domain, one transmembrane domain, and a short intracellular C-terminal domain (35). FC-1 has not been studied as extensively as PC1 or PC2, however, the extracellular domain contains protein-protein interaction regions and numerous N-glycosylation sites while the C-terminal tail contains potential phosphorylation sites for protein kinase A (PKA) or protein kinase C (PKC), all of which are consistent with a membrane receptor function.

ARPKD is a fast-progressing disease, typically occurring in infants and juveniles, and although rare, it is clinically significant as it often causes neonatal death. Death in neonates is due to the gross enlargement of both kidneys and impaired development of the liver and lungs, often leading to respiratory failure. In patients that survive the neonatal period, 20-45% reach end-stage renal disease by 15 years of age (14). Arterial hypertension and liver fibrosis commonly contribute to the morbidity and mortality of these children (33, 36). While massive renal enlargement due to the presence of cysts is classically found in both ADPKD and ARPKD, the cysts in ARPKD differ from those in ADPKD in that they originate as expansions of only the collecting duct segments of the nephron and remain associated with the nephron of origin.

Primary cilia and PKD

Renal epithelial cells have a single, non-motile primary cilium extending from their apical surface into the lumen of the tubules and collecting ducts (Figure 2.4A). The primary cilium consists of a basal body and an axoneme (Figure 2.4A) (37). Basal bodies anchor the cilia and serve as the nucleation site for the growth of the axoneme. Basal bodies are formed from one of the centrioles, or short cylindrical arrays of microtubules which comprise the centrosomes, the microtubule organizing centers within the cell. The axoneme of the primary cilia consists of a cylindrical arrangement of 9 pairs of microtubules as well as many proteins and protein complexes which support its structure, function in intraflagellar transport (IFT) and allow it to bend in response to luminal fluid flow. One microtubule in each doublet is attached to outer and inner dynein arms and a radial spoke, a multi-unit protein complex involved in ciliary motility (Figure 2.4B). Bending of the cilium is achieved by the sliding of microtubule doublets relative to each other as a result of the 'walking' of the dynein arms on one microtubule up the adjacent microtubule, powered by the ATPase activity of dynein. Highly elastic proteins called nexins link the microtubule doublets so that they only slide a short distance, resulting in the bending of the entire axoneme (37).

Figure 2.4. Primary cilia in renal epithelia
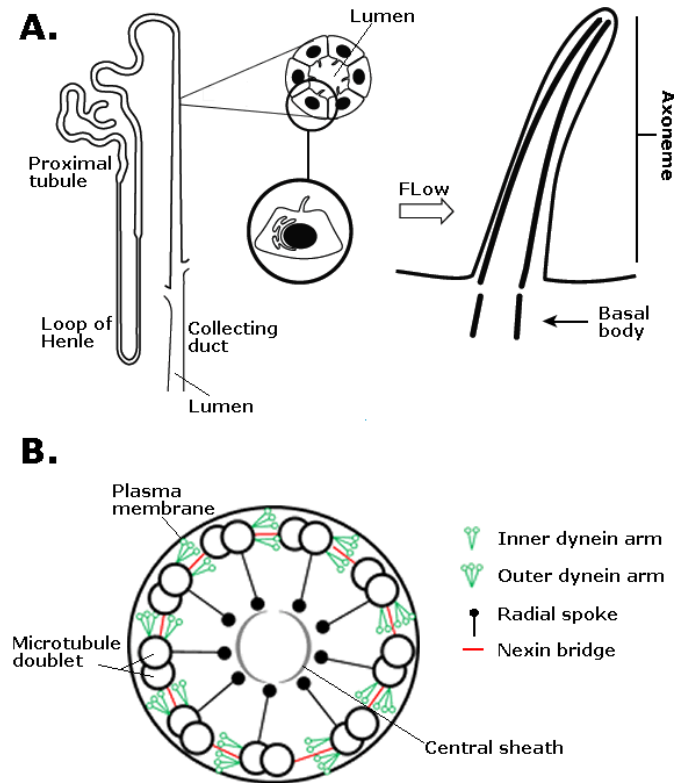
Figure 2.4. Primary cilia in renal epithelial cells. (A) A monolayer of epithelial cells line the tubules and collecting ducts of the nephrons. A single, primary cilium extends from the apical membrane of each cell. The primary cilium is comprised of a basal body which anchors the cilia to the cell and an axoneme. (B) Cross section of the axoneme consisting of nine pairs of microtubules arranged in a circular pattern. The nine microtubule doublets carry outer and inner dynein arms, radial spokes, and nexin bridges which together control the movement and sliding of the microtubules, allowing the cilium to bend. Illustration in (A) courtesy of Don Connor at the College of Veterinary Medicine, University of Missouri, adapted from Zhang *et al*, 2004 (38).

There is a growing body of evidence that these cilia impart a vital signaling function which contributes to the proper establishment of extracellular matrix components, cell polarity, and differentiation of renal epithelial cells during kidney development, all of which are disrupted in PKD. Several PKD-related proteins have been reported to associate with the cilia or basal bodies in renal cells and

13

alterations in these proteins are detrimental to normal kidney pathology (Table

2.1) (39-54). Further evidence that PKD is a ciliary disease is that Polycystin 1,

Polycystin 2 and Fibrocystin have all been shown to localize to the primary cilia

of renal epithelial cells (Figure 2.5) (28, 44, 47, 52-55).

Figure 2.5. PKD proteins localize to the cilia
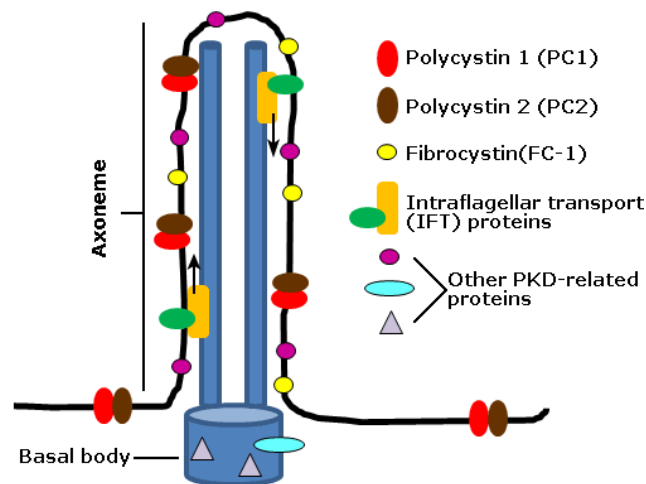
Figure 2.5. Many PKD-related proteins localize to the cilium or basal body, including the Polycystins
and Fibrocystin, which are the gene products of *PKD1*, *PKD2*, and *PKHD1*, respectively. Cilia are
predicted to act as mechanosensors, where changes in luminal flow are detected by the PC1/PC2
complex, resulting in an influx in calcium and an intracellular signaling response.

Ciliary signaling is predicted to be important for establishing and

maintaining proper cell polarity, extracellular matrix organization and

differentiation of renal epithelial cells during kidney development.   Defects in

ciliogenesis or ciliary dysfunction are thought to be fundamental in the

pathophysiology of PKD, as all of these characteristics are disrupted in PKD

epithelial cells. The general hypothesis of ciliary signaling is that renal cilia act

as sensory transducers within a complex signaling pathway and PC1 and PC2

are essential components of that pathway (56).

Table 2.1. Animal models of PKD and cilia expression

Model	Gene	Protein	Cilia and/or basal body expression	Reference
cpk	*Cys1*	Cystin	YES	Hou *et al*, 2002 (41); Yoder *et al*, 2002 (53)
bpk	*Bicc1*	Bicaudal C	NO	The current work; Stagner *et al*, 2009 (57)
jcpk	*Bicc1*	Bicaudal C	NO	The current work ; Stagner *et al*, 2009 (57)
orpk	*TgN737Rpw*	Polaris	YES	Taulman *et al*, 2001 (51); Yoder *et al*, 2002 (54)
inv	*Invs*	Inversin	YES	Otto *et al*, 2003 (45); Watanabe *et al*, 2003 (58)
jck	*Nek8*	Nek8	YES	Mahjoub *et al*, 2005 (43); Liu *et al*, 2002 (59)
kat	*Nek1*	Nek1	YES	Mahjoub *et al*, 2005 (43); Shalom et al, 2008 (48)
Han:SPRD +/*Cy*	*Anks6*	SamCystin	NO	Stagner *et al*, 2009 (57)
pck	*Pkhd1*	Fibrocystin	YES	Menezes *et al*, 2004 (44); Masyuk *et al*, 2003 (55); Ward *et al*, 2003 (52)

Table 2.1. Animal models for PKD and cilia expression. PKD, polycystic kidney disease; *cpk*, congenital polycystic kidneys; *bpk*, BALB/c polycystic kidneys; *jcpk*, juvenile polycystic kidney; *orpk*, Oak Ridge polycystic kidney; *inv*, inversin of embryonic turning; *jck*, juvenile cystic kidney; *kat,* kidney anemia testis; *pck*, polycystic kidneys. Table modified from Guay-Woodford, 2003 (60).

The specific mechanism by which primary cilia mediate cell signaling is

not well understood. Characterization of the molecular pathways involved in

ciliary signaling which result in a cystic phenotype may provide the missing link in

understanding the pathogenesis of PKD.

Wnt signaling in PKD

Wnt signaling is an important part of embryonic development and organogenesis and is proposed to play a role in the maintenance of adult tissue homeostasis (61). *Wnt* genes encode a large family of secreted, cysteine-rich glycoproteins that are defined by sequence homology to the proto-oncogene *wingless-related mouse mammary tumor virus (MMTV) integration site 1* (*Wnt-1*) in the mouse (62, 63) and the *Drosophila* homolog, *wingless* (*wg*) (64-67). Genetic studies in *Drosophila* (65, 66, 68-71) and *C. elegans* (72-78), ectopic expression in *Xenopus* (79-82) and gene knockouts in the mouse (83-97) have demonstrated the involvement of Wnts in numerous diverse processes such as segmentation, axis specification, limb development, patterning of the central nervous system, cell migration and polarity, control of asymmetric cell divisions and kidney tubule formation.

Wnt signaling affects the transcription of genes involved in cell cycle regulation (*c-Myc, Cyclin D*), angiogenesis (*vascular endothelial growth factor, VEGF*), genes encoding tissue remodeling proteins (matrix metalloproteinases, ephron receptors, adhesions), transcription factors as well as tissue-specific genes. Wnt signaling also affects gene transcription of members within the Wnt pathway in an autoregulatory mechanism (98-103).

The components of the Wnt signaling pathway include secreted Wnt ligands, Frizzled transmembrane receptors, the phosphoprotein Dishevelled and downstream effectors including β-catenin and the transcription factor T-cell

factor/lymphoid enhancer-binding (TCF/LEF). Dishevelled is an essential

component that transduces Wnt signals into one of three distinct branches, the

canonical (standard), non-canonical, also known as the planar cell polarity

pathway (PCP), and Ca^{2+} pathways (104). Branch-specific activation is partly

dependent upon which Wnt ligand and receptor initiated the signal (Figure 2.6).

Canonical Wnt signaling is primarily involved in cell proliferation and cell

fate specification and is tightly regulated (105-109). In the absence of Wnt

ligand, cytoplasmic β-catenin is sequestered by a complex of proteins, composed

of glycogen synthase kinase-β (GSKβ, adenomatous polyposis coli (APC), and

axin, which target β-catenin for destruction via the ubiquitin-proteosome pathway.

Upon ligand binding, Dishevelled, upstream of β-catenin, is phosphorylated and

activated. Activated Dishevelled disrupts the β-catenin destruction complex,

releasing β-catenin and allowing for its accumulation in the cytoplasm and

translocation to the nucleus. Nuclear β-catenin binds transcription factors, such

as TCF/LEF, to initiate transcription of Wnt target genes.

Canonical Wnt signaling is essential during nephrogenesis. Kidney

organogenesis is initiated by reciprocal induction of the ureteric bud and

nephrogenic mesenchyme mediated by Wnt signals and several growth factors

including fibroblast growth factor (FGF), transforming growth factor (TGF) and

bone morphogenic protein (BMP) (110-113). This reciprocal induction results in

the condensation of the mesenchymal tissue and formation of pre-tubular

aggregates which undergo morphogenesis and patterning, differentiating to form

the nephrons (11, 97, 114-117). Wnt signals are also involved in tubular

morphogenesis and epithelialization of the tubules (97, 110, 118).   While

canonical Wnt signaling is imperative to the proper development of the kidney,

constitutive canonical Wnt signaling has been shown to result in developmental

defects and the formation of renal cysts in both mice and humans (119).

Figure 2.6. Wnt signaling pathways
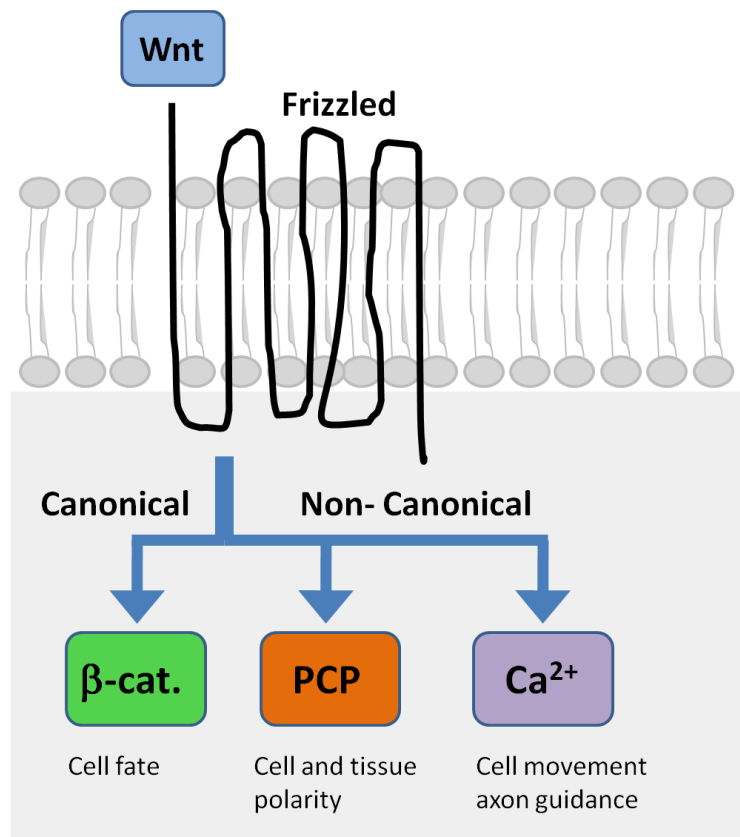
Figure 2.6. Wnt signaling pathways. Wnt signaling consists of canonical and non-canonical pathways and requires the interactions of specific secreted Wnt ligands and Frizzled membrane receptors. Both the canonical and non-canonical pathways are absolutely required for proper kidney organogenesis and continued maintenance of renal tubular architecture. β-cat., β-catenin; PCP, planar cell polarity. Figure adapted from Cadigan and Nusse, 1997 (120).

Casein kinase II (CK2), a ubiquitous kinase, is a strong positive regulator of canonical Wnt signaling, enhancing the signal through constitutive activation and stabilization of cytosolic β-catenin (121-123). Interestingly, CK2 has also been shown to interact with the Polycystins, PC1 and PC2, suggesting an involvement in PKD pathogenesis (124).

The non-canonical Wnt pathway regulates cell migration, cytoskeletal rearrangements and planar cell polarity (11, 120, 125). Planar cell polarity (PCP) involves coordinated cell movements within the same plane and orientation into regular, organized arrays, which is required for the formation of complex functional structures, such as the inner ear, eye and kidney tubules. The specific effectors of non-canonical (PCP) signaling are not well defined, although a specific subset of Wnt ligands (Wnts 4, 5a, and 11) and Frizzled receptors (Fzds 2, 3, 4, and 6) are found to transduce the signal (126-129). In PCP signaling, Wnt ligands bind to Frizzled receptors which interact with the Dishevelled protein at the membrane, inducing the activation of the small GTPases Rho and Rac. Rho activation leads to cytoskeletal re-organization (130-132), while activation of Rac stimulates JNK kinase activity, resulting in a transcriptional response (133). Overall, the gene transcription events and cytoskeletal rearrangements stimulated by PCP signaling lead to the terminal differentiation of cells (61, 125).

The third branch of Wnt signaling also involves interactions of particular Wnts (Wnts 4, 5a, and 11) and members of the Frizzled family of receptors (Fzds 2, 3, 4, and 6) (127). Activation of the Wnt Ca^{2+} pathway results in an increase of intracellular calcium ions (134). This calcium influx is sufficient to activate

calcium sensitive enzymes like protein kinase C (PKC), calcium-calmodulin dependent kinase 2 (CamK2) and calcineurin (CaCN). The Wnt Ca^{2+} pathway is important for dorso-ventral patterning of the embryo, cell adhesion, regulating cell migration and may play a role in tumor suppression (134, 135).

The PCP and Ca^{2+} branches of Wnt signaling utilize the same Wnt ligands and Frizzled receptors, suggesting that they are activated through similar mechanisms (135-137) and perhaps act synergistically in kidney epithelial cells in tubular morphogenesis.

Interestingly, several recent studies have established a link between Wnt signaling and primary cilia (9, 124, 138), providing further evidence that Wnt signaling may play an important role in PKD pathogenesis. Inversin, a ciliary protein that when altered results in cystic kidneys, has been shown to act as a molecular switch between the canonical and PCP pathways in kidney epithelial cells (139). Simons *et al,* show that Inversin inhibits canonical signaling by targeting cytoplasmic Dishevelled for degradation and that in the absence of Inversin, cysts develop as a result of unopposed canonical Wnt signaling. Inversin does not inhibit or degrade membrane-associated Dishevelled, which is presumably involved in PCP signaling; thus Inversin indirectly promotes the PCP pathway. It has been proposed that this switch between the canonical and PCP pathways is necessary to organize the shape and function of the nephron during development and that cross-talk between the PCP pathway and other signaling pathways is important for the continued maintenance of tubular structure, polarity and integrity in adult tissues (138-140).

It is important to note than many signaling pathways have been implicated in PKD, including mammalian target of rapamycin (mTOR), Map kinase (MAPK), c-Jun N-terminal kinase (JNK), epidermal growth factor (EGF), protein kinase B (AKT/PKB) and cAMP signaling. Recognizing that cross-talk between multiple signaling pathways is a common occurrence in biology; it is likely that the integration of multiple pathways is involved in the mechanisms of cyst formation.

PKD rodent models

The molecular mechanisms involved in cyst formation in PKD are not well understood; therefore, major efforts have been directed at generating animal models that closely resemble human PKD to gain a better understanding of these disease processes.

_j_uvenile _c_ongenital _p_olycystic _k_idney (_jcpk_): The _j_uvenile _c_ongenital _p_olycystic _k_idney (_jcpk_) mouse model for PKD mimics the phenotype of PKD in humans and is attributed to a mutation in the mouse _bicaudal C_ (_Bicc1_) gene (3). The coding region of _Bicc1_ is approximately 3 kb; two _Bicc1_ transcripts exist, one consisting of exons 1-22, excluding exon 21 (transcript A) and the other containing exons 1-21 (transcript B). The _jcpk_ mutation was identified during a chlorambucil mutagenesis study and is a point mutation (A<u>G</u> to A<u>A</u>) in the splice acceptor site of exon 3. The consequence of the mutation is the exclusion of exon 3 from both transcripts A and B, resulting in a premature stop codon and severely truncated proteins, which are predicted to be non-functional (141). The

jcpk mouse is a phenotypic model for both ADPKD and ARPKD in that

homozygous mutants exhibit bilateral cysts in all parts of the nephron, similar to

ADPKD and they have an early age of onset, similar to ARPKD. These mice are

runted and exhibit distended abdomens due to the gross enlargement of the

kidneys as early as 2 days after birth and they die within 10 days of age (Figure

2.7) (141).

Figure 2.7. PKD phenotype of the *jcpk* mouse model
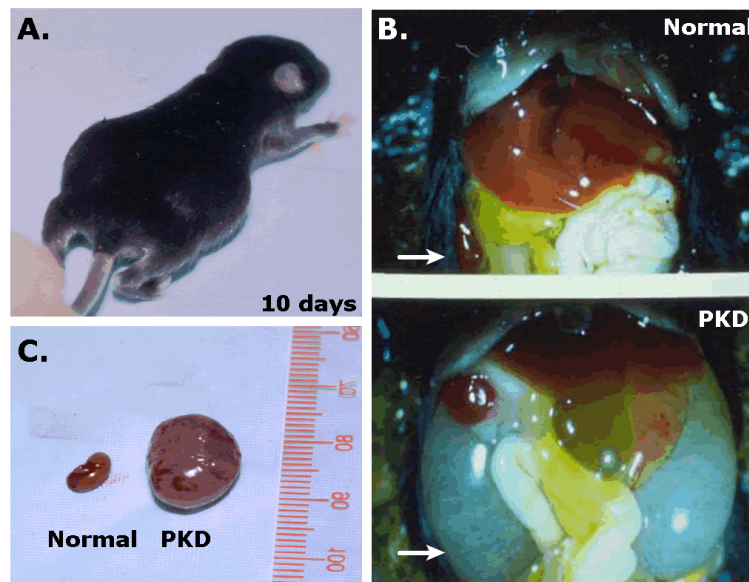
Figure 2.7. Phenotype of *jcpk* mouse model. (A) Photograph of a 10-day old homozygous *Bicc1^{jcpk}/Bicc1^{jcpk}* mutant pup with a severely distended abodomen. (B) Gross images of a normal littermate (top panel) compared to a homozygous *Bicc1^{jcpk}/Bicc1^{jcpk}* mutant (lower panel). White arrows indicate the kidney. (C) Dissected kidneys to demonstrate actual size of a normal versus a *Bicc1^{jcpk}/Bicc1^{jcpk}* kidney at 10 days of age. Photographs reprinted with the permission of Dr. Elizabeth Bryda.

The *bicaudal C* (*BicC*) gene was originally described in *Drosophila* and is

essential for various aspects of oogenesis including follicle cell migration and

proper anterior-posterior (AP) patterning in fruitflies (4, 142). The gene was so

named because females carrying mutations in *BicC* produce embryos displaying

a range of AP patterning defects, including bicaudal embryos. Orthologs of *BicC*

have been reported in *C. elegans, Xenopus,* mouse and human (3, 143-145).

    Drosophila BicC plays a role in the posterior localization and translational

regulation of maternal RNAs during oogenesis (142). Restricted localization of

specific maternal RNAs coordinated with their precise translational control during

oogenesis are necessary to define the dorsal-ventral and anterior-posterior body

axes of the developing embryo. These axes are established in part by dorsal

excretion of Gurken (a TGF-α homolog) and posterior accumulation of Oskar.

BicC is a translational repressor of *oskar* (142) and has recently been shown to

exert post-transcriptional repression of its own mRNA by controlling the poly(A)-

tail length through the recruitment of a deadenylase complex (146, 147). Other

potential targets of BicC regulation include components of the actin/tubulin

cytoskeleton (146, 147). Overexpression of *BicC* induces a posterior phenotype

similar to that of BicC mutants and also results in rapid cytoplasmic streaming

(147), suggesting that tightly controlled BicC expression and localization is

essential for normal patterning of the *Drosophila* embryo. A recent study

identified a novel function of BicC in the secretion of Gurken (148). Kugler *et al.,*

describe BicC mutant oocytes as having disrupted microtubule organization and

mislocalized Gurken trapped in actin-coated structures; preventing its activation

of epidermal growth factor receptor (EGFR) signaling in the dorsal-anterior follicle

cells. Interestingly, this phenotype closely resembled oocytes with mutations in a

Sm-like protein homolog, *trailer hitch* (146). Sm-like proteins associate with RNA

and form a core heptameric ring of ribonucleoprotein particles which aid in mRNA

processing and degradation (149-152). *BicC* and *trailer hitch* have been shown

to genetically interact (146), suggesting that they function in a common molecular

pathway important for embryo patterning and cytoskeletal regulation.

Xenopus Bicc1 is maternally expressed and has been shown to play a role

in germ layer specification during early embryonic development (5). Deletion of

the KH domains prevents *Xenopus* Bicc1 from inducing endoderm in animal cap

assays (145). Hypothetical models which suggest that *Xenopus* Bicc1 may

function to either repress an ectodermal determinant or activate an ectodermal

determinant through translational control have been proposed; however, the in

vivo targets of *Xenopus* Bicc1 are still unknown (145).

The function of mammalian *Bicc1* remains unknown, although it is

predominantly expressed in the heart and kidney of the mouse, with low levels

detected in the testes (143). Similar to what is observed in *Drosophila* and

Xenopus, maternal expression of *Bicc1* can be detected in the ovaries of 8 week

old mice (143). Mouse Bicc1 expression is first observed by in situ hybridization

in Hensen's node, the rostral tip of the primitive streak, during the late streak

stage. In 13 day-old mice, Bicc1 expression was detected in regions not

previously reported in *Xenopus*, including sites of cartilage formation, the

diaphragm, pericardium, and lung (143). Interestingly, *Xenopus* Bicc1 was only

found in the pronephros (the first kidney structure to develop), but mouse Bicc1

was also detected in the mesonephric and metanephric kidneys, which develop progressively from the pronephros (143).

The predicted Bicc1 protein in all species shows strong conservation of two functional domains, three tandem K-homology (KH) domains at the N-terminus and a sterile alpha motif (SAM) domain at the carboxyl end (3, 57, 153-155). KH domains are known to bind RNA, while SAM domains mediate protein-protein interactions (154-163). Recent work specifically indicates that the *Drosophila* BicC and mouse Bicc1 proteins bind RNA via their KH domains (146-148, 164). Chicoine *et al.* demonstrate that *Drosophila* BicC binds the 5' UTR of its target RNAs and recruits a deadenylase complex, presumably destabilizing and repressing the target RNA translation. They also showed that not only is BicC involved in the regulation of oogenesis, but it also plays a role in cytoskeletal organization, as well as its own translational regulation (146, 147).

The K homology (KH) domain was first described in the human hnRNP K protein from nuclear ribonuclear-protein complexes (165). The motif consists of approximately 50 amino acids expanded around a conserved GxxG core sequence, where x is any amino acid, with a preference for positive residues (158). Multiple copies of the KH motif appear in several proteins, for example, vigilin contains 15 KH motifs, IGF-II mRNA-binding protein 1 (IMP1) contains four KH domains, and FMRP, the protein affected in fragile X syndrome patients, contains two KH domains (3, 166, 167). KH motifs have demonstrated cooperative binding of RNA in some proteins such as hnRNP K which has three KH domains and P-element somatic inhibitor protein (PSI) which has four KH

domains (163, 168). However, several proteins, such as Mer1p, contain single

KH motifs suggesting that these domains can also function independently (169).

A common property among KH-domain containing proteins is that they all

function in RNA metabolism. KH domain-containing proteins have been shown

to function in diverse ways; including mRNA splicing, stabilizing target RNAs,

directing particular RNAs towards degradation pathways, or they may play a role

in the translational regulation of certain mRNAs (161, 170).

     The sterile alpha motif (SAM) domain was first described in yeast sexual

differentiation and *Drosophila* homeotic proteins and consists of approximately

70 amino acids (157). It has been proposed that SAM is an evolutionary

conserved protein binding domain involved in the regulation of numerous

developmental processes in diverse eukaryotes (156). Proteins containing SAM

domains include the Eph family of receptor tyrosine kinases, serine-threonine

kinases, Src homology (SH2) domain-containing adapter proteins, ETS

transcription factors, among others (171-173). These types of proteins are often

part of complex signaling cascades. SAM domains may interact through their

ability to homo- and hetero-oligomerize with other SAM domains (174, 175).

SAM domain oligomerization is thought to be important in creating binding sites

for additional proteins and the subsequent assembly of large protein complexes

(173). SAM domains can also bind proteins without SAM domains, such as

protein tyrosine phosphatases (PTPs), and PDZ-domain containing proteins

(176), suggesting that SAM domain-containing proteins may have multiple

protein targets in a given pathway.

Han:SPRD +/Cy: The Han:SPRD +/Cy rat model for PKD was the result of a spontaneous mutation in a Hannover colony of Sprague Dawley rats and is the only PKD rat model with an autosomal dominant mode of inheritance (177). Physiological and morphological phenotypes closely resemble those of human ADPKD with a slow disease progression and a gender bias towards males exhibiting more disease severity (178). Homozygous Cy/Cy mutant rats exhibit severe cystic disease and die within 3 weeks, while renal insufficiency is apparent in heterozygous male +/Cy affected rats between 9-12 weeks of age, and in heterozygous female +/Cy affected rats at 15 weeks of age (Figure 2.8).

Recent work identified the disease-causing gene in the Han:SPRD +/Cy rat model as *Anks6*, located on rat Cchromosome 5 (179). The function of *Anks6* is unknown; however it encodes a novel protein, SamCystin, which is predicted to contain two functional domains involved in protein interactions; 10 ankyrin repeat domains near the N-terminus and a single sterile alpha motif (SAM) domain at the C-terminus. A point mutation in *Anks6* results in the substitution of a conserved arginine to tryptophan at amino acid 823 (R823W), which is located within the SAM domain of SamCystin (179). Due to differences in the biochemical properties of these amino acids this mutation is predicted to reduce the stability of the SamCystin protein (57). Other proteins containing SAM domains often participate in the assembly of larger protein complexes, but they have a preference for self-association, including dimerization, polymerization, and oligomerization with other SAM domains (180).

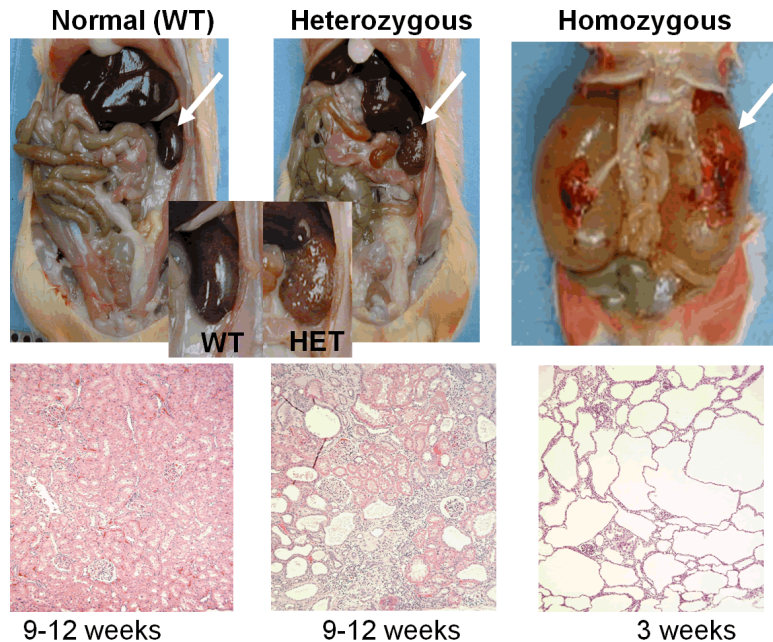**Figure 2.8. PKD phenotype of the rat Han:SPRD *+/Cy* model**

Figure 2.8. Phenotype of the Han:SPRD *+/Cy* rat PKD model. Gross images of wild type (far left), heterozygous at the *Cy* locus (center), and a homozygous *Cy/Cy* mutant (right). Kidneys are noticeably cystic and enlarged in the affected rats (white arrows). The bottom panels are micrographs of hemotoxylin and eosin stained transverse sections through the outer renal cortex of the animals pictured above. Numerous cysts (white spaces) are clearly visible in affected rats, with the homozygotes only surviving to 3 weeks of age. Micrograph images were captured using a Zeiss Axiophot microscope and Oympus DP70 digital camera at 400X. Photographs reprinted with permission from the Rat Resource and Research Center (RRRC) at the University of Missouri (www.nrrrc.missouri.edu), supported by NIH grant #P40 RR16939).

The observation that two PKD-related proteins, Bicc1 and SamCystin, both contain conserved SAM domains which are known to be involved in protein-protein interactions led us to investigate whether these proteins interact with each other. This recent work demonstrated that the SamCystin protein homodimerizes via its SAM domain and that this self-association is disrupted by the *Anks6* mutation (57). Importantly, the SamCystin protein has been shown to interact with the Bicc1 protein, not via their SAM domains, but rather indirectly, in

an RNA-dependent manner, suggesting that these proteins are part of a complex that function in a common molecular pathway involved in cyst formation (57).

      *k*idney, *a*nemia, *t*estes (*kat*): The *k*idney, *a*nemia, *t*estes (*kat*) mouse model is similar to human ADPKD, with mutant *kat* mice experiencing a late onset, slowly progressing form of PKD (181-184). In addition to polycystic kidneys, these mice exhibit pleiotropic phenotypes such as facial dysmorphism, dwarfing, male sterility, anemia, and cystic choroid plexus (59, 183). The underlying defect in the *kat* mouse model is a mutation in the kinase domain of the never in mitosis A (NIMA)-related kinase, *Nek1* gene located on chromosome 4 (183). NIMA-related kinases are known to be involved in cell cycle control, growth and differentiation (185, 186). Mouse *Nek1* is highly expressed in testes and ovaries (187, 188), as well as in peripheral and motor neurons (188), which could account for the pleiotropic phenotypes observed in the homozygous *Nek1^{kat}/Nek1^{kat}* mice. The Nek1 protein consists of an N-terminal catalytic kinase domain and a C-terminal regulatory tail, comprised of multiple coiled-coil domains thought to mediate protein interactions. Nek1 is a dual-specificity kinase, meaning it is capable of transferring a phosphate group to either serine, threonine, or tyrosine residues of target proteins. In addition to its kinase activity, Nek1 has been shown to participate in diverse protein interactions (138, 189-192). Yeast two hybrid studies using the coiled-coil region of mouse Nek1 as bait identified 11 interacting proteins (192). Recent reports have shown that Nek1 localizes primarily in the cytoplasm (186) and specifically to the centrosomes and the basal bodies of primary cilia (43). These data suggest that

Nek1 may have multiple roles at different points within the cell cycle, including potential involvement in cilia assembly or function. Apical primary cilia are a common feature of renal epithelial cells and are thought to function as mechanosensors, bending in response to fluid flow through the lumen of the tubules, and transducing extracellular signals into the cells (193). Several PKD disease genes encode proteins that localize to the primary cilia (Figure 2.5), suggesting that defects in cilia assembly, structure, and/or function may play a role in cystogenesis (12, 28, 39, 40, 50, 56, 60, 190, 194-199). Interestingly, some PKD cilia-associated proteins are substrates of Nek1 phosphorylation, including Kif3a and tuberin. Kif3a is a subunit of the kinesin II motor protein and is important for cilia assembly, neuronal polarity and the development of laterality during embryogenesis (186). Kidney-specific knockout of *Kif3a* results in a cystic kidney phenotype in the mouse (42). Tuberin is a tumor suppressor and has been shown to interact with polycystin 1 (PC1) (200) and is responsible for its localization to the ciliary membrane (201, 202). Mutations in another NIMA-related kinase, *Nek8*, results in PKD in the mouse (the *jck* mouse model), and zebrafish (43, 59), and the Nek8 protein also localizes to the basal bodies of primary cilia, suggesting that *Nek1* and *Nek8* may be involved in a similar signaling pathway specific to the kidney that is important for normal ciliary function (43).

Interestingly, recent microarray analysis and qRT-PCR have shown altered gene expression of *Nek1* in homozygous *Bicc1^{jcpk}/Bicc1^{jcpk}* mice (153). Additionally, altered expression of *Kif3a* was observed in homozygous

Anks6^{Cy}/Anks6^{Cy} affected rats (Stagner and Bryda, unpublished data). These

data suggest that there may be an interaction between these proteins in these

models.

Zebrafish as a model

While rodent models for PKD continue to provide valuable information in

disease gene identification; the unique features of zebrafish offer distinct

advantages over the use of rodent models to study disease pathogenesis.

Zebrafish are small and inexpensive to maintain. While zebrafish have a similar

generation time as rodents, they produce considerably more offspring, with one

female laying up to 200 eggs per week. The transparent, externally developing

embryos are easily manipulated during all stages of development. Zebrafish are

genetically amenable for use in mutational analysis as well as loss and gain of

function assays, making the zebrafish a powerful tool for functional genomics.

The zebrafish genome sequencing project (www.sanger.ac.uk) is nearing

completion, providing a database to search for disease gene orthologs of mouse

and human genes. Molecular tools are available for use in zebrafish that allow

us to design experiments that would prove particularly challenging to perform in

any other animal model. For example, elucidating gene function is enhanced

through gene knockdown techniques using morpholinos, as opposed to gene

knockout techniques in rodents. Morpholinos are short pieces of single-stranded

DNA, or oligonucleotides, typically 18-25 nucleotides in length, which are

designed to specifically recognize and bind via base-pairing the mRNA of a gene

of interest (Figure 2.9).

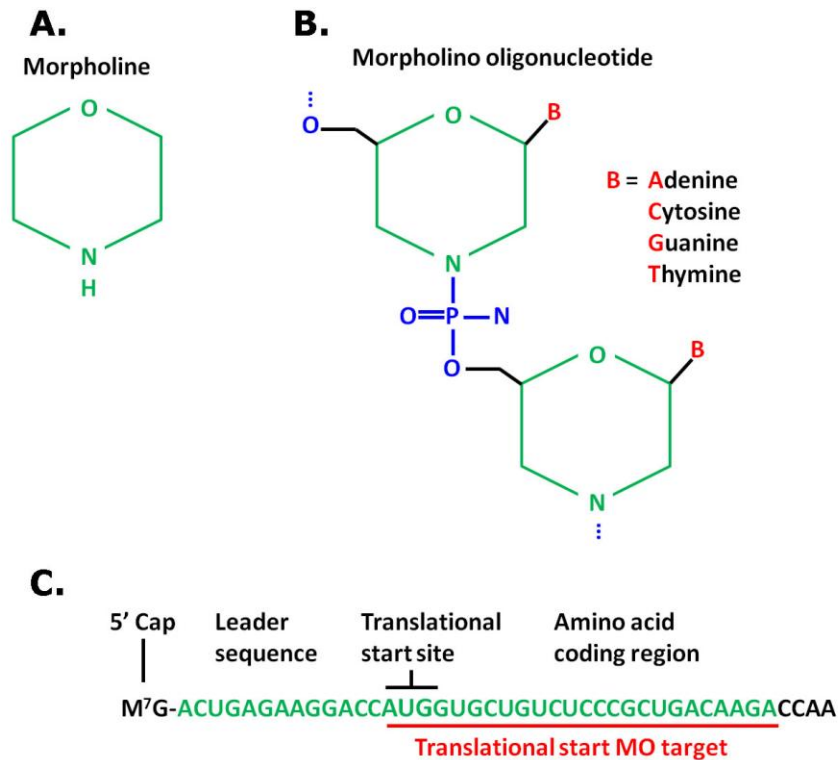**Figure 2.9. Morpholino oligonucleotide (MO)**

Figure 2.9. Morpholino (MO) oligonucleotide structure and function. (A) Structure of a morpholine ring. (B) Structure of a morpholino oligonucleotide with a morpholine backbone instead of ribose. Morpholinos (MO) are highly stable, extremely resistant to nucleases, and can remain active in the zebrafish embryo for up 5-7 days. (C) Morpholinos (MO) are typically 18-25 antisense oligonucleotides that bind to their target RNAs with high specificity. The binding of a MO to its target RNA blocks the translational start site and prevents translation from occurring, resulting in transient gene knockdown. Figure adapted from Gene Tools, LLC (www.gene-tools.com).

This allows for rapid assessment of phenotypic disturbances, in a matter

of hours or days compared to a minimum of two generations in the mouse (59).

Morpholino oligos have a high affinity for the target transcript and if injected into

zebrafish embryos will bind the mRNA of interest, knocking down function of the gene by blocking translation of the mRNA. Splice-blocking morpholinos can also be designed to target a splice donor or acceptor site in the pre-mRNA transcript, resulting in an altered transcript. This technique can be useful when there are not antibodies available to confirm knockdown of the gene, since the morpholino targeted mRNA can be characterized using RT-PCR (www.gene-tools.com). The advantages offered by the zebrafish model in combination with the accessibility of specific molecular tools makes this model a powerful tool for functional genomics.

Developmental processes in zebrafish, including organogenesis and tissue type differentiation, while less complex, are conserved in form and function to those of higher vertebrates; thus studies using this model can easily be translated into relevant experiments in mammals. The pronephros is the first kidney to develop in vertebrates and is functional in larval zebrafish (203). The pronephros consists of two fused glomeruli at the midline, paired tubules and collecting ducts, which empty into the cloaca (Figure 2.10). Unlike other alternative vertebrate model systems, such as *Xenopus*, zebrafish have a closed nephron system which is more similar to the mammalian nephron (204). While the zebrafish pronephros is more primitive than the metanephric mammalian kidney, it still contains the same specialized renal cell types in the glomerulus and tubules as is seen in the mouse.

The zebrafish pronephros develops within two days after fertilization, compared to 3-4 weeks in the mouse, and morphogenetic events parallel those

in mammalian kidney development (Figure 2.11) (205). Plus, the process can

be monitored in the live, transparent zebrafish embryos, while mouse kidney

development occurs *in utero*.
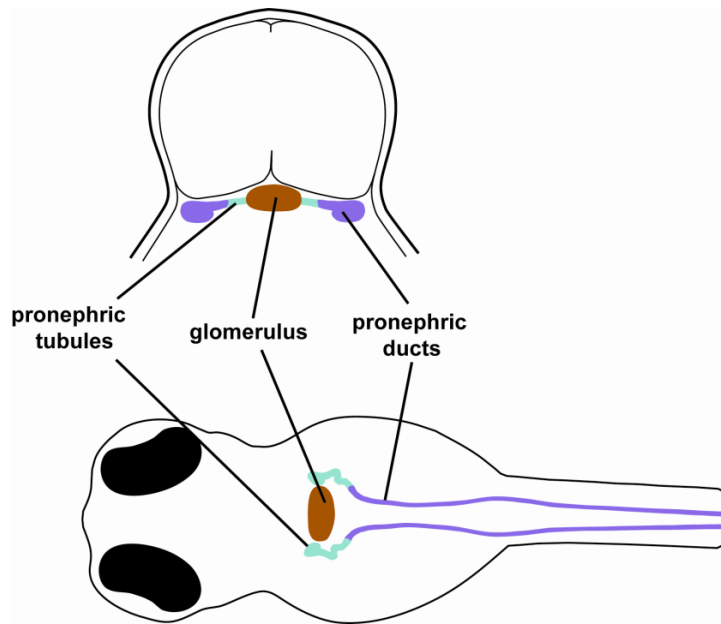
Figure 2.10. Zebrafish pronephros

Figure 2.10. Diagram of the zebrafish kidney (pronephros). Top panel is a cross section through the pronephros and the bottom panel represents a dorsal view of a 3-day old zebrafish embryo. The pronephric ducts are represented in dark blue; the tubules in light blue; and the glomerulus in brown. Zebrafish pronephric development begins as early as 10 hours post fertilization (hpf), and is complete by 72 hpf, yielding a primitive, but fully functioning kidney. Illustration courtesy of Don Connor at the College of Veterinary Medicine, University of Missouri, adapted from Drummond, 1998 (206).

Notably, several studies have demonstrated that mutations in zebrafish

orthologs of human and mouse PKD genes result in cystic phenotypes in fish

(45, 50, 59). These mutants also demonstrate extrarenal defects in other organs,

including the brain and heart (207). This is consistent with PKD phenotypes in

human disease and rodent models, suggesting that these genes maintain

multiple functions in different tissues. Taken together, the unique characteristics

of zebrafish combined with the available molecular tools and the conservation of

organogenesis make the zebrafish an attractive alternative model in which to

perform in vivo analyses of gene function.

Figure 2.11. Kidney organogenesis is highly conserved
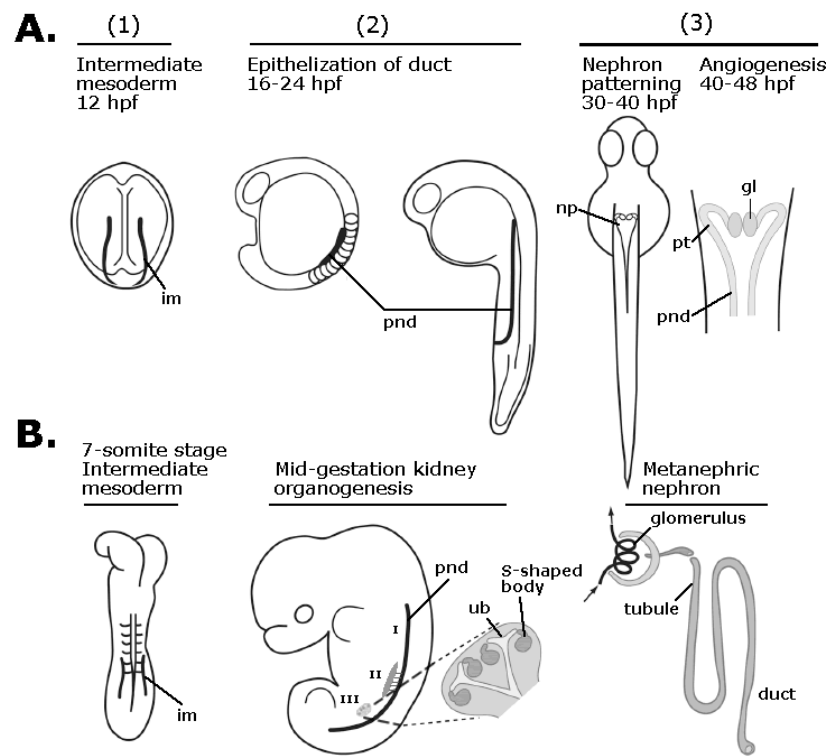

Figure 2.11. Kidney organogenesis is highly conserved between mouse and zebrafish. (A) Stages in zebrafish pronephros (kidney) development. (1) Specification of mesoderm to a nephric fate. The dark line represents the expression of an early marker of intermediate mesoderm (im). (2) Mesenchymal-epithelial transition of the pronephric duct (pnd). (3) Patterning of the nephron primordia (np) gives rise to the glomerulus (gl) and pronephric tubules (pt). Blood vessels from the dorsal aorta invade the glomerulus and form the capillary loop. (B) Processes in mammalian kidney development. At the 7-somite stage, expression of an early marker for intermediate mesoderm is observed. At mid-gestation, the growth and epithelialization of the pronephric (Wolffian) ducts occurs. From here, three distinct kidneys progressively form during embryogenesis in mammals; (I) the pronephros, which is vestigial and degenerate; (II) the mesonephros, an embryonic kidney that later contributes to the male reproductive tract; and (III) the metanephros, the adult mammalian kidney. Branching morphogenesis is unique to the metanephros (enlarged region). S-shaped bodies undergo patterning induced by the ureteric bud (ub) to become the glomerulus and tubules. The joining of the tubules with the branched collecting system forms the familiar mammalian nephron. Illustration courtesy of Don Connor at the College of Veterinary Medicine, University of Missouri, adapted from Drummond, 2003 (208).

CHAPTER III

MATERIALS AND METHODS

In vitro RNA binding assays

Computer-based peptide analysis: The putative functional domains of the Bicc1 protein were identified using the web interface PROSITE (209). Protein characteristics were determined using ProtParam (210). The GenBank accession numbers for the Bicaudal C protein sequences used in the analysis were: *Mus musculus* (mouse) (NP_113574); *Homo sapiens* (human) (NP_001073981); *Rattus norvegicus* (rat) (XP_342127); *Pan troglodytes* (chimpanzee) (XP_507803); *Gallus gallus* (chicken) (XP_421490); *Xenopus laevis* (frog) (AAF69826); *Danio rerio* (zebrafish) (XP_981965); *Anopheles gambiae* (mosquito) (XP_320061); *Drosophila melanogaster* (fruitfly) (NP_723948) and *Caenorhabditis elegans* (nematode) (NP_502067). CLUSTAL W2, Jalview, (211-213) and DS Gene (Accelrys, San Diego, CA) software programs were used for multiple sequence alignments and comparisons.

Construct generation: The reagents and materials used for these studies have been described previously (153). Briefly, clones encoding various portions of the mouse *Bicc1* gene were generated by PCR using a cDNA clone (GenBank Access. No. AW240366) as template. Primers used to amplify the various *Bicc1* fragments are listed in Appendix A. All primers were synthesized

by the Marshall University DNA Core facility (Huntington, WV). PCR products were gel extracted using the QIAGEN gel extraction kit (QIAGEN, Inc., Valencia, CA), directionally cloned into the Champion™ pET101/D-TOPO® expression vector containing a V5 epitope tag and ampicillin resistance gene. These constructs were transformed into OneShot® TOP10 chemically competent *E. coli* (Invitrogen, Carlsbad, CA) and sequence analysis was performed using an ABI Prism® 310 genetic analyzer (Applied Biosystems, Foster City, CA) to confirm the orientation and nucleotide sequence of the inserts.

Expression and isolation of fusion proteins: For protein expression, the plasmids containing various portions of the mouse *Bicc1* coding sequence in-frame with a V5 epitope tag described previously ("Construct generation"), were transformed into BL21 Star™ (DE3) chemically competent *E. coli* (Invitrogen). BL21 Star™ (DE3) competent cells (50 μl per vial) were removed from the -80°C freezer and thawed on ice. Fifty nanograms of each cloned plasmid DNA was added to one vial of competent cells and mixed by gently tapping the sides of tubes. The cells were incubated on ice for 20 minutes and then heat-shocked in a 42°C water bath for exactly 30 seconds. The heat-shocked cells were placed on ice for 2 minutes before adding 250 μl of SOC high growth media (2% Tryptone, 0.5% yeast extract, 10 mM NaCl, 2.5 mM KCl, 10 mM MgCl$_2$, 10 mM MgSO$_4$, and 20 mM glucose). The transformed cells were cultured for 1 hour in a shaking incubator at 37°C and 225 rpm, with the tubes placed on their sides. After 1 hour, 50 μl and 100 μl of the transformed cells were spread on Luria-Bertani (LB) agar plates containing 100 μg/ml of ampicillin for selection and

37

grown at 37°C overnight. Twenty individual colonies were picked and used to

inoculate 3 ml each of LB + 100 μg/ml ampicillin media. The clones were

cultured overnight at 37°C and 225 rpm and plasmid DNA was extracted from

each clone using a crude boil-prep method. Briefly, the cells were pelleted at

15,000 x g at 4°C for 3 minutes, the supernatants were removed and the pellets

were resuspended in 110 μl of STETL (8% sucrose, 0.5% Triton X-100, 50 mM

Tris, pH 8.0, 0.5 mg/ml lysozyme). The STET solution was pre-made and stored

at 4°C, but the lysozyme was added just before use. The cells were mixed by

pipetting and vortexed briefly to ensure the pellets were dissolved completely.

The cells were lysed by boiling for 30 seconds followed by centrifugation at

15,000 x g at 4°C for 15 minutes. The resulting pellets containing genomic DNA,

cell debris and proteins were plucked and discarded using a sterile toothpick. To

precipitate the plasmid DNA, 110 μl of room temperature isopropanol was added

to the remaining solution, mixed by inverting 4-5 times and immediately

centrifuged at 15,000 x g at 4°C for 15 minutes. The plasmid DNA pellet was

resuspended in 25 μl of nuclease free water and the concentration determined by

A_{260} using a Nano-drop spectrophotometer (Thermo-Fisher, Waltham, MA). The

plasmid DNA from each clone was screened for the presence of the various

Bicc1 inserts by restriction endonuclease digest using *Sac*I and *Xba*I restriction

enzymes (New England Biolabs, Ipswich, MA). One microgram of DNA was

digested at 37°C overnight using 10U of each enzyme, 1X NEB buffer #4 and 1X

BSA in a total reaction volume of 25 μl. Five microliters of each of the digested

DNAs were separated by gel electrophoresis on a 1% agarose gel containing 0.5

μg/ml ethidium-bromide in 1X Tris-acetate-EDTA (TAE) buffer (40 mM Tris, 0.1%

glacial acetic acid, 1 mM EDTA, pH 8.0) at 80V for 80 minutes. Insert-positive

clones were identified by visualization of the appropriate sized products using a

Gel Doc UV transilluminator (Bio-Rad, Hercules, CA). To obtain higher quality

plasmid DNA for clone sequence verification, the insert-positive clones were

cultured overnight in 3 ml LB + 100 μg/ml ampicillin media at 37°C, 225 rpm and

plasmid DNA was extracted using the QIAGEN mini-prep plasmid DNA extraction

kit (QIAGEN). The nucleotide sequence and orientation of the various *Bicc1*

inserts was confirmed by sequence analysis on an ABI Prism® 310 genetic

analyzer (Applied Biosystems) using vector-specific sequencing primers; T7

forward, 5'-TATACGACTCACTATAGGG-3' and T7 reverse, 5'-

TAGTTATTGTCAGCGGTGG-3' (Invitrogen).

For larger-scale protein expression of the various Bicc1-V5 fusion

proteins, the sequence-confirmed positive clones in BL21 Star™ (DE3) cells

were grown overnight in 20 ml of LB media containing 100 μg/ml ampicillin and

1% sterile glucose at 37°C. Five ml of the overnight cultures were used to seed

250 ml of LB containing 100 μg/ml ampicillin and 1% sterile glucose. Cultures

were grown for two hours or until an A_{600} of 0.4-0.6 was reached. Protein

expression was induced with isopropyl-β-D-thiogalactoside (IPTG) (Fisher

Scientific International, Hampton, NH) at a final concentration of 0.5 mM.

Induced cultures were grown overnight and pelleted by centrifugation at 6,000

rpm for 20 minutes at 4°C. Cell pellets were resuspended in a volume of 5

ml/gram weight of pellet (w/v) in denaturing lysis buffer (100 mM NaH_2PO_4, 10

mM Tris-Cl, 8 M urea, pH 8.0, 1 mg/ml lysozyme, and 1X Complete protease inhibitor (Roche Applied Science, Indianapolis, IN), sonicated on ice for 1 minute, and incubated on a rotating shaker at 4°C for 30 minutes. Lysates were sonicated again for 1 minute and incubated at 4°C for another 30 minutes with rotation. Lysates were then centrifuged at 4°C at 16,000 rpm for 20 minutes to produce a cleared cell lysate. The cleared cell lysates were concentrated to a volume of approximately 5 ml using Centri-prep centrifugal filtration units with molecular weight cut-offs of 100, 30, or 10 kDa (Millipore Corp., Billerica, MA). The filtration units contain a regenerated cellulose membrane that retains proteins at the molecular weight cut-off size or greater. Briefly, cleared cell lysates were added to the appropriate Centri-prep column and centrifuged in an Allegra 6R centrifuge using a GH3.8 rotor for 30 minutes at 15°C and 2,500 rpm (Beckman Coulter, Inc., Fullerton, CA). The filtrate was poured off and discarded and this process was repeated two more times. After the third centrifugation, the concentrated protein retentate was collected.

Protein detection: Concentrated, cleared bacterial cell lysates were diluted in equal volumes of 2X Laemmli sample buffer (4% SDS, 20% glycerol, 10% β-mercaptoethanol, 0.004% bromophenol blue, 0.125 M Tris-Cl, pH 6.8) and boiled for 5 minutes. The samples were loaded onto SDS-PAGE gels (10, 12 or 15% depending on protein size) and separated at 200V for 45 minutes in 1X SDS-PAGE running buffer (25 mM Tris, 192 mM glycine, 0.1% SDS). The separated proteins were transferred onto 0.45 μm nitrocelluose membranes (Bio-Rad) at 100V for 1 hour with an ice pack and constant stirring. Membranes were

blocked in 5% dry milk/PBST (1X phosphate-buffered saline, pH 7.4 containing 0.1% Tween-20) overnight at 4°C with constant rotation on a Belly Dancer™ shaker (Stovall, Greensboro, NC). Membranes were rinsed 2 times at room temperature for 10 minutes in 0.5% dry milk/PBST. Membranes were incubated overnight at 4°C with constant rotation in 0.5% dry milk/PBST and a 1:5,000 dilution of horseradish peroxidase-conjugated (HRP) mouse anti-V5 monoclonal antibody (Invitrogen). Membranes were washed 3 times with 0.5% dry milk/PBST for 15 minutes at room temperature with continuous rotation. Protein bands were visualized on x-ray film using chemiluminescence (Amersham Biosciences, Piscataway, NJ). Briefly, chemiluminescent detection uses the horseradish peroxidase (HRP) enzyme to catalyze a reaction that results in the generation of visible light. This is accomplished by incubating the membranes with a HRP substrate which is prepared fresh by adding equal parts luminol and peroxide reagents. The HRP enzyme catalyzes the reduction of peroxide (H_2O_2) to H_2O, and then recovers the electrons used for this reduction from luminol, generating an oxidized luminol radical, which emits light as it decays. The membranes were incubated with the HRP substrate solution for 1 minute, blotted on a paper towel to remove excess solution, wrapped in plastic wrap and exposed to x-ray film for 1-30 minutes.

RNA-binding assays: The binding reaction consisted of 200 μl of Bicc1 concentrated cleared cell lysate derived from a 250 ml IPTG-induced overnight bacterial culture, 40 μl of 10X RNA binding buffer (250 mM Tris-HCl, pH 7.4, 1.5 M NaCl, 10% Triton X-100, 1X Complete protease inhibitor cocktail (Roche), 159

μl of nuclease-free water (Ambion, Inc., Austin, TX), 1 μl of RNAseOUT (Invitrogen), and either 10 mg of poly(U) Sepharose beads or 30 ul of poly(G) or Sepharose 4B (Sigma-Aldrich, St. Louis, MO) sepharose bead slurry. Experiments designed to test the strength of the interaction were performed in the same manner but the NaCl concentration was adjusted appropriately in the RNA binding buffer to give final salt concentrations of 250 mM, 500 mM or 750 mM. Reaction mixtures were incubated at 4°C with end-over-end constant mixing on a Labquake® rotator (Barnstead Thermolyne, Dubuque, IA). Beads were pelleted at 13,000 rpm for 2 minutes at 4°C and washed 4 times with ice cold 1X RNA binding buffer. Between each rinse, the beads were vortexed briefly and centrifuged at 13,000 rpm for 2 minutes. Proteins were separated from the beads by adding 25 μl of Laemmli sample buffer and boiling for 5 minutes prior to loading the supernatant on 10% SDS-PAGE gels for protein detection as described previously ("Protein detection").

RNA interactions of Bicc1

RNA extraction: Whole kidneys were dissected from 3-5 day old wild type and *Bicc1^{jcpk}/Bicc1^{jcpk}* mice, flash frozen in liquid nitrogen and stored at -80°C. Total RNA was isolated from age-matched pooled wild type and *Bicc1^{jcpk}/Bicc1^{jcpk}* kidneys using RNeasy (QIAGEN). Kidneys were weighed and added to an appropriate volume of supplied lysis buffer (RLT) containing β-mercaptoethanol. The tissue was homogenized on ice using a rotor-stator

homogenizer (Ultra-turrax T-25 basic, IKA®Werke, Wilmington, NC) in 30 second

bursts until a homogenous solution was achieved. The resulting lysate was

centrifuged for 3 minutes at 13,000 rpm at room temperature. The supernatant

(cleared cell lysate) was removed carefully and transferred to a new tube; the

pellet was discarded. An equal volume of 70% ethanol was added to the cleared

cell lysate and mixed immediately by pipetting. This mixture was applied to an

RNeasy spin column containing a silica-based membrane and centrifuged for 15

seconds at 10,000 rpm; the flow through was discarded. In-column digestion of

DNA was achieved by adding RNase-free DNase I (QIAGEN) directly to the

column and incubating for 10 minutes at room temperature. The column was

washed three times followed by centrifugation for 15 seconds at 10,000 rpm.

The column was washed a fourth time and centrifuged for 2 minutes at 10,000

rpm; the longer centrifugation time helps to dry the membrane and avoid

carryover of ethanol from the wash buffer during elution. The column was placed

in a new collection tube and RNA was eluted with an appropriate volume of RNA

storage solution (Ambion) and stored -80°C. The RNA concentration was

estimated based on A_{260} (Nano-drop) measurements. The RNA was separated

by gel electrophoresis on a 1% formaldehyde gel (0.5 g agarose, 42.4 ml

nuclease-free water, 2.6 ml 37% formaldehyde, and 5 ml 10X MOPS buffer; 200

mM 4-morpholino-propanesulfonic acid, 50 mM sodium acetate, pH 7.0). The

RNA ladder and samples were prepared as follows: 5 μl RiboRuler High Range

(Fermentas) + 5 μl 2X RNA loading buffer (Fermentas; 95% formamide, 0.025%

SDS, 0.025% bromophenol blue, 0.025% xylene cyanol FF, 0.025% ethidium

bromide, 0.5 mM EDTA); and 5 μl in vitro transcribed RNA + 5 μl 2X RNA loading

buffer. Samples were heated at 65°C for 15 minutes, then loaded in the gel and

separated at 80V for 80 minutes in 1X MOPS buffer (20 mM 4-morpholino-

propanesulfonic acid, 5 mM sodium acetate, pH 7.0). The RNA was visualized in

the gel using a Gel Doc UV transilluminator (Bio-Rad).

Wnt PCR Superarray: First strand cDNA synthesis was performed using

Reaction Ready synthesis kit (SABiosciences Corp., Frederick, MD). An

annealing mixture was prepared by adding 1 μg of input RNA from wild type or

Bicc1^{jcpk}/Bicc1^{jcpk} kidneys, 1 μl Buffer P, and RNase-free water to a volume of 10

μl. The solution was mixed by pipetting and placed on ice. The reverse

transcription (RT) cocktail was prepared by adding 4 μl 5X RT buffer, 4 μl RNase-

free water, 1 μl RNase inhibitor and 1 μl M-MMLV reverse transcriptase. The RT

cocktail was mixed by pipetting, added to the annealing mixture, and mixed again

gently by pipetting. The tube was centrifuged briefly and incubated at 37°C for 1

hour, and then 95°C for 5 minutes.   The cDNA was diluted with 80 μl ddH$_2$O and

placed on ice. Real-time PCR was performed using RT^2 Profiler^{TM} PCR Array

specific for the Wnt pathway in the mouse (SABiosciences) in a 96-well format.

This array contains gene-specific primers for 84 Wnt-related genes as well as

gene-specific primers for 5 housekeeping genes (Appendix C). Five 10-fold

serial dilutions of the cDNA were added to the primers for one housekeeping

gene to estimate the linear dynamic range of the assay. To ensure that there

was not genomic DNA contamination in the RNA preps, a no reverse

transcriptase (NRT) control was set up using RNA from either wild type or

Bicc1^{jcpk}/Bicc1^{jcpk} mice. Additional controls included a no template control (NTC)

for each primer set. The real-time PCR reaction was prepared as follows in a

master mix: 12.5 μl 2X RT^2 Real-Time SYBR Green/ROX PCR supermix

(SABiosciences), 2 μl diluted cDNA, 10.5 μl ddH$_2$O in a final volume of 25 μl. A

separate master mix was prepared for the serial dilutions and negative controls in

a final volume of 25 μl. The 96-well plate was centrifuged briefly and cycled in an

ABI Prism® 7000 sequence detection system as follows: 95°C for 10 minutes,

then 40 cycles of 95°C for 15 seconds and 60°C for 1 minute. A dissociation

melting curve analysis was performed to verify only the target genes were

amplified. The fold changes in gene expression between wild type and

Bicc1^{jcpk}/Bicc1^{jcpk} homozygous mice were determined by the $\Delta\Delta C_t$ method of

analysis (214), normalizing to *β-actin* and *GAPDH*.

   Real time PCR confirmation: The following gene-specific primers were

designed using Primer Express software (Applied Biosystems) and manufactured

by Sigma-Genosys (The Woodlands, TX): *CK2*, 5'-

GAACGCTTTGTCCACAGTGA-3' and 5'-GCCTGGTCCTTCACAACAGT-3';

Pitx2, 5'-TTCCAGAGAAACCGCTACCCA-3' and 5'-

CGTTCCCGCTTTCTCCATTT-3'; *Tle2*, 5'-CCAGCGAGAAGACAGAAATGC-3'

and 5'-GAGGCGTTTCACAATCTCAGC-3'; *Fzd6*, 5'-

GCAAAAAGACGTGCACAGAA-3' and 5'-TCACAGGACTCTTGCAGCAC-3';

Wnt7a, 5'-GCCTGGACGAGTGTCAGTTT-3' and

5'CGATAATCGCATAGGTGAAGG3'; *β-actin,* 5'-GATCTGGCACCACACCTTCT-

3' and 5'-GGGGTGTTGAAGGTCTCAAA-3' and *GAPDH,* 5'-

TGCATCCTGCACCACCAACT-3' and 5'-TGCCTGCTTCACCACCTT-3'. First

strand cDNA synthesis was performed using Reaction Ready synthesis kit

(SABiosciences) as described in "Wnt PCR Superarray". The cDNA was diluted

with 80 μl ddH$_2$O and placed on ice. The real-time PCR reactions were

assembled as follows: 12.5 μl 2X RT^2 Real-Time SYBR Green/ROX PCR

supermix (SABiosciences), 2 μl diluted cDNA, 0.2 μM gene-specific primers, 10.5

μl ddH$_2$O in a final volume of 25 μl. Controls included a no reverse transcriptase

(NRT) using RNA from either wild type or *Bicc1^{jcpk}/Bicc1^{jcpk}* kidneys and no

template controls (NTC) for each primer set. The reactions were performed in

triplicate for each set of gene-specific primers. The 96-well plate was centrifuged

briefly and cycled in an ABI Prism® 7000 sequence detection system as follows:

95°C for 10 minutes, then 40 cycles of 95°C for 15 seconds and 60°C for 1

minute. A dissociation melting curve analysis was performed to verify only the

target gene was amplified. Fold changes in gene expression were determined by

the $\Delta\Delta C_t$ method of analysis (214), normalizing to *β-actin* and *GAPDH*.

CK2 protein analysis: Protein extraction: Whole kidneys were dissected

from 0 and 5 day-old wild type and *Bicc1^{jcpk}/Bicc1^{jcpk}* mice, flash frozen in liquid

nitrogen and stored at -80°C. Total protein was isolated from age-matched

pooled wild type and *Bicc1^{jcpk}/Bicc1^{jcpk}* kidneys using RIPA buffer (50 mM Tris-Cl

pH 7.4, 150 mM NaCl, 1 mM PMSF (phenylmethylsulphonyl fluoride), 1 mM

EDTA, 5 μg/ml aprotinin, 5 μg/ml leupeptin, 1% Triton X-100, 1% sodium

deoxycholate, 0.1% SDS). Frozen kidneys were weighed and added to 2 ml

RIPA buffer/100 mg tissue in a 50 ml conical tube and placed on ice. The

kidneys were homogenized on ice using a rotor-stator homogenizer (Ultra-turrax

T-25 basic, IKA® Werke) three times in 45 second intervals until a homogenous

solution was achieved. The homogenate was sonicated on ice in 10 second

bursts for 1-2 minutes and then incubated for 30 minutes on ice, sonicating

periodically during the incubation period. The samples were transferred to

microfuge tubes and centrifuged at 4°C for 10 minutes at 13,000 rpm. The

supernatant was transferred to a fresh tube and treated with DNase I (2.5 μl per

300 μl, QIAGEN) and RNase A (2 μl per 300 μl, USB, 10 mg/ml stock) to

eliminate DNA and RNA contaminants from the protein solution. The samples

were incubated for 20 minutes at room temperature after the addition of DNase I

and RNase A. Total protein concentrations were determined using the BCA

method (Sigma). The protein solutions were separated into small aliquots and

stored at -80°C. <u>Western blot analysis:</u> A rabbit monoclonal antibody to the

alpha subunit of CK2 which recognizes a 42 kDa protein product was obtained

from Epitomics (Burlingame, CA). Fifteen micrograms of total protein extracted

from 0 and 5 day-old wild type and $Bicc1^{jcpk}/Bicc1^{jcpk}$ kidneys was analyzed by

SDS-PAGE as described previously (see "In vitro RNA binding assays, Protein

detection") with the following modifications. The proteins were separated by gel

electrophoreses at 200V for 45 minutes and transferred to a 0.2 μm nitrocellulose

membrane (Whatman, Piscataway, NJ) at 100V for 1 hour. The membrane was

blocked for 2 hours at room temperature in 5% milk/PBST (1X PBS containing

0.1% Tween-20) and then incubated overnight at 4°C in rabbit-anti-CK2 antibody

diluted 1:250 in 0.5% milk/PBST. The membrane was washed two times for 5

minutes, once for 10 minutes and once for 15 minutes in 0.5% milk/PBST. The blot was incubated for 1 hour at room temperature with goat-anti-rabbit-HRP conjugated secondary antibody (Sigma) at a 1:100,000 dilution in 0.5% milk/PBST. The membrane was washed two times for 5 minutes, once for 10 minutes and once for 15 minutes in 0.5% milk/PBST. Proteins were detected using chemiluminescence as described previously (see "In vitro RNA binding assays, Protein detection") using Immobilon HRP substrate (Millipore) and subsequent exposure to x-ray film. The membrane was stripped for 1 hour in 25 mM glycine, pH 2.0 and washed for 30 minutes in 1% SDS. The membrane was washed 7 times for 5 minutes each in 1X PBST (1X PBS containing 0.2% Tween-20). The stripped blot was incubated for 2 hours at room temperature with mouse-anti-acetylated α-tubulin antibody (Sigma) diluted 1:2,000 in 0.5% milk/PBST. The membrane was washed two times for 5 minutes, once for 10 minutes and once for 15 minutes in 0.5% milk/PBST. The blot was incubated for 1 hour at room temperature with rabbit-anti-mouse-HRP conjugated secondary antibody (Sigma) at a 1:100,000 dilution in 0.5% milk/PBST. The membrane was washed two times for 5 minutes, once for 10 minutes and once for 15 minutes in 0.5% milk/PBST. Proteins were detected using Immobilon chemiluminescence HRP substrate (Millipore) and exposure to x-ray film.

Construct generation: As described previously (57), cDNA encoding the Bicc1 protein (GenBank Access. No. NM_031397) was amplified from IMAGE clone 2655954 (ATCC) by PCR using primers 5'-ATGGCCTCGCAGAGCGAG-3' and 5'-CTACCAGCGGCCACTGACGCT-3' and cloned into the pcDNA3.1/nV5-

DEST expression vector (Invitrogen). The following *GAPDH* gene-specific

primers, 5'-CGCATCTTCTTGTGCAGTG-3' and 5'-

AGGCCCCTCCTGTTATTATG-3', were designed using Primer 3 (215) and

manufactured by Sigma-Genosys (The Woodlands, TX) to amplify the full length

coding region of *GAPDH* (GenBank Access. No. NM_001001303). Total RNA

extracted from 3-5 day old wild type mouse kidneys (see "RNA extraction") and

was used as template for first strand cDNA synthesis. First strand cDNA

synthesis was performed using a High Capacity first strand synthesis kit (Applied

Biosystems). All kit components were thawed on ice. A 10 μl reverse

transcription (RT) master mix was prepared on ice by adding 2 μl 10X RT buffer,

0.8 μl 25X dNTP mix (100 mM), 2 μl 10X RT random primers, 1 μl MultiScribe™

reverse transcriptase (MuLV), 1 μl RNase inhibitor and 3.2 μl nuclease free

water. The RT reaction was mixed gently by pipetting, centrifuged briefly and

placed on ice. One microgram of input RNA was added to nuclease free water to

a volume of 10 μl mixed by pipetting and centrifuged briefly. The RNA solution

was added to the RT reaction mix, mixed gently by pipetting, centrifuged briefly

and then incubated for 10 minutes at 25°C, 2 hours at 37°C, 85°C for 5 minutes,

and then held at 4°C. A 25 μl PCR reaction was assembled by adding 2 μl

cDNA, 1U Platinum *Taq* High-Fidelity DNA polymerase (Invitrogen), 0.2 μM

GAPDH gene-specifc primers, 1.5 mM MgCl$_2$, 1X PCR buffer and 0.2 mM

dNTPs. The reaction was cycled at 94°C for 2 minutes, then 30 cycles of 94°C

for 30 seconds, 55°C for 30 seconds, and 68°C for 3 minutes, followed by a 7

minute final extension at 68°C, holding at 4°C. The resulting 1,170 bp amplicon

was subcloned into pCR2.1-TOPO® (Invitrogen), clones were screened by restriction endonuclease digest with FastDigest® *EcoR*I (Fermentas) and sequenced at the University of Missouri DNA Core facility on an ABI Prism® 3730 DNA analyzer (Applied Biosystems).

Cell culture: Mouse inner medullary collecting duct (IMCD) cells were obtained from the American Type Culture Collection (ATCC, Manassas, VA) and cultured in DMEM/F-12 (IMCD) containing 10% fetal bovine serum (Gibco-Invitrogen, Carlsbad, CA) at 37ºC and 5% CO_2.

Bicc1 immunoprecipitation: Mouse IMCD cells were transiently transfected using Lipofectamine 2000 (Invitrogen). Briefly, IMCD cells were seeded in a 6-well culture plate at a density of 2 x 10^5 cells/well and cultured to 80-90% confluency at 37°C/5% CO_2. In separate tubes, 4 μg of Bicc1-pcDNA3.1/nV5-DEST plasmid DNA was added to 250 μl of Opti-Mem (Gibco) and 12 μl of Lipofectamine 2000 was added to 250 μl of Opti-Mem. The solutions were incubated separately for 5 minutes at room temperature, combined, and then mixed by inversion. The transfection cocktail was incubated an additional 20 minutes at room temperature and then added to the cells dropwise while swirling. Cells were harvested 48 hours after transfection using a mammalian-specific cell lysis system (M-PER, Pierce, Rockford, IL) which provides rapid but gentle disruption and a high yield of native proteins. Culture medium was decanted and cells were washed once with ice cold 1X TBS (Tris-buffered saline, pH 7.4). Two hundred microliters of M-PER reagent containing 1X Complete protease inhibitor cocktail (Roche), was added to each well and

agitated gently for 10 minutes on a Belly Dancer™ shaker at room temperature.

Cells were scraped and lysates were transferred to a 1.5 ml microfuge tube.

Lysates were cleared by centrifugation for 20 minutes at 16,000 x g at 4°C.

Supernatants were transferred to fresh 1.5 ml tubes and protein concentration

was measured by BCA assay (Sigma). V5-Bicc1 was immunoprecipitated from

IMCD cell lysates using UltraLink Protein A/G agarose beads (Pierce). One

hundred microliters of UltraLink Protein A/G agarose beads (provided as 50%

slurry) was centrifuged at 2,500 x g for 1 minute at 4°C, the supernatant was

removed and the beads were resuspended in 100 μl M-PER lysis buffer (Pierce)

containing 1X Complete protease inhibitor (M-PER/Complete). The resuspended

protein A/G beads were added 100 μl of Bicc1 transfected cell lysates (~220 μg

protein) and incubated with gentle end-over-end mixing for 30 minutes at 4°C on

a Labquake® shaker (Barnstead Thermolyne). The mixture was centrifuged at

2,500 x g for 1 minute at 4°C and the supernatant (pre-cleared lysate) was

transferred to a new microfuge tube. Two microliters (2 μg protein) of mouse

anti-V5 monoclonal antibody (Invitrogen) was added to the pre-cleared lysate

and incubated overnight at 4°C on the Labquake®. Controls included non-

transfected cell lysates with or without anti-V5 antibody; Bicc1 transfected cell

lysates with or without anti-V5 antibody; and anti-V5 antibody plus protein A/G

beads without cell lysate. A new 100 μl aliquot of UltraLink Protein A/G agarose

beads was resuspended in M-PER/Complete, and this was added to the protein-

antibody complexes and incubated overnight at 4°C on the Labquake®. The

samples were centrifuged at 2,500 x g for 1 minute at 4°C and the supernatant

51

was saved on ice in a separate tube for future analysis. The beads were washed 3 times with 400 μl M-PER/Complete for 10 minutes at 4°C on the Labquake®; all washes were saved on ice in separate tubes for future analysis. The beads were resuspended in 100 μl Laemmli sample buffer, boiled for 5 minutes and centrifuged at 2,500 x g for 1 minute. Thirty five microliters of the supernatant was analyzed by 10% SDS-PAGE and Western blot analysis as described previously (see "In vitro binding assays, Protein detection"). Twenty five microliters of the saved supernatant and washes were also evaluated. Briefly, the gel was transferred to a nitrocellulose membrane and probed with mouse anti-V5-HRP antibody (Invitrogen) at a dilution of 1:5,000. The protein was detected using chemiluminescence as described previously (see "In vitro binding assays, Protein detection") with Immobilon HRP substrate (Millipore) and exposed to x-ray film.

RNA and protein isolation from Bicc1 immunoprecipitates: IMCD cells cultured and transfected as described previously (see "Cell culture" and "Bicc1 immuno-precipitation"). Immunoprecipitation of Bicc1 was performed as described in "Bicc1 immunoprecipitation", except for the final step. Rather than resuspending the beads in Laemmli sample buffer for SDS-PAGE, the beads were instead resuspended in 1 ml TRIZOL reagent (Invitrogen), mixed by inversion and incubated for 5 minutes at room temperature. RNA and protein were then extracted from the beads. Briefly, to extract RNA, 200 μl chloroform was added to the TRIZOL-bead mixture and shaken vigorously for 15 seconds under a fume hood. The phases were separated by centrifugation at 10,000 x g

for 15 minutes at 4°C. The aqueous layer was removed and placed in a clean microfuge tube. To facilitate precipitation of the RNA, 500 μl isopropanol was added, mixed by inversion and incubated for 10 minutes at room temperature. The RNA was pelleted by centrifugation at 12,000 x g for 10 minutes at 4°C. The pellet was washed with 500 μl 70% ethanol, air-dried for 5 minutes and resuspended in 30 μl RNA Storage solution (Ambion). The RNA concentration was determined by A_{260} (Nano-drop) and utilized for RT-PCR as described in the next section. The proteins were separated from the phenol-ethanol supernatant using isopropanol. One and one half milliliters of isopropanol was added to the phenol-ethanol supernatant and the mixture was incubated for 10 minutes at room temperature. The protein precipitate was pelleted by centrifugation at 12,000 x g for 10 minutes at 4°C. The protein pellet was washed 3 times with 2 ml 0.3 M guanidine hydrochloride in 95% ethanol. During each wash cycle, protein was incubated for 20 minutes in wash solution at room temperature, followed by centrifugation at 7,500 x g for 5 minutes at 4°C. After the final wash, the pellet was vortexed in 2 ml 100% ethanol, incubated for 20 minutes at room temperature, and centrifuged at 7,500 x g for 5 minutes at 4°C. The protein pellet was dissolved in 50 μl Laemmli buffer, boiled 5 minutes, and analyzed by SDS-PAGE and Western blot analysis as described previously (see "In vitro binding assays, Protein detection"), using the mouse anti-V5-HRP antibody to detect the presence of the Bicc1 protein.

RT-PCR: The RNA that was isolated from the Bicc1 immunoprecipitates with TRIZOL was subjected to RT-PCR using gene- specific primers (listed in

"Real-time PCR confirmation") for *CK2*, *Fzd6*, *GAPDH*, and *β-actin*. Gene-specific primers for *Nek1* were 5'-TGGGACAGTGCAGCTTGGAGA-3' and 5'-TGAGACAGCAAGCTGCGGAGA-3' (153). The following primers were used to amplify a 570 bp region of the coding sequence for nucleoporin 210 kDa-like (*Nup210L*, GenBank Access. No. XM_622896), 5'-CAGGTTCTCACTTTTCGGATCG-3' and 5'-TATTTCCTTCACATCAGGGTGGTT-3', as a negative control. First strand cDNA synthesis was performed using a High Capacity first strand kit (Applied Biosystems) as described previously (see "RNA interactions of Bicc1, Construct generation"). Briefly, after thawing kit components on ice, a 10 µl reverse transcription (RT) master mix was prepared on ice by adding 2 µl 10X RT buffer, 0.8 µl 25X dNTP mix (100 mM), 2 µl 10X RT random primers, 1 µl MultiScribe™ reverse transcriptase (MuLV), 1 µl RNase inhibitor and 3.2 µl nuclease free water. The RT reaction was mixed gently by pipetting, centrifuged briefly and placed on ice. One microgram of input RNA from the Bicc1 immunoprecipitate was added to nuclease free water to a volume of 10 µl mixed by pipetting and centrifuged briefly. The RNA solution was added to the RT reaction mix, mixed gently by pipetting, centrifuged briefly and then incubated for 10 minutes at 25°C, 2 hours at 37°C, 85°C for 5 minutes, and then held at 4°C. The cDNA was diluted to 10 ng/µl and PCR reactions were assembled using 5 µl diluted cDNA (~50 ng), 2 mM MgCl$_2$, 0.2 µM of each primer, 1X PCR buffer, 0.2 mM dNTPs, 1U FastStart® *Taq* DNA polymerase (Roche) and ultra pure water to a total reaction volume of 25 µl. Cycling conditions were as follows: 95°C for 4

minutes, then 35 cycles of 95°C for 30 seconds, 60°C for 30 seconds, and 72°C

for 45 seconds, followed by a final extension at 72°C for 7 minutes and held at

4°C. Fifteen microliters of the PCR products were separated by gel

electrophoresis on a 3% agarose gel containing 0.5 µg/ml ethidium bromide in 1X

TBE buffer at 90V for 1 hour. The expected product sizes of 152, 101, 77, 75,

294 and 570 bp for *CK2*, *Fzd6*, *GAPDH, β-actin, Nek1* and *Nup210L*,

respectively, were visualized in the gel using a Gel Doc UV Transilluminator (Bio-

Rad).

Bicc1 cellular localization

Cell culture: Human embryonic kidney cells (HEK293) and mouse inner

medullary collecting duct (IMCD) cells were obtained from the American Type

Culture Collection (ATCC, Manassas, VA) and cultured in DMEM (HEK293) or

DMEM/F-12 (IMCD) containing 10% fetal bovine serum (Gibco-Invitrogen,

Carlsbad, CA) at 37ºC and 5% CO_2.

Generation of a GFP-Bicc1 construct: The coding sequence of *Bicc1*

(GenBank Access. No. NM_031397) was amplified from a clone kindly provided

by Oliver Wessely (LSU) by PCR using primers 5'-

CACCATGGCCTCGCAGAGCGAGC-3' and 5'-

CTACCAGCGGCCACTGACGCT-3'. Primers were designed using Primer 3

(215) and manufactured by Integrated DNA Technologies (IDT, Coralville, IA).

The resulting 2,938 bp amplicon was directionally cloned into the mammalian

expression vector pcDNA3.1/NT-GFP-TOPO® using the directional TOPO® TA

cloning system (Invitrogen) and transformed into One Shot® TOP 10 chemically competent *E. coli* (Invitrogen). Briefly, 4 μl of the PCR product was mixed with 1 μl salt solution (final concentration 200 mM NaCl, 10 mM MgCl$_2$) and 1 μl pcDNA3.1/NT-GFP-TOPO® linearized vector (10 ng/μl). The TOPO® reaction was incubated for 5 minutes at room temperature. TOP10 chemically competent cells (50 μl per vial) were thawed on ice. Two microliters of the TOPO® reaction was added to the competent cells and transformed as described previously (see "In vitro RNA binding assays, Expression and isolation of fusion proteins").

Twenty individual colonies were picked and plasmid DNA was extracted using a boil-prep method as described previously (see "In vitro RNA binding assays, Expression and isolation of fusion proteins). Cloned plasmids were screened by restriction endonuclease digest using *Bgl*II and *Xmn*I. A 30 μl digest reaction was assembled by adding 1 μg plasmid DNA, 7U *Bgl*II, 5U *Xmn*I, 1X NEB buffer #3, 1X bovine serum albumin (BSA) and ultra pure water. Five microliters of digested DNA was separated by gel electrophoresis on a 1% agarose gel containing 0.5 μg/ml ethidium bromide in 1X TAE buffer at 80V for 80 minutes.

Insert-positive clones were identified by visualization of the expected 5,397 and 3,713 bp digest products using a Gel Doc UV transilluminator (Bio-Rad). To obtain higher quality plasmid DNA for clone sequence verification, the insert-positive clones were cultured overnight in 3 ml LB + 100 μg/ml ampicillin media at 37°C, 225 rpm and plasmid DNA was extracted using the QIAGEN mini-prep plasmid DNA extraction kit (QIAGEN). The GFP-Bicc1 sequence, orientation and reading frame were verified by nucleotide sequence analysis using vector-

specific primers, GFP-forward 5'-CGACACAATCTGCCCTTTCG-3' and BGH reverse 5'-TAGAAGGCACAGTCGAGG-3', by SeqWright (Houston, TX) on an ABI Prism® 3730xl DNA sequencer (Applied Biosystems).

Transfection and immunofluorescence microscopy: HEK293 cells were transiently transfected with the Bicc1-pcDNA3.1/NT-GFP-TOPO® expression construct using Lipofectamine 2000 (Invitrogen). Briefly, a 12-well cell culture plate containing one 12 mm-round coverslip (Fisher cat#12-545-81, 1.5) was seeded with HEK293 cells at a density of 5×10^4 cells/well and grown to 80-90% confluency at 37°C and 5% CO_2. In separate tubes, 4-5 μg of Bicc1-pcDNA3.1/NT-GFP-TOPO® plasmid DNA was added to 100 μl of Opti-Mem (Gibco) and 12 μl of Lipofectamine 2000 was added to 100 μl of Opti-Mem. The solutions were incubated separately for 5 minutes at room temperature, combined, and then mixed by inversion. The transfection cocktail was incubated an additional 20 minutes at room temperature and then added to the cells dropwise while swirling, followed by incubation at 37°C and 5% CO_2 for 48-72 hours, changing the medium each day. The coverslips were then removed from the cell culture plate using forceps and placed in a new 12-well plate, cell side up. Coverslips were washed gently once with 500 μl 1X PBST (1X phosphate-buffered saline containing 0.1% Tween-20), fixed for 3 minutes in 500 μl acetone: methanol (1:1) and then washed gently 3 times for 5 minutes with 500 μl 1X PBST. To stain the nuclei, 10 μl of DAPI (Roche, 1 μg/ml stock, stored in the dark at 4°C) was added, just enough to cover the coverslips completely, and incubated 2-3 minutes in the dark. The cells were washed gently 5 times for 5

minutes with 500 μl 1X PBST in the dark with gentle rocking to remove DAPI.

Coverslips were mounted on slides (cell side down) in 5 μl of Mowiol

(Calbiochem, San Diego, CA) and the DAPI/GFP fluorescence was visualized

using a Zeiss Axiophot microscope. Images were acquired with an Olympus

DP70 digital camera at 400X and 1000X (oil immersion).

Immunohistochemistry (endogenous Bicc1): The expression of

endogenous Bicc1 was evaluated in mouse IMCD cells using a rabbit anti-Bicc1

polyclonal antibody (MU92) raised against the first 81 amino acids of the Bicc1

protein (153). The pre-immune serum was utilized as a negative control. IMCD

cells were seeded in a 12-well cell culture plate containing one 12 mm-round

coverslip at a density of 5 x 10^4 cells/well and grown to confluency in DMEM/F-12

containing 10% fetal bovine serum at 37°C and 5% CO_2. The medium was

decanted and cells were washed 2 times for 5 minutes in 1X PBS. The cells

were fixed in 0.5 ml acetone: methanol (1:1) for 3 minutes, washed 2 times for 5

minutes in 1X PBS, and permeabilized for 10 minutes in PBS containing 0.1%

Triton-X 100. The cells were rinsed briefly in 1X PBST (1X phosphate-buffered

saline containing 0.2% Tween-20), then incubated for 30 minutes in 0.1% bovine

serum albumin (BSA) diluted in PBST. The cells were rinsed briefly in 1X PBST,

and incubated for 1 hour in blocking buffer (1X PBST containing 2.5% BSA and

2.5% normal goat serum). After blocking, the cells were washed 2 times for 5

minutes in 1X PBST. The following steps (except washes) were performed in the

12-well culture plate in a humidity chamber to prevent evaporation. Cells were

incubated with 15 μl of rabbit anti-Bicc1 (MU92) antibody or 15 μl of the pre-

immune serum, diluted 1:200, 1:100, and 1:50 in blocking buffer for 1 hour. The cells were washed 3 times for 5 minutes in 1X PBST with gentle agitation. Cells were incubated with 15 μl fluorochrome-conjugated Alexa Fluor 488 (green) goat anti-rabbit antibody (Molecular Probes, Eugene, OR) diluted 1:200 in blocking buffer. Cells were washed 3 times for 5 minutes in 1X PBST in the dark with gentle agitation. Nuclei were stained by adding 15 μl of DAPI (Roche, 1 μg/ml stock) to coverslips and incubating in the dark for 2-3 minutes. After incubation with DAPI, cells were washed 3 times for 5 minutes in 1X PBST in the dark with gentle agitation. Coverslips were mounted on slides; cell side down, in 5 μl Mowiol (Calbiochem) and fluorescence was visualized using a Zeiss Axiophot microscope. Images were acquired with an Olympus DP70 digital camera at 400X and 1000X (oil immersion).

To assess Bicc1 protein localization within the primary cilia, IMCD cells were seeded in 6-well tissue culture plates containing 22 mm-round collagen-coated coverslips (BD Biosciences, San Jose, CA) at a density of 2 x 10^5 cells/well and cultured two days post-confluency to promote cilia growth. Immunohistochemistry was performed as described previously (see "Transfection and immunofluorescence microscopy") with the addition of mouse anti-acetylated α-tubulin primary antibody (Sigma) as a marker for cilia and Alexa Fluor 568 (red)-conjugated goat anti-mouse secondary antibody (Molecular Probes), both diluted 1:200 in blocking buffer for 1 hour.

Protein interactions of Bicc1

Construct generation: The reagents and materials used in this study have been previously described (57). Briefly, *Anks6* cDNA (GenBank Access. No. NM_001015028) was obtained from IMAGE clone 7108955 (Open Biosystems, Huntsville, AL) and amplified by PCR to generate a full length SamCystin, SamCystin with the ankyrin repeats deleted (SamCystinΔANK), and SamCystin with the SAM domain deleted (SamCystinΔSAM). cDNA encoding the mutated form of SamCystin for the c-Myc-SamCystin (R823W) construct was obtained by RT-PCR using total kidney RNA from a *Cy/Cy* rat as template, cloned into the pCMV-3Tag-2A expression vector (Stratagene, La Jolla, CA). cDNA encoding the Bicc1 protein (GenBank Access. No. NM_031397) was amplified from IMAGE clone 2655954 (OpenBiosystems) by PCR to generate a full length Bicc1, Bicc1 with the KH domains deleted (Bicc1ΔKH), and Bicc1 with the SAM domain deleted (Bicc1ΔSAM). Amplicons were cloned into pcDNA3.1/nV5-DEST expression vectors (Invitrogen). All primers were manufactured by Sigma-Genosys (The Woodlands, TX). The sequence and orientation of the inserts for all clones were confirmed by nucleotide sequence analysis performed at the University of Missouri DNA Core facility on an ABI Prism® 3730 DNA analyzer (Applied Biosystems).

Cell culture and transfection: Mouse inner medullary collecting duct (IMCD) cells were cultured as described previously (see "Bicc1 cellular localization, Cell culture"). Full length V5-Bicc1 and c-Myc-SamCystin

expression constructs were transiently co-transfected as described previously (see "Bicc1 cellular localization, Transfection and Immunofluorescence microscopy") into IMCD cells using 4 μg of each DNA (total 8 μg DNA) and 20 μl of Lipofectamine 2000 (Invitrogen). Cells were harvested 48 hours post-transfection using M-PER (Pierce) and protein concentration was determined by BCA assay (Sigma) as described in "RNA interactions of Bicc1, Bicc1 immunoprecipitation". For cells that were singly transfected with the V5-Bicc1 or c-Myc-SamCystin expression construct, 4 μg of DNA and 12 μl of Lipofectamine 2000 were used.

Bicc1 and SamCystin co-localization: IMCD cells were cultured in 12-well culture plates with 12 mm-round coverslips and immunohistochemistry was performed as described in "Bicc1 cellular localization, Immunohistochemistry endogenous Bicc1" with the following modifications. The cells were incubated with primary antibodies diluted 1:200 in blocking buffer for 1 hour; mouse anti-V5 monoclonal antibody (Invitrogen) was used to detect V5-Bicc1 and rabbit anti-c-Myc polyclonal antibody (Novus Biologicals, Littleton, CO) was used to detect c-Myc-SamCystin. The following fluorochrome-conjugated secondary antibodies were used: Alexa Fluor 568 (red) goat anti-mouse antibody for visualization of V5-Bicc1 and Alexa Fluor 488 (green) goat anti-rabbit antibody for visualization of c-Myc-SamCystin.

For experiments to determine whether either Bicc1 or SamCystin also localize to the primary cilia or basal body, the cellular structure that anchors the cilia, 4 μg of GFP-Bicc1 or c-Myc-SamCystin expression construct DNA was

61

transfected into IMCD cells in 6-well culture plates and 22 mm-round collagen-coated coverslips, as described previously (see "Bicc1 cellular localization, Transfection and Immunofluorescence microscopy"). Bicc1 localization was visualized directly by GFP fluorescence; c-Myc-SamCystin was visualized using the Alexa Fluor 488 (green) goat anti-rabbit antibody. The ciliary structures were labeled using mouse anti-acetylated α-tubulin antibody (Sigma) to mark the cilia as described earlier, and mouse anti-γ tubulin antibody (Santa Cruz Biotech, Santa Cruz, CA) to label the basal body. Alexa Fluor 568 (red) goat anti-mouse antibody was used to visualize both the cilia and basal bodies. Cell nuclei were stained with DAPI (Roche) and mounted using Mowiol (Calbiochem) as described previously (see "Bicc1 cellular localization, Transfection and immunofluorescence microscopy). Images were obtained with a Zeiss Axiophot microscope and Olympus DP70 digital camera and software.

Co-immunoprecipitation: Immunoprecipitation and co-immunoprecipitation were performed using the Profound Mammalian c-Myc Tag/Co-IP kit (Pierce). The principle is that a specific antibody to the c-Myc tag is covalently immobilized to a beaded agarose gel, enabling immediate use in co-IP experiments with the c-Myc-SamCystin as the primary target protein. Controls for the co-IP studies include: (1) a non-activated gel (negative control); (2) a quenched c-Myc activated gel, which serves as a control for non-specific binding to the c-Myc agarose gel matrix; (3) a control bacterial cell lysate with a GST-c-Myc fusion protein as a positive control for c-Myc binding and (4) lysates from singly transfected cells using either the V5-Bicc1 and c-Myc-SamCystin

expression construct. Briefly, V5-Bicc1 and c-Myc SamCystin co-tranfected cell lysates (400 μg protein) were applied to spin columns containing 10 μl immobilized c-Myc antibody agarose (0.5 μg/μl), as well as the four controls described earlier. For RNase treated samples, transfected lysates were first treated with 1 μl RNase A (10 mg/ml stock, USB, Cleveland, OH) at 37°C for 40 minutes, prior to application to the columns. Columns were incubated with end-over-end mixing at 4°C overnight and centrifuged for 10 seconds. The flow-through was placed in a clean microfuge tube and saved for future analysis. Columns were washed 3 times with 500 μl 1X TBST (1X Tris-buffered saline, pH 7.4, containing 0.05% Tween-20). Each wash was placed in a new tube and saved for future analysis. Immunoprecipitates were eluted from the columns with the addition of 25 μl 2X ImmunoPure Lane Marker Non-Reducing Sample Buffer (Pierce) non-reducing sample buffer. The tubes were tapped to mix, boiled for 5 minutes and centrifuged for 10 seconds. Additionally, 25 μl of the flow-through and wash samples were added to an equal volume of 2X non-reducing sample buffer and boiled five minutes. One microliter of β-mercaptoethanol was added to all samples; samples were boiled for 5 minutes and loaded on duplicate 10% SDS-PAGE gels. Gels were electrophoresed and stained with a reversible zinc stain (Pierce), followed by Western blot analysis (described in the next section), probing one blot with a mouse anti-c-Myc antibody (Clontech, Mountain View, CA) and the other with the mouse anti-V5 antibody (Invitrogen) in order to detect the co-IP protein complex.

Western blot analysis: Western blot analysis was performed as described previously (see "In vitro RNA binding assays, Protein detection") with the following modifications. Twenty micrograms of protein from transfected cell lysates and 12.5 µl of co-immunoprecipitation eluates were separated at 200V for 45 minutes in 1X SDS-PAGE running buffer on duplicate 10% SDS-PAGE gels. The gels were equilibrated in 1X transfer buffer and transferred onto 0.45 µm nitrocellulose membranes (Bio-Rad) at 100V for 1 hour. The membranes were blocked 3 hours in 5% milk/PBST (1X phosphate-buffered saline, pH 7.4, containing 0.2% Tween-20) and incubated overnight in 0.5% milk/PBST, containing primary antibodies diluted as follows: mouse anti-c-Myc monoclonal antibody (Clontech) 1:5,000; mouse anti-V5-HRP antibody (Invitrogen) 1:5,000. After washing, anti-c-Myc blots were incubated for 1 hour in goat anti-mouse-HRP antibody (Novagen, San Diego, CA) diluted 1:100,000 in 0.5% milk/PBST. Proteins were detected using chemiluminescence by incubating the membranes in the Immobilon (Millipore) HRP substrate for 5 minutes, wrapping the membranes in plastic wrap and exposing to x-ray film for 30 seconds to 5 minutes.

Generation of *bicc1 and anks6* zebrafish PKD models

Animals: Wild type zebrafish were bred and raised in-house using breeding pairs that have been maintained as a closed colony for several generations. Fish were reared under the guidelines described in the Guide for

the Care and Use of Laboratory Animals (216) and the Zebrafish Book (217).

The protocol for the experimental use of fish was approved by the University of

Missouri Institutional Animal Care and Use Committee. Adult fish were kept in a

filtered, UV-treated recirculating aquatic system at 28.5°C on a 14:10 hour light:

dark cycle. The adult fish were fed brine shrimp (*Artemia nauplii*) twice daily.

Fish were spawned and embryos collected using a mesh-bottom tank system.

Embryos were collected in 90 mm petri dishes in E3 embryo medium (Appendix

B) and kept in an incubator at 28.5°C for 4 days post fertilization (dpf). At 4 dpf,

embryos were fed live paramecia (*Paramecia multimicronucleatum*) twice daily.

At 9 dpf, embryos were moved to baby-rearing containers in the nursery and fed

both paramecia and brine shrimp twice daily. Containers were cleaned carefully

and replaced with clean system water twice daily. The proportion of brine shrimp

was increased gradually while phasing out the paramecia until 21 dpf, at which

point babies were moved to adult tanks and fed live brine shrimp twice daily.

Throughout the text, the developmental age of the embryos corresponds to the

hours elapsed since fertilization (hours post fertilization (hpf) at 28.5°C).

Expression constructs: A construct containing the full length wild type

mouse *Bicc1* (GenBank Assess. No. NM_031397) cDNA in pCS2$^+$ (University of

Michigan) was kindly provided by Oliver Wessely (LSU). A cDNA clone

containing the entire coding region of zebrafish *anks6* (GenBank Assess. No.

NM_001005928) was obtained from Open Biosystems (IMAGE clone 6967963,

GenBank Access. No. BC083503).

Sequence analysis: A putative zebrafish ortholog of mouse *Bicc1* was identified using Basic Local Alignment Search Tool (BLAST) (Ensembl assembly Zv8) (218) and was designated *bicc1a.* Another distant *bicc1* paralog was also identified and designated *bicc1b*. A single zebrafish *anks6* ortholog was identified similarly, (218) against rat *Anks6* and was designated *anks6.* Multiple sequence alignments were performed using Clustal W2 (211, 212) and were viewed using Jalview (212, 213). The following nucleotide and (protein) accession numbers were used: zebrafish *bicc1a*, NM_203420 (NP_981965); zebrafish *bicc1b*, XM_691516.3 (XP_696608.3), zebrafish *anks6,* NM_001005928 (NP_001005928); mouse *Bicc1*, NM_031397 (NP_113574); mouse *Anks6*, NM_ 001024136 (NP_001019307); human *BICC1*, ENST000000373886 (ENSP000000362993), Ensembl release 55, human *ANKS6*, NM_173551 (NP_775822); and rat *Anks6*, NM_001015028 (NP_001015028). Conserved protein domains were identified using multiple programs available at ExPASy (219), including MotifScan, PROSITE, and Pfam (154, 155, 220-222).

RNA isolation and RT-PCR: Total RNA was isolated from 20-30 dechorinated zebrafish embryos at various stages of development. Staged embryos were dechorinated using forceps in a glass dish in E3 embryo medium (Appendix B) and transferred to a 1.5 ml microfuge tube. Excess media was removed and 1 ml of TRIZOL reagent (Invitrogen) was added to the embryos. Embryos <30 hpf were homogenized by vortexing vigorously for 2-3 minutes; embryos >30 hpf were sonicated on ice in 5 second bursts for 1 minutes using a

Sonic dismembrator Model 100 (Fisher Scientific, Pittsburgh, PA) at remote

setting 6. Homogenized embryos were incubated for 5 minutes at room

temperature. Under a fume hood, 0.2 ml of chloroform (Sigma) was added to the

samples; the tubes were capped securely and shaken vigorously for 15 seconds.

The samples were incubated for an additional 3 minutes at room temperature.

Phase separation was achieved by centrifugation at 12,000 x g for 15 minutes at

4°C. The RNA remains in the upper aqueous phase. The aqueous phase was

transferred to a fresh 1.5 ml microfuge tube and the RNA and mixed with 0.5 ml

room temperature isopropanol. The sample was incubated for 10 minutes at

room temperature before centrifuging at 12,000 x g for 10 minutes at 4°C to

precipitate the RNA. The supernatant was removed carefully, and the RNA pellet

was washed with 1 ml 75% ethanol. The samples were mixed by flicking the

bottom of the tube and then centrifuged at 7,500 x g for 5 minutes at 4°C. The

pellet was air dried for 5 minutes and dissolved in 30μl RNA storage solution

(Ambion).

Gene-specific primers were designed using Primer 3 (223) and

manufactured by Sigma-Genosys (The Woodlands, TX) for *bicc1a,* 5'-

CATGACTGCAAACACTCCTTTGT-3' and 5'-AAGGTCACGCTTCTCTGCAT-3';

bicc1b, 5'-CAGAGCACTCGCATGTCATT-3' and 5'-

TGAGCTTGATGTTTGCTCCA-3'; and *anks6,* 5'-AAGCGTCCTCAGTCAGGAAA-

3', 5'-CATCCTCGTCAGTGATGGTG-3'. Gene-specific primers for the

housekeeping gene *ef1α* were 5'-TCACCCTGGGAGTGAAACAGC-3' and 5'-

ACTTGCAGGCGATGTGAGCAG-3' (224). One-step RT-PCR was performed

using Superscript III™/Platinum *Taq* (Invitrogen). A 25 μl reaction containing

100 ng of template RNA, 0.2 μM gene-specific primers, 1X Reaction buffer

containing 1.6 mM MgCl$_2$ and 0.2 mM each dNTP, and 2 μl SuperScript™III

RT/Platinum *Taq* enzyme mix was amplified under the following conditions: 45°C

for 30 minutes, 94°C for 2 minutes, 40 cycles of 94°C for 30 sec, 58.5°C (*bicc1a,*

bicc1b), 63.1°C (*anks6*) or 66$^{\text{o}}$C (*ef1α*) for 30 sec, 68°C for 1 minutes with a final

extension of 7 minutes at 68°C. Following PCR, 15 μl of the amplified products

were separated by gel electrophoresis at 90V for 2 hours on a 3% agarose gel in

1X Tris-borate, EDTA (TBE) buffer (100 mM Tris, 90 mM boric acid, 2 mM EDTA,

pH 8.0) containing 0.5 μg/ml ethidium bromide. Expected products of 179 bp,

643 bp, 217 bp and 648 bp for *bicc1a, bicc1b, anks6* and *ef1α*, respectively,

were visualized using a Gel Doc UV transilluminator (Bio-Rad).

Morpholinos: Translation-blocking or splice-blocking antisense

morpholino oligonucleotides were designed by Gene Tools, LLC (Philomath, OR)

and obtained from Open Biosystems, Inc. (Huntsville, AL). The sequences for

the morpholinos used are as follows: *bicc1a* (GenBank Access. No.

NM_203420) translation blocking*,* 5'-TCTCTGAGGCCGCCATAGCAAGACT-3';

bicc1a splice blocking, 5'-GGAAGCATGACTTTCCTCACCTTTC-3'; *bicc1b*

(GenBank Access. No. XM_691516.3) translation blocking, 5'-

AAACTCAACGGTTCGGCCATTGTCC-3', *anks6* #1 (GenBank Access. No.

BC083503) translation blocking*,* 5'-TCAGCGCCGTGTTTCCATCCTCATC-3' and

anks6 #2 (GenBank Access. No. BC083503) translation blocking*,* 5'-

CGGCAGCTCTCCAGATCTCCGTCAT-3', and *pkd2* (GenBank Access. No.

AY618926) translation blocking, 5'-AGGACGAACGCGACTGGAGCTCATC-3'

(50). A *Gli2* antisense mismatch morpholino, 5'-

CCTCTTACCTCAGTTACAATTTATA-3', was used as a control (225).

In vitro RNA synthesis: Full-length synthetic mRNA was transcribed

using mMessage mMachine™ (Ambion) and mouse *Bicc1*/pCS2$^+$ as template:

Fifteen micrograms of the *Bicc1* plasmid DNAs were incubated with 40U *Not*I

(New England Biolabs), 5 μl 10X NEB buffer #3, and 0.5 μl 100X NEB BSA in a

total reaction volume of 50 μl at 37°C overnight. The linearized DNA was purified

by phenol chloroform extraction by adding 50 μl of ultra pure water and 100 μl of

phenol: chloroform: isoamyl alcohol 25:24:1 (USB), vortexing briefly and

centrifuging at 15,000 x g for 10 minutes at 4°C. The aqueous phase was

transferred to a new 1.5 ml centrifuge tube and an equal volume of chloroform

(Sigma) was added. The mixture was shaken vigorously for 15 seconds and

centrifuged at 15,000 x g for 10 minutes at 4°C. The aqueous layer was

transferred to a new 1.5 ml tube, 1/10 volume of 3 M sodium acetate, pH 5.2,

was added and the sample was mixed by tapping the sides of the tube. Three

volumes of 100% ethanol was added, the sample was mixed by inversion and

incubated at -80°C overnight. The sample was centrifuged for 20 minutes at

15,000 x g, 4°C and the pellet was washed with 250 μl of 70% ethanol. The

pellet was air dried for 5 minutes and the DNA was resuspended in 25 μl of ultra

pure water and the DNA concentration was determined by A$_{260}$ (Nano-drop). To

verify that the DNA was linearized, 5 μl of digested DNA was evaluated by gel

electrophoresis on a 1% agarose gel containing 0.5 μg/ml ethidium bromide in 1X

TAE buffer at 80V for 80 minutes and visualized using a Gel Doc UV transilluminator (Bio-Rad).

The transcription reaction was prepared by combining 1 μg of linearized DNA, 10 μl 2X NTP/CAP buffer mix, 2 μl 10X transcription buffer mix, and 2 μl 10X SP6 enzyme mix and nuclease free water to a final volume of 20 μl in a 1.5 ml centrifuge tube. The reaction was mixed gently by pipetting, centrifuged briefly, and incubated at 37°C for 3 hours. To remove any remaining DNA template, 1 μl of Turbo DNase I (RNase-free) was added, mixed by flicking the tube, and incubated at 37°C for an additional 10 minutes. The reaction was stopped by adding 30 μl nuclease free water and the RNA was recovered by adding 30 μl lithium chloride precipitation solution (7.5 M lithium chloride, 50 mM EDTA), mixed by pipetting, and stored at -20°C overnight. To precipitate the RNA, the sample was centrifuged at 15,000 x g for 20 minutes at 4°C, the pellet was washed with 70% ethanol, air dried for 5 minutes and resuspended in 25 μl RNA storage solution (Ambion). RNA concentration was determined by A_{260} (Nano-drop). The RNA quality was evaluated by gel electrophoresis on a 1% formaldehyde gel at 80V for 80 minutes and visualized using a Gel Doc UV transilluminator (Bio-Rad) as described previously (see "RNA interactions of Bicc1, RNA extraction").

Morpholino and RNA injections: Translation or splice-blocking antisense morpholinos and in vitro transcribed RNA were suspended in Danieau buffer (58 mM NaCl, 0.7 mM KCl, 0.4 mM $MgSO_4$, 0.6 mM $Ca(NO_3)_2$, 5 mM HEPES, pH 7.6) (226) containing 0.1% Phenol red, loaded into microcapillary

needles (Stoelting, Wood Dale, IL), and injected into 1-4 cell stage zebrafish embryos using a microinjector (ASI, Eugene, OR). Dose-response experiments were performed to determine the concentration range in which the morpholinos (MO) were effective without non-specific toxicity. Dose ranges were 1-20 ng per embryo for MO and 150-750 pg per embryo for RNA dose studies. At higher MO doses, the injected embryos exhibited non-specific defects and died. Similarly, dose-response experiments defined the highest RNA dose at which non-specific or toxic effects were absent.

Immunohistochemistry: Embryos were fixed overnight at 4°C in Dent's (80% v/v methanol, 20% v/v DMSO), treated with 10% H_2O_2/Dent's (227) for 2 hours at room temperature, and placed in 100% methanol. A monoclonal antibody against the chicken alpha 1 subunit of Na^+/K^+ ATPase (228) was acquired from the Developmental Studies Hybridoma Bank (Iowa City, IA) and used at a 1:10 dilution. All washes and incubations were performed at room temperature on a rotating shaker. Embryos were washed 4 times for 30 minutes in incubation buffer, IB (1X PBS, 1% BSA, 0.5% Triton X-100, 1% DMSO) and then 1 time for 30 minutes in IB containing 1% horse serum (Vector Labs, Burlingame, CA). Embryos were incubated overnight in primary antibody (anti-Na^+/K^+ ATPase antibody) diluted 1:10 in IB + 1% horse serum. The embryos were washed 2 times for 30 minutes in IB and then once for 30 minutes in IB containing 1% horse serum. Embryos were incubated for 8 hours in secondary antibody (anti-mouse-biotinylated antibody, Vector Labs) diluted 1:250 in IB + 1% horse serum. Embryos were washed 3 times for 30 minutes in IB. The Avidin

and Biotinylated horseradish peroxidase (A/B) solution (VECTASTAIN® ABC-AP kit, Vector Labs) was prepared by adding 1% Reagent A (Avidin DH) to IB, vortexing to mix, and then adding 1% Reagent B (biotinylated horseradish peroxidase H) and vortexing to mix. The A/B solution was allowed to stand for 30 minutes to promote formation of the Avidin DH-Biotinylated horseradish peroxidase Complexes (ABC). After the 3rd wash in IB, embryos were incubated in A/B solution overnight, allowing the ABC complexes to interact with the biotinylated secondary antibody. Embryos were washed 6 times for 15 minutes in 1X PBS + 1% DMSO, then incubated for 15 minutes in 0.5 mg/ml diaminobenzidine (DAB, Sigma, a peroxidase substrate), 1X PBS, and 1% DMSO solution. The peroxidase reaction was initiated by adding 0.1 volume of 0.003% H_2O_2. The reaction was stopped by replacing the DAB solution with cold 1X PBS + 0.1% sodium azide. The embryos were washed 3 times for 5 minutes in 1X PBS and fixed overnight in 4% paraformaldehyde in 1X PBS (PFA-PBS). Embryos were washed 3 times for 5 minutes in 1X PBS and transferred gradually to 70% glycerol for mounting. The 1X PBS was replaced with a 25% glycerol solution and embryos were incubated for 10 minutes. The 25% glycerol solution was replaced with 50% glycerol and embryos were incubated for 10 minutes. The 50% glycerol was replaced with 70% glycerol and embryos were incubated for 10 minutes. Embryos were stored in 70% glycerol at 4°C. For mounting, embryos were deyolked as necessary in 70% glycerol and placed on a slide. The excess glycerol was removed, and a coverslip was secured using Vaseline at the corners. Slides were allowed to dry and the coverslips sealed with clear

nail polish. Mounted embryos were observed and images were captured using an Olympus BX60 fluorescence microscope and digital camera.

In situ hybridization: The probes used for *anks6* in situ hybridization were derived from IMAGE clone 6967963 (GenBank Access. No. BC083503) obtained from Open Biosystems. The probes used for *bicc1* in situ hybridization were derived from EST clones AL923800, AL926659, EB910780, AL919843, or by PCR of the 3' end of *bicc1a* and *bicc1b* cDNAs using the following primers: *bicc1a*, 5'-GGGTGTGAGCACATTTGGAG-3', 5'-AACGTGAATAAAAGCAAAGTGT-3', and *bicc1b*, 5'-CAGCAACAGGAGATTGATCT-3', 5'ACAACATAAGCATCGGCTGGT-3'. The resulting 511 bp (*bicc1a*) and 643 bp (*bicc1b*) amplicons were cloned using the TOPO® TA cloning system (Invitrogen) and transformed into One Shot® TOP 10 chemically competent *E. coli* (Invitrogen). Briefly, 4 μl of the PCR products were mixed with 1 μl salt solution (final concentration 200 mM NaCl, 10 mM MgCl$_2$) and 1 μl pCR2.1-TOPO® linearized vector (10 ng/μl). The TOPO® reaction was incubated for 5 minutes at room temperature. TOP10 chemically competent cells (50 μl per vial) were thawed on ice. Two microliters of the TOPO® reaction was added to the competent cells and transformation was carried out as described previously (see "In vitro RNA binding assays, Expression and isolation of fusion proteins"). Twenty individual colonies were picked and plasmid DNA was extracted using a boil-prep method as described previously (see "In vitro RNA binding assays, Expression and isolation of fusion proteins"). Cloned plasmids were screened by restriction endonuclease digest using FastDigest® *EcoR*I

73

(Fermentas). A 20 μl reaction was prepared containing 1 μg of DNA, 1 μl

FastDigest® *EcoR*I and 2 μl 10X FastDigest® buffer. The digest reaction was

incubated for 5 minutes at 37°C. Five microliters of the digested DNA was

separated by gel electrophoresis on a 1% agarose gel containing 0.5 μg/ml

ethidium bromide in 1X TAE buffer at 80V for 80 minutes. Insert-positive clones

were identified by visualization of the appropriate size products (511 bp for

bicc1a and 643 bp for *bicc1b*) in the gel using a Gel Doc UV transilluminator (Bio-

Rad). To verify the orientation of the inserts, sequence analysis was performed

at the MU DNA Core facility on an ABI Prism® 3730 DNA analyzer (Applied

Biosystems) using the vector-specific sequencing primers: M13 forward, 5'-

GRAAAACGACGGCCAG-3' and M13 reverse, 5'-CAGGAAACAGCTATGAC-3'

(Invitrogen). Clones positive for the insert and in the correct orientation were

selected for subcloning into the expression vector, pCRScriptSK⁺, at the *EcoR*I

restriction site. Five micrograms of pCRScriptSK⁺ DNA was linearized with 30U

of *EcoR*I in 1X *EcoR*I buffer (New England Biolabs). A 10 μl ligation reaction (4:1

insert:vector) was prepared by mixing 50 ng of linearized pCRScriptSK⁺, 1 μl 10X

T4 DNA ligase buffer (New England Biolabs), 1 μl T4 DNA ligase (400U, New

England Biolabs) and 25 ng *bicc1a* PCR product or 32 ng *bicc1b* PCR product.

The ligation reactions were incubated overnight at 16°C. Two microliters of the

ligation reactions were used to transform One Shot® TOP 10 chemically

competent cells (Invitrogen). Colonies were picked and plasmid DNA was

extracted as described previously (see "In vitro RNA binding assays, Expression

and isolation of fusion proteins"). The *bicc1a* and *bicc1b* pCRScriptSK⁺ cloned

plasmids were screened by restriction digest using FastDigest® *EcoR*I as described earlier in this section; the sequence and orientation of insert-positive clones was verified by sequence analysis at the University of Missouri DNA Core facility on an ABI Prism® 3730 DNA analyzer (Applied Biosystems). <u>Probe synthesis</u>: Sense and anti-sense digoxigenin-dUTP labeled probes were synthesized using DIG RNA labeling mix (Roche). A 20 µl reaction mixture was prepared containing 1 µg linearized plasmid DNA, 1X DIG RNA labeling mix, 1X Transcription buffer, and 40U RNA polymerase (SP6, T7 or T3).

Plasmid DNAs for the detection of *bicc1* were linearized as follows:

Plasmid DNA	sense/antisense	enzyme	polymerase	insert size (bp)
AL919843	antisense	*Xho*I	T3	539
AL919843	sense	*Not*I	T7	539
AL923800	antisense	*Xho*I	T3	539
AL923800	sense	*Xba*I	T7	539
AL926659	antisense	*Xho*I	T3	539
AL926659	sense	*Not*I	T7	539
EB910780	antisense	*Xba*I	T7	522
EB910780	sense	*EcoR*I	SP6	522
3'-PCR *bicc1a*	antisense	*Xho*I	T3	511
3'-PCR *bicc1a*	sense	*Not*I	T7	511
3'-PCR *bicc1b*	antisense	*Xho*I	T3	643
3'-PCR *bicc1b*	sense	*Sac*I	T7	643

The full length *anks6* clone was linearized as follows:

Plasmid DNA	sense/antisense	enzyme	polymerase	insert size
BC083503	sense	*Not*I	SP6	3 kb
BC083503	antisense	*EcoR*I	T7	3 kb
BC083503	antisense	*PshA*I	T7	1 kb (3')
BC083503	antisense	*SgrA*I	T7	464 bp (3')

The transcription reaction was mixed by pipetting, centrifuged briefly and incubated 2 hours at 37°C. Two microliters of DNase I (RNase-free) was added and the reaction mixture was incubated an additional 15 minutes at 37°C to remove template DNA. To stop the reaction, 2 µl 0.2 mM EDTA was added. To

facilitate RNA precipitation, 1 μl pre-chilled glycogen (20 μg/μl), 0.1 volume of

pre-chilled 4 M LiCl, and 2.5 volumes 100% pre-chilled ethanol were added,

mixed by inversion and stored at -20°C overnight. The samples were centrifuged

at 15,000 x g for 20 minutes at 4°C, the RNA pellets were washed once with 250

μl 70% ethanol, and then centrifuged again at 15,000 x g 10 minutes at 4°C. The

pellets were air dried for 5 minutes and resuspended in 25 μl RNA Storage

solution (Ambion). The RNA ladder and samples were prepared by adding 5 μl

RiboRuler High Range (Fermentas) + 5 μl 2X RNA loading buffer (Fermentas)

and 5 μl RNA probes + 5 μl 2X RNA loading buffer. The samples were heated at

65°C for 15 minutes and then loaded on a 1% formaldehyde gel (0.5 g agarose

melted in 42.4 ml nuclease-free water + 2.6 ml 37% formaldehyde, 5 ml 10X

MOPS buffer). The RNA probes were separated by gel electrophoresis in 1X

MOPS buffer (200 mM MOPS, 50 mM sodium acetate, 10 mM EDTA, pH 7.0) at

80V for 80 minutes and visualized using a Gel Doc UV transilluminator (Bio-Rad).

RNA probe concentrations were estimated based on A_{260} (Nano-drop)

measurements. In situ hybridization: Embryos were fixed in 4%

paraformaldehyde in 1X PBS (PFA-PBS) overnight. Embryos were washed

twice for 5 minutes in 1X PBS, 1 time for 5 minutes in 50% PBS/50% MeOH, and

then once for 10 minutes in 100% MeOH. Dehydrated embryos were stored in

fresh MeOH at -20°C overnight. Embryos were rehydrated by washing once for

5 minutes in 50% MeOH/50% PBST (0.1% Tween-20), once for 5 minutes in

30% MeOH/70% PBST, and twice for 5 minutes in 1X PBST. Embryos were

fixed for 1 hour in PFA-PBS and washed 3 times for 5 minutes in 1X PBST.

Embryos were digested with 10 μg/ml Proteinase K (Sigma) in 1X PBST (1 μl of 10 mg/ml Proteinase K + 999 μl PBST). Treatment times varied with age - no Proteinase K for 10 hpf and younger; 5 minutes for 20 hpf, and up to 20 minutes for 48 hpf or older embryos. Digested embryos were washed twice for 5 minutes in 1X PBST and fixed for 1 hour in PFA-PBS. Embryos were washed 3 times for 5 minutes in 1X PBST and transferred to 0.5 ml microcentrifuge tubes. Embryos were washed once for 10 minutes in 50% hybridization buffer/50% PBST. Hybridization buffer (hyb) consists of 50% formamide, 5X SSC (0.75 M NaCl, 750 mM sodium citrate), 50 μg/ml Heparin, 500 μg/ml yeast tRNA, 0.1% Tween-20, 9.2 mM citric acid, pH 6.0 prepared in DEPC (diethyl pyrocarbonate, Sigma) treated water. <u>Pre-hybridization</u>: Embryos were added to 450 μl hyb buffer which was first equilibrated to room temperature. The embryos in the hyb buffer were incubated for 2 hours at 65°C. The tubes were rocked gently on a platform rocker in the incubator. <u>Hybridization</u>: The pre-hybridization buffer was removed and 200 μl hyb buffer containing 100 ng of labeled probe equilibrated to 65°C was added to the embryos. One hundred microliters is enough for ≤ 20 embryos. The embryos were incubated overnight (9-12 hours) at 65°C on a tilted platform without rocking, such that the embryos were distributed along the wall of the tubes and covered completely by the hyb-probe solution. The used probe was saved, stored at -20°C, and reused up to 2-3 times. The hyb-probe solution was replaced with hyb buffer pre-warmed to 65°C and rinsed for 1 hour at 65°C. <u>Washes</u>: Washes were performed at 65°C on a platform rocker in the incubator. The embryos were washed twice for 30 minutes in Wash A (50% formamide, 2X

SSC, 0.1% Tween-20) and once for 30 minutes in Wash B (2X SSC, 0.1% Tween-20). Embryos were washed twice for 30 minutes in Wash C (0.2X SSC, 0.1% Tween-20), and then rinsed for 10 minutes in 50% Wash C/50% 1X Maleic Acid buffer, pH 7.5 containing 0.1% Tween-20 (MAT) at room temperature on a rotating rocker. Embryos were washed twice for 10 minutes in MAT at room temperature and then equilibrated for 10 minutes in Block solution (1X Maleic Acid buffer, pH 7.5 + 1X Blocking Reagent, Roche, catalog #11 096 176 001). Fresh Block solution was added and embryos were blocked for 3 hours at room temperature on a rotating rocker. Detection: The embryos were incubated overnight with 450 μl of anti-digoxigenin alkaline phosphatase-conjugated antibody (Fab fragments, Roche) diluted 1:5000 in Block solution at room temperature on a rotating rocker. Embryos were washed 8 times for 15 minutes in MAT, then 3 times for 10 minutes in TMNT (100 mM Tris-Cl, pH 9.5, 50 mM MgCl$_2$, 100 mM NaCl, 1 mM levamisole, 0.1% Tween-20). Embryos were transferred to a 24 well microtiter plate after the second TMNT wash and 1 ml of TMNT was used for the third wash. NBT/BCIP Color reaction: The alkaline phosphatase substrate coloration solution was prepared by adding 45 μl nitro-blue tetrazolium chloride (NBT, Roche) and 35 μl 5-bromo-4-chloro-3'-indolyphosphate p-toluidine salt (BCIP, Roche) to 10 ml TMNT. One milliliter of coloration solution was used per well of embryos. The embryos were incubated at 37°C in the dark for 15 minutes to 4 hours and observed for the development of dark blue staining in specific tissues. After the color reaction was complete, as determined by the appearance of non-specific background staining of the

78

embryo, the embryos were washed 2-3 times rapidly with 1X PBS and fixed overnight at 4°C in 4% paraformaldehyde in phosphate buffered saline (PFA-PBS). Mounting: Embryos were washed twice in 1X PBS, transferred gradually to 70% glycerol and mounted as described previously (see "Generation of *bicc1* and *anks6* zebrafish PKD models, Immunohistochemistry"). Mounted embryos were observed and images were captured using an Olympus BX60 fluorescent microscope and digital camera at 400X.

Histological analysis: Four day old *anks6* morphants and controls or five day old *bicc1* morphants and controls were fixed overnight in 2% glutaraldehyde, 2% paraformaldehyde in 0.1 M sodium cadodylate buffer, pH 7.35. Samples were rinsed in cadodylate buffer, followed by 3 washes for 5 minutes in ultra pure water. The embryos were dehydrated gradually by adding 1 ml of 20, 50, 70, and 90% ethanol and then 2 times with 95% ethanol. Dehydration was achieved by adding the ethanol solution to the embryos and microwaving them at 120W for 45 seconds in a Pelco 3440 Laboratory Microwave Oven (Ted Pella, Inc., Redding, CA) while under a vacuum and using the cold spot water recirculator. The embryos were infiltrated with JB-4 resin (Polysciences, Inc., Warrington, PA) by adding a 2:1 ethanol: resin solution and microwaving at 200W for 2 minutes; then 1:1 ethanol: resin and microwaving at 200W for 2 minutes; and then 1:2 ethanol: resin and microwaving at 200W for 2 minutes. Three pure resin exchanges followed by irradiation in the microwave at 250W for 2 minutes completed the infiltration process. Fresh pure resin was added to the samples and the embryos were incubated on a rocker at room

temperature for 1 hour. Embryos were orientated for cross section in a Teflon flat embedding mold with metal frame (Ted Pella, Inc. Redding, CA) and each well was filled with JB-4 resin. Two embryos were placed per well. The samples were covered with 22 x 60 mm Thermanox Plastic Coverslips to exclude oxygen and placed at 4°C overnight for polymerization.   The JB-4 blocks containing the embryos were first cut approximately 100 μm posterior to the eye prior to collecting sections. The remaining tissue was serially sectioned at 4 μm using a Leica Ultracut UCT Microtome (Leica Microsysystems Wien, Austria) and glass knives. Serial sections were collected up to the swim bladder, about mid-way through the yolk sac, comprising approximately 48 sections or 4 serial slides. Slides were stained with 1% (w/v) alkaline toluidine blue in 1%(w/v) sodium borate (229, 230) and observed using a Zeiss Axiophot microscope. Images were acquired with an Olympus DP70 digital camera at 400X and 1000X (oil immersion). Histological processing and sectioning were performed by the Electron Microscopy Core facility at the University of Missouri.

Rhodamine-dextran dye injections: Rhodamine-dextran injections were performed as described previously (195) with the following modifications. Embryos (3-3.5 days) were anesthetized with 0.02% Tricaine (Sigma) and mounted on slides in 3% (w/v) methyl-cellulose (Sigma). Briefly, the methyl-cellulose solution and microscope glass base plate were pre-warmed in a 55°C water bath. A drop of methyl-cellulose was placed on a slide; using a pin, the embryo was positioned laterally within the methyl-cellulose solution. A 5% (w/v) solution of 70 kDa tetramethylrhodamine-dextran (Invitrogen) was loaded into a

microcapillary needle (Stoelting) and injected into the common cardinal vein. The embryo was covered with a coverslip and examined with an Olympus BX60 fluorescence microscope at 400X.

Acetylated α-tubulin labeling of cilia: Embryos were fixed at 28-30 hpf in Dent's (80% MeOH/20%DMSO) at 4°C overnight. The embryos were slowly rehydrated into PBDT (1X PBS, 1% DMSO, 0.1% Tween-20) as follows: washed once for 5 minutes in 70%/30% Dent's/PBDT with agitation; washed once for 5 minutes in 50%/50% Dent's/PBDT with agitation; washed once for 5 minutes in 30%/70% Dent's/PBDT with agitation; and finally washed twice for 5 minutes in 100% PBDT with agitation. Embryos were incubated for 2 hours in a blocking solution of PBDT + 10% normal goat serum (NGS). Mouse anti-acetylated α-tubulin primary antibody (Sigma, T-6793) was added at a dilution of 1:400 in PBDT + 1% NGS and embryos were incubated overnight at room temperature on a rotating rocker. The embryos were washed 5 times for 30 minutes with PBDT + 1% NGS. Embryos were incubated with goat-anti-mouse Alexa-Fluor 568 (red) conjugated secondary antibody (Molecular Probes, A11031) at a dilution of 1:500 in PBDT + 1% NGS overnight in the dark at room temperature on a rotating rocker. DAPI (Roche) was added to the embryos at the same time as the secondary antibody at a final concentration of 13 μM to counterstain the nuclei. The embryos were washed 5 times for 30 minutes in PBDT + 1% NGS in the dark. Embryos were mounted in 70% glycerol as described previously (see "Generation of *bicc1* and *anks6* zebrafish PKD models, Immunochemistry") and evaluated by confocal microscopy at the Molecular Cytology Core facility at the

81

University of Missouri. A Zeiss LSM 510 META NLO two-photon point-scanning

confocal microscope was used to capture images at 400X and 630X (oil

immersion). Images were viewed using the Zeiss LSM Image Browser and a 3X

optical zoom was applied to the 400X images for better visualization of cilia. Cilia

measurements were estimated using the scale function. Comparisons were

made between at least five wild type embryos and *bicc1a* MO injected embryos.

CHAPTER IV

RESULTS

In vitro RNA binding assays

Characterization of the mouse Bicc1 protein: The entire mouse *Bicc1* coding region was sequenced previously (3). Several protein analysis programs including InterPro and MotifScan (155, 231) were used to analyze the predicted Bicc1 peptide sequence. Mouse Bicc1, like that of its counterparts in *Drosophila*, *Xenopus* (142, 145) and a number of other species, contains two functional domains: N-terminal K homology (KH) domains and a C-terminal sterile alpha motif (SAM) domain (Figure 4.1). There are three tandem KH motifs in mouse Bicc1 and comparison of the mouse KH domains with the consensus KH motif (GxxG, where x is usually a neutral or basic hydrophillic residue) indicates that KH domains 2 and 3 share more identity to the prototype KH domain than does KH domain 1 (Table 4.1). Comparison of the nucleotide and amino acid sequences of mouse Bicc1 with the sequence of Bicaudal C proteins from eleven other diverse species (*H. sapiens, R. norvegicus, P. troglodytes, C. familiaris, B. taurus, G. gallus, X. laevis, D. rerio, D. melanogaster, A. gambiae and C. elegans*) for which predicted sequences are available in public databases reveals a high degree of conservation at both the nucleotide and protein levels (Table 4.2; Appendix D, E). Based on Clustal W2 analysis (211, 212) of the complete

protein sequence, mouse Bicc1 shares overall amino acid identity ranging from

97% when compared with rat Bicc1 to 27% when compared with *C. elegans* Bic-

C (Table 4.3).

Figure 4.1. Mouse Bicaudal C (Bicc1) protein
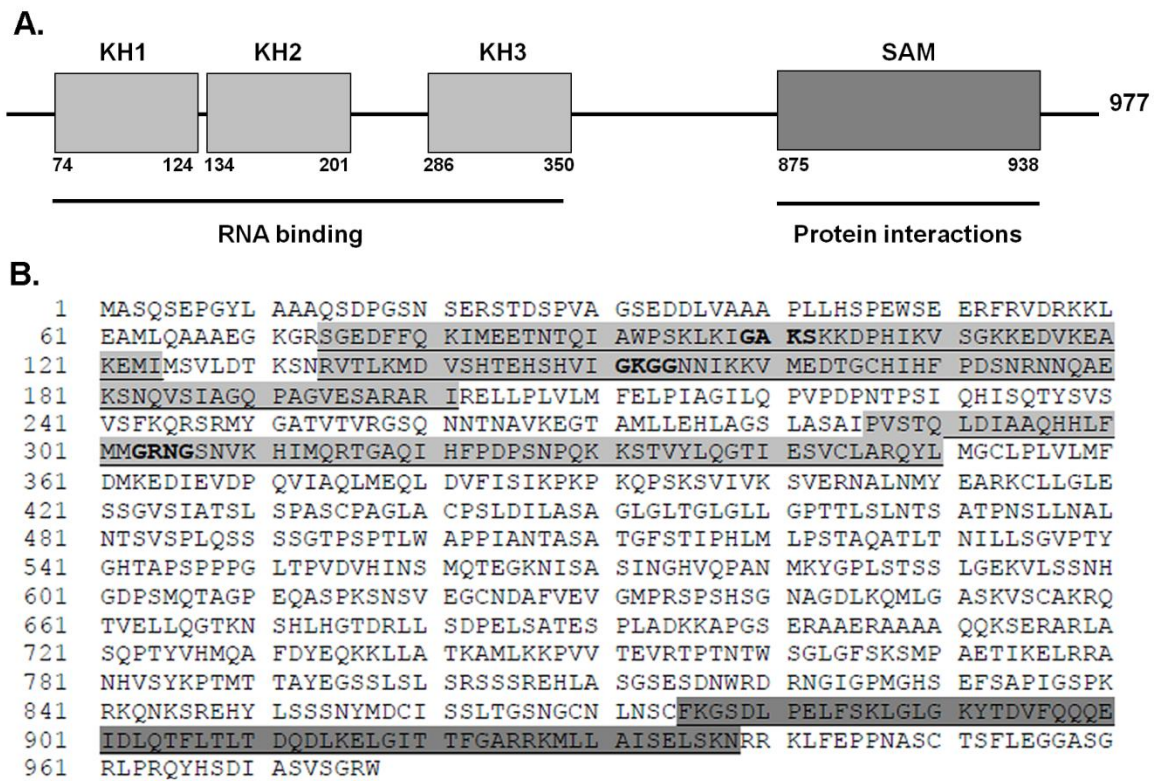
Figure 4.1. Analysis of the mouse Bicc1 protein. (A) Schematic of the predicted functional domains of mouse Bicc1. The KH domains are represented by light gray boxes while the sterile alpha motif (SAM) domain is represented by the dark gray box. The positions of the amino acid residues defining the boundaries of each domain are indicated under the boxes. The putative functions of the KH and SAM domains are also indicated. The full-length mouse Bicc1 protein is predicted to be 977 amino acids. (B) Primary amino acid sequence of mouse Bicc1 based on the known cDNA sequence. The amino acids representing each KH domain are underlined and highlighted in light gray. The residues corresponding to the conserved GxxG core defining each KH domain are bolded. The sterile alpha motif (SAM) domain is underlined and highlighted in dark gray. Figure is from Bouvrette *et al.*, 2008 (164), copyright permission granted from S. Karger AG, Basel.

Table 4.1. Mouse Bicc1 KH domain consensus sequence

	KH1	KH2	KH3
KH Consensus	**GxxG**	**GxxG**	**GxxG**
Mouse Bicc1	GAKS	GKGG	GRNG

Table 4.1. Conserved GxxG core defining each KH domain of the mouse Bicc1 protein sequence. This tetrapeptide is found between the first two □-helices of the KH domain and are predicted to be an unstructured surface loop important for nucleotide binding (232). The KH2 and KH3 domains more closely fit the prototype KH domain than does KH1.

A similar pairwise analysis was performed on the sequences for each functional domain. Overall, the percent amino acid identity between the functional domains of mouse Bicc1 and the functional domains of Bicaudal C of other species was greater than the percent amino acid identity of the full-length Bicaudal C proteins (Table 4.3). For example, the amino acid identity between mouse and frog (*X. laevis*) Bicaudal C proteins was 81%, however when the functional domains were compared, the amino acid identity was 95%, 95% and 92% for KH domains 1, 2 and 3 respectively, and 96% for the SAM domain. The high degree of amino acid identity specifically over the KH and SAM domain sequences suggests that these functional domains have been conserved among diverse species and most likely share an important, common function.

Table 4.2. Conservation of *Bicc1*

	GenBank Accession No. nucleotide (protein)	Chr. #	amino acid % identity	nucleotide % identity
Mus musculus **vs.**	NM_031397 (NP_113574)	10		
Homo sapiens	NM_001080512 (NP_001073981)	10	93	84
Rattus norvegicus	NM_001108531 (NP_001102001)	20	97	87
Pan troglodytes	XM_507803 (XP_507803)	10	92	83
Canis familiaris	XM_845706 (XP_850799)	4	92	81
Bos taurus	XM_617983 (XP_617983)	28	92	84
Gallus gallus	XM_421490 (XP_421490)	6	85	73
Xenopus laevis	AF224746 (AAF69826)	?	81	70
Danio rerio	NM_203420 (NP_981965)	14	44	24
Drosophila melanogaster	NM_165144 (NP_723948)	2L	29	17
Anopheles gambiae	XM_320061 (XP_320061)	3R	30	23
Caenorhabditis elegans	NM_069666 (NP_502067)	IV	27	9

Table 4.2. Multiple sequence alignments were performed using Clustal W2 (211, 212) comparing the nucleotide and amino acid sequences of *Bicc1* orthologs in eleven different species to the mouse *Bicc1* nucleotide and protein sequences.

Table 4.3. Percent amino acid identity across Bicc1 functional domains

M. musculus **vs.**	Full length Bicc1	KH1	KH2	KH3	SAM
H. sapiens	93	100	100	100	98
R. norvegicus	97	95	98	100	100
P. troglodytes	92	97	97	98	98
C. familiaris	92	NA	100	98	98
B. taurus	92	98	97	98	98
G. gallus	85	91	97	98	97
X. laevis	81	95	95	92	96
D. rerio	44	82	87	72	83
A. gambiae	29	55	66	52	50
D. melanogaster	30	55	66	47	45
C. elegans	27	42	54	39	29

Table 4.3. The amino acid sequences of the KH and SAM domains of Bicc1 from eleven different species were compared to that of mouse Bicc1 and the percent of identical residues was calculated. The percent identity across the functional domains is greater than the overall protein sequence identity in all cases. NA indicates that sequence data is unavailable.

Mouse Bicc1 binds synthetic RNA in vitro: A common property among proteins in the KH domain family is that they all function in close association with RNA (146-148, 159-161, 163, 168, 233-235). KH-domain-containing proteins are involved in many aspects of RNA metabolism, including mRNA splicing, translation and RNA stability (160, 161, 165, 236, 237). We predict that Bicc1 is a RNA binding protein and that this function is important to the biological role of Bicc1 in the kidney. Earlier work involving *BicC*, the *Drosophila* ortholog of mouse *Bicc1*, showed that the BicC protein was able to bind homoribopolymers in vitro and that this RNA binding appeared to be mediated by the KH domains (142). In this study, we tested the RNA-binding capabilities of the mouse Bicc1 protein and determined which KH domains played a role in binding.

Using a recombinant Bicc1 construct containing nucleotide sequence encoding a region including all 3 KH domains but not the SAM domain, we tested whether the resulting recombinant Bicc1 protein exhibited differential binding to any of the four possible homoribopolymers, poly(A), poly(C), poly(G) and poly(U) (164). Differential binding of polyribonucleotides has been demonstrated for other KH domain proteins, such as FMRP, which binds strongly to poly(G) and poly(U) but not to poly(A), while Sam68 binds with a preference for poly(U) and poly(A) (235, 237). In RNA-binding studies involving *Drosophila* BicC, poly(U) and poly(G) were more effective competitors of binding to poly(U)-Sepharose than poly(A) or poly(C) (142). For our experiments, cleared cell lysates from bacterial cultures expressing recombinant protein with a V5 epitope tag were the source of mouse Bicc1 protein. Binding experiments were carried out as

described by others for similar RNA-binding assays (142, 159, 164). The results

of these experiments demonstrate that recombinant mouse Bicc1 protein

preferentially binds poly(G) and poly(U) in vitro (Figure 4.2A) (164). This is

consistent with the earlier work on *Drosophila* BicC.

Figure 4.2. Mouse Bicc1 binds homoribopolymers in vitro
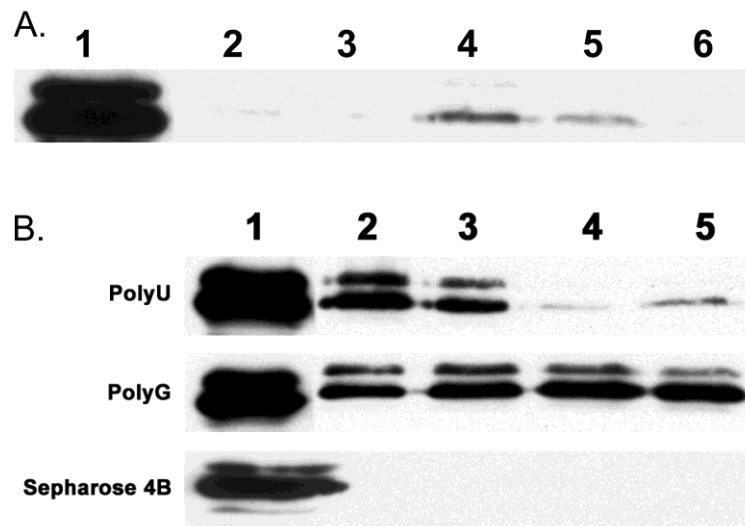
Figure 4.2. Homoribopolymer binding assays. (A) The ability of recombinant mouse Bicc1 protein to bind to homoribopolymers was assessed. Lane 1: cell lysate (positive control); Lane 2: poly(A); Lane 3: poly(C); Lane 4: poly(G); Lane 5: poly(U); Lane 6: Sepahrose 4B (negative control). The presence of a protein band indicates the ability of the protein to bind to the homoribopolymer. (B) RNA binding assay to test strength of interaction. The ability of recombinant Bicc1 protein to bind to either poly(U) or poly(G) in the presence of increasing salt concentration was assessed. The homoribopolymer used is indicated to the left of the panel. Sepharose 4B is the negative control. Lane 1: Bicc1 recombinant protein only, no homoribopolymer (positive control); Lane 2: 150 mM NaCl; Lane 3: 250 mM NaCl; Lane 4: 500 mM NaCl; Lane 5: 750 mM NaCl. Presence of a protein band indicates ability of the protein to bind to the homoribopolymer. Figure is from Bouvrette *et al.*, 2008 (164), copyright permission granted from S. Karger AG, Basel.

Mouse Bicc1 interaction with poly(G) is less salt labile than

interaction with poly(U): To test the contribution of electrostatic interactions,

88

binding of the recombinant mouse Bicc1 protein to poly(G) and poly(U) was

assessed at increasing ionic strength ranging from 150 mM to 750 mM NaCl

concentration (164). In typical binding experiments, 150 mM NaCl is commonly

used. As shown in Figure 4.2B, binding of recombinant Bicc1 protein to poly(U)

was decreased in the presence of salt concentrations greater than 150 mM

whereas binding to poly(G) was unaffected (164).

The third KH domain is important for in vitro binding: Previous work

demonstrated that the third KH domain is important to maintain the interaction

with RNA in vitro (153). Briefly, Price *et al.* designed experiments to investigate

which regions of the mouse Bicc1 protein were necessary for the capability to

bind to homoribopolymers. Constructs ranging from a full length Bicc1 construct

containing all 3 KH domains and the SAM domain to constructs that contained

the individual KH domains in isolation (Figure 4.3) (164). Cleared cell lysates

were incubated with homoribopolymer poly (U)-Sepharose. Similar incubation

with Sepharose 4B served as a control for non-specific binding. After washing,

the protein was eluted by boiling, separated by SDS-PAGE and analyzed by

immunoblot analysis using a commercially available anti-V5 antibody. The results

are shown in Figure 4.3. In every case where there was binding to poly(U), the

KH3 region was present in the recombinant mouse Bicc1 protein suggesting that

the KH3 domain is important for binding in vitro (164). When a recombinant

protein containing only the mouse Bicc1 KH3 domain was used in the assay, the

protein was still able to bind poly(U) suggesting that the third KH domain (KH3) of

mouse Bicc1 is sufficient for binding to occur in vitro (164). In addition, the

results of these experiments suggest that the SAM domain is not involved in these interactions since recombinant proteins lacking the SAM domain were still able to bind poly(U).

Figure 4.3. RNA binding properties of individual KH domains
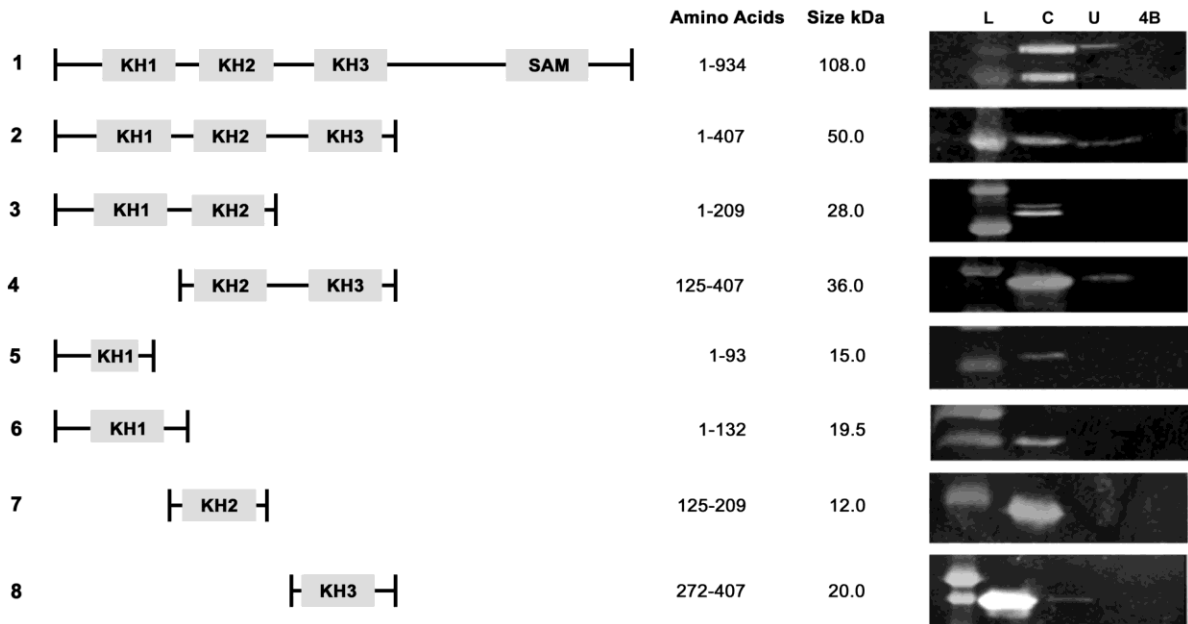
Figure 4.3. Poly(U) homoribopolymer binding assays involving mouse Bicc1 full-length and deletion construct recombinant mouse Bicc1 proteins. Eight regions of mouse Bicc1 were cloned into expression vectors to produce recombinant proteins. Each construct (1-8) is represented schematically to indicate which functional domains it contains. The N-terminal and C-terminal amino acids (based on the full-length mouse Bicc1 peptide sequence in Figure 1) for each protein and the predicted size in kilodaltons (kDa) are indicated. The results of the binding assays are shown to the right of each construct map. The lanes are (L) protein molecular weight ladder, (C) cleared cell lysate, no ribohomopolymer, which serves as a positive control for expression of each recombinant protein, (U) lysate incubated with poly(U) Sepharose and (4B) lysate incubated with Sepharose 4B which serves as a negative control. Presence of recombinant protein in Lane U indicates successful binding of the protein to poly(U). Figure from Bouvrette *et al.*, 2008 (164), copyright permission granted from S. Karger AG, Basel.

RNA interactions of Bicc1

Wnt signaling pathway PCR Superarray: Several signaling pathways have been implicated in PKD pathogenesis, including the Wnt signaling pathway, which is essential for kidney development (11, 61, 97, 115, 120, 125, 139, 140). KH domain-containing proteins often regulate translation of their target RNAs or target them for degradation (147, 238-243). We hypothesized that Bicc1 may be a novel regulator of Wnt signaling. To determine whether Bicc1 regulates RNAs involved in Wnt signaling, we used a Wnt pathway-specific PCR Superarray (SABiosciences, Inc.) to screen for misregulated genes in the kidneys of homozygous *Bicc1^{jcpk}/Bicc1^{jcpk}* mutant mice as compared to wild type controls. This array allowed us to examine 84 Wnt-related genes and 5 housekeeping genes (Figure 4.4, Appendix C).

Quantitative real-time PCR (qPCR) using this Wnt pathway-specific PCR Superarray identified five differentially expressed Wnt-related genes that in the kidneys of 3-5 day old *Bicc1^{jcpk}/Bicc1^{jcpk}* homozygous mice when compared to age-matched wild type controls (Figure 4.5). One of these five genes*, Casein kinase II (CK2)*, a strong regulator of Wnt signaling, was of particular interest because it has previously been implicated in PKD (124).

91

Figure 4.4. Wnt PCR Superarray principle

A.

Isolate RNA

Reverse transcribe
mRNA to cDNA

AAAA

mRNA

cDNA

Template for PCR

B. cDNA template +
SYBR PCR master mix

SYBR® Green I Dye Chemistry

Denature

Anneal

Extend

Wnt PCR Superarray

84 Wnt-related genes +
5 housekeeping genes
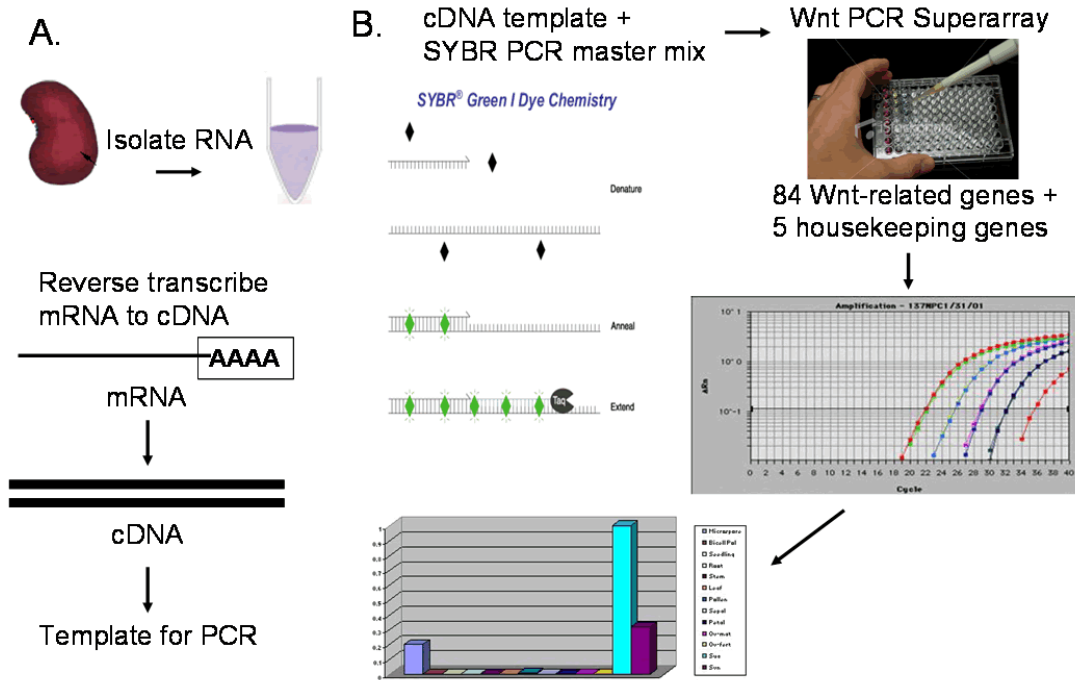
Figure 4.4. Wnt pathway-specific PCR superarray. The Wnt pathway is important during kidney development and has been implicated in PKD pathogenesis. This Superarray allows us to examine 84 Wnt-related genes at once. (A) RNA isolation and first strand cDNA synthesis (High Capacity, Applied Biosystems).   (B) PCR array of 84 Wnt-related genes using the SYBR green detection method and an ABI Prism 7000 sequence detection system.

Figure 4.5. Five Wnt pathway genes are misregulated in *Bicc1^jcpk/Bicc1^jcpk* mice
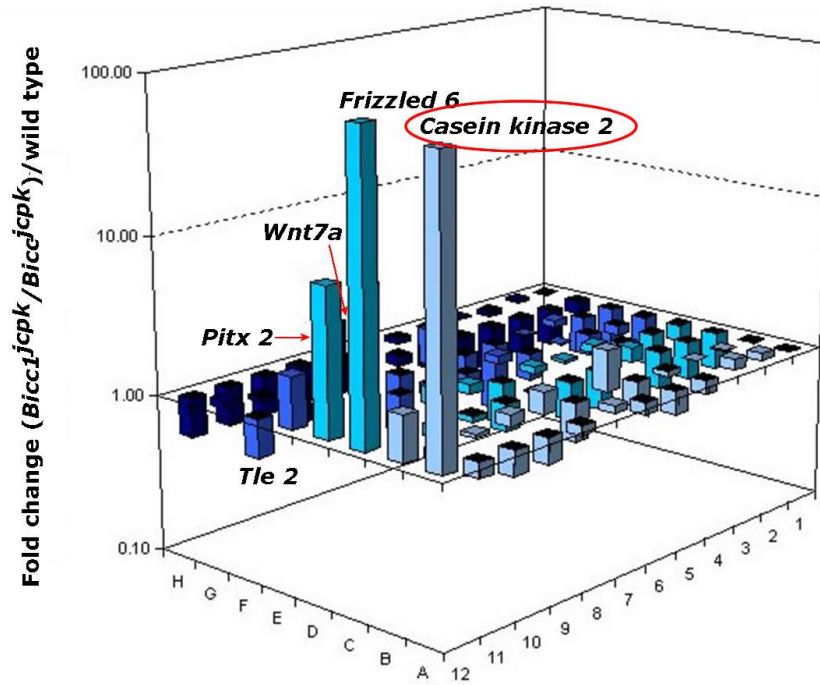
Figure 4.5. Wnt pathway PCR Superarray results (n=1). Each column represents the fold change in gene expression as determined by the $\Delta\Delta C_T$ method (214), normalizing to β–*actin* and *GAPDH*. A fold change greater than 2 was considered to be biologically relevant. Five genes demonstrated differential expression in the kidneys of 3-5 day old *Bicc1^jcpk/Bicc1^jcpk* homozygous mice when compared to age-matched wild type controls. These genes are indicated; however, *Wnt7a* is hidden behind *Pitx2* and indicated with an arrow. *Pitx2* and *Tle2* are transcription factors involved in canonical Wnt signaling. *Frizzled 6* is a receptor for Wnt ligands involved in PCP-Wnt signaling. *Casein kinase II* (*CK2*) encodes a ubiquitous kinase that has also been shown to interact with and regulate other PKD proteins.

While the PCR Superarray allowed us to look at many genes at once, it did not allow for replicates in the same experiment. Therefore, we wanted to confirm the results for these five genes by performing additional qPCR using independently designed gene-specific primers. We decided to use the relative quantitation and the $\Delta\Delta C_T$ methods of analysis (214), normalizing to one or more

housekeeping genes. The relative quantitation method requires several validation procedures (214, 244).

First, the dynamic range of the assay was determined using an RNA-based standard curve for all 5 genes to be tested, as well as the *β-actin* and *GAPDH* housekeeping genes. The dynamic range establishes the upper and lower limits of input RNA concentrations required to achieve efficient reverse transcription. The optimal range was defined as the amount at which a cycle threshold (C_T) less than 35 was achieved; C_T is the number of PCR cycles required for the SYBR green fluorescent signal to exceed the background fluorescence. C_T levels are inversely proportional to the amount of target in the sample (i.e., the lower the C_T, the greater amount of target). A C_T of ≥ 35 indicates little to no target is present in the sample. Serially diluted RNA samples were used as template for first strand cDNA synthesis, which was then used in the real-time PCR experiment.   In our study, the optimal range of input RNA was between 0.5 ng and 500 ng (Figure 4.6).

Next, we verified that there is no significant difference in the expression of the housekeeping genes *β-actin* and *GAPDH* in the kidneys of 3-5 day old wild type and PKD affected (*Bicc1^{jcpk}/Bicc1^{jcpk}*) animals (Figure 4.7), validating the use of these genes as normalizers.

Figure 4.6. Dynamic range for qPCR of Wnt genes
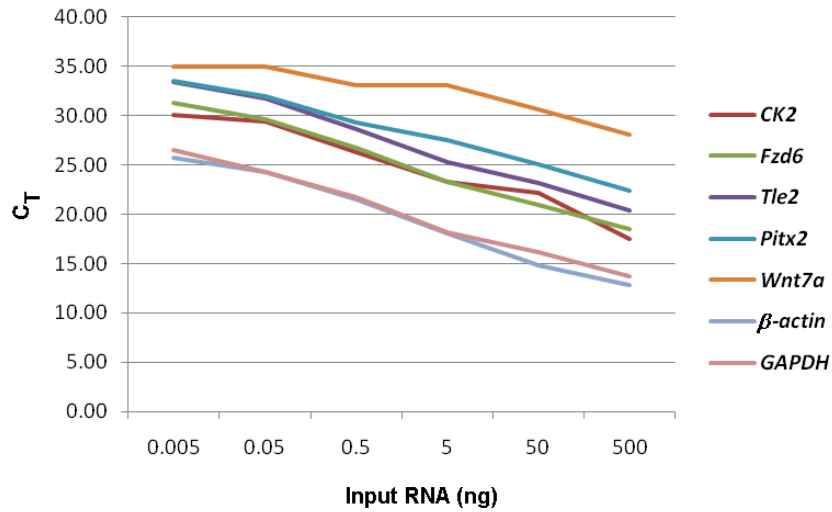
Figure 4.6. Determination of the dynamic range using gene-specific primers for the five Wnt-related genes and controls, *β-actin* and *GAPDH*. Serial dilutions of RNA ranging from 5 pg to 500 ng were used as template for cDNA synthesis followed by qPCR with each of the gene-specific primer set and the Cycle Threshold (C_T) was determined.

Figure 4.7. Validation of housekeeping genes
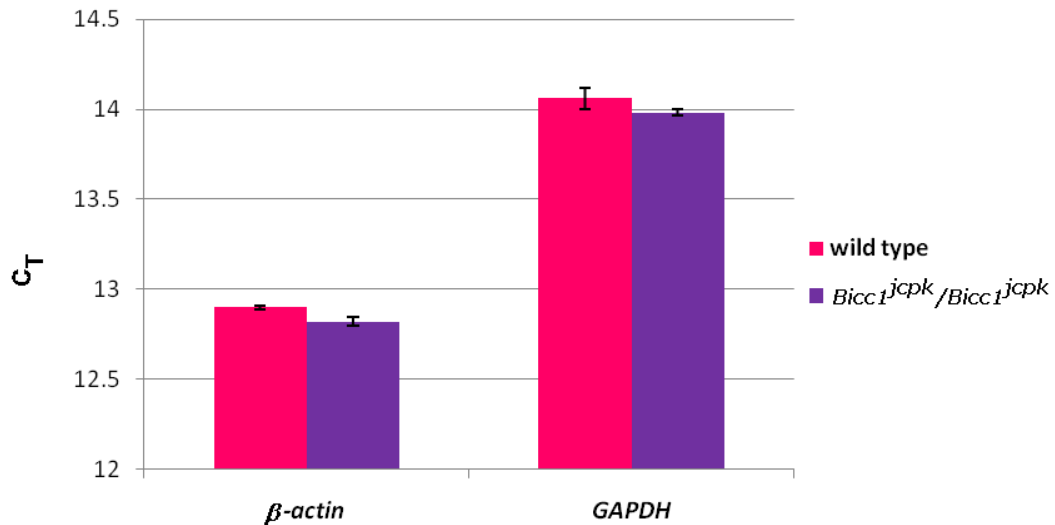
Figure 4.7. Comparison of gene expression levels for *β-actin* and *GAPDH* in the kidneys of 3-5 day old wild type and *Bicc1^{jcpk}/Bicc1^{jcpk}* mice. There is no difference in the expression of these genes between wild type and PKD mice, thus validating their use as normalizing genes for relative quantitation in subsequent qPCR experiments. Statistical analysis was performed using the Mann-Whitney Rank Sum Test (Sigma Plot). There was no significance difference ($p > 0.05$) in gene expression levels of *β-actin* or *GAPDH* between wild type and *Bicc1^{jcpk}/Bicc1^{jcpk}* kidneys.

As a final control, the PCR efficiency of each gene-specific primer set was validated against the PCR efficiency of the housekeeping gene primer sets (Table 4.4). The threshold for differences in PCR efficiencies in this study was set at ≤ 20% (244). The efficiencies for *Pitx2* and *Wnt7a* fell outside the acceptable range, therefore were not utilized to evaluate gene expression levels.

Table 4.4. PCR efficiencies of gene-specific primers

Gene	Slope	Slope difference (β-*actin*)	Slope difference (*GAPDH*)	Acceptable within ≤ 20%
CK2	-2.97	0.11	0.08	yes
Fzd6	-3.14	0.06	0.09	yes
Tle2	-3.09	0.01	0.04	yes
Pitx2	-2.85	0.23	0.20	no
Wnt7a	-2.77	0.21	0.28	no
β-actin	-3.08	0	0.03	yes
GAPDH	-3.05	0.03	0	yes

Table 4.4. The PCR efficiency of each primer set was determined by establishing a standard curve using five 10-fold serial dilutions of input cDNA and plotting the C_T versus log (input cDNA). The slopes of the resulting trendlines were compared to those of β-*actin* and *GAPDH*. The difference in slope represents the percent difference in PCR efficiencies (i.e., a difference of 0.1 indicates that the difference in PCR efficiencies is ≤ 10%).

Finally, the real-time qPCR experiment was repeated two additional times, with each reaction in triplicate, comparing expression in the wild type versus *Bicc1^{jcpk}/Bicc1^{jcpk}* homozygous kidneys. Upregulation of *CK2* and *Fzd6* in *Bicc1^{jcpk}/Bicc1^{jcpk}* kidneys were confirmed, although not to the degree observed in the Wnt PCR Superarray (Figure 4.8); this difference was found to be statistically signiicant. There was no significant difference in the expression levels of *Tle2*, β-*actin*, o*r GAPDH*. These data provide the first evidence linking *Bicc1* to the Wnt

pathway. As a RNA-binding protein, we hypothesize that *Bicc1* may function to regulate the *CK2* and *Fzd6* mRNAs and thus may be a novel regulator of Wnt signaling.

Figure 4.8. Real-time qPCR confirmation of Wnt Superarray results
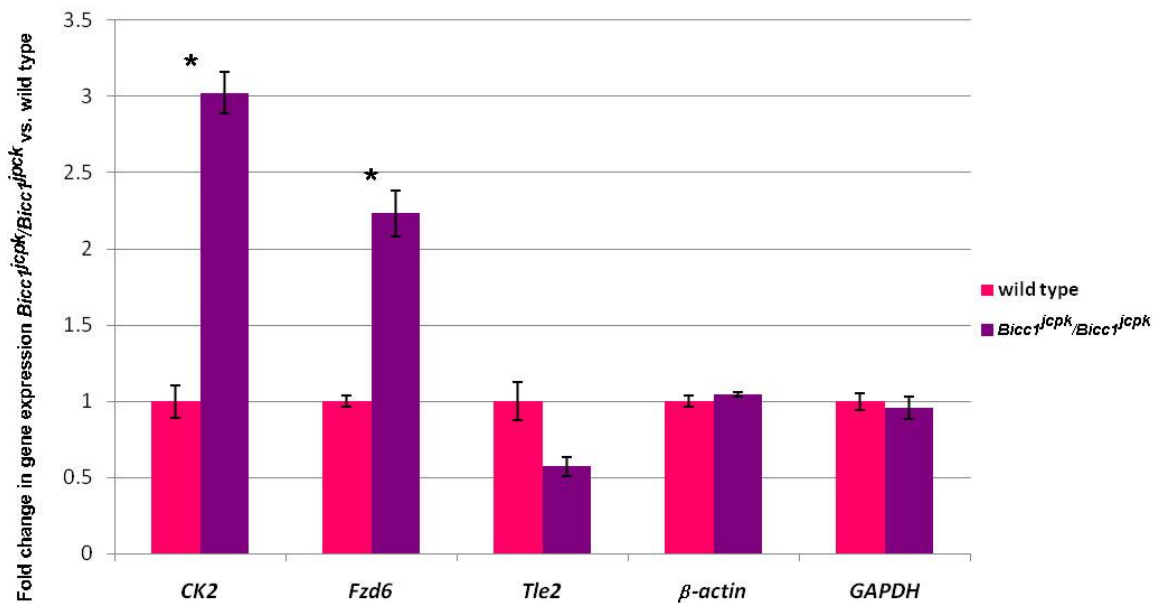
Figure 4.8. Graphical representation of the fold change in gene expression of five select Wnt-related genes in *Bicc1^{jcpk}/Bicc1^{jcpk}* homozygous kidneys compared to wild type controls. Total RNA was collected from three pooled kidneys of 4 day-old wild type or *Bicc1^{jcpk}/Bicc1^{jcpk}* homozygous kidneys. First strand synthesis was performed and equal amounts of cDNA were amplified in real time using an ABI Prism 7000 sequence detection system and the SYBR green detection method. Changes in gene expression were normalized to *β-actin* and *GAPDH* using the $\Delta\Delta C_T$ method. A fold change of >2 was considered biologically relevant. Statistical analysis was performed using the Mann-Whitney Rank Sum Test. There were significant differences in the gene expression levels of *CK2* and *Fzd6* ($p<0.05$) between wild type and *Bicc1^{jcpk}/Bicc1^{jcpk}* kidneys, as indicated by an asterisk (*). There was no significant difference in the gene expression levels of *Tle2*, *β-actin* or *GAPDH* ($p>0.05$).

To determine if a change in CK2 or Fzd6 protein expression accompanies the changes observed in gene expression in *Bicc1^{jcpk}/Bicc1^{jcpk}* homozygous

kidneys, Western blot analysis was performed using commercial antibodies to CK2 (Epitomics) and Fzd6 (Santa Cruz) and total protein extracted from the kidneys of wild type and $Bicc1^{jcpk}/Bicc1^{jcpk}$ mice at days 0 and 5. Despite repeated attempts at optimization, the Fzd6 antibody did not yield any usable data. There appeared to be a slight difference in CK2 expression in the kidneys of $Bicc1^{jcpk}/Bicc1^{jcpk}$ homozygous mice at 5 days old as compared to wild type (Figure 4.9A). However, the α-tubulin also appeared slightly increased in this sample. To determine whether this was a true difference, the densities of the protein bands were analyzed with Image J (245)(Figure 4.9B,C). These data show that the level of CK2 protein expression is slightly elevated in the kidneys of 0 day old $Bicc1^{jcpk}/Bicc1^{jcpk}$ homozygous mice, while a larger increase is observed in the 5 day old $Bicc1^{jcpk}/Bicc1^{jcpk}$ homozygous mice as compared to wild type controls; similar results were achieved in two independent experiments.

Bicc1 protein-RNA interactions: Since both the mRNA and protein levels of CK2 are elevated in the kidneys of $Bicc1^{jcpk}/Bicc1^{jcpk}$ homozygous mice, we suspect that Bicc1 may be involved in the regulation of *CK2* mRNA, presumably through binding via its KH domains. To test whether the Bicc1 protein and *CK2* mRNA interact directly, we performed immunoprecipitation of a recombinant Bicc1 protein containing a V5 epitope using an anti-V5 antibody (Invitrogen) and examined the immunoprecipitate, extracted protein and RNA using Trizol reagent (Invitrogen), and analyzed the protein by SDS-PAGE and RNA by RT-PCR (Figure 4.10).

Figure 4.9. CK2 protein expression in *Bicc1^jcpk^/Bicc1^jcpk^* kidneys vs. wild type
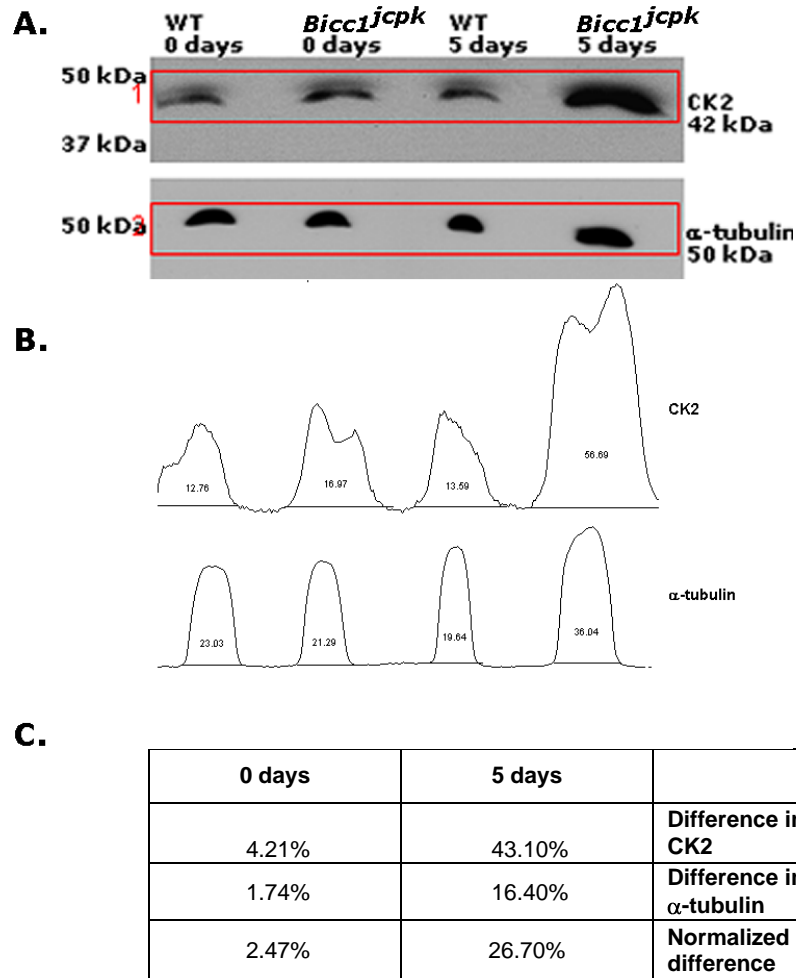
Figure 4.9. (A) Western blot analysis of CK2 protein expression. Total protein was extracted from kidneys of 0 and 5 day-old wild type and *Bicc1^jcpk^/Bicc1^jcpk^* homozygous mice. Twenty micrograms of total protein was loaded onto an SDS-PAGE gel and probed with an antibody to CK, detecting a 42 kDa protein. The same blot was stripped and re-probed with an antibody to acetylated α-tubulin (Sigma) as a loading control. (B) Densitometry analysis was performed using Image J. Protein bands were selected as indicated by rectangles (Panel A) and the data converted to lane profile plots represented as peaks. The numerical peak sizes, shown within each peak, are based on the peak size (area under the curve) as measured as a percent of the total size of all the peaks. (C) The differences between the peaks for the wild type and homozygous *Bicc1^jcpk^/Bicc1^jcpk^* samples were calculated for the 0 and 5 day time points for both CK2 and α-tubulin. The actual difference in protein expression was determined by normalizing to α-tubulin expression; the difference in α-tubulin expression was subtracted from the difference in CK expression.

Figure 4.10. Schematic of RNA-protein interactions
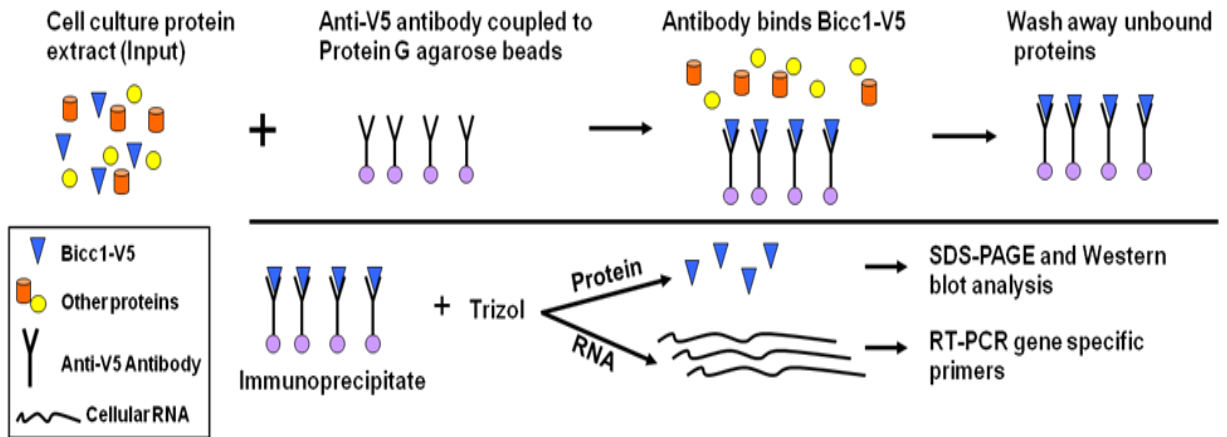
Figure 4.10. Method to detect RNA-protein interactions. Bicc1-V5 was transiently transfected into mouse inner medullary collecting duct cells (IMCD) and protein was extracted using M-PER (Pierce). Bicc1-V5 was immunoprecipitated using anti-V5 antibody coupled to Protein G agarose beads (Pierce). The beads were washed to remove unbound proteins, yielding the Bicc1-V5 immunoprecipitate. Protein and RNA were extracted from the beads using Trizol reagent (Invitrogen). Extracted protein was analyzed by SDS-PAGE and Western blot using the V5 antibody to verify presence of Bicc1 in the immunoprecipitate. Extracted RNA was used as a template for RT-PCR to detect the presence of RNAs that may be interacting with Bicc1.

Using gene-specific primers, we looked for the presence of *CK2* mRNA in the Bicc1-V5 immunoprecipitate by RT-PCR. As a negative control, we used primers to detect the presence of *GAPDH* and *β-actin* mRNA. As we suspected, *CK2* mRNA was found in the immune-precipitate (Figure 4.11). However, *β-actin* and *GAPDH* transcripts were also detected. This is not entirely surprising, as *Drosophila BicC* has been shown to regulate components of the actin cytoskeleton (147). Further investigation of GAPDH reveals that it is also an inducer of apoptosis (246, 247); increases in apoptosis is one of the hallmarks of PKD (60). In previous experiments, we showed however that the transcript levels for *β-actin* and *GAPDH* are unchanged in the kidneys from

Bicc1^{jcpk}/Bicc1^{jcpk} homozygous mice. We hypothesize that these housekeeping

genes are tightly regulated by multiple mechanisms within the cell and while

Bicc1 may interact with these RNAs, the loss of Bicc1 alone does not result in

aberrant gene expression.

Figure 4.11. RNA detected in Bicc1 immunoprecipitates
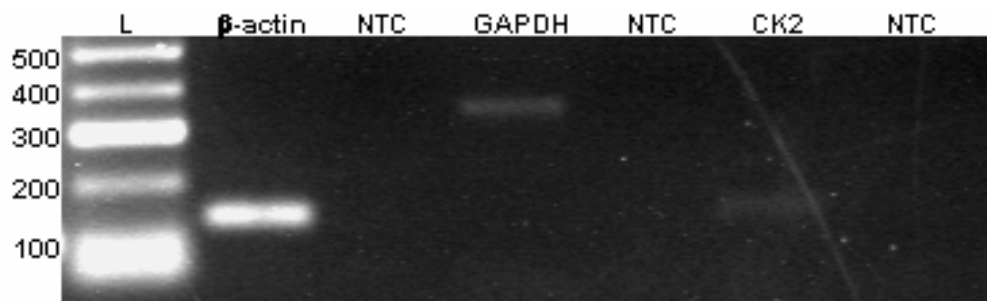
Figure 4.11. RT-PCR of the Bicc1 immunoprecipitate from mouse IMCD cells. (L) is Hyper V ladder (Bioline), (NTC) represents no template controls. Fifteen microliters of PCR products were separated on a 3% agarose (TBE) gel. Bands of the appropriate sizes (156 bp, 350 bp, 152 bp for *β-actin*, *GAPDH*, and *CK2* respectively) were detected, indicating that these RNAs were pulled down with the Bicc1 protein.

To determine whether these potential RNA-protein interactions are true

interactions and not due to non-specific binding to the protein A/G beads, we

performed immunoprecipitation of Bicc1 in both transfected and non-transfected

mouse IMCD cells, followed by RT-PCR. As a negative control, we used primers

designed towards a nucleoporin, *Nup210L*, which we suspect will not interact

with Bicc1. Additionally, we tested another PKD-related gene, *Nek1* (*Nema-*

related kinase 1), as this gene was shown to be down-regulated approximately 5-

fold in the kidneys of *Bicc1^{jcpk}/Bicc1^{jcpk}* homozygous mice (153). Figure 4.12A

shows the presence of Bicc1 protein before and after immunoprecipitation from

mouse IMCD cells. We designed and tested primers to all the genes of interest

using total RNA extracted from mouse IMCD cells as template (Figure 4.12B).

Next, we performed the RT-PCR experiments using RNA extracted from the

Bicc1 immunoprecipitates as template. *β-actin*, *GAPDH*, *CK2*, and *Nek1* mRNAs

were detected in the transfected immunoprecipitate (Figure 4.12C). *GAPDH* was

also clearly observed in the immuno-precipitate from non-transfected cells. This

could be a result of insufficient washing, as *GAPDH* is a highly abundant

transcript. The other genes were not detected in the non-transfected immuno-

precipitates, suggesting that there is no non-specific binding to the beads. We

did test if *Fzd6* mRNA could be pulled down by Bicc1, however, in three

independent experiments; *Fzd6* mRNA was never detected in the Bicc1

immunprecipitate (data not shown).

Figure 4.12. Potential RNA targets of Bicc1
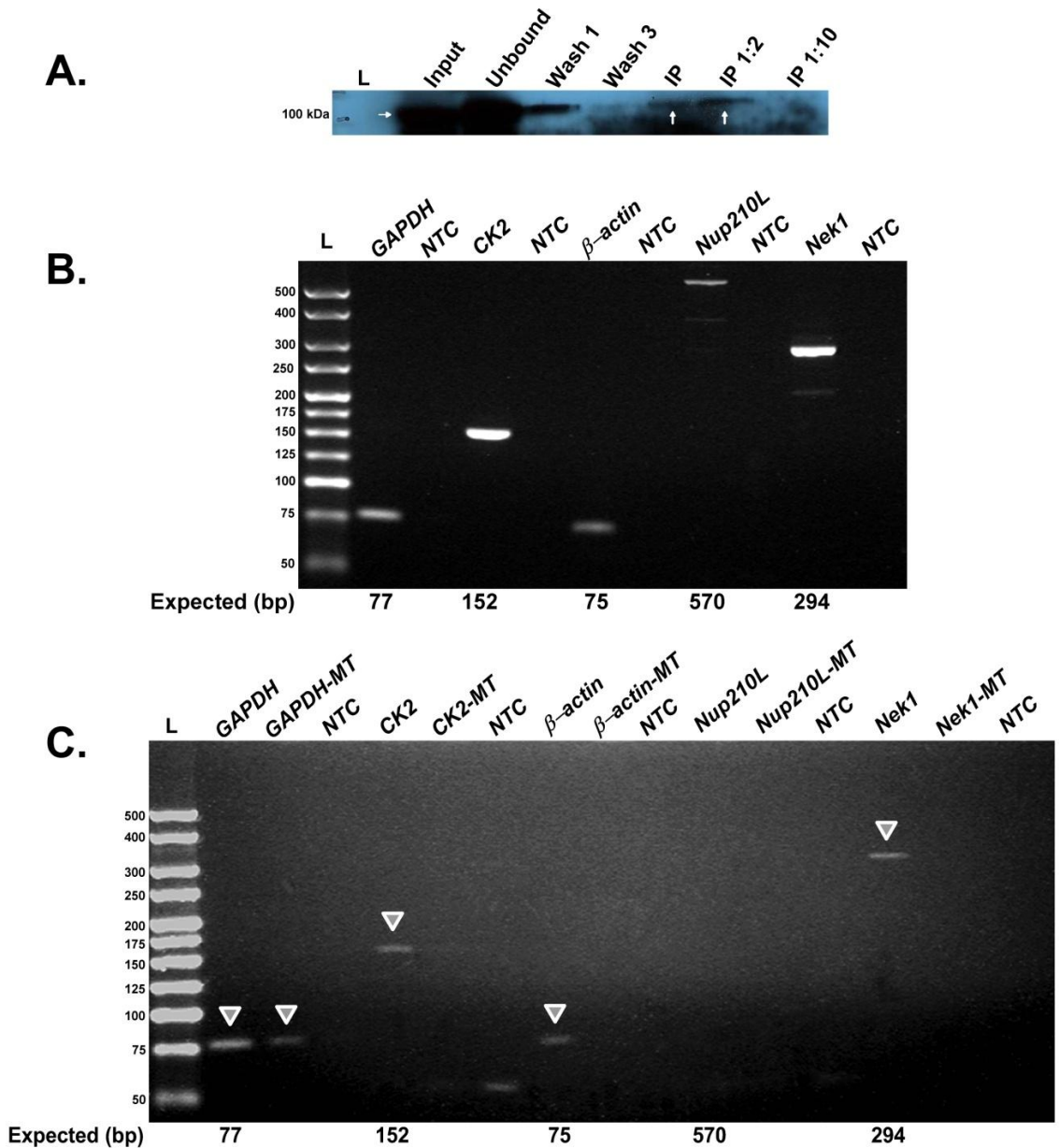
Figure 4.12. Potential RNA binding partners of Bicc1. (A) Protein was extracted from Bicc1-V5 immunoprecipitate using Trizol reagent and analyzed by SDS-PAGE and Western blot analysis using anti-V5 antibody. Shown are 10 μg cleared cell lysate, prior to immunoprecipitation (Input), 20 μl of the flow through (Unbound), 20 μl of wash 1, 3, 20 μl undiluted eluate after immunoprecipitation (IP), and 20 μl of the IP diluted 1:2, 1:10. Efficient precipitation of the 105 kDa Bicc1-V5 recombinant protein is demonstrated. (B) All primer sets were tested by two step RT-PCR using cDNA template from IMCD cells (amplification control); 15 μl of PCR products were separated by electrophoresis on a 3% agarose (TBE) gel at 90V for 1hr. The first lane (L) contains Hyperladder V (Bioline), NTC=no template control. (C) RNA was extracted from Bicc1-V5 immunoprecipitates using Trizol reagent. First strand cDNA synthesis was performed followed by PCR using a Hot Start Fast*Taq* polymerase (Roche) and gene specific primers; 15 μl of PCR products were separated by electrophoresis on a 3% agarose (TBE) gel at 90V for 1hr. The first lane (L) contains Hyperladder V (Bioline), NTC=no template control, MT=mock transfected.

Bicc1 cellular localization

Recombinant Bicc1 localization: To examine the cellular localization of the Bicc1 protein, the full length coding sequence for mouse *Bicc1* was cloned into a GFP-expression plasmid, pcDNA3.1/NT-GFP-TOPO, containing a N-terminal GFP tag. Human embryonic kidney (HEK293) cells were transiently transfected using Lipofectamine 2000 (Invitrogen) and 4 μg of plasmid DNA in a 12-well culture plate containing glass coverslips. The cell nuclei were counterstained with DAPI and Bicc1-GFP recombinant protein expression was observed by direct fluorescence 48-72 hours post-transfection using a Zeiss Axiophot microscope. The Bicc1-GFP recombinant protein was expressed diffusely, primarily in the cytoplasm (Figure 4.13); however, punctate expression was also noted in the nucleus on occasion. The transfection efficiency varied between experiments, as determined by the number of cells expressing GFP, sometimes as low as 12% or as high as 56%. Three separate experiments were performed and at least 100 cells were evaluated in each experiment. Bicc1 localization was independently confirmed by Stagner *et al.* (2009) using mouse inner medullary collecting (IMCD) cells (57) and the same plasmid DNA construct.

Figure 4.13. Immunofluorescence microscopy Bicc1-GFP in HEK293 cells
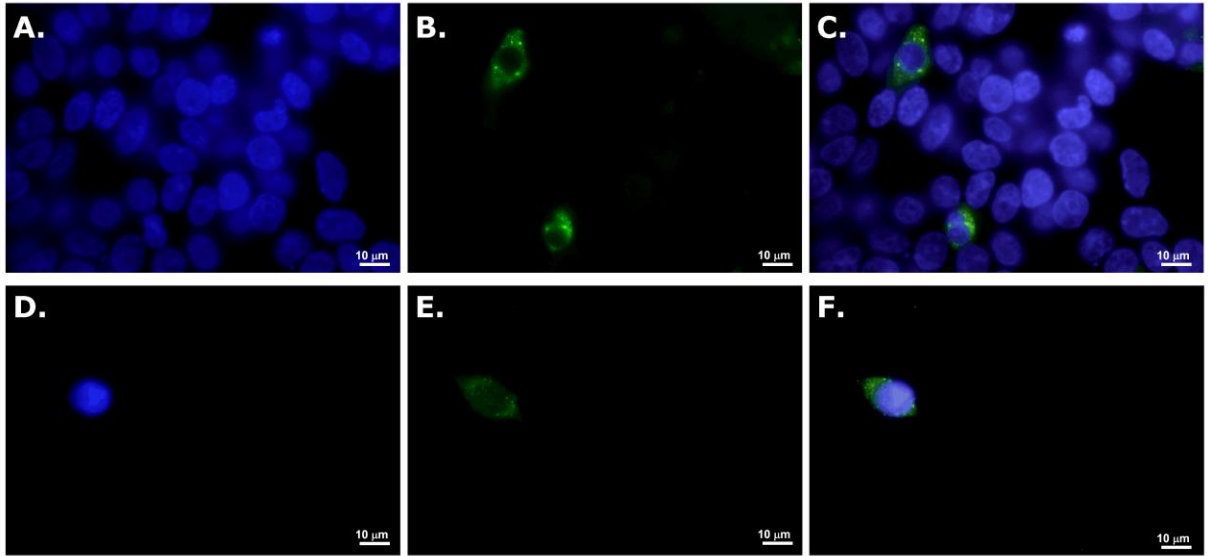
Figure 4.13. Immunofluorescence microscopy of Bicc1-GFP transiently transfected human embryonic kidney (HEK293) cells. Cells were transfected with *Bicc1*/pcDNA3.1/NT-GFP-TOPO plasmid DNA and observed for GFP fluorescence 48-72 hours post-transfection using a Zeiss Axiophot microscope. (A) Nuclei were counterstained with DAPI, (B) GFP fluorescence of successfully transfected cells, (C) Merged image of (A) and (B). (D) Another representative cell showing DAPI counterstained nucleus, (E) Bicc1-GFP fluorescence, and (F) Merged image of (D) and (E). In all cases, Bicc1 expression was observed primarily in the cytoplasm with occasional punctate expression in the nucleus. Images were acquired with an Olympus DP70 digital camera at 1000X (oil immersion).

Immunofluorescence microscopy of endogenous Bicc1: The

localization of the endogenous Bicc1 was examined using mouse inner medullary

collecting duct (IMCD) cells, which have been shown to express Bicc1 at a

readily detectable level by Western blot (Figure 4.14). A Bicc1-specific rabbit

polyclonal antibody (MU92) was used in combination with an anti-rabbit Alexa

Fluor 488 (Green) conjugated secondary antibody to detect the presence of the

endogenous Bicc1 protein by immunofluorescence microscopy.

Figure 4.14. Mouse IMCD cells express endogenous Bicc1
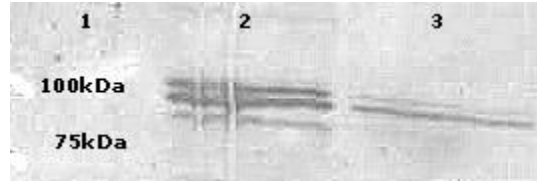
Figure 4.14. Western blot analysis of Bicc1 expression. (1) Precision Plus All Blue protein standard, 10 μl, Bio-Rad. (2) Thirty micrograms of cleared cell lysate from Bicc1-transfected HEK293 cells. (3) Thirty micrograms of cleared cell lysate from non-transfected mouse IMCD cells. Blot was probed with a rabbit polyclonal antibody specific to Bicc1 (MU92) which detects a band between 75-100 kDa. Note: Bicc1 is present in multiple isoforms which may also be detected.

Mouse IMCD cells were cultured as described previously (see "RNA interactions of Bicc1, Cell culture") with glass coverslips and labeled with various dilutions (1:50, 1:100, 1:200) of MU92 antibody as well as the pre-immune serum as a negative control. The observed expression of endogenous Bicc1 confirmed the expression pattern that was observed with the Bicc1-GFP recombinant protein. Three independent experiments demonstrated that endogenous Bicc1 was present in a diffuse pattern throughout the cytoplasm in all cells examined (n=1,182) and punctate expression in the nucleus was also noted in an average of 50% of the cells (Figure 4.15).

Bicc1 is not expressed in the primary cilia of mouse IMCD cells: To assess Bicc1 protein localization in the cilia, immunofluorescence microscopy was performed with the addition of a mouse monoclonal antibody to acetylated α-tubulin as a marker for cilia. Mouse IMCD cells were cultured 2 days post-confluency in 6-well plates with collagen-coated coverslips to promote cilia growth.

Figure 4.15. Expression of endogenous Bicc1 in mouse IMCD cells
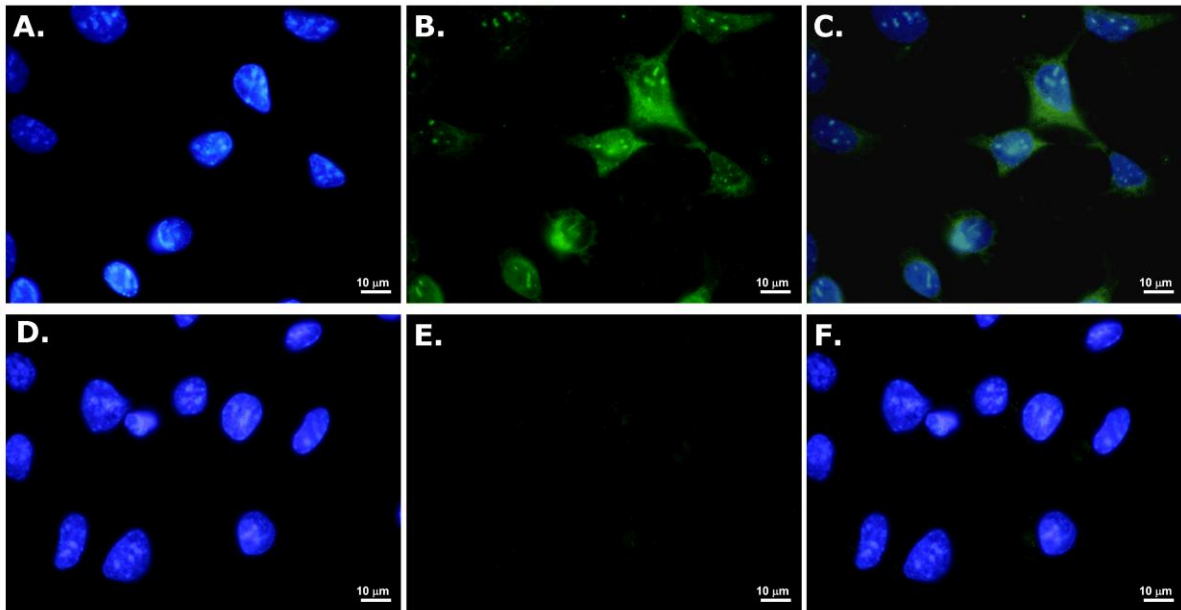
Figure 4.15. Mouse inner medullary collecting duct cells (IMCD) were cultured on coverslips and labeled with a Bicc1-specific polyclonal antibody developed in rabbit (MU92) and Alexa-Fluor 488 conjugated secondary antibody to observe fluorescence (top panels, green). The pre-immune serum was utilized as a negative control (bottom panels). (A) Nuclei were counterstained with DAPI, (B) Bicc1 expression primarily in cytoplasm and punctate expression in the nucleus, (C) Merged image of (A) and (B). (D) DAPI counterstained nuclei, (E) pre-immune serum expression demonstrating very low background, and (F) Merged image of (D) and (E). In all cases, Bicc1 expression was observed primarily in the cytoplasm with occasional punctuate expression in the nucleus and this expression was well above the background fluorescence of the pre-immune samples. Images were acquired with an Olympus DP70 digital camera at 1000X (oil immersion).

Anti-mouse Alexa Fluor 568 (Red) conjugated secondary antibody was used to detect the presence of α-tubulin. Dual labeling of endogenous Bicc1 and α-tubulin revealed that Bicc1 does not localize to the primary cilia (Figure 4.16). Three separate experiments were performed and at least 100 cells were examined in each experiment. Cilia were present and expressing α-tubulin on 36-96% of cells.

Figure 4.16. Bicc1 is not expressed in the primary cilia
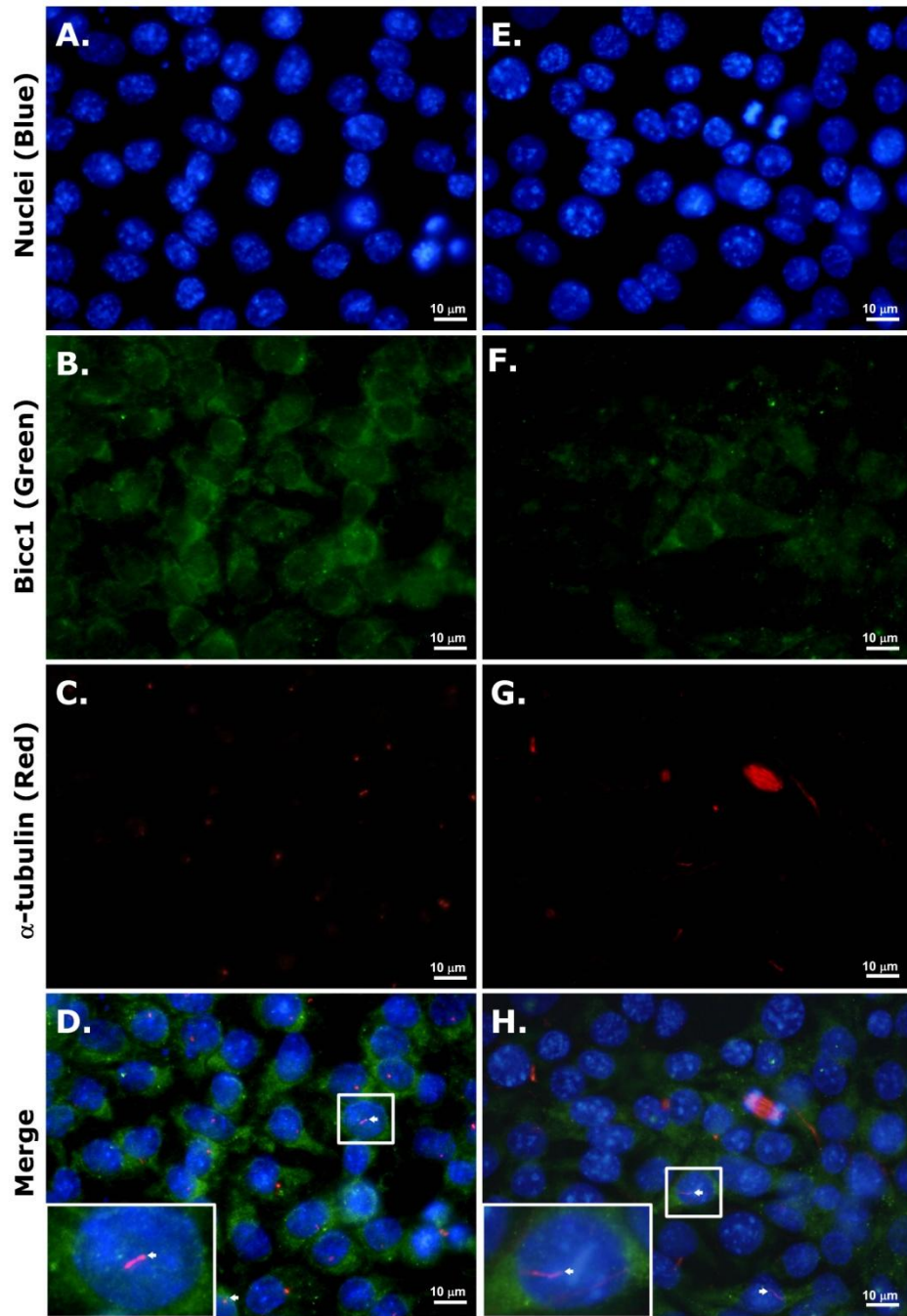
Figure 4.16. Immunofluorescence microscopy of Bicc1 and primary cilia in mouse inner medullary collecting duct cells (IMCD). To observe fluorescence, cilia were labeled with anti-acetylated α-tubulin mouse monoclonal antibody and Alexa-Fluor 568 (Red) conjugated secondary antibody; Bicc1 was labeled with the Bicc1-specific polyclonal antibody (MU92) and Alexa-Fluor 488 (Green) conjugated secondary antibody. (A, E) Nuclei were counterstained with DAPI, (B, F) Bicc1 expression primarily in cytoplasm and punctate expression in the nucleus, (C, G) α-tubulin expression in the primary cilia, and (D, H) Merged images of all three, inset is a 2X zoom of the boxed-in area. Images were acquired with an Olympus DP70 digital camera at 1000X (oil immersion).

Protein interactions of Bicc1

Mouse Bicc1 interacts with PKD-related protein SamCystin:

Mutations in either the *bicaudal C (Bicc1)* or *Anks6* genes result in polycystic

kidney disease (PKD), as characterized by the *jcpk* mouse and Han:SPRD *Cy* rat

models for the disease (3, 248-250). *Bicc1* and *Anks6* encode the Bicc1 and

SamCystin proteins respectively, both of which contain a C-terminal sterile alpha

motif (SAM) functional domain, which are known to participate in protein

interactions (156). The molecular functions of Bicc1 and SamCystin are

unknown; however, the recognition of a SAM domain in two PKD-related proteins

suggests that they may be involved in protein-protein interactions. We speculate

that both the Bicc1 and SamCystin proteins may function in a common molecular

pathway involved in cyst formation, present in both the mouse and the rat, in

which they specifically interact with each other via their SAM domains. In this

study, we investigated whether the Bicc1 and SamCystin proteins physically

interact in a specific, predictable manner.

Using recombinant mammalian expression constructs containing the

coding sequences for *Bicc1* and *Anks6* and a N-terminal V5 or c-Myc epitope

tag, respectively, we tested whether these proteins physically interact (57).

Briefly, these constructs were co-transfected into mouse inner medullary

collecting duct (IMCD) cells to produce recombinant proteins. Cleared cell

lysates were collected and utilized for co-immunoprecipitation using Profound

Mammalian c-Myc-Tag/Co-IP kit (Pierce). Co-IP experimental design is

illustrated in Figure 4.17. Recombinant Bicc1 and SamCystin protein expression

in IMCD cells was demonstrated by Western blot analysis using anti-c-Myc or

anti-V5 antibodies (Figure 4.18, Input). The co-IP experiments reveal that the

Bicc1 and SamCystin proteins physically interact (Figure 4.18, IP). Co-IP

experiments performed with the mutant form of c-Myc tagged SamCystin and V5-

Bicc1 indicate that the mutation in *Cy* does not affect the interaction between

SamCystin and Bicc1 (57).

Figure 4.17. Schematic of co-immunoprecipitation procedure
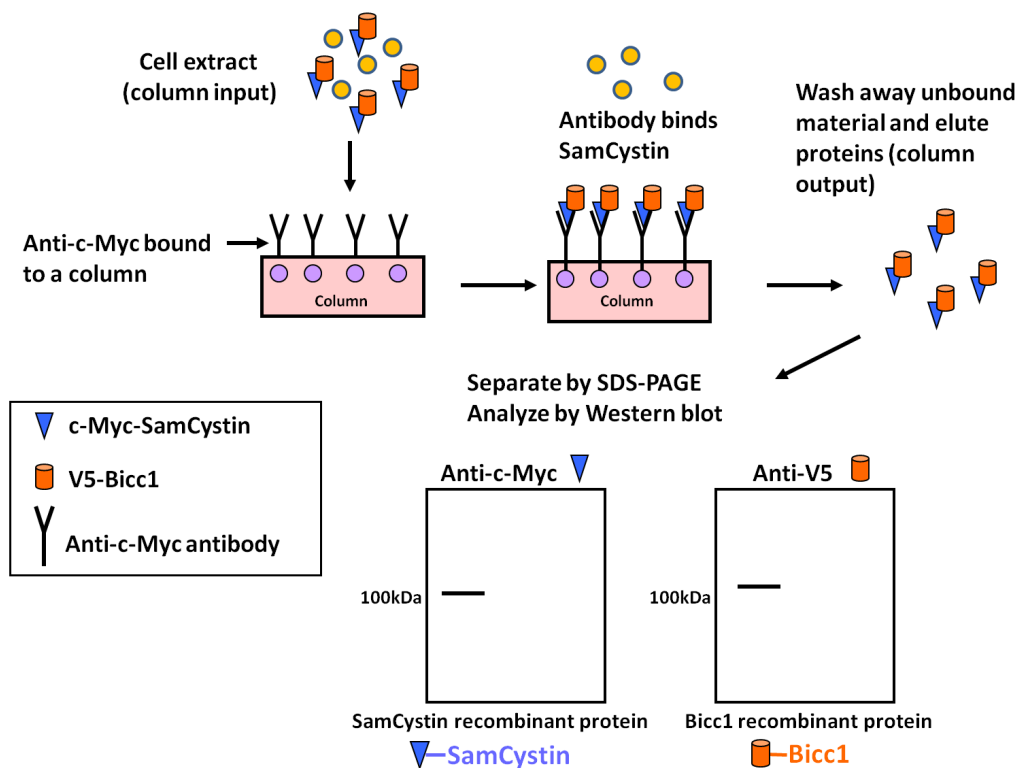
Figure 4.17. Co-Immunoprecipitation principle. Mouse IMCD cells are transiently transfected with plasmid constructs encoding the c-Myc-SamCystin and V5-Bicc1 recombinant proteins. The cell extracts (column input) are applied to a column containing a c-Myc-coupled agarose. The c-Myc-SamCystin recombinant protein binds to the column, along with any interacting partners. The column is washed to remove unbound proteins; while the bound proteins are eluted from the column (column output). Proteins are separated by SDS-PAGE gel electrophoresis and analyzed by Western blot analysis using antibodies to the c-Myc or V5 epitopes.

110

Figure 4.18. Co-immunoprecipitation of SamCystin and Bicc1
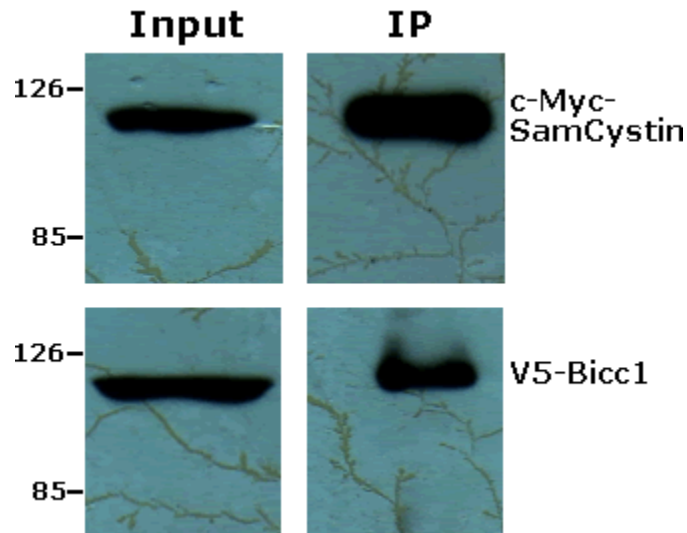
Figure 4.18. The polycystic kidney disease proteins Bicc1 and SamCystin physically interact. The input column represents the expression of the recombinant V5-Bicc1 and c-Myc-SamCystin proteins in mouse IMCD cells. The IP column indicates whether the protein was pulled down in the immunoprecipitation. The presence of Bicc1 in the SamCystin-immunoprecipitate confirms that these proteins physically interact.

To further delineate which functional domains of Bicc1 and SamCystin participate in the interaction, a series of deletion constructs were used in co-immunoprecipitation experiments (Figure 4.19) (57). These studies determined that interaction between Bicc1 and SamCystin is mediated by the SAM domain of SamCystin and the KH domains of Bicc1 (57). The finding that the KH domains of the Bicc1 protein were necessary for the interaction with the SamCystin protein was surprising, since it is well known that proteins containing KH domains bind and regulate RNA (147, 148, 158, 159, 161-164, 251).

Figure 4.19. Schematics of Bicc1 and SamCystin recombinant proteins
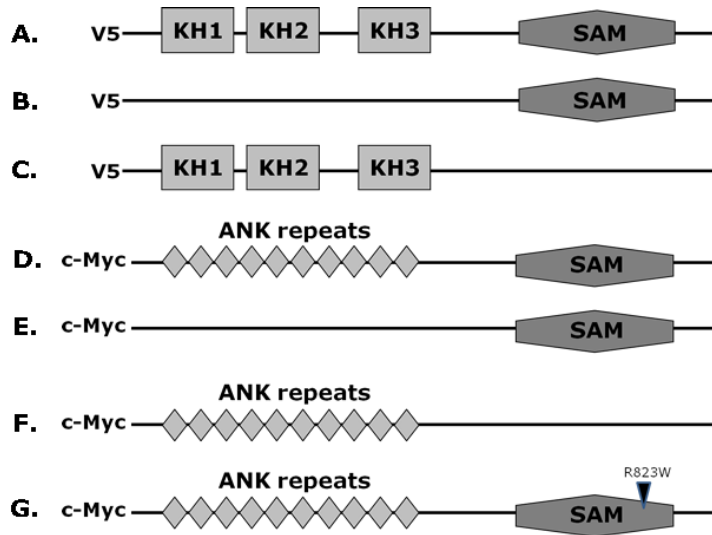
Figure 4.19. Schematic representation of recombinant proteins used in co-immunoprecipitation experiments. (A) Full length Bicc1, (B) Bicc1 with the KH domains deleted, (C) Bicc1 with the SAM domain deleted, (D) Full length SamCystin, (E) SamCystin with the ankryin repeats deleted, (F) SamCystin with the SAM domain deleted, and (G) the altered form of SamCystin as a result of the point mutation in the *Cy* gene resulting in PKD in the rat.

It is important to note that the lysis buffer used to collect the cell lysates does not rid the lysates of the presence of RNA. Given what is known about the RNA binding properties of Bicc1, we predict that this is an indirect interaction, perhaps facilitated by a RNA intermediate. To test this possibility, we treated Bicc1 and SamCystin co-transfected cell lysates with RNase A prior to performing the co-immunoprecipitation experiment. The interaction between Bicc1 and SamCystin was notably reduced with the addition of RNase A (Figure 4.20), supporting the hypothesis that an RNA intermediate is involved in the interaction.

Figure 4.20. Protein interaction of Bicc1 and SamCystin is RNA-dependent
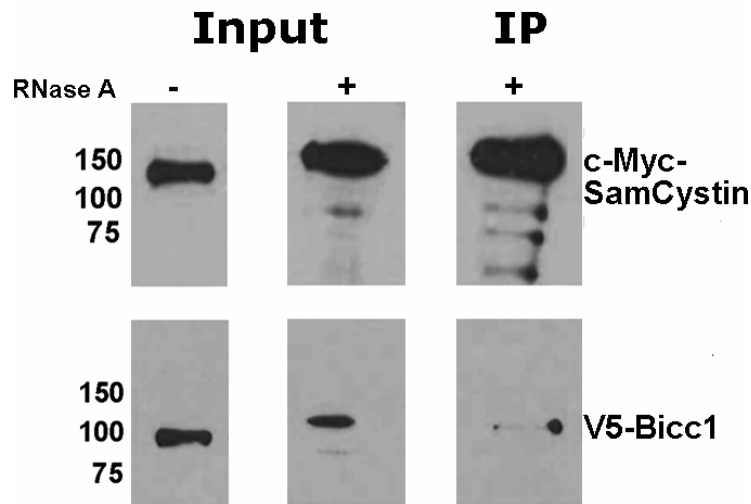
Figure 4.20. Bicc1-SamCystin interaction is mediated by RNA. The input column represents the expression of the c-Myc-SamCystin and V5-Bicc1 recombinant proteins in mouse IMCD cells. Co-IP was performed using transfected cell lysates in the presence or absence of RNase A. The IP column represents the elution (output) from the co-IP experiments, indicating whether the proteins were pulled down in the immunoprecipiation. There is a notable reduction in Bicc1 in the immunoprepitate in the presence of RNase A.

Taken together, these data suggest that Bicc1 and SamCystin physically interact and function in a common molecular pathway. Our current model is that the SAM domains of SamCystin, which are predicted to form homomers in a head to tail fashion, interact with unidentified RNA-associated protein complexes, while Bicc1 binds the same target RNAs through interactions of its KH domains (Figure 4.21) (57). Studies in *Drosophila* have shown that BicC specifically binds the 5'-UTR of its target RNAs and recruits a deadenylase complex to the 3'-UTR of the RNA (147), creating instability in the RNA and leading to its degradation. While we have not yet determined whether the interaction between SamCystin and the RNA intermediate is direct or indirect, we hypothesize that the SAM domain of SamCystin interacts with proteins within this deadenylase complex

rather than a direct interaction with the RNA. However, we cannot rule out this

possibility as the SAM domains of certain proteins have been shown to bind RNA

(252, 253). To determine whether the SamCystin-RNA interaction is direct or

indirect, we plan to immunoprecipitate SamCystin from mouse IMCD cells and

evaluate the immunoprecipate for the presence of *CK2* mRNA by RT-PCR, as

described earlier in "RNA interactions of Bicc1).

Figure 4.21. Proposed model for Bicc1-SamCystin interaction
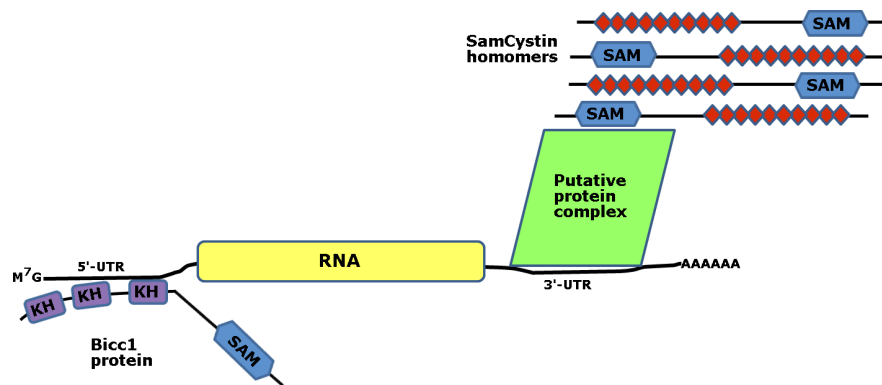
Figure 4.21. Our current model is that Bicc1 associates with the 5'-UTR of target RNAs via its KH
domains, while another protein complex associates with the 3'-UTR. Bicc1 interacts with SamCystin in
a RNA-dependent manner; therefore, we predict that SamCystin may be part of this putative protein
complex. This illustration is adapted from Stagner *et al.*, 2009 (57).

Generation of *bicc1* zebrafish PKD model

Identification and sequence analysis of zebrafish *bicc1* orthologs:

Using Basic Local Alignment Search Tool (BLAST) (218) to compare the

nucleotide sequence of mouse *Bicc1* (GenBank Access. No. NM_031397) to

sequences deposited in the public database maintained by the National Center for Biotechnology Information (NCBI) as well as the zebrafish Vega and Ensembl databases (254, 255), we identified a zebrafish *bicc1* ortholog (GenBank Access. No. NM_203420) which we designate *bicc1a.* This *bicc1* ortholog maps to zebrafish chromosome 14 (Ensembl assembly, Zv8). We also identified a somewhat distant paralog (GenBank Access. No. XM_691516.3) mapping to chromosome 17 (Ensembl assembly, Zv8) which we designate *bicc1b.* Since the genomes of teleost fish, including zebrafish, have undergone an additional round of duplication compared to mammals (256, 257), it is not unexpected that there may be multiple *bicc1* genes in zebrafish. The *bicc1a* and *bicc1b* genes are approximately 2.9 and 3.2 kb in length, respectively, encoding proteins of 849 and 973 amino acids. *Bicc1a* and *bicc1b* share homology at both the nucleotide (24%) and amino acid (42%) levels, with an even higher degree of conservation across the KH and SAM domains, suggesting that they are paralogs (Table 4.5).

Table 4.5. Comparison between zebrafish *bicc1* paralogs

	Chr.#	nucleotide % identity	amino acid % identity	KH1	KH2	KH3	SAM
bicc1a	14	24	41	85	70	43	67
bicc1b	17						

Table 4.5. Multiple sequence alignment analysis of the predicted zebrafish *bicc1* paralogs. There is a high degree of conservation between *bicc1a* and *bicc1b*, particularly across the KH and SAM functional domains, indicating that these genes are paralogous.

Often, paralogous genes persist in zebrafish because they have diverged and acquired distinct functions (258, 259). We hypothesize that this is the case with *bicc1a* and *bicc1b* based on the studies that are described in the subsequent sections.

Characterization of the bicc1a protein: Using the suite of protein analysis programs publicly available at the ExPASy Molecular Biology server, we analyzed the predicted zebrafish bicc1a peptide sequence and found that it contains two types of functional domains: a K homology (KH) domain and a sterile alpha motif (SAM) (Figure 4.22A, B). The KH domain region is at the N-terminus of the protein and consists of 3 KH domains in tandem while the SAM domain is located at the C-terminus. KH domains have been shown to bind RNA, and SAM domains have been implicated in protein-protein interactions during development (156, 158). There is 44% overall amino acid identity between zebrafish bicc1a and mouse and human Bicc1. Importantly, the KH and SAM domains exhibit very high levels of amino acid conservation across all three species (Figure 4.22C), suggesting strongly that these domains are important for Bicc1 function.

Zebrafish *bicc1a* is expressed throughout early development: To determine the temporal expression pattern of *bicc1a* in the developing zebrafish embryo, RT-PCR was performed using total RNA from embryos ranging in age from 1-72 hours post fertilization (hpf) (Figure 4.23A). The constitutively-expressed elongation factor alpha gene (*ef1α*) served as a control (224).

Figure 4.22. Bicaudal C (Bicc1) protein comparison
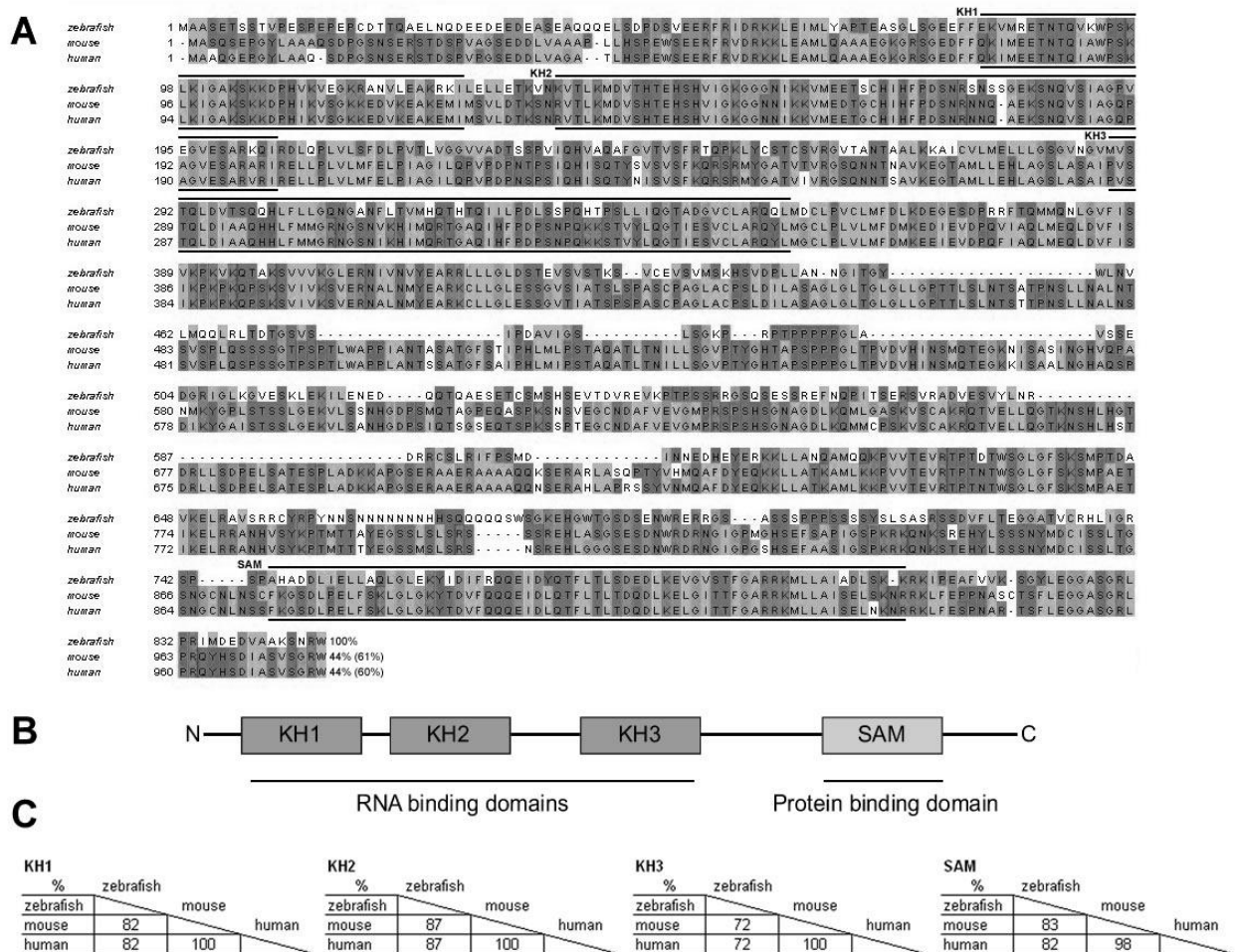
Figure 4.22. Bicaudal C (Bicc1) protein comparison. (A) Comparison of human, mouse and zebrafish bicc1a protein sequences. The number immediately following the peptide sequences represent the % identity of that sequence compared to the zebrafish sequence and the number in parentheses represents the overall conservation of the peptide sequence compared to the zebrafish sequence. Light gray blocks of amino acids indicate residues that are conserved between at least 2 of the species, while dark gray blocks of amino acids represent residues that are conserved among all three species. (B) Schematic of the predicted Bicc1 protein and its functional domains. (C) Comparison of human, mouse, and zebrafish amino acid sequences for Bicc1 functional domains. The percent amino acid conservation for the three KH domains and the SAM domain are listed.

Zebrafish *bicc1a* transcripts were present in all stages tested. Expression at the 1 hour stage is a result of maternally contributed *bicc1a* transcripts, consistent with *BicC* expression in *Drosophila* and *Xenopus* (4, 145). While

quantitative RT-PCR was not performed, comparison to *ef1α* expression

suggests that *bicc1a* expression is robust from 6 hpf through 72 hpf. These

results indicate that *bicc1a* is expressed continuously during the period of

pronephros development. To determine the spatial expression pattern of *bicc1*,

we performed whole-mount in situ hybridization on 12-48 hpf embryos. We used

a digoxygenin-labeled probe derived from EST clone AL923800 which contains

nucleotide sequence near the 5' end of the gene and includes part of the KH

domains. We observed transient *bicc1* expression in 10-18 hpf embryos in the

developing pronephric ducts as well as at the midbrain-hindbrain boundary

(Figure 4.23B, C).

Figure 4.23. Spatial and temporal expression of zebrafish *bicc1a*
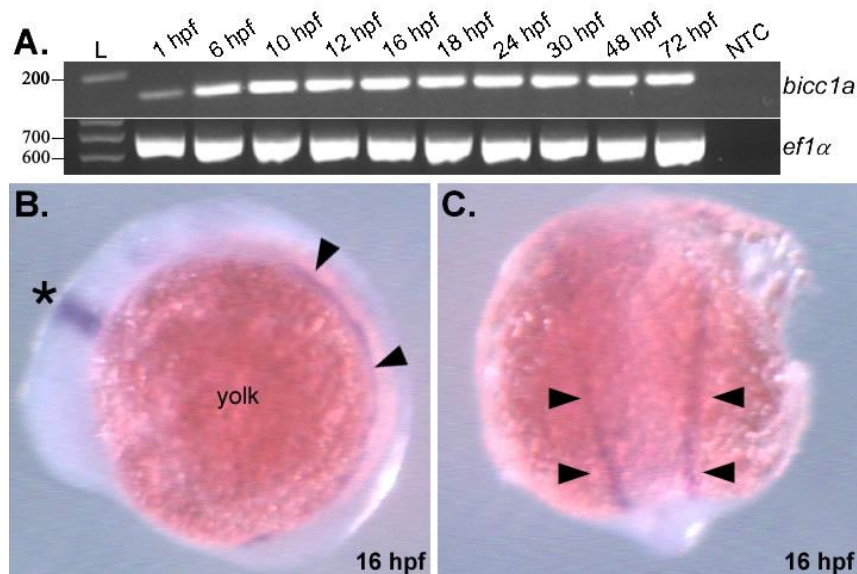
Figure 4.23. Expression of *bicc1a* in whole embryos. (A) Primers specific for zebrafish *bicc1a* or *ef1α* (control) were used in RT-PCR to amplify total RNA from whole embryos. Amplicon size is 179 bp for *bicc1a* (upper panel) and 648 bp for *ef1α* (lower panel). L: 100 bp ladder (Promega); hpf=hours post fertilization; NTC=no template (negative control). (B) Whole-mount in situ hybridization of 16 hpf embryo. In this lateral view, *bicc1* expression is seen at the midbrain-hindbrain boundary (asterisk) and in the developing pronephric duct (arrowheads). (C) Dorsal view of the same embryo with *bicc1* expression seen bilaterally in both pronephric ducts.

Bicc1a knockdown generates kidney cyst-associated morphological

defects: To test whether *bicc1a* plays a role in kidney development and

physiology, we examined the effects of loss of *bicc1a* using a translation-blocking

antisense morpholino oligonucleotide (MO) to transiently knock down expression

of the gene (226). We initially performed dose-response experiments to

determine the MO concentration range in which specific, non-toxic effects could

be obtained. As a positive control, we injected MOs against *pkd2* which were

shown previously to generate kidney cysts in zebrafish (50). Abnormal

morphology was similarly observed in the *bicc1a* and *pkd2* morphants, while the

control embryos developed normally (Figure 4.24).

Figure 4.24. Percent abnormal morphology in *bicc1a* morphants
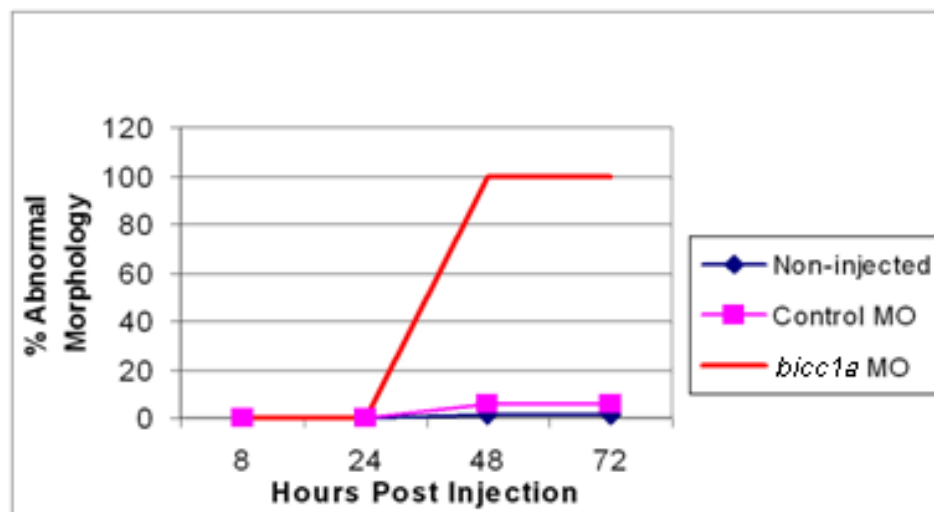
Figure 4.24. Abnormal morphology. Various doses (1-20 ng) of a *bicc1a* antisense morpholino (MO) were used while 1 ng of either a mismatch morpholino (control MO) or a *pkd2* antisense morpholino was used. Animals were observed for gross morphological abnormalities at various time points post injection. The results for all doses of *bicc1a* MO and the *pkd2* MO were the same and are represented by the line labeled *bicc1a* MO.

Injection of *bicc1a* MO over a broad range (1-20 ng/embryo) induced

dorsal curvature in the trunk and tail, with the severity of phenotype directly

proportional to the dose (Figure 4.25D-F; Table 4.6). This phenotype was similar

to the phenotype of *pkd2* MO-injected embryos (Figure 4.25C). In contrast,

uninjected and control MO-injected embryos developed normally (Figure 4.25A,

B). At a dose of 5 ng or higher of the *bicc1a* MO, the trunk phenotype was fully

penetrant, with 100% of embryos exhibiting dorsal curvature (Table 4.6). All

injected embryos exhibited no morphological defects up to 30 hpf. In *bicc1a* and

pkd2 MO injected embryos the trunk phenotype became visible by 40 hpf, and

was fully expressed by 48-60 hpf, suggesting that this phenotype is a specific

effect of MO injection. Many embryos also exhibited varying degrees of

pericardial edema, but the penetrance of this phenotype was variable between

experiments, ranging from 0-50%. Therefore, we used only the trunk phenotype

as a reliable indicator of *bicc1a* morphant activity in all subsequent experiments.

Table 4.6. Summary of *bicc1a* morphant phenotypes

	Dorsal curvature		Kidney cysts
	%	n	
Non-injected	0	266 (7)	0/10
Control MO 1 ng	5	112 (4)	0/4
bicc1a MO 1 ng	97	29 (1)	5/5
bicc1a MO 2.5 ng	100	265 (7)	13/13
bicc1a MO 5 ng	100	84 (3)	8/8
bicc1a MO 10 ng	100	84 (3)	NA
bicc1a MO 20 ng	100	18 (1)	NA
pkd2 MO 1 ng	100	87 (3)	14/14
Bicc1 RNA 150 pg	22	37 (1)	0/4
bicc1a MO 2.5 ng + *Bicc1* RNA 150 pg (rescue)	44	39 (1)	0/6

Table 4.6. Summary of observed phenotypes in *bicc1a* morpholino and rescue studies, where n is the total number of embryos examined and the number in parenthesis refers to the number of experiments performed, NA=not available. Kidney cysts were assessed through histological examination.

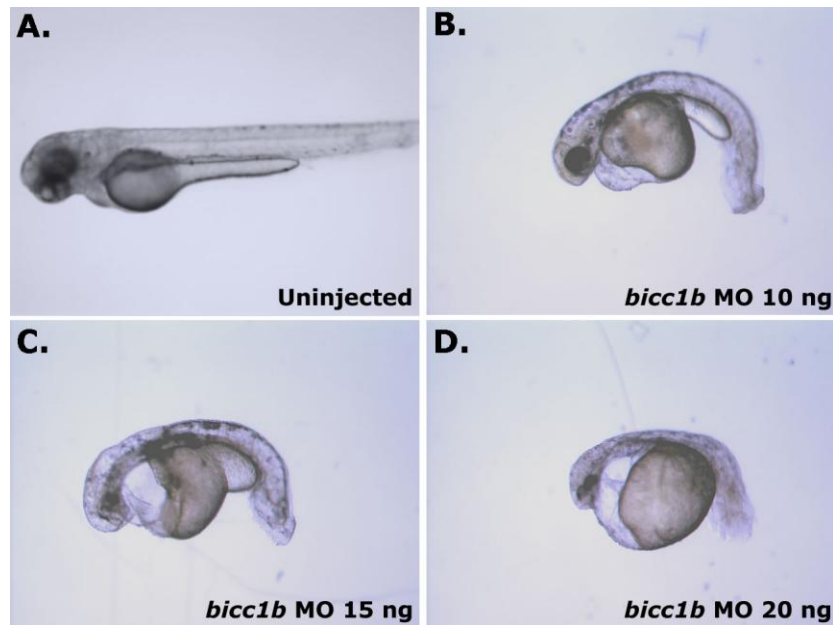**Figure 4.25. Gross morphology of *bicc1a* morphants**
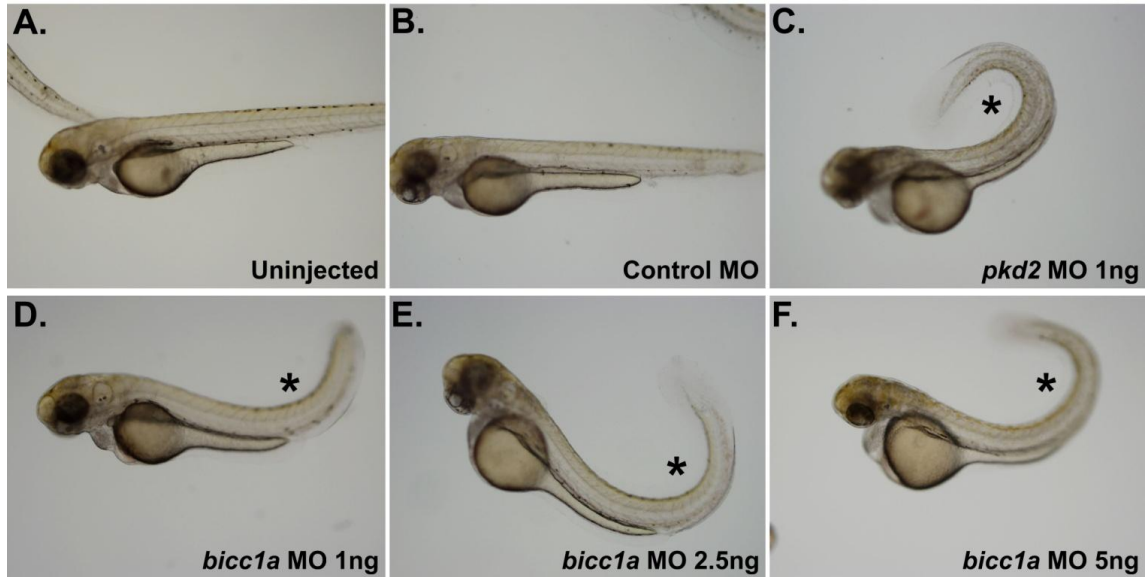
Figure 4.25. Morphological defects in *bicc1a* morphant embryos. Panels show bright-field 50X images of 72 hpf embryos: (A) uninjected fish (control); (B) control morpholino (MO); (C) *pkd2* MO at 1 ng dose; (D) *bicc1a* MO at 1 ng dose; (E) *bicc1a* MO at 2.5 ng dose; (F) *bicc1a* MO at 5 ng dose. No gross abnormalities were detected in uninjected animals or animals injected with the control MO. In embryos injected with the *pkd2* MO or the *bicc1a* MO, there was pronounced dorsal curvature of the trunk (asterisk).

Renal cysts develop in *bicc1a* morphants: Although the morphological defects of *bicc1a* morphants resemble previously described zebrafish mutants and morphants for PKD-causing genes (50, 205), kidney cysts were not visible in live embryos injected with *bicc1a* MO. Therefore, to determine if the loss of *bicc1a* results in kidney cysts, we examined cross-sections of 5 day-old zebrafish embedded in JB-4 (plastic) resin for structural defects in the larval pronephros (Figure 4.26). In uninjected embryos, the glomerulus and pronephric tubules were normal (Figure 4.27A, B), with cellular morphologies resembling those described previously for wild-type embryos (206, 207). In *bicc1a* morphants,

there were prominent cysts in the pronephric tubules as well as cystic dilations in

the glomerulus and pronephric ducts (Figure 4.27C-F). The cysts were lined by

epithelial cells, which appeared normal. The cysts were noted in every morphant

embryo examined (n=18). These results demonstrate that abrogation of *bicc1a*

expression leads to formation of cysts in the developing pronephros.

Figure 4.26. Serial cross sectioning of zebrafish larvae
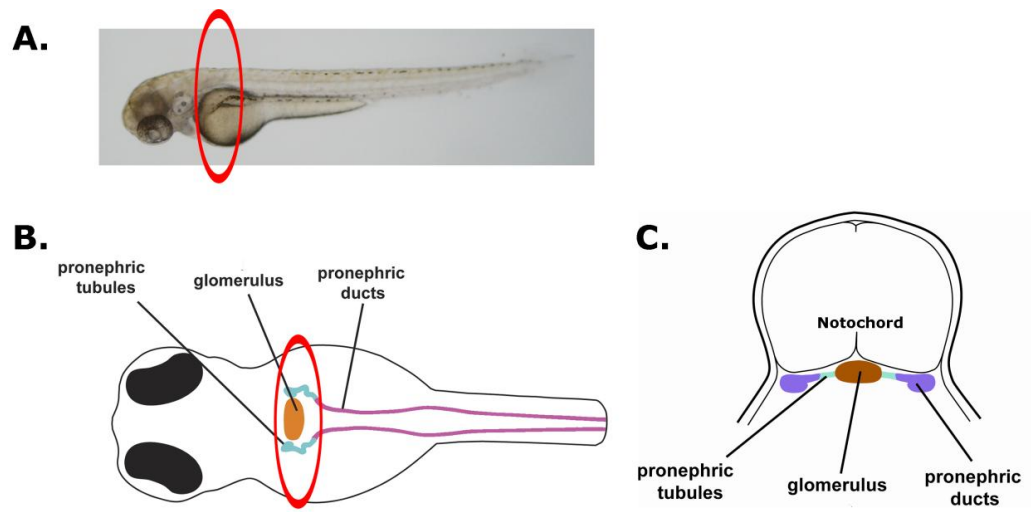
Figure 4.26. Zebrafish larvae were serially cross-sectioned for histological examination. (A) Five day old larval fish were fixed and embedded in JB-4 and serially cross-sectioned through the region containing the kidney, approximately 200 μm (red oval). (B) Illustration of a zebrafish larva (dorsal view) showing the pronephric structures, including the glomerulus, tubules and ducts. The red oval indicates the area included in the serial cross sections. (C) Illustration of the resulting cross sections through this region. The kidney tissues are horizontally orientated directly beneath the notochord. Illustrations kindly provided by Don Connor at the College of Veterinary Medicine, University of Missouri, modified from Drummond *et al.*, 1998 (206).

Figure 4.27. Histological analysis of *bicc1a* cystic morphants
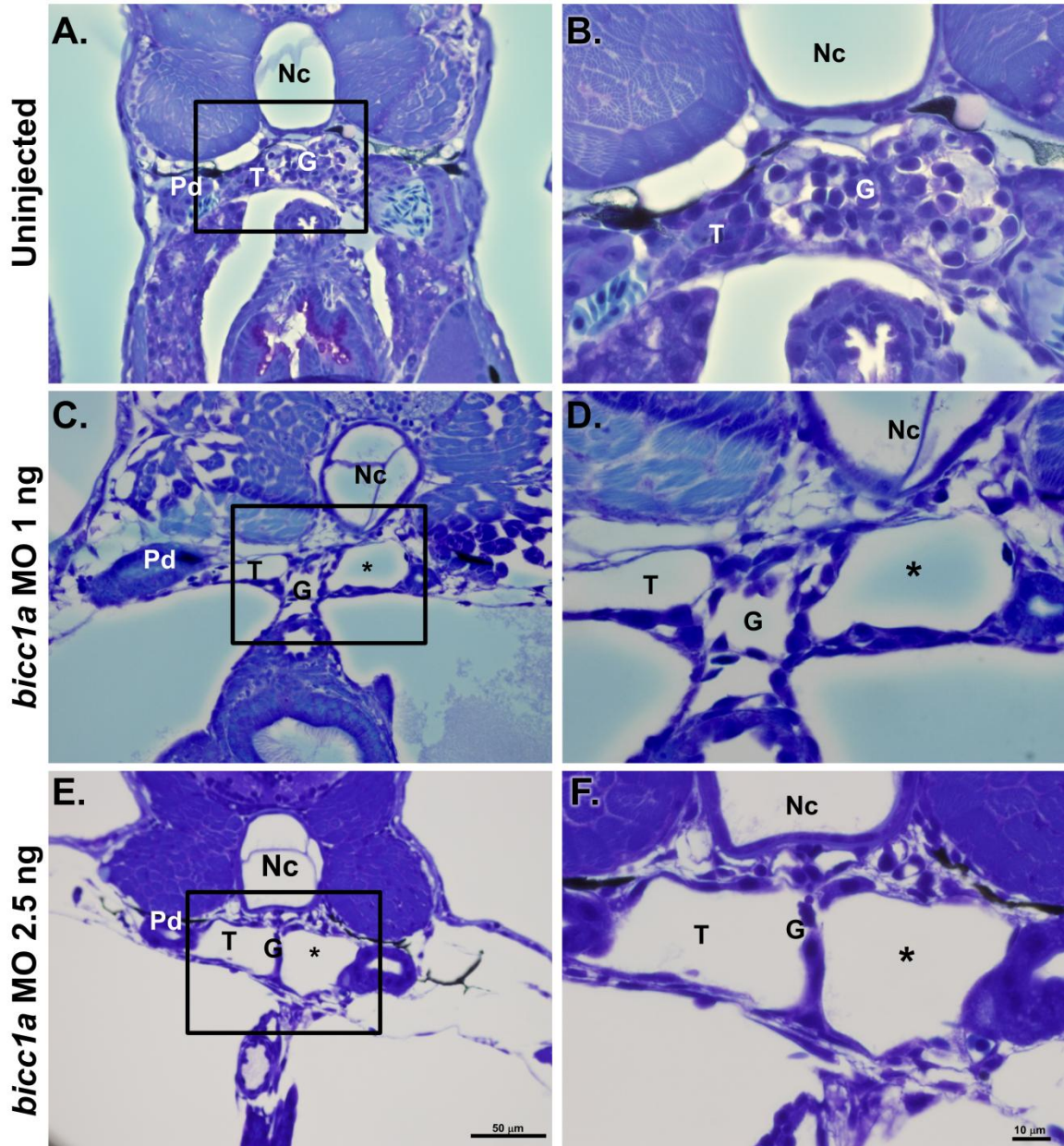
Figure 4.27. Histological analyses of transverse sections of 5 day old embryos provide evidence for cystic kidneys in *bicc1a* morphants. (A) Control morphant at 400X. (B) Boxed area in Panel A at 1000X. (C) *bicc1a* morphant at 1 ng dose of *bicc1a* MO at 400X. (D) Boxed area in Panel C at 1000X. (E) *bicc1a* morphant at 2.5 ng dose of *bicc1a* MO at 400X. (F) Boxed area in Panel E at 1000X. Nc: notochord; Pd: pronephric duct; T: pronephric tubule; G: glomerulus; asterisk: cysts. Sections are representative of embryos examined (n=18).

Similar gross morphology and cystic defects were observed using a broad

range of doses (2.5-20 ng) of a second *bicc1a* morpholino designed to target the

splice junction between exons 2 and 3, resulting in the exclusion of exon 3 in the

final transcript (Figure 4.28, Table 4.7). The exclusion of exon 3 leads to a

frameshift and premature stop codon, mimicking the *Bicc1^{jcpk}* transcript. While

we were unable to confirm the action of the splice-blocking morpholino by RT-

PCR, we never observed cysts in the control morpholino-injected embryos,

suggesting that the cystic phenotype in the *bicc1a* SPL morphants is due to the

loss of *bicc1a* and not a non-specific affect of morpholino injection. The

observation that two independent morpholinos induce a similar phenotype

strongly suggests that the formation of pronephric cysts is specific to the loss of

bicc1a function.

Table 4.7. Summary of *bicc1a* SPL morphant phenotypes

	Dorsal curvature		Kidney cysts
	%	n	
Uninjected	0	102 (3)	0/8
Control MO 1 ng	4	51 (3)	0/3
bicc1a SPL MO 2.5 ng	52	69 (2)	NA
bicc1a SPL MO 5 ng	59	85 (3)	NA
bicc1a SPL MO 10 ng	80	99 (3)	5/5
Bicc1a SPL MO 15 ng	81	21 (1)	NA
bicc1a SPL MO 20 ng	89	29 (2)	NA

Table 4.7. Summary of observed phenotypes in *bicc1a* splice-blocking morpholino studies, where n is the total number of embryos examined and the number in parenthesis refers to the number of experiments performed, NA=not available. Kidney cysts were assessed by histological examination.

Figure 4.28. Morphology and histology of *bicc1a* SPL morphants
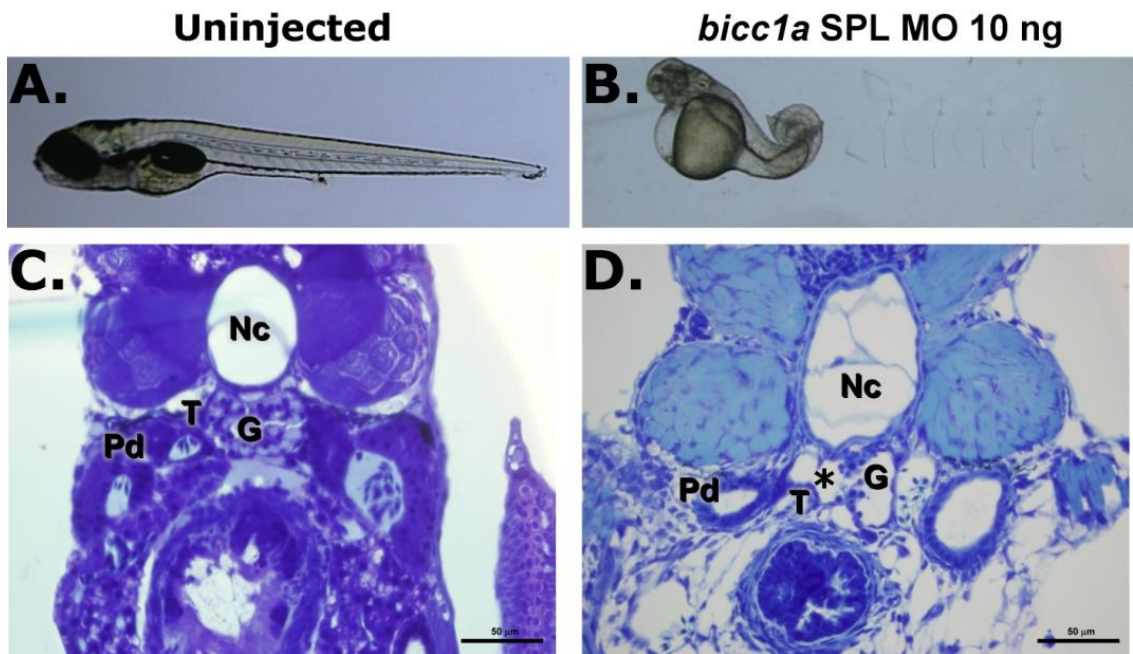
Figure 4.28. Gross morphology and histological analyses of 5 day old embryos provide evidence for cystic kidneys in *bicc1a* morphants using a splice-blocking morpholino. (A) Bright-field image of an uninjected embryo at 250X. (B) Bright-field image of an embryo injected with 10 ng *bicc1a* SPL MO at 250X. (C) Transverse section of uninjected embryo at 400X (D) Transverse section of *bicc1a* SPL morphant (10 ng *bicc1a* SPL MO) at 400X. Nc: notochord; Pd: pronephric duct; T: pronephric tubule; G: glomerulus; asterisk: cysts. Sections are representative of embryos examined (n=5).

Kidney morphogenesis and function appear normal in *bicc1a* morphants: We tested whether formation of cysts in *bicc1a* morphants was accompanied by changes in kidney development and physiology. To examine pronephros development, we stained 48 hpf embryos with anti-Na+/K+ ATPase alpha subunit monoclonal antibody alpha 6F, which labels the pronephric ducts and tubules (206). The morphology and arrangement of these structures was not affected in *bicc1a* morphants (Figure 4.29A-B), indicating that cyst formation does not result from aberrant development of the pronephros.

Disruption of fluid flow in the zebrafish pronephros, either due to defects in cilia or any mechanical barrier, can lead to tubule luminal expansion and cyst formation (195). To test for proper fluid flow through the pronephros, we examined the excretion of rhodamine-dextran from the cloaca immediately following injection into the common cardinal vein of 3-3.5 day-old larvae (195) In control animals, boli of fluorescent material were excreted within 2-3 minutes of injection (Figure 4.29C). Rhodamine dextran was excreted efficiently by *bicc1a* morphants (Figure 4.29D), although the process was slightly slower than in controls. These results suggest strongly that the formation of cysts in morphants does not interfere with fluid flow.

Cilia are not affected in *bicc1a* morphants: To examine the pronephric cilia, we performed immunostaining using mouse monoclonal anti-acetylated-α-tubulin in 28-30 hpf wild type and *bicc1a* morphant embryos using confocal fluorescence microscopy. The length, number, and direction of the cilia in *bicc1a* morphants closely resembled that of the wild-type controls (n=6) (Figure 4.29E, F). Taken together, these results suggest that the formation of cysts in *bicc1a* morphants is not due to overt defects in cilia formation or structure, nor the inhibition of fluid flow.

Figure 4.29. Kidney morphogenesis and function in *bicc1a* morphants
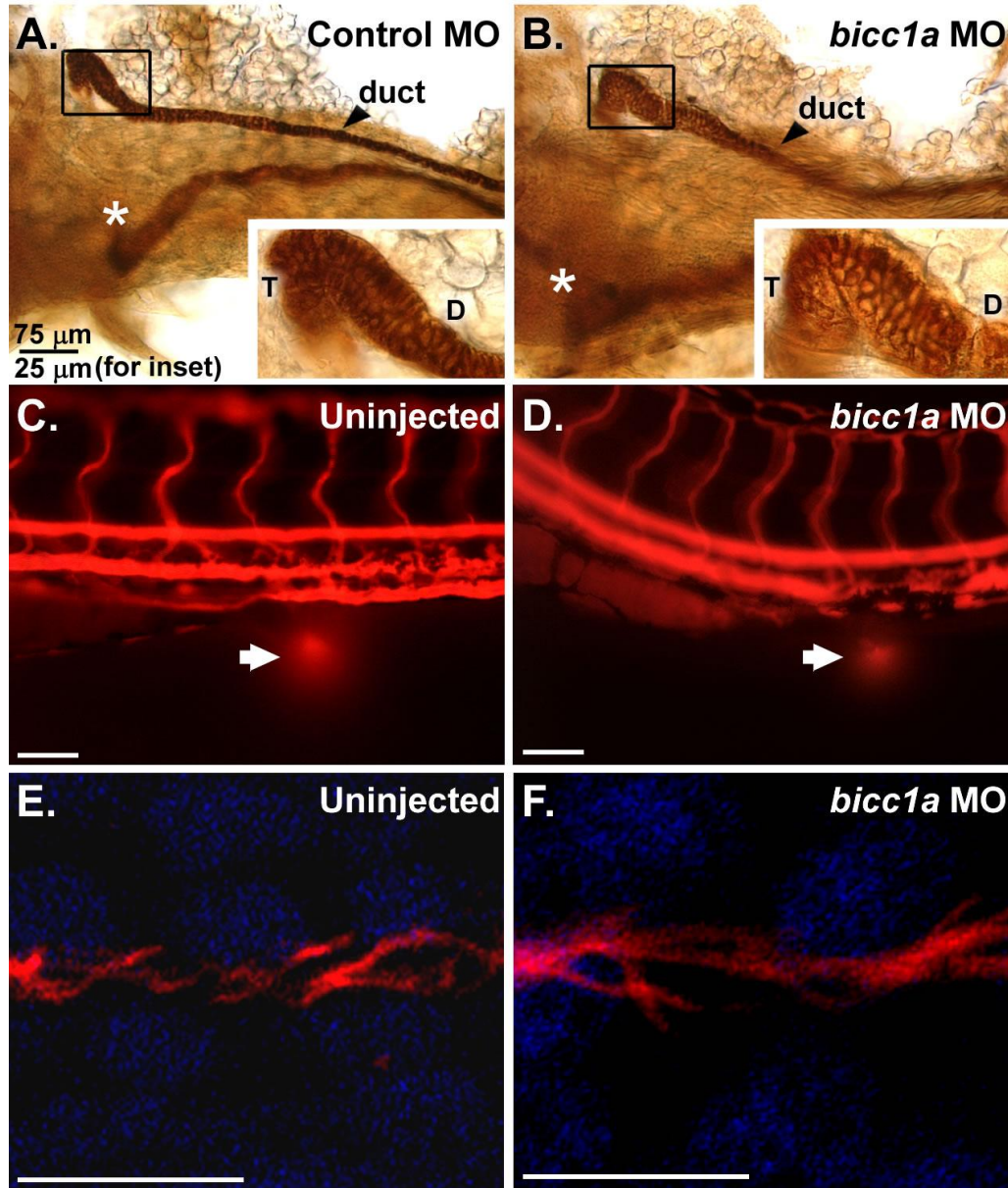
Figure 4.29. Kidney morphogenesis and function. The upper panels show whole-mount immunostaining of 72 hpf embryos with α6F antibody. (A) Injected with the control MO, (B) Injected with *bicc1a* MO. Both panels (A) and (B) are dorsal views, with anterior to the left. Arrowhead indicates duct and asterisk indicates location of paired tubule (out-of-focus). D=Duct, T=Tubule. The boxed region at 200X is magnified in the inset at 600X. A total of 8 embryos were examined in each group. Panels (C) and (D) show uninjected control and *bicc1a* morphant animals respectively, injected with fluorescently labeled dextran. Arrows indicate excretion of the labeled dextran from the cloaca via the pronephros. A total of 10 uninjected and 8 *bicc1a* morphant embryos were examined. Images were acquired with an Olympus BX60 fluorescent microscope at 400X. (E, F) Confocal microscopy of pronephric cilia in 28-30 hpf wild type and *bicc1a* morphant embryos using a Zeiss LSM 510 META NLO two-photon point-scanning microscope at 400X and 3X optical zoom. Comparisons were made between at least 5 wild type and morphant embryos.

127

Expression of mouse *Bicc1* can prevent cyst formation in *bicc1a*

morphants: It is important to demonstrate that pronephric cysts in morphants

are specifically due to knockdown of *bicc1a* expression. Therefore, we tested

whether expression of the mouse *Bicc1* ortholog could prevent cyst formation in

bicc1a morphants. Synthetic full-length mRNA encoding mouse *Bicc1* that lacks

the *bicc1a* MO-binding site was co-injected with *bicc1a* MO, and embryos were

examined for morphological defects as well as for cyst formation by histological

analysis (Figure 4.20, Table 4.8). Uninjected or mouse *Bicc1* RNA alone-injected

embryos were indistinguishable up to 5 days post fertilization (Figure 4.30A-D),

indicating that overexpression of mouse *Bicc1* has no detrimental effects on

larval development or physiology. In embryos co-injected with both the *bicc1a*

MO, and mouse *Bicc1* RNA, the occurrence of dorsal tail curvature and

pronephric cysts was significantly reduced (Figure 4.30G-I), with almost 60% of

the rescued embryos demonstrating normal morphology (Figure 4.30E, F, I).

Importantly, co-injection of *bicc1a* MO and mouse *Bicc1* mRNA representative of

the *jcpk* mutation into zebrafish embryos was unable to rescue the cystic

phenotype (data not shown), providing further evidence that the development of

renal cysts is a direct result of the loss of *bicc1a* and that mouse and zebrafish

Bicc1 are functionally conserved.

Figure 4.30. Mouse Bicc1 rescues cystic *bicc1a* morphants
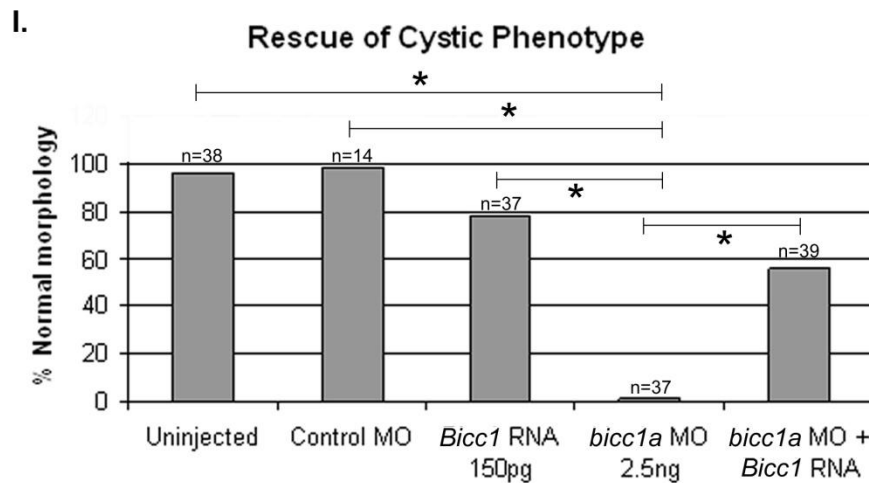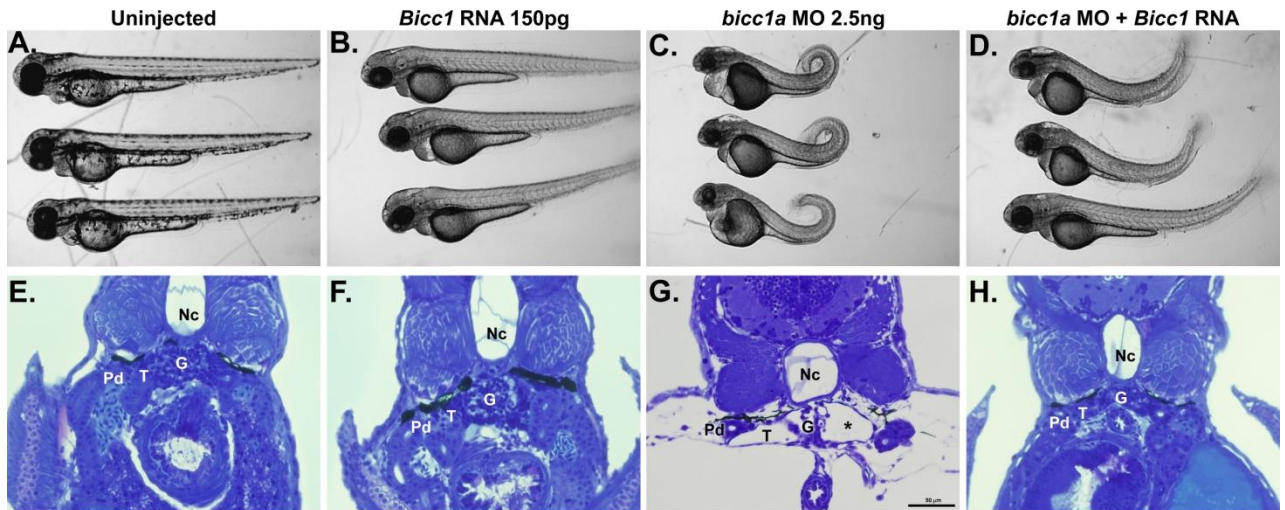
Figure 4.30. Mouse *Bicc1* rescues the zebrafish *bicc1a* morphant phenotype. Bright-field images of embryos that were (A, E) uninjected, (B,F) injected with 150 pg of mouse *Bicc1* RNA, (C,G) injected with 2.5 ng of zebrafish *bicc1a* MO, or (D,H) co-injected with 150 pg of mouse *Bicc1* RNA and 2.5 ng of zebrafish *bicc1a* MO at 250X. In embryos injected with the *bicc1a* MO, there was pronounced dorsal curvature of the trunk. Panels (E-H) show histological analysis of cross-sections of representative fish from each treatment group at 400X. Nc: notochord; Pd: pronephric duct; T: pronephric tubule; G: glomerulus; asterisk: cysts (as in Legend for Fig 4). Panel (I) A graphical depiction of the number of animals observed in each group and the percent exhibiting normal outward morphology. In the morphants that were also injected with mouse *Bicc1* RNA, 56% did not exhibit outward morphological defects and showed little or no dorsal curvature of the trunk. Statistical analysis comparing proportions using Fisher's Exact test (Sigma Plot) showed a significant difference (p<0.05) between groups as indicated with an asterisk (*).

Characterization of the bicc1b protein: Comparison of zebrafish bicc1b with the mouse and human Bicc1 proteins by multiple sequence alignment (211, 212) showed that the zebrafish bicc1b protein shares 62% identical amino acids in the overall protein (Figure 4.31A). Taking into account conserved amino acid substitutions as calculated by JalView (213), the bicc1b protein shares 71% overall conservation with mouse Bicc1 and human BICC1 (Figure 2.31A). As seen before with zebrafish bicc1a, the degree of conservation is even higher in the regions of the KH and SAM functional domains, as illustrated in Figure 4.31C. It is interesting that while both bicc1a and bicc1b are very similar to human and mouse Bicc1 across the functional domains, bicc1b appears to have more similarity to the mouse and human proteins in the regions between the functional domains (Figure 4.31A).

Zebrafish *bicc1b* is expressed throughout early development: To determine the temporal expression pattern of *bicc1b* in the developing zebrafish embryo, RT-PCR was performed using total RNA from embryos ranging in age from 4-72 hours post fertilization (hpf) (Figure 4.32A). The constitutively-expressed elongation factor alpha gene (*ef1α*) served as a control (224). *Bicc1b* transcripts are present in all stages tested. Expression at the 4-8 cell stage is a result of maternally contributed *bicc1b* transcripts, consistent with BicC expression in *Drosophila* and *Xenopus* (4, 145). These results indicate that *bicc1b* is expressed continuously during the period of pronephros development.

Figure 4.31. bicc1b protein comparison with mouse and human Bicc1

Figure 4.31. Bicaudal C (Bicc1) protein comparison. (A) Comparison of the human and mouse Bicc1 protein sequences with zebrafish bicc1b. The number immediately following the peptide sequences represent the % identity of that sequence compared to the zebrafish sequence and the number in parentheses represents the overall conservation of the peptide sequence compared to the zebrafish sequence. Light gray blocks of amino acids indicate residues that are conserved between at least 2 of the species, while dark gray blocks of amino acids represent residues that are conserved among all three species. (B) Schematic of the predicted bicc1b protein and its functional domains. (C) Comparison of human, mouse, and zebrafish amino acid Bicc1 sequences across the functional domains. The percent amino acid conservation for the three KH domains and the SAM domain are listed.

Figure 4.32. Temporal expression of *bicc1b* in zebrafish
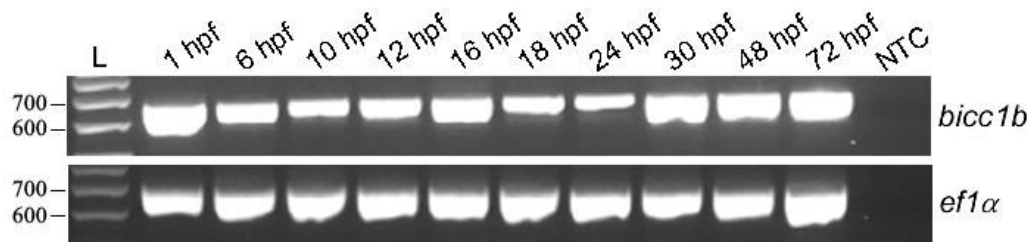
Figure 4.32. Expression of *bicc1b* in whole embryos. (A) Primers specific for zebrafish *bicc1b* or *ef1α* (control) were used in RT-PCR to amplify total RNA from whole embryos. Amplicon size is 643 bp for *bicc1b* (upper panel) and 648 bp for *ef1α* (lower panel). L: 100 bp ladder (Promega); hpf=hours post fertilization; NTC=no template (negative control).

Unfortunately, attempts to determine the spatial expression pattern of *bicc1b* using whole-mount in situ hybridization failed to delineate its expression in zebrafish embryos. Multiple digoxigenin-labeled probes derived from EST clones which contain nucleotide sequences specific to *bicc1b*, as well as a PCR-derived probe containing sequence specific to the 3'-UTR of *bicc1b* were utilized for in situ hybridization in embryos from 6 hpf to 72 hpf. A signal was not achieved for any of the probes tested, despite various alterations to the in situ hybridization protocol (260-263).

***Bicc1b* knockdown generates abnormal morphology:** To test whether *bicc1b* also plays a role in kidney development and cyst formation, we examined the effects of knocking down *bicc1b* expression using a translation-blocking antisense morpholino oligonucleotide (MO) (226). We again performed dose-response experiments to determine the MO concentration range in which specific, non-toxic affects could be obtained. Abnormal morphology was

observed in the *bicc1b* morphants at MO doses between 2.5-20 ng, while the

control embryos developed normally (Figure 4.33, Table 4.8).

Figure 4.33. Gross morphology of *bicc1b* morphants

Figure 4.33. Morphological defects in *bicc1b* morphant embryos. Panels show bright-field 50X images of 54 hpf embryos: (A) uninjected fish (control); (B) *bicc1b* morpholino (MO) at 10 ng dose; (C) *bicc1b* MO at 15 ng dose; (D) *bicc1b* MO at 20 ng dose. No gross abnormalities were detected in uninjected animals or animals injected with the control MO (not shown). In embryos injected with the *bicc1b* MO, we observed a downward curvature of the trunk, a shortened trunk and pericardial and tail edema.

The *bicc1b* morphants exhibited a downward curvature of the trunk, a

shorter trunk region, and edema in the pericardium and tip of the tail. Embryos

injected with >10 ng of the *bicc1b* MO also showed delayed or abnormal eye

development. *Bicc1b* morpholino-injected embryos appeared to develop

normally until 20-24 hpf, at which point the abnormal phenotype began to

emerge. The severity of the phenotype was directly proportional to the dose

(Figure 4.33B-D; Table 4.8), suggesting that the phenotype is specific. In

contrast, uninjected and control MO-injected embryos developed normally

(Figure 4.33A). Unlike the *bicc1a* morphants which exhibited a survival rate of 5-

7 days, the *bicc1b* morphants only survived 3-4 days post-fertilization.

Table 4.8. Summary of *bicc1b* morphant phenotypes

	Abnormal Morphology	
	%	n
Non-injected	0	68(3)
Control MO 1 ng	2	56(3)
bicc1b MO 2.5 ng	10	29(1)
bicc1b MO 5 ng	31	32(2)
bicc1b MO 10 ng	68	25(2)
bicc1b MO 15 ng	73	22(2)
bicc1b MO 20 ng	100	11(1)

Table 4.8. Summary of observed phenotypes in the *bicc1b* morpholino studies. The percent of
embryos with abnormal morphology are indicated for various doses of the *bicc1b* MO; n represents the
total number of embryos examined and the number in parenthesis refers to the number of experiments
performed.

Kidney tissues are not evident in *bicc1b* morphants: The outwardly

visible morphological defects of *bicc1b* morphants do not resemble those of the

bicc1a morphants. However, it was unclear from the gross morphological

examination whether the kidneys of *bicc1b* morphants were affected. To

determine if the loss of *bicc1b* also resulted in the formation of kidney cysts, we

examined cross-sections of 3 day-old zebrafish embedded in JB-4 plastic resin

for structural defects in the larval pronephros. In uninjected embryos, the

glomerulus and pronephric tubules were normal, with cellular morphologies

resembling those described previously for wild-type embryos (206, 207).

134

However, in all *bicc1b* morphant embryos examined (n=4) at the 10 ng dose, kidney tissues were not evident. This could be due to artifacts that occurred during the processing or sectioning of the embryos or perhaps the pericardial edema and fluid accumulation in these embryos may have displaced the kidney tissues. As a result of the lack of any discernible kidney tissue in the *bicc1b* morphants, at this time we cannot determine if the loss of *bicc1b* results in the formation of cysts. However, the morpholino used to knockdown *bicc1a* does not prevent translation of *bicc1b* (Table 4.9), yet *bicc1a* morphants develop cystic kidneys, suggesting that *bicc1b* is not able to compensate for the loss of *bicc1a* in the kidney. Further studies are required to determine whether the abnormalities observed in the *bicc1b* morphants are due to developmental defects or failure kidney organogenesis. While *bicc1b* may play an important role during zebrafish development, it does not appear to contribute to renal cystogenesis, therefore, we did not pursue further analysis of *bicc1b* in this study.

Table 4.9 Comparison of *bicc1a* and *bicc1b* morpholino binding sequences

Gene	Morpholino target sequence
bicc1a *bicc1b*	AGTCTTGCTATGGCGGCCTCAGAGACGAGCAGCA ----GGACAATGGCCGAACCGTTGAGTTTTATGC
mismatch	XXX X X XXX XXX XXXX

Table 4.9. Comparison of the *bicc1a* and *bicc1b* nucleotide sequences targeted by morpholinos. The sequence of *bicc1a* and *bicc1b* genes targeted by their corresponding morpholinos is shaded in gray with the ATG translational start site indicated in yellow. Mismatched base pairs between the two sequences are indicated by red X's. More than 5 mismatch base pairs will prevent a morpholino from binding a target sequence. There are 15 mismatched base pairs between the *bicc1a* and *bicc1b* sequences; therefore, the *bicc1a* morpholino will not bind to *bicc1b* and the *bicc1b* morpholino will not bind to *bicc1a.*

Generation of *anks6* zebrafish PKD model

Identification and sequence analysis of a zebrafish ortholog of

Anks6: Mutations in rat *Anks6* result in polycystic kidney disease (179, 249).

We have shown that Bicc1 and SamCystin, the protein encoded by *Anks6*,

physically interact, suggesting that they may function in a common molecular

pathway (57). The zebrafish model system could facilitate further investigation

into this pathway and the molecular functions of Bicc1 and SamCystin. Using

Basic Local Alignment Sequence Tool (BLAST) (218) to compare the nucleotide

sequence of the rat *Anks6* gene (GenBank Access. No. NM_001015028) to

sequences deposited in the zebrafish Vega and Ensembl databases identified a

single zebrafish *anks6* ortholog (GenBank Access. No. NM_001005928). This

anks6 ortholog has yet to be mapped, however it is approximately 3 kb in length,

encoding a protein consisting of 739 amino acids. Reciprocal BLAST analysis

identified human, rat, and mouse *Anks6* as putative orthologs. Clustal W2 (211,

212) alignment of the human, rat, and mouse cDNAs with the zebrafish

sequence showed a high degree of sequence similarity at both the nucleotide

and amino acid levels (Figure 4.34A, Table 4.10).

Table 4.10. Conservation of *Anks6*

Rattus norvegicus vs.	GenBank Accession No. nucleotide (protein)	Chr. # 5	amino acid % identity	nucleotide % identity
Mus musculus	NM_ 001024136 (NP_001019307)	4	94	89
Homo sapiens	NM_173551 (NP_775822)	9	85	50
Danio rerio	NM_001005928 (NP_001005928)	?	56	55

Table 4.10. Multiple sequence alignment using Clustal W2 (211, 212) comparing the mouse, human and zebrafish *Anks6* sequences to rat *Anks6*.

The predicted zebrafish SamCystin protein contains 2 functional domains: ten tandem N-terminal ankyrin repeats (ANK) and a single C-terminal sterile alpha motif (SAM) (Figure 4.34B)(155). As observed in the Bicc1 proteins, when the protein sequences of SamCystin for different species were compared, the percent amino acid identity across the ANK and SAM functional domains was higher than the percent amino acid identity of the protein sequences overall (Figure 4.34C, Table 4.11).

Table 4.11. Percent amino acid identity across SamCystin functional domains

Rattus norvegicus vs.	Full length SamCystin	ANK repeats	SAM
Mus musculus	94	95	100
Homo sapiens	85	93	98
Danio rerio	56	59	95

Table 4.11. The amino acid sequences of the ANK and SAM domains of mouse, human and zebrafish SamCystin were compared to that of rat SamCystin and the percent of identical residues was calculated. The percent identity across the functional domains is greater than the overall protein sequence identity in all cases.

Figure 4.34. SamCystin protein comparison
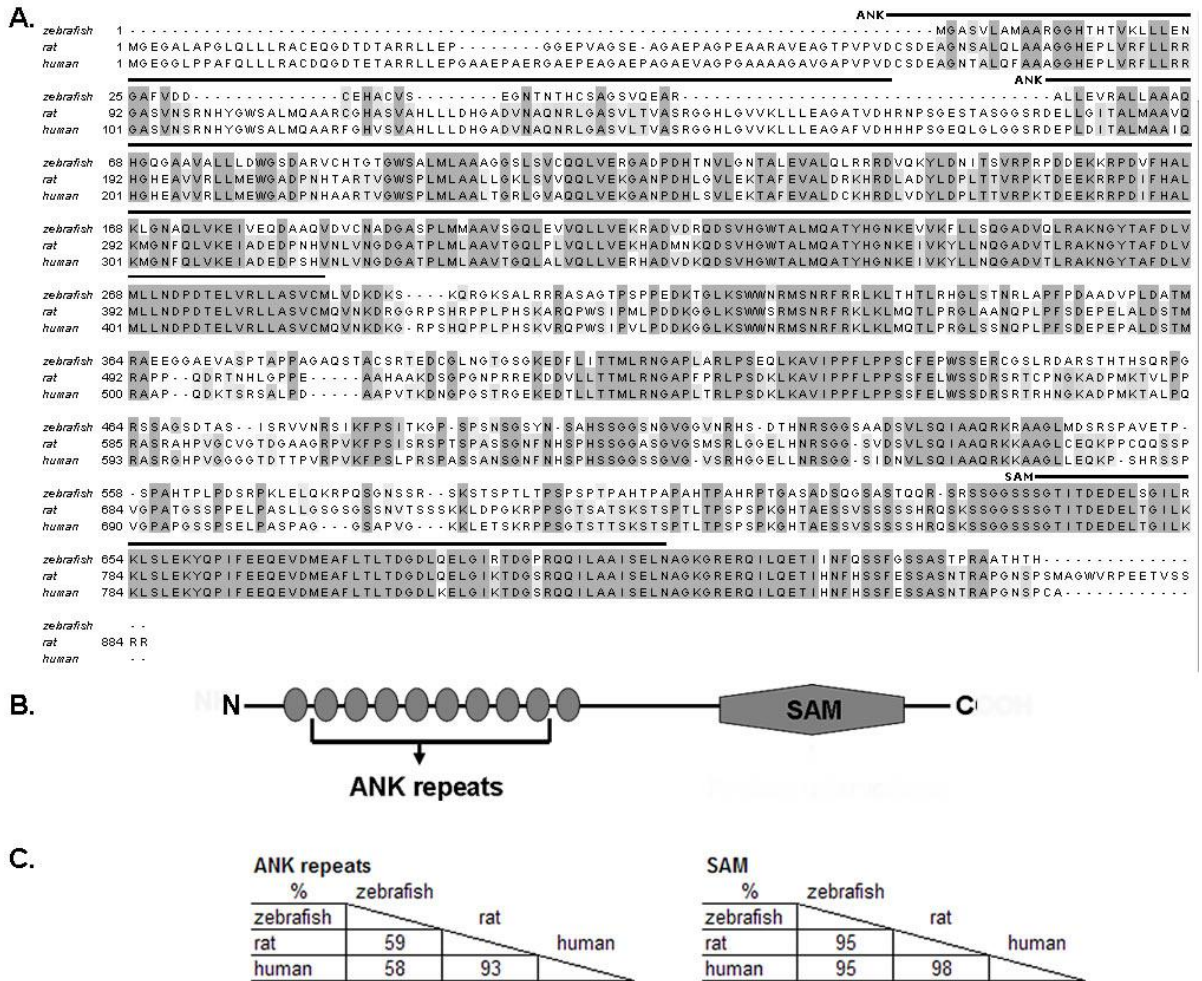
Figure 4.34. (A) Clustal W2 (211, 212) alignment of human, rat, and zebrafish SamCystin protein sequences. Light gray shading indicates identical residues in at least 2 species, while dark gray shading represents identical residues in all three species. Unshaded residues are likely divergent. (B) Schematic of the predicted SamCystin protein and its functional domains. (C) Comparison of human, rat, and zebrafish amino acid sequences for the SamCystin functional domains. The percent amino acid identity for the ankyrin repeats and the SAM domain are listed.

Zebrafish *anks6* is expressed throughout early development: To determine the temporal expression pattern of *anks6* in the developing zebrafish embryo, RT-PCR was performed using total RNA from embryos ranging in age from 4-72 hours post fertilization

(hpf) (Figure 4.35). The constitutively-expressed elongation factor alpha gene (*ef1α*)

served as a control (224). *Anks6* transcripts are present in all stages tested. Expression at

the 4-8 cell stage can be attributed to maternal expression of *anks6*. These results indicate

that *anks6* is expressed continuously during the period of pronephros development.

Figure 4.35. Zebrafish expression of *anks6*
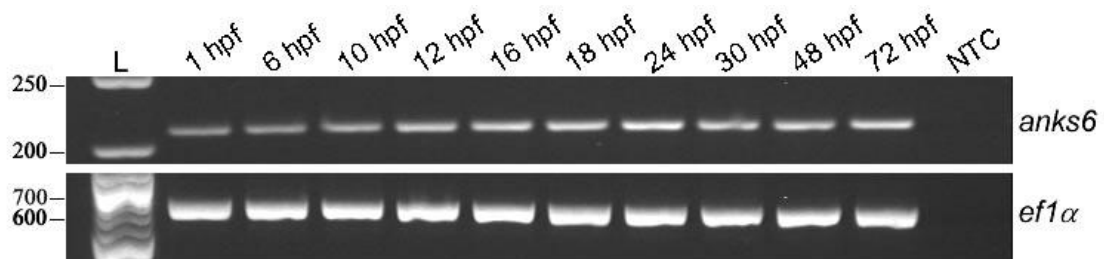
Figure 4.35. Expression of *anks6* in whole embryos. (A) Primers specific for zebrafish *anks6* or *ef1α* (control) were used in RT-PCR to amplify total RNA from whole embryos. Amplicon size is 217 bp for *anks6* (upper panel) and 648 bp for *ef1α* (lower panel). L: 100 bp ladder (Promega); hpf=hours post fertilization; NTC=no template (negative control).

To determine the spatial expression pattern of *anks6*, we performed

whole-mount in situ hybridization on 10-48 hpf embryos. We used a

digoxygenin-labeled probe derived from a full length clone BC083503,

approximately 3 kb, as well as two truncated probes aligning at the 3' end, 1 kb

and 464 bp in length. Unfortunately, we did not see expression in embryos

ranging from 10-48 hpf with any of these probes. Adjustments to the

hybridization protocol and hydrolyzation of the probes did not improve the results.

In the rat, *Anks6* is expressed in many tissues including the brain, heart, kidney,

liver, and testis; kidney expression is specific to the proximal tubules (179). We

suspect that the expression pattern of zebrafish *anks6* in the kidney is similar to that of the rat, but as of yet cannot provide confirming evidence.

Knockdown of *anks6* generates kidney cyst-associated morphological defects: To determine whether *anks6*, like *bicc1a*, plays a role in pronephros development and physiology, we examined the effects of loss of *anks6* function by knocking down *anks6* using translation-blocking antisense morpholino oligonucleotides (MOs) (226). As before, we performed dose-response experiments to determine the MO concentration range in which specific, non-toxic effects could be obtained. Injection of *anks6* MO over a broad range (1-20 ng/embryo) induced a slight dorsal curvature in the trunk and tail and pericardial edema, with the severity of phenotype proportional to the dose (Figure 4.36B-F, Table 4.11). In contrast, uninjected control embryos developed normally (Figure 4.36A, Table 4.11). MO injected embryos developed normally for the first 20-24 hours. Morphological defects became apparent at approximately 24 hpf, suggesting that this phenotype is a specific effect of MO injection. Interestingly, *anks6* morphant embryos also exhibited defects reminiscent of some convergent extension mutants (264), displaying a shortened and broadened body axis (Figure 4.27D-F, Table 4.8). Since there was a relatively low penetrance (25-40%) of the phenotype in *anks6* morphants (Table 4.11), we repeated the experiments with a second translation-blocking morpholino designed to target a different region of *anks6*. Embryos injected with this morpholino mirrored the phenotyped observed with the first, carrying a similar penetrance (data not shown). The induction of similar phenotypic defects

140

using two separate morpholinos suggests that the observed phenotype is specific

to the loss of *anks6* and not due to non-specific effects. For future studies, it may

be necessary to inject both morpholinos to increase the penetrance of the

phenotype.

Figure 4.36. Gross morphology of *anks6* morphants
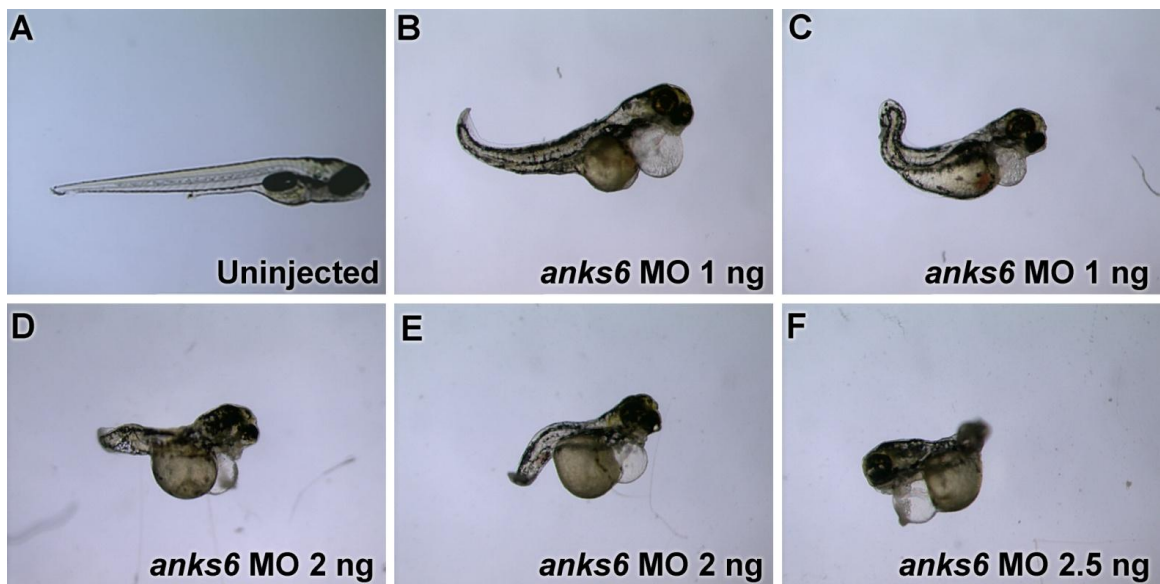
Figure 4.36. Morphological defects in *anks6* morphant embryos. Panels show bright-field 50X images of 72 hpf representative embryos: (A) Uninjected (control); (B) and (C) Injected with *anks6* MO at 1 ng dose; (D) and (E) Injected with *anks6* MO at 2 ng dose; (F) Injected with *anks6* MO at 2.5 ng dose.

Renal cysts develop in *anks6* morphants: To determine whether the

morphological defects in *anks6* morphants are accompanied by a cystic kidney

phenotype, we examined transverse sections of 4 day old zebrafish embedded in

JB-4 for structural defects in the larval pronephros (Figure 4.37).

Table 4.12. Summary of *anks6* morphant phenotypes

	Dorsal curvature/ Shortened body		Kidney cysts
	%	**n**	
Uninjected	0	192 (4)	0/2
Control MO 1 ng	0	148 (4)	0/3
anks6 MO 1 ng	27	163 (4)	3/3
anks6 MO 1.5 ng	40	10 (1)	3/3
anks6 MO 2 ng	48	10 (1)	2/2
anks6 MO 2.5 ng	46	56 (3)	1/1
anks6 MO 5 ng	41	22 (2)	NA
anks6 MO 10 ng	38	24 (2)	NA
anks6 MO 15 ng	26	15 (1)	NA
anks6 MO 20 ng	36	11 (1)	NA

Table 4.12. Summary of observed phenotypes in morpholino studies, where n is the total number of embryos examined, the number in parenthesis refers to the number of experiments performed, and NA=not available. Kidney cysts were assessed by histological examination.

For hisological examination, we used 4 day old embryos rather than 5 day old embryos because the *anks6* morphants did not have a high survival rate beyond 4 days post fertilization. In uninjected embryos, the glomerulus and pronephric tubules were normal (Figure 4.37A, B), with cellular morphologies resembling those described previously for wild-type embryos (206, 207). In *anks6* morphants, there were notable cystic dilatations in the glomerulus and tubules (Figure 4.37C, D, Table 4.12); dilated pronephric ducts were also observed. The cysts were lined by epithelial cells, which appeared normal. The cysts were noted in every morphant embryo examined (n=9) and absent from all controls (n=5). These results demonstrate that abrogation of *anks6* expression leads to formation of cysts in the developing pronephros.

Figure 4.37. Histology of *anks6* morphants
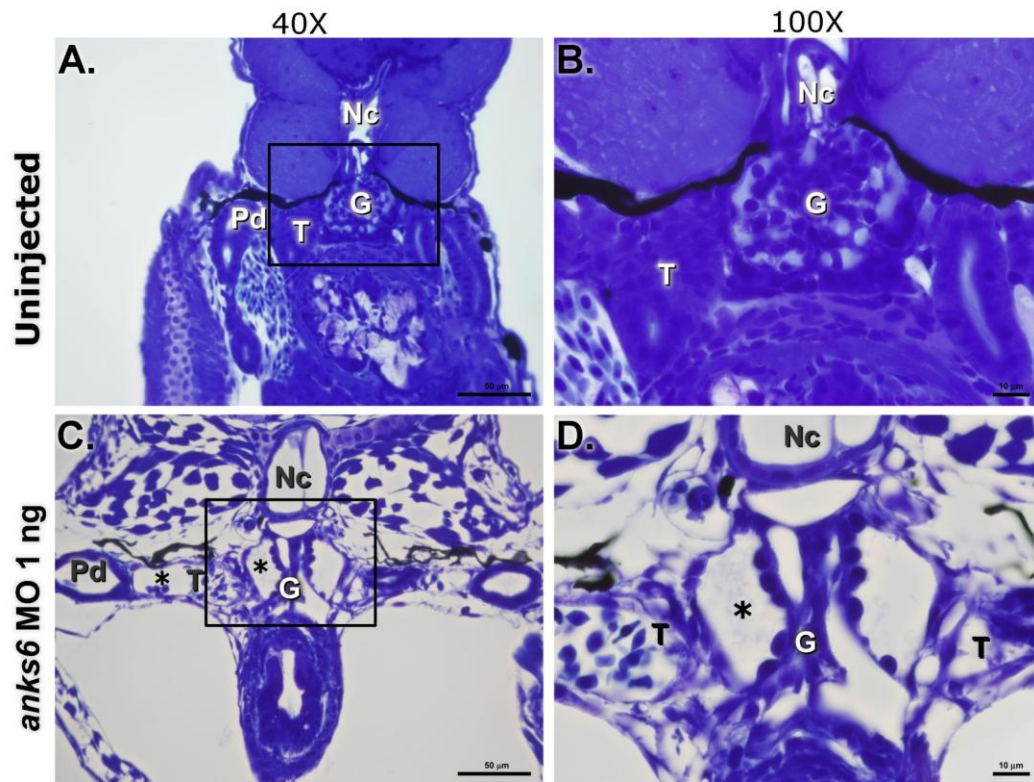
Figure 4.37. Kidney cysts in *anks6* morphant embryos. Histological analysis of transverse sections from 4 day old embryos. (A) Uninjected at 400X. (B) Boxed area in Panel A at 1000X. (C) *anks6* morphant at 1 ng dose of *anks6* MO at 400X. (D) Boxed area in Panel C at 1000X. Nc: notochord; Pd: pronephric duct; T: pronephric tubule; G: glomerulus; asterisk: cysts. Sections are representative of embryos examined (n=9).

CHAPTER V

DISCUSSION

Summary and conclusions

Cystic kidney diseases are a heterogenous group of clinically relevant genetic disorders having a similar morbidity-associated phenotype and kidney pathology. Given that a multitude of cystic diseases with distinct underlying genetic defects share specific phenotypic aspects, it is likely that a common molecular mechanism of cyst formation has evolved. Therefore, for more than a decade extensive studies have been instituted in animal models to investigate the mechanism of cyst initiation and disease progression, in an effort to glean information to use in the treatment of human polycystic kidney disease (PKD). Abnormalities common in all models of polycystic kidney disease include increased cell proliferation and apoptosis, alterations in cell matrix composition, reversal of renal epithelial apical-basolateral cell polarity and increased luminal fluid accumulation (265).

Several rodent models have been established that mimic aspects of human PKD as related to the age of onset and the morphology and location of cysts (Figures 2.7 and 2.8). Rodent models have been instrumental in the identification of novel genes required for the establishment of normal renal epithelial morphology and function. Studies in these models have greatly increased the current understanding of the molecular etiologies of PKD. In one

such model, the *juvenile congenital polycystic kidney* (*jcpk*) mouse, the cystic kidney phenotype is caused by defects in the *bicaudal C* (*Bicc1*) gene.

The objective of the current body of work is to investigate the biological role of *Bicc1* as it relates to cyst formation. Similar to its *Drosophila* counterpart, the mammalian Bicc1 protein contains N-terminal K homology (KH) domains and a C-terminal sterile alpha motif (SAM) domain (Figure 4.1). These functional domains are highly conserved among 11 diverse species, suggesting that they are vital to Bicc1 function (Tables 4.2 and 4.3). It is well documented that KH domain-containing proteins bind and regulate RNAs while SAM domain-containing proteins participate in protein interactions (57, 148, 156-163, 172, 173, 180, 234, 238, 239). However, the specific RNA targets, mode of post-transcriptional regulation or identification of interacting proteins of mammalian Bicc1 are not known.

In these studies, we examined the RNA binding properties of the mammalian Bicc1 protein. Our data demonstrate that mouse Bicc1 is able to bind synthetic RNA in vitro (Figure 4.2) and that this binding is mediated by its KH domains (Figure 4.3), similar to what was described previously in *Drosophila* (142). Many RNA binding proteins exhibit differential binding of specific nucleotide sequences (i.e., U>G>C/A) (164, 232, 234, 266). Our studies established that Bicc1 binds preferentially to poly(G) and poly(U) synthetic RNAs (Figure 4.2). Interestingly, binding of Bicc1 to poly(U) was significantly decreased under high salt conditions, while binding to poly(G) was unaffected, suggesting that Bicc1 has a higher affinity for poly(G). We show that the third KH

domain, KH3, is important and sufficient for binding RNA (Figure 4.3). In

Drosophila, two alleles which exert a strong bicaudal phenotype, *BicC^{RU35}* and

BicC^{AB79} affect the third KH domain. The *BicC^{AB79}* allele deletes portions of both

KH2 and KH3, while the *BicC^{RU35}* allele replaces a consensus glycine with an

arginine residue in the RNA-binding motif of KH3 (142). These data support our

finding that the KH3 domain is important for Bicc1 function. Additionally, amino

acid sequence comparisons of Bicaudal C across 11 different species reveal a

great deal of conservation in all three KH domains (Table 4.3). In all cases, the

KH2 and KH3 domains contain a more consistent GxxG binding motif than does

KH1 (Table 4.1). Structural analysis indicates that this tetrapeptide, a key

characteristic of KH domains, is located between the first two α-helices of the KH

domain structure and is predicted to be an unstructured surface loop important

for nucleotide binding (158, 232). The consensus of this region in KH2 and KH3

of Bicc1 suggests that these domains may be the regions directly involved with

the binding of target RNA sequences. Based on the studies described earlier in

Drosophila, it is likely that Bicc1 regulates multiple RNAs; therefore, it is possible

that the KH2 and KH3 domains confer binding specificity for binding different

target RNAs. Interestingy, another strong allele in *Drosophila*, *BicC^{IIF34}*, has a

mutation downstream of the KH domains which results in a frameshift and

premature stop, truncating the protein and eliminating the C-terminal SAM

domain, but leaving the KH domains presumably intact (142). This suggests that

the C-terminal portion of Bicc1 is also important to BicC function; either through

interactions of the SAM domain or perhaps it is simply necessary to maintain the

secondary structure or stability of the protein. However, recent studies in

Xenopus where *Bicc1* has been transiently knocked down using antisense

morpholinos demonstrated that only the portion of Bicc1 containing the KH

domains, and not the SAM, could rescue the defective phenotype by recovering

the expression of terminal differentiation genes in the late distal pronephric tubule

of *bicc1* morphants (145). It is important to note that the studies presented here

were all performed in vitro with synthetic ribohomopolymers and that the KH

domains may behave differently in vivo.

Several reasons have been proposed to explain the presence of multiple

KH domains in RNA binding proteins. In other proteins containing multiple KH

domains different RNA binding properties have been described. The hnRNP

protein, which contains three KH domains, shows enhanced RNA binding

capability when all three KH domains are present than when only single KH

domains were present (163), suggesting that in this protein, the KH domains bind

their target RNAs in a cooperative fashion. However, in studies involving Nova-

1, which also contains three KH domains, the KH3 domain alone was sufficient

for RNA binding (160). Our data indicate that Bicc1 is similar to Nova-1 in that

the third KH domain is important for binding and this binding does not seem to

require the cooperation of the other KH domains (Figure 4.3). In vitro studies

involving the *Drosophila* P-element somatic inhibitor protein (PSI), containing four

KH domains show that mutations in KH2 and KH3 were more deleterious to RNA

binding capability than mutations in the outer KH domains (KH1, KH4) (168).

The authors also demonstrate using various lengths of in vitro transcribed PSI

target RNA, that the participation of multiple KH domains in RNA binding allows the recognition of a longer and more specific RNA sequence than can be discerned by a single KH domain. Collectively, these data suggest that while individual KH domains may be able to bind RNA, the presence of multiple KH domains in tandem may be important to form specific and stable interactions with target RNAs.

In some multiple KH domain-containing proteins, the relative importance of each KH domain seems to vary with the RNA target. For example, the *Xenopus* Vg1RBP protein consists of four KH domains and two RNA recognition motifs (RRM). A recent study examined the contributions of each KH domain of Vg1RBP to RNA binding through UV crosslinking to ^{32}P-labeled *vegetal localization element* (*Vle)* RNA and in vitro binding to poly(C) homoribiopolymers (267). The authors demonstrate different crosslinking efficiencies of the individual KH domains to the same RNA (*Vle*), with KH1 and KH3 playing a greater role. Conversely, the KH1 and KH2 domains are required for efficient binding of poly(C). Additionally, the authors noted cooperative binding of the KH domains to *Vle*, while binding appeared to be additive when poly(C) was the target. Similar results were achieved in studies involving the human Vg1RBP homolog, IMP-1 (167), suggesting that individual KH domains may play a role in the affinity and binding specificity of the protein to different target RNAs. Interestingly, the KH3 and KH4 domains of Vg1RBP promote self-association which is stabilized by RNA, suggesting a potential role for KH domains in not only RNA-protein interactions but also protein-protein interactions (267). Similar

studies involving the RNA binding proteins Sam68, GRP33, GLD-1, and Qk1 demonstrated self association mediated by the KH domains in a RNA-dependent manner (268). These properties of KH domains may be important in the formation of RNA-regulating multiprotein complexes.

While mutations in *bicaudal C* lead to early developmental defects in *Drosophila* and *Xenopus*, mice with mutations in *bicaudal C* instead develop polycystic kidneys (3). The *Bicc1^{jcpk}* allele results in a frameshift and premature stop codon resulting in a truncation. This truncated protein is missing most of KH1, all of KH2 and KH3 and the entire SAM domain (3). We predict that the Bicc1^{jcpk} protein is non-functional. In our binding assays, a recombinant protein representing the predicted Bicc1^{jcpk} protein was unable to bind poly(U) homoribopolymers (Figure 4.3). We hypothesize that the RNA-binding function of Bicc1 is necessary for the development of normal renal tubules and that abrogation of this function contributes to cyst formation, which is the hallmark of polycystic kidney disease. While mutations in many different genes can lead to polycystic kidney disease, this is the first evidence of a RNA binding protein as the causative agent in polycystic kidney disease.

However, KH domain-containing proteins have been implicated in a number of other diseases. FMRP, the protein responsible for Fragile X syndrome, contains two KH motifs and has been shown to associate with polyribosomes, mediate RNA binding and post-trascriptionally regulation protein translation (162, 269-271). Additional studies have established that mutations in either of the FMRP KH domains, including the I$_{304}$N mutation in KH2 which is

associated with severe mental retardation (272), affect RNA binding in vitro (237). Nova-1 and Nova-2 are target antigens in paraneoplastic opsoclonus myoclonus ataxia (POMA) (273, 274). Patients with this neurogenerative disorder have high levels of auto-antibodies directed to the Nova KH domains, which disrupt the ability of the Nova proteins to bind RNA (160, 233, 273, 274).

There is increasing evidence that aberrant Wnt signaling (Figure 2.6) contributes to the pathogenesis of polycystic kidney disease (9, 11, 45, 124, 125, 138, 139, 190, 199), however, a direct link between *Bicc1* and Wnt signaling has not been investigated. Wnt signaling is essential during all phases of kidney organogenesis (93, 97-99, 111, 114, 115, 118, 120, 167). Recent reports indicate that the PKD-associated ciliary protein Inversin acts as a molecular switch between different branches of Wnt signaling, inhibiting the canonical (standard) pathway and inducing the non-canonical (planar cell polarity, PCP) cascade in kidney epithelial cells (139). Canonical Wnt signaling is mostly involved in proliferation and cell fate specification, while the PCP pathway regulates cell migration and polarity. It has been proposed that the transition from canonical to PCP signaling is imperative for the proper establishment and maintenance of renal tubular architecture, polarity and integrity (61).

To explore the possibility that Wnt signaling plays a role in cyst development in the *jcpk* mouse model for PKD, we performed a PCR Superarray analysis specific to the Wnt pathway (Figures 4.4 and 4.5), followed by confirmatory qRT-PCR (Figure 4.8), identifying two Wnt-related genes, *Casein kinase II* (*CK2*) and *Frizzled 6* (*Fzd6*), that were upregulated in the kidneys of

Bicc1^{jcpk}/Bicc1^{jcpk} affected mice when compared to wild type controls. Our data

demonstrate that the observed increase in gene expression of *CK2* translates to

an increase in CK2 protein expression in the kidneys of *Bicc1^{jpck}/Bicc1^{jcpk}* mice

versus wild type controls (Figure 4.9). CK2 activity is tightly controlled through

various mechanisms including protein kinase C and inositol phosphates (275-

279) and previous work demonstrated that CK2 kinase activity directly correlates

with protein expression levels (280); therefore we suspect that CK2 activity is

also increased in the kidneys of *Bicc1^{jpck}/Bicc1^{jcpk}* affected mice.

Casein kinase 2 (CK2) is a ubiquitous, pleiotropic serine/threonine kinase

involved in the regulation of cell signaling, protein expression and ion channel

activity (281). Studies in mice show high levels of *CK2* expression in all tissues

involved in organogenesis beginning at mouse embryonic day 16.5 (280) and

CK2 kinase activity is significantly increased in human kidney tumors (282). CK2

positively regulates canonical Wnt signaling by stabilizing the active forms of the

main effectors of the pathway, cytoplasmic Dishevelled and β-catenin (121-123).

Of interest, CK2 has also been shown to interact with Polycystin 1 (PC1) and

modify Polycystin 2 (PC2) by phosphorylation (124). It is hypothesized that

binding of CK2 to PC1 allows the close proximity of CK2 to Polycystin-2 (PC2),

which associates with PC1 at the ciliary membrane of renal epithelial cells to

form a semi-permeable calcium channel. Studies have shown that constitutive

phosphorylation of PC2 by CK2 results in increases in channel sensitivity and

activity (283), resulting in an increase of intracellular calcium and subsequent

activation of calcium-dependent enzymes, including calcineurin. One substrate

of calcineurin phosphatase activity is nuclear factor activated T-cell (NF-AT), a

transcription factor that is normally phosphorylated and sequestered at the

membrane. The removal of phosphate groups from NF-AT allows it to

translocate to the nucleus where it stimulates transcription of cytokine genes

(284). Cytokines promote canonical Wnt signaling (285-287), therefore, CK2

may function to activate the canonical Wnt pathway at two different cellular

levels.

Interestingly, *Frizzled 6* (*Fzd6*) represses canonical Wnt signaling

downstream of β-catenin through activation of calcium-calmodulin-dependent

kinase 2 (CaMK2), which activates the NEMO-like kinase pathway. NEMO-like

kinase phosphorylates the TCF/LEF transcription factors, masking their DNA

binding domains and preventing transcription of Wnt target genes (127). Frizzled

6 is also one of the subset of Frizzled family receptors that is known to promote

the PCP and Ca^{2+} branches of Wnt signaling. *CK2* expression is upregulated 3

fold, while *Fzd6* is upregulated 2.2 fold in the absence of *Bicc1* (Figure 4.8). It is

interesting that these two genes are upregulated in the *jcpk* mouse model as they

seemingly demonstrate antagonistic downstream effects. We hypothesize that in

normal kidney cells, Bicc1 regulation ensures the appropriate levels of CK2 and

Fzd6 proteins required to preserve the balance between the canonical and PCP

Wnt signaling pathways necessary for the maintenance and homeostasis of

kidney tubules.

To determine whether *CK2* or *Fzd6* are RNA targets of Bicc1, we

immunoprecipitated Bicc1 from mouse IMCD cells and examined the precipitated

material by RT-PCR for the presence of *CK2* or *Fzd6* RNAs (Figure 4.10). In

addition to these two Wnt-related RNAs, we decided to examine whether Bicc1

may regulate the RNA of another PKD-related gene, *Nek1*. Mutations in *Nek1*

are the underlying cause of polycystic kidney disease in the *kat* mouse model

(183). *Nek1* belongs to a family of NIMA-related kinases that are known to be

involved in cell cycle control, growth and differentiation (186). The *Nek1* protein

has been shown to localize to the basal bodies and centrosomes of primary cilia

(43, 48). The reason we are interested in this gene is that previous work

described a 5-6 fold decrease in the expression of the *Nek1* in mice homozygous

for the *Bicc1^{jpck}* allele (153). Therefore, we also investigated whether *Nek1* may

be a target for Bicc1 regulation. We utilized primers detecting *GAPDH* and β-

actin as negative controls, as we already demonstrated that expression of these

genes are unaltered in *Bicc1^{jpck}*/*Bicc1^{jpck}* affected mice. Our data provide

evidence that *CK2* and *Nek1* RNAs are present in the Bicc1 protein

immunoprecipitate, suggesting that they may be RNA targets of Bicc1 (Figures

4.11, 4.12). Interestingly, β-*actin* and *GAPDH* transcripts were also detected in

the Bicc1 protein immunoprecipitate (Figures 4.11, 4.12). This is not entirely

surprising, as *Drosophila BicC* has been shown to regulate components of the

actin cytoskeleton (147). GAPDH serves an additional function in the cell

besides being involved in glycolysis; it is also an inducer of apoptosis (246, 247).

An increase in apoptosis is one of the hallmarks of PKD (60) and microarray data

implicate increased expression of pro-apoptotic genes coupled with decreased

expression of anti-apoptotic genes in the *jcpk* mouse model (153). As

mentioned, previous experiments demonstrated that the transcript levels for β-actin and *GAPDH* are unchanged in *Bicc1^{jcpk}/Bicc1^{jcpk}* homozygous mice (Figure 4.7). One explanation for this is that these housekeeping genes are most likely tightly regulated by multiple mechanisms within the cell and while Bicc1 may truly interact with these RNAs, the loss of *Bicc1* alone does not result in aberrant gene expression. Taken together, these data provide the first evidence linking Bicc1 to both Wnt signaling and the primary cilia, supporting our hypothesis that Bicc1 may function downstream or parallel to the ciliary pathway leading to cystogenesis.

Mutations in *Bicc1* and *Anks6* result in polycystic kidney disease in the *jcpk* mouse and Han:SPRD *+/Cy* rat models for PKD, respectively (3, 179); however, the function of the corresponding proteins, Bicc1 and SamCystin, are unknown. SamCystin contains ten ankryin repeats (ANK) at the N-terminus and a sterile alpha motif (SAM) domain at the C-terminus (Figure 4.34). ANK and SAM domains are common functional motifs found in a wide variety of proteins and have been well documented as protein-binding modules (288, 289). Other proteins containing ANK and SAM domains, including Shank, tankyrase, and Sans function as scaffolding proteins, forming large protein complexes via self-association, while also binding multiple interaction partners (290-292).

The presence of a SAM domain in both the Bicc1 and SamCystin proteins led us to examine whether these proteins physically interact. Until now, there were no known protein-binding partners for Bicc1 or SamCystin. In this study, we show that Bicc1 and SamCystin co-localize in the cytoplasm of mouse inner

medullary collecting duct (IMCD) cells (Figures 4.13 and 4.14) (57). This agrees

with previously published in situ hybridization data demonstrating specific

cytoplasmic localization of *Anks6* mRNA in rat proximal tubules (179). Co-

immunoprecipitation assays demonstrated that Bicc1 and SamCystin interact

(Figure 4.18) and that the interaction is mediated by the SAM domain of

SamCystin and the KH domains of Bicc1 (57). This was surprising because the

primary function of KH domains is RNA-binding; however some studies have

demonstrated a role for KH domains in self-association (268). To establish

whether the KH domains of Bicc1 were involved directly in the protein interaction

or indirectly through a RNA intermediate, we performed the co-immuno-

precipitation experiments in the presence of an RNase. RNase treatment

abrogated the interaction between Bicc1 and SamCystin, suggesting that these

proteins interact indirectly in a RNA-dependent manner (Figure 4.20). Similar to

other ANK and SAM domain-containing proteins, a recent study found that

SamCystin self-associates and interacts with other proteins and deletion of either

the ANK or SAM domains abolished SamCystin self-association (57). These

data suggest that both the ankyrin repeats and the SAM domain are necessary

for the interaction and are consistent with a model whereby SamCystin proteins

associate via interactions between the ankyrin repeats of one SamCystin protein

and the SAM domain of another SamCystin protein, in a 'head to tail' fashion

(Figure 4.21). It cannot be ruled out, however, that the inability of SamCystin to

self-associate in the absence of either the ANK or SAM domain may be due to

gross alterations in protein conformation. The single amino acid change that is

linked to PKD in the *Cy* rat occurs at a highly conserved residue within the SamCystin SAM domain, suggesting that it is functionally important (179) The presence of this arginine-to-tryptophan change was shown to disrupt SamCystin self-association (57).

Taken together, the association of Bicc1, a RNA-binding protein, with SamCystin, a probable scaffolding protein, suggests that SamCystin and Bicc1 may act together to localize and regulate the translation of specific mRNAs that are important in the kidney. We propose a model (Figure 4.21) in which SamCystin homomers associate in a head-to-tail manner, while the SAM domains interact with another as yet unidentified protein or protein complex that concurrently binds to specific RNAs, perhaps *Bicc1* RNA. Bicc1 would associate with these specific RNAs via its KH domains, thus the interaction between Bicc1 and SamCystin is indirect, facilitated by a RNA intermediate (Figure 4.21). This model could explain how the KH domains of Bicc1, which so far have only been described as nucleic acid-binding or self-association modules (293) are critical for the Bicc1-SamCystin interaction.

Collectively, our data support the hypothesis that SamCystin and Bicc1 act together in a common molecular pathway, perhaps to regulate translation of particular mRNAs, although the exact mechanisms are unclear. Perhaps SamCystin is important in the recruitment of other RNA-binding proteins necessary to promote the interaction of Bicc1 with polyadenylation proteins and prompt RNA degradation. Further studies are required to elucidate the effects of the Bicc1-SamCystin interaction on the expression of specific genes.

Several PKD-disease genes encode proteins that localize to the primary cilium or basal body of renal epithelial cells (Table 2.1, Figure 2.5) and defects in these proteins result in abnormal cilia structure or function that leads to cystogenesis (48, 51-53). Importantly, we show that Bicc1 and SamCystin do not localize to the primary cilia or basal bodies (Figure 4.16)(57), providing further evidence that these proteins function downstream of cilia-related proteins or in a parallel cilia-independent pathway. Furthermore, studies in the frog and zebrafish demonstrate that morpholino-induced knockdown of *bicc1* does not affect the number or length of primary cilia in the pronephric kidney, providing evidence that *bicc1* is not involved in cilia formation (Figure 4.29) (5, 294). Continued elucidation of additional proteins that interact with SamCystin or Bicc1, as well as the identification of in vivo RNA targets of Bicc1 will provide important clues to understanding how these proteins function in the mammalian kidney. This in turn will provide a better understanding of the underlying molecular pathways that are perturbed due to mutations in either *Bicc1* or *Anks6*.

Armed with the information that these two PKD-related proteins interact, we set out to generate zebrafish animal models with which to accelerate the studies of the roles of *Bicc1* and *Anks6* in cystogenesis. The primary goal of this study was to demonstrate evolutionary conservation of *Bicc1* and *Anks6* function in the kidneys of zebrafish and rodents, validating the use of a zebrafish model as a complementary alternative system in which to study the roles of *Bicc1* and *Anks6* in cystogenesis.

Two conserved zebrafish homologs of *bicc1* and a single zebrafish *anks6* ortholog were identified using Basic Local Alignment Search Tool (BLAST) (Ensembl assembly Zv8) (Table 4.5). Since zebrafish genomes have undergone an additional round of duplication compared to mammals (256, 257), it is not unexpected to find multiple *bicc1* genes. Protein analysis using MotifScan (155) demonstrated that zebrafish bicc1a and bicc1b, similar to mouse, consist of three tandem KH domains and a C-terminal SAM domain (Figures 4.22 and 4.31). Likewise, zebrafish SamCystin, similar to rat has 10 ankyrin repeat regions and a C-terminal SAM (Figure 4.34). While the amino acid sequences of the zebrafish bicc1 and SamCystin proteins were overall very similar to their mammalian counterparts (44-60%), we observed an even higher degree of conservation (59-95%) in the regions of the functional domains, suggesting that these domains are important (Tables 4.3 and 4.11; Figures 4.22, 4.31 and 4.34).

To determine whether these genes are expressed in the developing kidneys (pronephros) of zebrafish, we examined the spatial and temporal expression patterns of *bicc1* and *anks6* in zebrafish embryos. RT-PCR data demonstrated that *bicc1a, bicc1b* and *anks6* are temporally expressed throughout all stages of zebrafish pronephros (kidney) development (Figures 4.23, 4.32 and 4.35). In situ hybridization demonstrated specific expression of zebrafish *bicc1* in the pronephric tubules and collecting ducts, as well as at the midbrain-hindbrain boundary (Figure 4.23). In the mouse, *Bicc1* is strongly expressed in heart and kidney, weakly expressed in the testes, and not present at all in the lung, brain, spleen, liver or skeletal muscle (143). It is important to

note that the sequence of the EST probe used for in situ hybridization overlaps with part of the KH domains; therefore, due to the conservation of this region, it is possible that the observed expression pattern represents both *bicc1a* and *bicc1b*. Unfortunately, efforts to delineate the specific expression of each gene using several additional ESTs (specific to the sequence of either *bicc1a* or *bicc1b*) as probes as well as probes generated by PCR-cloning of the 3'-UTR regions of *bicc1a* and *bicc1b* were unfruitful. However, given that we detect *bicc1* in two distinct tissues (brain and kidney) and expression in the brain is inconsistent with *Bicc1* expression in the mouse, it is tempting to consider that perhaps these represent distinct patterns of the two genes; *bicc1a* in the kidney and *bicc1b* in the brain. Often, paralogous genes persist in zebrafish because they have diverged and acquired distinct functions (258, 259). We hypothesize that this may be the case with *bicc1a* and *bicc1b* in part because of the results of our morpholino studies. We established that morpholino gene knockdown of *bicc1a* using a morpholino specific to only *bicc1a* (Table 4.9) results in the formation of cystic kidneys, strongly suggesting that *bicc1b* function is not redundant of *bicc1a* function. We hypothesize that *bicc1a* and *bicc1b* have developed separate and distinct functions in the zebrafish, with *bicc1a* being important in kidney development and PKD.

While RT-PCR indicates that *anks6* expression is continuous in the early embryonic and larval stages of zebrafish development (Figure 4.35), we were unable to determine the spatial expression pattern of *anks6* in the zebrafish embryo by in situ hybridization. One explanation is that *anks6* expression levels

159

may be below the detection limit of the in situ hybridization assay (261-263),

however increasing the amount of probe, which should saturate binding of the

target sequence, did not rectify the problem. Interestingly, similar problems were

met when these studies were attempted in the mouse embryo (personal

communication, Glasco and Chandrasekhar).

To investigate the consequence of the loss of *bicc1a* and *anks6* function,

we utilized antisense morpholino oligonucleotides to transiently knockdown the

genes in zebrafish embryos. We show that the morpholino-induced loss of

zebrafish *bicc1a* or *anks6* results in abnormal morphology (Figures 4.25, 4.28

and 4.36) as well as the formation of kidney cysts (Figures 4.27 and 4.37) and

that the *bicc1a* cystic phenotype can be reversed with the addition of mouse

Bicc1 (Figure 4.30)*,* suggesting that mouse and zebrafish *Bicc1* are evolutionarily

conserved. Two distinct morpholinos specifically targeting *bicc1a* or *anks6* were

used in these studies and yielded similar phenotypes and penetrance,

suggesting that the cystic phenotypes are a direct result of the loss of *bicc1a* or

anks6 function. Similar to human ADPKD, *bicc1a* morphants exhibit cysts in all

parts of the nephron, including the glomerulus, pronephric tubules and

pronephric ducts (Figure 4.27). The ability to rescue this cystic phenotype using

mouse *Bicc1* mRNA is further evidence that the role of zebrafish and mouse

Bicc1 in the kidney is conserved.

Numerous PKD-associated protein localize to the primary cilia, suggesting

that the structure and/or function of cilia is important in cystogenesis (295).

Likewise, a number of cystic zebrafish mutants are due to defects in genes

known to be involved in ciliogenesis or maintenance (50, 195). Electron microscopy studies of *Bicc1^{jcpk}/Bicc1^{jcpk}* homozygous affected mice reveal morphologically normal cilia present on the apical surface of the renal epithelial cells (Bryda, unpublished data) and we have demonstrated that the mouse Bicc1 protein does not localize to the primary cilia of IMCD cells (Figure 4.16). In addition, *Xenopus* embryos injected with morpholinos to knockdown expression of *bicc1* display a cystic phenotype but do not have any obvious differences in the number or length of cilia (5). To assess the primary cilia in zebrafish *bicc1a* morphants, we examined embryos using a fluorescent immunostaining technique for acetylated α-tubulin, a marker for cilia. Similar to the previous study in *Xenopus*, the zebrafish *bicc1a* morphants revealed no apparent defects in cilia (Figure 4.29). Additionally, fluid flow through the pronephros was not compromised (Figure 4.29). Based on all of these independent pieces of data, we propose that *Bicc1* is not involved directly in the structure or function of cilia but instead, in either a downstream or parallel cilia-independent pathway that when perturbed, leads to cystogenesis.

The precise molecular function of mammalian *Bicc1* in the kidney is unclear. *Drosophila* BicC localizes RNA and regulates translation by interacting with components of the polyadenylation machinery, and associating with specific mRNAs, including the 5'-UTR of its own mRNA (142, 147, 296, 297). Studies in *Xenopus* suggest that it is the KH domains and not the SAM domain that are important for Bicc1 function in the pronephros (5). A recent report indicates that *Xenopus* Bicc1 functions to repress translation of Polycystin 2 (PC2)(298).

Furthermore, the investigators indicate that Bicc1 and PC2 work together and that PC2 is required for the activity of Bicc1. Interestingly, in this report, Bicc1 protein expression was noted in P-bodies, cytoplasmic processing centers involved in mRNA turnover and in sequestering mRNAs away from the translational machinery. Unlike *Drosophila*, in mice and zebrafish, mutations in *Bicc1* do not result in developmental defects, but instead lead to cyst formation in the kidney. Previous to the current body of work, the RNA and protein targets of mammalian Bicc1 were unknown. The current research provides the first evidence of involvement of a RNA binding protein in polycystic kidney disease, identifies another PKD-related protein, SamCystin as a protein-binding partner of Bicc1 and identifies four potential RNA targets of Bicc1 regulation, supporting earlier reports of Bicc1 regulation of cytoskeletal components in *Drosophila* and, most importantly, providing the first evidence linking Bicc1 to Wnt signaling and primary cilia. Additionally, a new alternative zebrafish model was established and characterized for the further study of *Bicc1* function in vivo. The use of this comparative zebrafish model will allow us to readily and rapidly delineate the precise functional role of *Bicc1* in terms of cyst formation and PKD pathogenesis.

Future directions

The establishment of a *Bicc1* zebrafish animal model for PKD and the identification of putative RNA targets as well as a novel protein-binding partner of Bicc1 in kidney epithelial cells are preliminary steps in elucidating the molecular pathways involving *Bicc1* in relation to the pathogenesis of PKD in the *jcpk*

mouse model. More information is needed to better define the specific biological role of *Bicc1* in normal kidney development and organogenesis.

To further strengthen the *bicc1* zebrafish PKD model, we should attempt to rescue the *bicc1a* morphants using a *Bicc1^jcpk^/Bicc1^jcpk^* mutant RNA. Since the Bicc1^jcpk^ protein is predicted to be non-functional, we hypothesize that the co-injection of *Bicc1^jcpk^/Bicc1^jcpk^* RNA with the *bicc1a* MO will not be able to rescue the cystic phenotype of the morphants. I have already generated an expression construct representing the *Bicc1^jcpk^* allele; therefore these studies can be readily accomplished.

Additionally, since we have established a link between *Bicc1* and Wnt signaling, it would be interesting to evaluate the effects of Wnt and CK2 inhibitors on the developing zebrafish embryos. Small molecules can easily be added to the water of *bicc1a* MO injected embryos and thus we can investigate whether such inhibitors are able ameliorate cyst formation in this model. These studies would allow us to determine if aberrant Wnt signaling is a major factor in cyst formation in the *jcpk* model. A zebrafish model also facilitates genetic interaction studies. Therefore, we can investigate whether there is a genetic interaction between *bicc1a* and members of the Wnt pathway, particulary the PCP pathway, as this seems to be important in the kidney.

In our studies to develop an *anks6* zebrafish model for PKD, we observed a low penetrance of the morpholino, with only 25-40% of the embyros having the abnormal phenotype. This phenomenon makes it difficult to attempt to correct the phenotype with rat *Anks6* RNA, as it would be impossible to distinguish

between rescued embryos and those that were not affected by the morpholino.

To address this issue, we need to establish the optimal dose of both *anks6*

morpholinos for co-injection which yields a penetrance of at least 80% of the

embryos having the phenotype. Additionally, we have already generated *Anks6*

deletion constructs containing either the ANK domains only or the SAM domain

only; therefore, we could also attempt to rescue the *anks6* cystic morphants with

these RNAs and determine which domain(s) is most important in cystogenesis.

These experiments will provide evidence as to whether *Anks6* is evolutionarily

conserved in zebrafish and rat.

Importantly, unlike the *jcpk* mutation which presumably represents a total

loss of protein function, the mutation in *Anks6* responsible for the PKD phenotype

in the Han:SPRD *+/Cy* rat model is a point mutation within the SAM domain. The

effects of this mutation are not known, although it has been shown to inhibit self-

association and is predicted to decrease the stability of the protein (57). Studies

in the rat using a lentivirus transgene delivery of mutant *Anks6* and GFP reporter

into normal rat embryonic stem cells and subsequent implantation into a recipient

female were performed in an attempt to produce an in vivo transgenic rat model

for PKD (Stagner and Bryda, unpublished data). The lentivirus system results in

the random insertion of multiple copies of the transgene; therefore, depending

upon the insertion sites, it is possible to have overexpression of the transgene.

We hypothesize that the mutant SamCystin protein may act in a dominant

negative fashion, as no rats positive for the transgene were ever produced. This

can easily be tested in zebrafish by injecting the *Anks6* mutant RNA and

evaluating the embryos for a dominant-negative effect. Accomplishment of these short term goals will bring us closer to understanding the roles of *Bicc1* and *Anks6* in normal kidney pathology.

We have shown that the Bicc1 and SamCystin proteins interact and we hypothesize that they function together in a pathway downstream of primary cilia-associated proteins or in a parallel cilia-independent pathway. Our data indicates that the cilia in *bicc1a* morphants are not affected; however we have not yet evaluated the cilia in the *anks6* morphants. Therefore this is another area for further investigation.

We would also like to explore whether other proteins interact with Bicc1 and SamCystin. Tandem Affinity Purification (TAP) can be used to identify potential binding partners. A commercially available TAP system is available (Stratagene, LaJolla, CA). The strategy is to clone *Bicc1* and *Anks6* into a TAP expression vector containing two tandem affinity tags, a streptavidin binding peptide (SBP) and a calmodulin binding peptide (CBP) and use this construct to transfect mammalian cells in culture. The proteins are purified in a two step method, first by applying the cell lysate to a streptavidin column to bind the protein of interest and wash away other proteins. The protein of interest is eluted with biotin and applied to a second column containing calmodulin, which will bind the protein of interest. The column is washed to remove any remaining contaminants and the protein and its binding partner(s) are released by removing calcium from the column with a chelator. These elution conditions are very gentle and do not disrupt protein-protein interactions. Plus the two-step

purification leads to an ultra-pure sample of the protein of interest and any binding partners. The purified interacting complex can then be analyzed by SDS-PAGE and Western blot analysis. Our data demonstrates that Bicc1 and SamCystin interact indirectly through an RNA intermediate. As proposed in our model, we hypothesize that there also exists another protein complex that facilitates this interaction between SamCystin and the RNA. It is possible that Bicc1 may be involved in the recruitment of some of these proteins. A more complete understanding of the complex interactions between these PKD-related proteins will help to define the critical biological pathways involved in cyst formation and PKD pathogenesis.

We identified several putative RNA targets of Bicc1; however, further investigation is required to confirm the interaction. One method would be to perform in vitro binding assays with in vitro transcribed RNAs (*CK2, Nek1, β-actin, GAPDH*) and purified recombinant Bicc1. To achieve this, purified recombinant Bicc1 protein would be incubated with in vitro transcribed RNAs in binding buffer supplemented with tRNA, a non-specific competitor, which reducs non-specific binding to the target RNAs and thus reduces noise in the system.

The resulting RNA-Bicc1 complexes can be resolved on a 6% TBE/polyacrylamide gel and visualized by ethidium bromide staining. In addition, to show specificity for the RNA-Bicc1 interaction, a separate set of binding reactions would be analyzed which include the Bicc1-specific antibody. Under UV illumination, those RNAs which interact with Bicc1 will migrate through the gel more slowly resulting in a mobility shift; the binding reactions which included the

166

Bicc1-specific antibody will demonstrate a supershift. To verify that the mobility

shifts are specifically due to RNA-Bicc1 complex formation, we can excise the gel

bands and analyze them by Western blot analysis using the Bicc1-specific

antibody.

Once we have confirmed that these RNAs interact with Bicc1, we would

want to investigate which region of the Bicc1 protein is required to maintain the

interaction. We can begin to narrow the region using the recombinant deletion

proteins we created for our in vitro RNA binding assays in our in vitro binding and

mobility shift experiments. We could induce specific mutations in each of the KH

domains by PCR, perhaps in the GxxG consensus, to determine how these

mutations affect RNA binding capability. Additionally, it would be beneficial to

know what sequence/motif within the target RNA is the Bicc1 binding region.

This could be accomplished by repeating the in vitro binding assays using

various regions of the target RNA sequences. These experiments may also

provide insight into other protein-binding partners of Bicc1 which contain a similar

sequence/motif.

One of the most important areas of research to explore is the nature by

which Bicc1 regulates its target RNAs. Studies in *Drosophila* demonstrated that

BicC represses its own translation (147). We can investigate this in vitro by

incubating in vitro transcribed RNAs with Bicc1 recombinant protein and

subsequently translating the RNA in the presence of ^{35}S methionine (299, 300).

An aliquot of the reaction can be analyzed by SDS-PAGE and phosphorimaging

to determine if Bicc1, like *BicC* in *Drosophila*, represses translation of its target

RNAs. An alternative method to assess mRNA translation efficiency is to quantify the amount of a given RNA associated with polyribosomes (301). This could be accomplished by comparing the association of putative Bicc1 target RNAs with polyribosomes in cytoplasmic extracts from the kidneys of $Bicc1^{jcpk}/Bicc1^{jcpk}$ and wild type mice. Understanding the mode of Bicc1 regulation on its target RNAs may begin to provide some insight into the processes that Bicc1 helps to control and thus begin to outline the mechanism of cyst formation in the *jcpk* mouse model.

APPENDIX A

List of primers used for in vitro RNA binding assays:

	Forward 5' to 3'	Reverse 5' to 3'
Full-length (a.a. 1-934)	CACCATGGCCTCGCAGAGC	GAGATTGCCAGCAGCATTTTCCCT
Bicc1^{jcpk}/Bicc1^{jcpk} (a.a. 1-93)	CACCATGGCCTCGCAGAGC	GAGATTGCCAGCAGCATTTTCCCT
KH1 (a.a. 1-132)	CACCATGGCCTCGCAGAGC	GCTTTTTGTGTCTAAGACAGAC
KH2 (a.a. 125-209)	CACCATGTCTGTCTTAGACACA	CAGCACCAAAGGAAGCAGCTCCG
KH1+KH2 (a.a. 1-209)	CACCATGGCCTCGCAGAGC	CAGCACCAAAGGAAGCAGCTCCG
KH3 (a.a. 272-407)	CACCATGCTGTTGGAACACCTT	TAAGGCATTTCGCTCAACACT
KH2+KH3 (a.a. 125-407)	CACCATGTCTGTCTTAGACACA	TAAGGCATTTCGCTCAACACT
KH1+KH2+KH3 (a.a. 1-407)	CACCATGGCCTCGCAGAGC	TAAGGCATTTCGCTCAACACT

Recipes for zebrafish embryo medium solutions (217):

E3 zebrafish embryo medium

  1.0 ml Hank's Stock #1
  0.1 ml Hank's Stock #2
  1.0 ml Hank's Stock #4
95.9 ml milli-Q water
  1.0 ml Hank's Stock #5
  1.0 ml fresh Hank's Stock #6

Use approximately 10 drops of 1 M NaOH to bring pH to 7.2

Hank's Stock #1
8.0 g NaCl
0.4 g KCl
in 100 ml milli-Q water

Hank's Stock #2
0.358 g Na_2HPO_4, anhydrous
0.60 g KH_2PO_4
in 100 ml milli-Q water

Hank's Stock #4
0.72 g $CaCl_2$
in 50 ml milli-Q water

Hank's Stock #5
1.23 g $MgSO_4$ x $7H_2O$
in 50 ml milli-Q water

Hank's Stock #6
0.35 g $NaHCO_3$
in 10 ml milli-Q water

APPENDIX C

Gene chart for Wnt PCR Superarray (SABiosciences, cat# PAMM-043)

Position	Unigene	GeneBank	Symbol	Description
A01	Mm.180013	NM_010347	Aes	Amino-terminal enhancer of split
A02	Mm.7883	NM_007462	Apc	Adenomatosis polyposis coli
A03	Mm.23684	NM_009733	Axin1	Axin 1
A04	Mm.87600	NM_029933	Bcl9	B-cell CLL/lymphoma 9
A05	Mm.119717	NM_009771	Btrc	Beta-transducin repeat containing protein
A06	Mm.299735	NM_023465	Ctnnbip1	Catenin beta interacting protein 1
A07	Mm.273049	NM_007631	Ccnd1	Cyclin D1
A08	Mm.333406	NM_009829	Ccnd2	Cyclin D2
A09	Mm.246520	NM_007632	Ccnd3	Cyclin D3
A10	Mm.26908	NM_146087	Csnk1a1	Casein kinase 1, alpha 1
A11	Mm.216227	NM_139059	Csnk1d	Casein kinase 1, delta
A12	Mm.298893	NM_007788	Csnk2a1	Casein kinase II, alpha 1 polypeptide
B01	Mm.7286	NM_013502	Ctbp1	C-terminal binding protein 1
B02	Mm.246240	NM_009980	Ctbp2	C-terminal binding protein 2
B03	Mm.291928	NM_007614	Ctnnb1	Catenin (cadherin associated protein), beta 1
B04	Mm.87417	NM_172464	Daam1	Dishevelled associated activator of morphogenesis 1
B05	Mm.82598	NM_178118	Dixdc1	DIX domain containing 1
B06	Mm.214717	NM_010051	Dkk1	Dickkopf homolog 1 (Xenopus laevis)
B07	Mm.3400	NM_010091	Dvl1	Dishevelled, dsh homolog 1 (Drosophila)
B08	Mm.5114	NM_007888	Dvl2	Dishevelled 2, dsh homolog (Drosophila)
B09	Mm.258397	NM_177821	Ep300	E1A binding protein p300
B10	Mm.28017	NM_134015	Fbxw11	F-box and WD-40 domain protein 11
B11	Mm.4465	NM_013890	Fbxw2	F-box and WD-40 domain protein 2
B12	Mm.254739	NM_013907	Fbxw4	F-box and WD-40 domain protein 4
C01	Mm.4956	NM_010202	Fgf4	Fibroblast growth factor 4
C02	Mm.6215	NM_010235	Fosl1	Fos-like antigen 1
C03	Mm.4496	NM_008238	Foxn1	Forkhead box N1
C04	Mm.4573	NM_008043	Frat1	Frequently rearranged in advanced T-cell lymphomas
C05	Mm.314721	NM_011356	Frzb	Frizzled-related protein
C06	Mm.249525	NM_008045	Fshb	Follicle stimulating hormone beta

C07	Mm.246003	NM_021457	Fzd1	Frizzled homolog 1 (Drosophila)
C08	Mm.36416	NM_020510	Fzd2	Frizzled homolog 2 (Drosophila)
C09	Mm.243722	NM_021458	Fzd3	Frizzled homolog 3 (Drosophila)
C10	Mm.86755	NM_008055	Fzd4	Frizzled homolog 4 (Drosophila)
C11	Mm.150813	NM_022721	Fzd5	Frizzled homolog 5 (Drosophila)
C12	Mm.4769	NM_008056	Fzd6	Frizzled homolog 6 (Drosophila)
D01	Mm.297906	NM_008057	Fzd7	Frizzled homolog 7 (Drosophila)
D02	Mm.184289	NM_008058	Fzd8	Frizzled homolog 8 (Drosophila)
D03	Mm.200770	NM_019827	Gsk3b	Glycogen synthase kinase 3 beta
D04	Mm.275071	NM_010591	Jun	Jun oncogene
D05	Mm.209989	NM_032396	Kremen1	Kringle containing transmembrane protein 1
D06	Mm.255219	NM_010703	Lef1	Lymphoid enhancer binding factor 1
D07	Mm.274581	NM_008513	Lrp5	Low density lipoprotein receptor-related protein 5
D08	Mm.321990	NM_008514	Lrp6	Low density lipoprotein receptor-related protein 6
D09	Mm.2444	NM_010849	Myc	Myelocytomatosis oncogene
D10	Mm.30219	NM_027280	Nkd1	Naked cuticle 1 homolog (Drosophila)
D11	Mm.9001	NM_008702	Nlk	Nemo like kinase
D12	Mm.246804	NM_011098	Pitx2	Paired-like homeodomain transcription factor 2
E01	Mm.153107	NM_023638	Porcn	Porcupine homolog (Drosophila)
E02	Mm.260288	NM_019411	Ppp2ca	Protein phosphatase 2 (formerly 2A), catalytic subunit, alpha isoform
E03	Mm.294138	NM_016891	Ppp2r1a	Protein phosphatase 2 (formerly 2A), regulatory subunit A (PR 65), alpha isoform
E04	Mm.295009	NM_009358	Ppp2r5d	Protein phosphatase 2, regulatory subunit B (B56), delta isoform
E05	Mm.273605	XM_134865	Pygo1	Pygopus 1
E06	Mm.168257	NM_133955	Rhou	Ras homolog gene family, member U
E07	Mm.297431	NM_029457	Senp2	SUMO/sentrin specific peptidase 2
E08	Mm.281691	NM_013834	Sfrp1	Secreted frizzled-related sequence protein 1
E09	Mm.19155	NM_009144	Sfrp2	Secreted frizzled-related sequence protein 2
E10	Mm.42095	NM_016687	Sfrp4	Secreted frizzled-related sequence protein 4
E11	Mm.27842	NM_012030	Slc9a3r1	Solute carrier family 9 (sodium/hydrogen exchanger), isoform 3 regulator 1
E12	Mm.279103	NM_011441	Sox17	SRY-box containing gene 17
F01	Mm.913	NM_009309	T	Brachyury
F02	Mm.321330	NM_009332	Tcf3	Transcription factor 3
F03	Mm.31630	NM_009331	Tcf7	Transcription factor 7, T-cell specific
F04	Mm.278444	NM_011599	Tle1	Transducin-like enhancer of split 1, homolog of Drosophila E(spl)

F05	Mm.38608	NM_019725	Tle2	Transducin-like enhancer of split 2, homolog of Drosophila E(spl)
F06	Mm.32831	NM_011915	Wif1	Wnt inhibitory factor 1
F07	Mm.10222	NM_018865	Wisp1	WNT1 inducible signaling pathway protein 1
F08	Mm.1123	NM_021279	Wnt1	Wingless-related MMTV integration site 1
F09	Mm.5130	NM_009518	Wnt10a	Wingless related MMTV integration site 10a
F10	Mm.22182	NM_009519	Wnt11	Wingless-related MMTV integration site 11
F11	Mm.137403	NM_053116	Wnt16	Wingless-related MMTV integration site 16
F12	Mm.33653	NM_023653	Wnt2	Wingless-related MMTV integration site 2
G01	Mm.10740	NM_009520	Wnt2b	Wingless related MMTV integration site 2b
G02	Mm.159091	NM_009521	Wnt3	Wingless-related MMTV integration site 3
G03	Mm.1367	NM_009522	Wnt3a	Wingless-related MMTV integration site 3A
G04	Mm.20355	NM_009523	Wnt4	Wingless-related MMTV integration site 4
G05	Mm.287544	NM_009524	Wnt5a	Wingless-related MMTV integration site 5A
G06	Mm.321818	NM_009525	Wnt5b	Wingless-related MMTV integration site 5B
G07	Mm.268282	NM_009526	Wnt6	Wingless-related MMTV integration site 6
G08	Mm.56964	NM_009527	Wnt7a	Wingless-related MMTV integration site 7A
G09	Mm.306946	NM_009528	Wnt7b	Wingless-related MMTV integration site 7B
G10	Mm.558	NM_009290	Wnt8a	Wingless-related MMTV integration site 8A
G11	Mm.88365	NM_011720	Wnt8b	Wingless related MMTV integration site 8b
G12	Mm.218794	NM_139298	Wnt9a	Wingless-type MMTV integration site 9A
H01	Mm.371672	NM_010368	Gusb	Glucuronidase, beta
H02	Mm.299381	NM_013556	Hprt1	Hypoxanthine guanine phosphoribosyl transferase 1
H03	Mm.2180	NM_008302	Hspcb	Heat shock protein 1, beta
H04	Mm.379644	NM_001001303	Gapdh	Glyceraldehyde-3-phosphate dehydrogenase
H05	Mm.297	NM_007393	Actb	Actin, beta, cytoplasmic
H06	Mm.297	NM_007393	Actb	Actin, beta, cytoplasmic
H07	Mm.297	NM_007393	Actb	Actin, beta, cytoplasmic
H08	Mm.297	NM_007393	Actb	Actin, beta, cytoplasmic
H09	Mm.297	NM_007393	Actb	Actin, beta, cytoplasmic
H10	Mm.297	NM_007393	Actb	Actin, beta, cytoplasmic
H11	Mm.297	NM_007393	Actb	Actin, beta, cytoplasmic
H12	Mm.297	NM_007393	Actb	Actin, beta, cytoplasmic

APPENDIX D

Multiple nucleotide sequence alignment of *Bicc1* species using Clustal W2 (211, 212) and aligning sequences in the Accelrys DS Gene 1.5.

KH1

KH3

```
              1230          1240          1250          1260          1270
Mus musculus        GCAGAGAAGAGTAACCAGGTG---TCTATAGCAGGACAGCC-AGCAGGAGT
Homo sapiens        GCAGAAAAAAGCAACCAGGT---ATCTATAGCGGGACAACC-AGCAGGAGT
Rattus norvegicus   GTGGAAAGAGAGTA---TCTATAGCAGGACAGCC-AGCAGGAGT
Pan troglodytes     GCAGAAAAAAGCAACCAGGTGGTATCTATAGCAGGACAACC-AGCAGGAGT
Gallus gallus       GCAGAAAAAAGCAACCAAGTG---TCTATAGCAGGACAGCC-AGCTGGAGT
Xenopus laevis      GCCGAGAAAAAGCAACCAGGTG---TCGATTGCAGGGCAACC-AGCTGGTGT
Danio rerio         G-AGAGAAGAGCAACCAGGTG---TCAATCGCTGGACCGGT-TGAAGGGGGT
Anopheles gambiae   ACCGAGAAGAGCAATCAGGTG---TCGAT-GTGCGGCAGCATCGAGGGGGT
Drosophila melanogaster ACGGAGAAATCCAACCAGGTG---TCGCT-GTGCGGCAGCCTAGAGGGCGT
Caenorhabditis elegans  TCGAACAAAAGCGATCAAGTT---TCTATATCCGGAACACC-TGTTAATGT

Consensus           gcrgArAaaagcaaAcCAGgTgGTATCtaTagcrgGacagccTaGcwggdGT
```

```
              1280          1290          1300          1310          1320
Mus musculus        AGAATCGGCCCCGAGCAAGGATTCGGGAGCTGCTTCCTTTGGTGCTGATGTT
Homo sapiens        AGAATCTGCCCCGAGTTAGAATTCGGGAGCTGCTTCCTTTGGTGCTGATGTT
Rattus norvegicus   AGAATCGGCCCCGAGCGAGGATTCGGGAGCTGCTTCCTTTGGTGCTGATGTT
Pan troglodytes     AGAATCTGCCCCGAGTTAGAATTCGGGAGCTGCTTCCTTTGGTGCTGATGTT
Gallus gallus       AGAGTCTGCAAGAGTTAGAATTCGGGAGCTGCTTCCATTGGTACTGATGTT
Xenopus laevis      GGAATCTGCAAGAGTACGAATAAGGGAGCTGCTTCCTTTGGTGCTGATGTT
Danio rerio         GGAGTCTGCACGGAAACAGATCCGGGACCTGCAGCCCCTGGTGCTGAGCTT
Anopheles gambiae   GGAACGGGCGGAGATCGCTGGTGCGCAACTCGACGCCGTTGCTGATCTCCTT
Drosophila melanogaster GGAGCGGAGCCCGGGCTCTCGTTCGGCTCTCCACACCGCTGCTCATCTCCTT
Caenorhabditis elegans  ATTTGAAGCTTTAAAACACTTGAGGTCAATGTGTCCGTTGACAGTCTACAT

Consensus           agaatckGCmcgagywmgraTtcGggagctgcttCCktTGgtgctTgatgtT
```

```
              1330          1340          1350          1360          1370
Mus musculus        TGAGTTACCGATTGCCGGGATTCTCCAG-CCAGTCCCCGATCCCAACACCC
Homo sapiens        TGAGCTACCAATTGCTGGAATTCTTCAA-CCGGTTCCTTTATCCTAATTCCC
Rattus norvegicus   TGAGTTACCGATCGCCGGGATTCTCTCAG-CCGGTTCCCAGATCCCAACACCC
Pan troglodytes     TGAGCTACCAATTGCTGGAATTCTTCAA-CCGGTTCCTGATCCTAATTCCC
Gallus gallus       TGAATTGCCTATTGCTGGAATTCTGCAA-CCAATCCCCTGATCCTAATTCTC
Xenopus laevis      TGAGCTGCCTATAGCCGGGATTCTGCAA-CCGATACCAGACCCGAACTCTC
Danio rerio         TGACCTCCCGGTGACCCTGGTGGGGGGGT-GTGGTTGCAGATACGAGCTCTC
Anopheles gambiae   CGAGCTGCCGGAT-ACTGGCGCGCGGGCAAGACGCGCCGTTGCTGATCTCCTT
Drosophila melanogaster CGAGATGCCCGT-AATGGGACCCAACAAGCGCAGCCCGACCACGAGACTC
Caenorhabditis elegans  GAAGCTTCC-----CTGGTATAATCCAGGTCAA--CCTGAT--------CTA

Consensus           tgAgcTrCCdaTtgctgggrattctscaaGccgrtyccWGAtccyaactCyc
```

```
              1380          1390          1400          1410          1420
Mus musculus        CGTCCATTCAGCACATCTCACAAACCTACAGCGTTTCTGTGTCCTTTAAGC
Homo sapiens        CCTCTATTCAGCATATATCACAGAACGTACAATATTTCAGTATCATTTAAAC
Rattus norvegicus   CCTCCATCCAGCACATATCACAGAACGTACAATATTTCCGTGTCATTTAAGC
Pan troglodytes     CCTCTATTCAGCATATATCACAAACGTACAATATTTCAGTATCATTTAAAC
Gallus gallus       ACACAATTCAACATATATCTCAGACATACAACATTTCAGTTTCCTTTAAAAC
Xenopus laevis      CCACAATTCAGCAAATATCCCAAACGTACAATTTAACGGTTTTCTTTCAAGC
Danio rerio         CGGTGATCCAGCATGTGGCGCAGGCGTTTGGAGTCACCGTGAGCTTCAGAA
Anopheles gambiae   CGTACGTGAAGGAGATCGAGGCGGGAGTACGGGGGTGCAGGTGATCTTCTCCA
Drosophila melanogaster CCTACATCAAGATGATCGAGACCAAGTTCAATGTTCAGGTCATATTCTCCA
Caenorhabditis elegans  CGTCCTCTCA-----TGTCACAAATG---GATTTAGATGTTTCTGTTGAAC

Consensus           cctchattcAgcabaTmtcrcaracgTacaayrTthcrGTktcmtTtaarc
```

```
              1430          1440          1450          1460          1470
Mus musculus        AGAGGTCTCGAATGTATGGTGCTACAGTCACAGTACGAGG--CTCTCAGAA
Homo sapiens        AGCGTTCCCGAATGTATGGTGCTACTGTCATAGTACGGAGG--GTCTCAGAA
Rattus norvegicus   AGAGGTCTCGAATGTATGGTGCTACCGTCATAGTGCGGAGG--GTCTCAGAA
Pan troglodytes     AGCGTTCCCGAATGTATGGTGCTACTGTCATAGTACGGAGG--GTCTCAGAA
Gallus gallus       AACGCTCTCGAATGTATGGTGCTACGGTCATTGTCAGAGG--GTCACAAAA
Xenopus laevis      AACGCTCACGTGTGTTTACGGCGCTACTGTTATAGTGAGGGG--TTCCCAGAA
Danio rerio         CGCAGCCCAAACTCTACTCGCAGCACCTGCAGTGTCAGTAGTGCAGACGCC
Anopheles gambiae   CCCGACCCGAAGCTCCACTCGTCGCTCGTGCTGGTGA-AGGG-GTCGGAAAA
Drosophila melanogaster CGCGTCCAAAATTGCATACCTCGCTGGTTTTTGGTCA-AGGG-ATCGAGAAA
Caenorhabditis elegans  AG------AATATTTATAGTTTGGCAATTAAAATGACAGGAAGTC------A

Consensus           agcgktCycgaaTgtAtggtgctacygtcatagTvagaGGrAgTChcAgaa
```

```
              1480          1490          1500          1510          1520          1530
Mus musculus        TAACACTAATGCT--GTGAAGGAAGGAACAGCCATGCTGTTGGAACACCTT
Homo sapiens        TAACACTAGTGCT--GTGAAGGAAGGAACTGCCATGCTGTTAGAACATCTT
Rattus norvegicus   TAACACTAATGCT--GTGAAGGAAGGACAGCCATGCTATTGGAACACCTC
Pan troglodytes     TAACACTAGTGCT--GTGAAGGAAGGAACTGCCATGCTGTTAGAACATCTT
Gallus gallus       TAATACTAGTGCT--GTGAAGGAAGGAACTGCCATGCTTCTGGAACACCTA
Xenopus laevis      TAACACCAGTGCT--GTGAAGGAGGGTACAGTCTATGCTCTTGAACATCTT
Danio rerio         -AACACTGCTGCA--CTCAAGAAGGCGATCTGTGTGCTGTTGGAGCTGCT-
Anopheles gambiae   GGA-GGGAG-CGCATGGTGAAGGAGGCGACCCGCCGGCTGATGGACCTGATG
Drosophila melanogaster GGA-ATCGGCGCA-GGTCCGAGATGCCACGCAGCTGCTGATCAACTTCGCC
Caenorhabditis elegans  AGACACCAGTGTA---TTATT--TGCAATTCGATTAGTTTACATCA-CTT

Consensus           taAcactagtGcttTGgTgaaggArGgrAcwgccatgctTgwTrgAacayctt
```

Mus musculus
Homo sapiens
Rattus norvegicus
Pan troglodytes
Gallus gallus
Xenopus laevis
Danio rerio
Anopheles gambiae
Drosophila melanogaster
Caenorhabditis elegans

Consensus

Block 1 (positions 1840–1880):

```
                          1840        1850        1860        1870        1880
Mus musculus             C A C A G C T - G A - - - - T G G A A C A - G C T G G A C G T C T T T A - - T C A G T A T T A A A C C
Homo sapiens             C G C A G T T - G A - - - - T G G A A C A - G C T T G A T G T C T T C A - - T C A G T A T T A A A C C
Rattus norvegicus        C A C A G C T - C A - - - - T G G A G C A - G C T A G A C G T C T T T A - - T C A G T A T T A A A C C
Pan troglodytes          C A C A G T T - G A - - - - T G G A A C A - G C T T G A T G T C T T C A - - T C A G T A T T A A A C C
Gallus gallus            C G C A G C T - A A - - - - T G G A A C A - G T T A G A T G T C T T C A - - T A A G C A T T A A G C C
Xenopus laevis           C T C A G C T - C A - - - - T G G A A C A - G T T A G A T G T T T T C A - - T C A G C A T T A A A C C
Danio rerio              C C C A G A T - G A - - - - T G C A G A A - C C T G G G C G T T T T C A - - T C A G C G T C A A A A C C
Anopheles gambiae        C C A A G C T - A A - - - - T G C T A A C - G C A C G A C G T G T T C A - - T C T C G G T G C G G C A
Drosophila melanogaster  T G A G C C T C A A - - - - C A C C A A - - G T A C G G C G T C T A C A - - T C A C G T T G C G C C A
Caenorhabditis elegans   T C C A G T T C A A C A A T T G G A A C A A G A A A G A G G A A T A C A A G T T A C G T G T A A A C G

Consensus                c v c a g c T C r A C A A T t g g a a c a A g c t n G a y G t c T t c A A G T c a g b a t t a a a C c
```

Block 2 (positions 1890–1930):

```
                          1890        1900        1910        1920        1930
Mus musculus             A A A G C C C A A A C A G C C G A G C A A G T C T G T G A T T G T G A A A A G T G T T G A G C G A A A
Homo sapiens             A A A G C C C A A A C A G C C A A G C A A G T C T G T G A T T G T G A A A A G T G T T G A G C G A A A
Rattus norvegicus        G A A G C C C A A A C A G C C C A G C A A G T C T G T G A T T G T G A A A A G T G T T G A G C G A A A
Pan troglodytes          A A A G C C C A A A C A G C C A A G C A A G T C T G T G A T T G T G A A A A G T G T T G A G C G A A A
Gallus gallus            G A A G C C A A A A G C A A C C A A G C A A G T C T G T G A T T G T A A A A A G T G T T G A A C G A A A
Xenopus laevis           C A A A C C T A A G C A G C C A A G T A A A T C C G T T A T A G T A A A A A G C G T G G A G C G A A A
Danio rerio              C A A G G T C A A G C A G A C A G C A A A G T C A G T G G T G G T G A A A G G T T T G G A G A G A A A A
Anopheles gambiae        A A A G T C C C G C C A G A G C A C G C T C T G C A T C G T G A T C A A G G G C A T C G A G A A G T T
Drosophila melanogaster  G A A A C A G C G G C A G A G C A C C C T G G C C A T T G T G G T C A A G G G A G T G G A G A A G T T
Caenorhabditis elegans   A A A A A A C G G G G A - - - T A T T A T G A C C A T A A C A A T G A A A T C A A C A G A A T C A A A

Consensus                r A A g c c c a a r c A g c c m a g c a a g t c y g T g a t k g T g A A a a g t g t k G A g c g a a a
```

Block 3 (positions 1940–1980):

```
                          1940        1950        1960        1970        1980
Mus musculus             T G C C T T A A A T A T G T A T G A A G C A A G G A A G T G T - C T C C T C G - G A C T T G A A - A G
Homo sapiens             T G C C T T A A A T A T G T A T G A A G C A A G G A A A T G T - C T C C T C G - G A C T T G A A - A G
Rattus norvegicus        T G C C T T A A A T A T G T A T G A A G C A A G G A A G T G T - C T C C T C G - G A C T T G A A - A G
Pan troglodytes          T G C C T T A A A T A T G T A T G A A G C A A G G A A A T G T - C T C C T C G - G A C T T G A A - A G
Gallus gallus            T G C C T T A A A T A T G T A T G A G G C A C G G A A A T G T - C T T C T C G - G A C T T G A A - A G
Xenopus laevis           T G C C T T A A A T A T G T A C G A A G C A A G A A A A T G C - C T T C T C G - G A C T C G A T - A G
Danio rerio              T A T T G T C A A T G T G T A T G A G G C C A G - A C G T C T G C T G C T C G - G C C T G G A C - T C
Anopheles gambiae        T A T C G C C A A C A T C T A C G A G G C C C C G - A C A T C A G C T G C T G A A G G G T G G T G - G G
Drosophila melanogaster  T A T A G A C A A A A T C T A C G A G G C C C C G - C C A G G A G A T C C T G C - G C C T G G C C - A C
Caenorhabditis elegans   A T T A G C A G A A G T T C T T C A A T C T C G T G A A T T A - C T G T T A G - - - C T C T A C C A C

Consensus                t g c c t t a a A t a T g t a t g A a g C a a G g a a a t g t G c T s c T c g A G a c T k g a m C a g
```

Block 4 (positions 1990–2040):

```
                          1990        2000        2010        2020        2030        2040
Mus musculus             C A G T G G G G T T T C C A T A G C A A - C C A G T C T A T C C C C A G C A T C G T G C C C T G C C G
Homo sapiens             C A G T G G G G T T A C C A T A G C A A - C C A G T C C A T C C C C A G C A T C C T G C C C T G C C G
Rattus norvegicus        C A G T G G G G T T T C C A T A G C A A - C C A G T C T A T C C C C A G C A T C G T G C C C T G C C G
Pan troglodytes          C A G T G G G G T T A C C A T A G C A A - C C A G T C C A T C C C C A G C A T C C T G C C C T G C C G
Gallus gallus            C A G T G G A G T C A C C A T A G C A T - C A A A T G C C T C T A C T G T C T C A T G T C C T G T T G
Xenopus laevis           C A G C G G C G T G A C C G T T A C A A A C C A G T C T A - - - - C G T T A T C C T G T C C G G T T C
Danio rerio              C A C G G A G G T C T C T G T - - - - - - G T C C A - - - C C A A G A G C G T G - - - - - - - - - - -
Anopheles gambiae        G C G C G - C G T T G T C G C C G A A A T A C - - - C G C G C A C G T A C T T C G G G C C - - - - - - -
Drosophila melanogaster  G C C A T T C G T G A A G C C C G A G A T C C - - - C C G A C T A C T A C T T C A T G C C - - - - - - -
Caenorhabditis elegans   C A A C A A C A T A T T C A T C T C C T - G A T G A T T A T G A T C C G A A T C C T G - - - - - - - -

Consensus                c a g y g g s g T b w c c a t a g c a a t c c a g t c y a t c h c c w g c a t C s t G c C C t G c c g
```

Block 5 (positions 2050–2090):

```
                          2050        2060        2070        2080        2090
Mus musculus             G C C T G G C C T G T - C C C A G C C T G G A T A T C T T A G C T T C G G C A G G C C T C G G A C T -
Homo sapiens             G C C T G G C A T G T - C C C A G C C T G G A T A T C T T A G C T T C A G C A G G C C T T G G A C T -
Rattus norvegicus        G C C T G G C A T G T - C C C A G C C T G G A T A T C T T A G C T T C G G C A G G C C T T G G A C T -
Pan troglodytes          G C C T G G C A T G T - C C C A G C C T G G A T A T C T T A G C T T C A G C A G G C C T T G G A C T -
Gallus gallus            G T T T G T C T T G T - C C T G G T G T T G G A T A T C T T G T C T T C A G C A G G A C T A G G A C T -
Xenopus laevis           C G A T G A A T T G C - C A C G G G T T G G A T A T T T T G G C - - - A G C G G G G C C T A G G T C T -
Danio rerio              - - - T G T G A G G T - C T C A G T - - - G A T G - - - - - - A G C A A A C A T - - - - - - - T -
Anopheles gambiae        - - - - - G A A C G A G C A C C C G C A G C A - A A C G A G C - - - C A G A A C A - - - - - T A T C G G
Drosophila melanogaster  - - - - - A A A G G A - C A A A G A C C T T A - A T C T C G C C T A C A C G C A C C C A G T T A A C T G
Caenorhabditis elegans   - - - - - T G A T G A G C A G A C C A C C T A G T T T A A C A C C T T T G C A A A C T G A A A T G G C

Consensus                g c c T G k m a t G t G C m c a g b c t g g A t a t c t t r g C t t c a G c a g g c c t w g g a c t g
```

Block 6 (positions 2100–2140):

```
                          2100        2110        2120        2130        2140
Mus musculus             C A C T G - - G - A C T A G G T T T A T T G - - G G G C C C A C C A C A T T G T C G C T C A A T A C G
Homo sapiens             C A C T G - - G - A C T A G G T C T T T T G - - G G A C C C A C C A C C T T A T C T C T G A A C A C T
Rattus norvegicus        C A C T G - - G - A C T A G G T C T T T T G - - G G G C C C A C C A C A C T T G T C C C T C A A C A C A
Pan troglodytes          C A C T G - - G - A C T A G G T C T T T T G - - G G A C C C A C C A C C T T A T C T C T G A A C A C T
Gallus gallus            C A C T G - - G - A C T T G G C C T T T T A - - G G T C C A A C A G C A C T G T C C A T C A A C A C C
Xenopus laevis           C T C T G - - G - A T T A G G T C T C T T G - - G G T C C C A A C A C C C T T T C A G T T A A T T C C
Danio rerio              C A G T G - - G - A C - - - - C C T C T G C - - T G G C C A A T A A C - - - - - - - - - - - - G G C A
Anopheles gambiae        C T C T G T T G - G C G G G C C C G G T - - - A G C G C C A C C G T - - - - T C - - T C G C C G C T
Drosophila melanogaster  C T C T G C T G - G C T G G G T A T G T G G A C A G C C C G A A G A C - - - - T C C A T C G C T G C T
Caenorhabditis elegans   A T C T G G A G T A C G A G T A T T T T T G - - A C T C C G C C C A T T G A A T C T C A A A A T C T

Consensus                c a c T G b t G T a c t a G g t c t n T t g A C g g k c C c a c c a c m t t r T C y c t c a a y r C h
```

178

Mus musculus
Homo sapiens
Rattus norvegicus
Pan troglodytes
Gallus gallus
Xenopus laevis
Danio rerio
Anopheles gambiae
Drosophila melanogaster
Caenorhabditis elegans

Consensus

```
                                 2450        2460        2470        2480        2490
Mus musculus            GCGTCTATA--AATGGACATGTGCAGCCTGCAAACATGAAATACGGTCCGCT
Homo sapiens            GCTGCTTTA--AATGGACATGCACAGTCTCCAGATATAAAATATGGGTGCAAT
Rattus norvegicus       GCTTCTATA--AATGGACACGTGCAGCCTCCGAACATGAAATACGGTCCGCT
Pan troglodytes         GCTGCTTTA--AATGGACATGCACAGTCTCCAAATATAAAATATGGTGCAAT
Gallus gallus           GCTTCTTTA--AATGGTCATGTGAAGGCCACAAATATCAAGTATGCTGCGCT
Xenopus laevis          TCCGCTTTG--AATGGTCATGTAAAGCCGACAAATATGAATATGGAACAAT
Danio rerio             ----------AAAGGA---GTGGAGTCTA-AGTTAGAGAAGAT----------
Anopheles gambiae       GG---------CGGTAGTTCGGCAGGG----AAGATGAACCATC--------
Drosophila melanogaster CC---------ACGGAACAGCTGCAGGTC-----AGAAT--ACCAGTGG-----
Caenorhabditis elegans  ACTAATGAACCATCCACAAATGGT-CCTCCAATGATGAATCAT---------

Consensus               gctkcTtttaCaatggacatgtgcagGyctmCaaabAtgaAatAtggtsCrmT
```

```
                         2500        2510        2520        2530        2540        2550
Mus musculus            GTCCACTTCATCGCTT-GGGGAAAAAGTGCTGAGTTCGAATCATGGTGACC
Homo sapiens            ATCCACTTCATCACTT-GGAGAAAAAGTGCTGAGTGCAAAATCACGGGGATC
Rattus norvegicus       TTCCACTTCATCGCTT-GGGGAAAAAGTGCTGAGTTCTAATCACGGCGATC
Pan troglodytes         ATCCACTTCATCACTT-GGAGAAAAAGTGCTGAGTGCAAATCACGGGGATC
Gallus gallus           GTCTGCCACTTCACTG-GGAGAAAAACGTGTTGAATGCAAACCACAGTGATT
Xenopus laevis          ATCTTCTTCATCTCTA-GGAGACAAGGTGTTGAACACAAATCTTGCGGAGG
Danio rerio             ----------TC---T-GGAGAAA------TGAGG----ATCA--------
Anopheles gambiae       ----------TTTCCA-GCCCCCA------TTTGCTCC-TG-ACGGTGAGC
Drosophila melanogaster ----------TTACCA-GAGCT--------TTAGCAGC-AGCACCACCTCC
Caenorhabditis elegans  ----------TCACAACGGGGACTTTGTAGTGTACGAGAAGAAG--------

Consensus               rTCcaCttCaTcaCtwCGgrgaaaaaGTgcTgagykcVAatcacggkgabc
```

```
                                     2560        2570        2580        2590        2600
Mus musculus            CATCCATGCAGACA---------GCTGGGCCCGAACAGGCTTCT-CCTAAA
Homo sapiens            CGTCCATCCAGACA---------AGTGGGTCTGAGCAGACATCT-CCCAAA
Rattus norvegicus       CATCCATGCAGACA---------GCTGGGCCCGAACAGGCTTCT-CCTAAA
Pan troglodytes         CATCCATCCAGACA---------AGTGGGTCTGAGCAGACATCT-CCCAAA
Gallus gallus           CAGCAAGACAAACAAGCACTCATGGTGCATCAGACAAGTAGCT-GCCAAG
Xenopus laevis          CGTCAAGGCAGTCAAACAACCACAGCTCGGCTGAAGAAGTGAAT-TCCAAA
Danio rerio             -------GCAGACA------CAAGCGGAGTCTGA---GACCTGT-AGCATG
Anopheles gambiae       C-----AGAA--CA---------GTAGCCACAACGATAT--CCATT
Drosophila melanogaster C-----TGGAG-CA-----------GTCGTATCCGCCGTATGCCCAAT
Caenorhabditis elegans  ------ATGAAGAGC---------TCTCTGATTTTTCAGCTTCATCCACTAA

Consensus               CatCcAtgcAgacaArCAmyCAhrstgsgtcbgaacagvcwtmTscccaaa
```

```
                                  2610        2620        2630        2640        2650
Mus musculus            TCA--AACTCGGTGGAAGGCTGCAATGATGCCTTTGTTGAAGTGGGCATGC
Homo sapiens            TCA--AGCCCCACTGAAGGTTGTAATGATGCTTTTGTTGAAGTAGGCATGC
Rattus norvegicus       TCA--AACTCAGTGGAAGGCTGCAATGATGCCTTTGTTGAAGTGGGCATGC
Pan troglodytes         TCA--AGCCCCACTGAAGGTTGTAATGATGCTTTTGTTGAAGTAGGCATGC
Gallus gallus           TCA--AATGGTACAGAAGGTTGTAATGATGCTTTTGTAGAAGTGGGCATGC
Xenopus laevis          ACA--GATCC---AGAAGGTTGTAATGATGCCTTTGTGGAAGTGGGAATGC
Danio rerio             TCA--CATTC---AGA--GGTG-ACCGACG---TCAGAGAAGT---CAAGC
Anopheles gambiae       CGA--GCGGCTACCAAAGCTTGAACTGT-----TCCAGCAACTCGCTCGAC
Drosophila melanogaster TGC--CGGGC-ACCGTGTCGTCCACTTCA----TCCTCCACCGCGGGAAGC
Caenorhabditis elegans  TTATGGAATGTCTAGAATCTTTGAACAACC---ACCTAGAAATGTGT-TCT

Consensus               tcaTGraybcyacngaaggtTgyAatgatgCyTtttgtwgAagtgggcatgc
```

```
                                  2660        2670        2680        2690        2700
Mus musculus            CTCGAAGTCCCTCCCATTCTGGAAACGCTGGCGACTTGAAGCAGATGCTGG
Homo sapiens            CTCGAAGTCCTTCCCATTCTGGGATGCTGGTGACTTGAAACAGATGATGT
Rattus norvegicus       CTCGAAGTCCTTCCCATTCGGAAAACGCTGGTGACTTGAAGCAGATGCTGG
Pan troglodytes         CTCGAAGTCCTTCCCATTCTGGGAATGCTGGTGACTTGAAACAGATGATGA
Gallus gallus           CAAGAAGTCCGTCCCATTCAGCAAATACCAGTGATCTGAAGCAGATGATGA
Xenopus laevis          CCAGAAGTCCGTCTCATTCTGCCAACACCAAGGATCTCAAGCAGATGCTCA
Danio rerio             C---AACACCATCA-------------------TCAAGGAGAGGCAG-
Anopheles gambiae       CAACAGTTCCAGAGCA-----------------ACTCGT---CCGCGTCCG-
Drosophila melanogaster CAAAA--TCGGGCGCATT---------------ATTCGC--CAGATTCCA-
Caenorhabditis elegans  CTGCATCAACGTCGGTTT---------------TCGATTCGAACTCACT

Consensus               CtmgAagtccktcscaTTCtGgrAAygCtggtGActtgaagcagatgctgd
```

```
                              2710        2720        2730        2740        2750
Mus musculus            GTGCCTCCAAGGTCTCCTGTGCCAAGCGGCAGACGGTTGAGCTACTGCAGG
Homo sapiens            GTCCCTCCAAGGTTTCCTGTGCCAAAAGGCAGACAGTGGAACTATTGCAAG
Rattus norvegicus       GTCCCTCCAAGGTCTCCTGTGCCAAGCGGCAGACACGTTGAGCTACTGCAAG
Pan troglodytes         GTCCCTCCAAGGTTTCCTGTGCCAAAAGGCAGACAGTGGAACTATTGCAAG
Gallus gallus           GCTCTTCCAAAACAGGCTTGTTCAAAGAGGCAAACAGTTGAATTACTGCAAG
Xenopus laevis          ACTCCACCAAAAGCTCGCAGTGTCCAACACAGACAGACCGTCAAACTATTACACG
Danio rerio             ------CCAA----TCAGAGT-CCTCGAGGGA----GTTCAAC----CAG-
Anopheles gambiae       ------GCT-----CGGTGTCGCAGGTGTC-----CTCCAACT----CGCT
Drosophila melanogaster ----CTTACG-GCAGTGAGGGTGGTGGC-----GT-----TT-----GGCG
Caenorhabditis elegans  -----TCCATA---TAATCTACAATGGGATA------TT-AATTATTTCACG

Consensus               gtyCctccaargtbycstgtgccavghGgcAgACmgTtgAacTAtTgcavg
```

180

Multiple sequence alignment (nucleotide positions 3070–3360)

Block 1 (positions 3070–3110):

```
                          3070        3080        3090        3100        3110
Mus musculus              TCAAAGTCCATGCCGGCAGAAACCATTAAGGAACTGAGGAGAGCCAACCAC
Homo sapiens              TCTAAATCCATGCCAGCTGAAAACTATCAAGGAGTTGAGAAGGGCCAATCAT
Rattus norvegicus         TCGAAGTCCATGCCGGCAGAAACCATCAAGGAACTGAGGAGAGCGAACCAT
Pan troglodytes           TCTAAATCCATGCCAGCTGAAACTATCAAGGAGTTGAGAAGGGCCAATCAT
Gallus gallus             TCTAAATCTATGCCTGCAGAAACGATCAAAGAACTAAGAAGAGCTAACCAT
Xenopus laevis            TCCAAATCCACGCCAGCGGAAACCATTAAGGAACTGAGACGGGCCAACCAT
Danio rerio               TCTAAATCGATGCCTACTGACGCTGTGAAAGAGCTGCGAGCCGTGAGCCGG
Anopheles gambiae         TACAAGGCGATGC-A-C--ATGTCGCCCCAGCAGGGTGAAATACGCACC--
Drosophila melanogaster   TACAAAGCCATGG-AGC--GCACCCCGGTGGCAGGG-GAGCTGCGAACA--
Caenorhabditis elegans    TTCAACTA-ATTC-----TTAAAACAATAA-----------------------

Consensus                 TcyAAatccATgcCagCwgaaacyatbaagGaactgaGaagrgcsaaccat
```

Block 2 (positions 3120–3160):

```
                          3120        3130        3140        3150        3160
Mus musculus              GTATCCTAT-A-AGCCCACGATGACCACCGCCTATGAGGGGCT-CCTCATTG
Homo sapiens              GTGTCCTAT-A-AGCCCACAATGACAACCACTTATGAGGGCT-CATCCATG
Rattus norvegicus         GTGTCTTAT-A-AGCCCACAATGACAACCGCCTATGAGGGCT-CCTCATTG
Pan troglodytes           GTGTCCTAT-A-AGCCCACAATGACAACCACTTATGAGGGCT-CATCCATG
Gallus gallus             GTATCATAT-A-AGCCATCTATGACAACTACATATGAGGGTT-CATCAATG
Xenopus laevis            GTGCCTTAC-A-AGCCCACCATGACTACGACATACGAGAACT-CCTC----
Danio rerio               CGCTGTTAC-AGACCCTACAACAACAGCAACA-ATAACAACAACAACAACC
Anopheles gambiae         ----CCGAC-ACTGTCCTGGCAGGGGCTCGGGC-TAAGCCAGTCGTCG---
Drosophila melanogaster   ----CCCACGACCG-CTTGGATGGGAATGGGCT-TGAGCAGCACCTCG---
Caenorhabditis elegans    ---------------------------------------------------

Consensus                 gtgtcctAtGAcagcCcacratgacaaccacmtAtgAgggctaCmtCvatg
```

Block 3 (positions 3170–3210):

```
                          3170        3180        3190        3200        3210
Mus musculus              TCC-CTCTCA--AGGTCCAGCAGTCGTG----------AGCACCTGGCAA
Homo sapiens              TCC-CTTTCA--CGGTCCAACAGTCGTG----------AGCACTTGGGAG
Rattus norvegicus         TCC-CTCTCA--AGGTCCAGCAGTCGTG----------AGCACCTGGCGA
Pan troglodytes           TCC-CTTTCA--CGGTCCAACAGTCGCG----------AGCACTTGGGAA
Gallus gallus             TCT-CTCTCA--CGATCCAACAGTCGGG----------AGCACCTGGGAA
Xenopus laevis            --C-CTGTCG--AGGTCTAACAGCCGGG----------AACAGCTGGGAA
Danio rerio               ACCACAGCCAGCAGCAGCAGTCGTGGAGTGGGAAGGAACACGGCTGGA
Anopheles gambiae         -CC-CGCCC---GCTCGAG-GCTTGCG-----------ATCTCAGCT
Drosophila melanogaster   -CC-CGCCCCT--GCCCC---GCTGGAG-----------AAC-------
Caenorhabditis elegans    --------------------------------------------------

Consensus                 tCcACtctCakCaGgtccArcagtcGbGGAGTGGGAAGGAgCAcctgggaa
```

Block 4 (positions 3220–3260):

```
                          3220        3230        3240        3250        3260
Mus musculus              GTGGAAGCGAGTCAGACAACTGGAGAGAGACCGGAATGGAATAGGCCCATGG
Homo sapiens              GTGGAAGCGAATCTGATAACTGGAGAGACCGAAATGGAATTGGACCTGGAA
Rattus norvegicus         GCGGAAGCGAGTCAGACAACTGGAGAGACCGAAACGGAATCGGCCCCATGG
Pan troglodytes           GTGGAAGCGAATCTGATAACTGGAGAGACCGAAATGGAATTGGACCTGGAA
Gallus gallus             CTGGCAGTGAATCTGATAACTGGAGAGATCGTAATGGCCTTTGGACCCACAG
Xenopus laevis            ACGGCAGCGACTCTGAACTGGAGGGGAAAGGAATGGGATTG-ACTCGT--
Danio rerio               CCGGAAGCGACTCTGAGAACTGGAGAGAAAGACGTGGATCTGCATCTTCAT
Anopheles gambiae         GGGCCA---ACACGAGCAGCTCGAG---CAGCACCGGCGGTGGCCGGGACG
Drosophila melanogaster   GGGGAA---AATGGGGCTGCTGGTG---GAGGAGCATC-------------
Caenorhabditis elegans    --------------------------------------------------

Consensus                 gyGgaAGcGAmtctgayaaCTgGaGaGAccGraatggaattGgaccyrbag
```

Block 5 (positions 3270–3310):

```
                          3270        3280        3290        3300        3310
Mus musculus              GTCACAGTGAATTCTCAGCACCAATCGGCAGCCCCAAGCGCAAGCAGAACA
Homo sapiens              GTCATAGTGAATTTGCAGCTTCTATTGGCAGCCCTAAGCGTAAACAAAAACA
Rattus norvegicus         GTCACAGTGAATTCTCGGCACCGATCGGCAGCCCCAAGCGCAAGCAGAACA
Pan troglodytes           GTCATAGTGAATTTGCAGCTTCTATTGGCAGCCCTAAGCGTAAACAAAAACA
Gallus gallus             CTCA---TGAATTTGTCTCCTCAATTGCCAGCCCCAAGCGGAAACAAAAATA
Xenopus laevis            CTCAGAACGACTACTCGTCTCCATAGGCAGCCGGAAAGCAGAAACAAAAACA
Danio rerio               CTCCTCCTCCTTCCTCCTCCTCC-TA--CAGTTT-----GTCAGCATC-CC
Anopheles gambiae         GTGGTGGCGGCAGCGGCTGCGCCAACACCAGTAC-------GAGCAGCTCA
Drosophila melanogaster   -TAGTGGGTG--GCGGCTGC-----CACCAGGAC-------TGG--GTTCC
Caenorhabditis elegans    --------------------------------------------------

Consensus                 gTcatagtgaattcgcmtcctChAtyggcAGccccAAGCGyaagCAraaca
```

Block 6 (positions 3320–3360):

```
                          3320        3330        3340        3350        3360
Mus musculus              AATCAAGAGAGCACTATCTAA--GCAGCAGCAACTACATGGACTGCATTTC
Homo sapiens              AATCAACGGAACACTATCTCA--GCAGTAGCAATTACATGGACTGCATTTC
Rattus norvegicus         AATCAAGAGAGCACTATCTAA--GCAGCAGCAACTACATGGACTGCATTTC
Pan troglodytes           AATCAACGGAACACTATCTCA--GCAGTAGCAATTACATGGACTGCATTTC
Gallus gallus             AATCAGCTGAACACTATCTCA--GTAGCAGTAACTACATGGACTGCATTTC
Xenopus laevis            AATCTGCAGAACACTATCTCA--GCAGCAGTAATTACATGGACTGCATTTC
Danio rerio               GATCATCGGATGTCTTTCTGACCGAGGGCGGGGCTAC--GGTATGCAGACA
Anopheles gambiae         AGC--AGCGGGGGCT---GCTGA--CTCGC-GCCACAACA-TGACGACC-ACC
Drosophila melanogaster   CCT--TACGGA-------CTGA--GT----GCCACCACC-GGACTCC-----
Caenorhabditis elegans    --------------------------------------------------

Consensus                 aatCaacgGarcaCTatCTsACCgcaGcaGcaactACaTgGactgCatttc
```

182

3370 3380 3390 3400 3410

Mus musculus
Homo sapiens
Rattus norvegicus
Pan troglodytes
Gallus gallus
Xenopus laevis
Danio rerio
Anopheles gambiae
Drosophila melanogaster
Caenorhabditis elegans

Consensus

3420 3430 3440 3450 3460

Mus musculus
Homo sapiens
Rattus norvegicus
Pan troglodytes
Gallus gallus
Xenopus laevis
Danio rerio
Anopheles gambiae
Drosophila melanogaster
Caenorhabditis elegans

Consensus

3470 3480 3490 3500 3510

Mus musculus
Homo sapiens
Rattus norvegicus
Pan troglodytes
Gallus gallus
Xenopus laevis
Danio rerio
Anopheles gambiae
Drosophila melanogaster
Caenorhabditis elegans

Consensus

3520 3530 3540 3550 3560 3570

Mus musculus
Homo sapiens
Rattus norvegicus
Pan troglodytes
Gallus gallus
Xenopus laevis
Danio rerio
Anopheles gambiae
Drosophila melanogaster
Caenorhabditis elegans

Consensus

3580 3590 3600 3610 3620

Mus musculus
Homo sapiens
Rattus norvegicus
Pan troglodytes
Gallus gallus
Xenopus laevis
Danio rerio
Anopheles gambiae
Drosophila melanogaster
Caenorhabditis elegans

Consensus

3630 3640 3650 3660 3670

Mus musculus
Homo sapiens
Rattus norvegicus
Pan troglodytes
Gallus gallus
Xenopus laevis
Danio rerio
Anopheles gambiae
Drosophila melanogaster
Caenorhabditis elegans

Consensus

Alignment blocks with species rows:

Mus musculus
Homo sapiens
Rattus norvegicus
Pan troglodytes
Gallus gallus
Xenopus laevis
Danio rerio
Anopheles gambiae
Drosophila melanogaster
Caenorhabditis elegans

Consensus

Percent Identity Key

0-9 %	50-59 %
10-19 %	60-69 %
20-29 %	70-79 %
30-39 %	80-89 %
40-49 %	90-99 %
	100 %

184

Conservation of the KH and SAM functional domains of Bicc1 in ten diverse species using Clustal W2 (211, 212) and aligning sequences in the Accelrys DS Gene 1.5 software system.

Mus musculus
Homo sapiens
Rattus norvegicus
Pan troglodytes
Gallus gallus
Xenopus laevis
Danio rerio
Anopheles gambiae
Drosophila melanogaster
Caenorhabditis elegans

Consensus

KH3

Alignment positions 510–560:

Species	Sequence
Mus musculus	A S A I P V S T Q L D I A A Q H H L F M M G R N G S N V K H I M Q R T G A Q I H F P D P - - - - S N
Homo sapiens	A S A I P V S T Q L D I A A Q H H L F M M G R N G S N I K H I M Q R T G A Q I H F P D P - - - - S N
Rattus norvegicus	A S A I P V S T Q L D I A A Q H H L F M M G R N G S N V K H I M Q R T G A Q I H F P D P - - - - S N
Pan troglodytes	A S A I P V S T Q L D I A A Q H H L F M M G R N G S N I K H I M Q R T G A Q I H F P D P - - - - S N
Gallus gallus	A S A I P V S T Q L D I A A Q H H L F M M G R N G S N I K H I M Q R T G A Q I H F P D P - - - - S N
Xenopus laevis	A T A I P V S T Q L D I A A Q H H L F M M G R N G C N I K H I M Q R T G A Q I H F P D P - - - - N N
Danio rerio	V N G V M V S T Q L D V T S Q Q H L F L L G Q N G A N F L T V M H Q T H T Q I I L P D L - - - - S S
Anopheles gambiae	A S Q I P V H M Q L E I S T Q H H P I V L G R S S S N L R E I M N R T G T Q I M F P D A N D V N I K
Drosophila melanogaster	A S Q I L V N V Q M E I S P Q H H E I V K G K N N V N L L S I M E R T Q T K I I F P D L S D M N V K
Caenorhabditis elegans	L N I S T Q V L A R E E L N Y Q L E N V E E H R E R L R E V C N K N N V T I Q T F P E T - - - - - -
Consensus	a s a i p v s t q l d i a a q h h l f m m g r n g s n X k h i m q r t g a q i h f P d p X D X N s n

Alignment positions 560–600:

Species	Sequence
Mus musculus	P Q K K S T V Y L Q G T I E S V C L A R Q Y L M G C L P L V L M F D M K E D I E V D P Q V I A Q L M
Homo sapiens	P Q K K S T V Y L Q G T I E S V C L A R Q Y L M G C L P L V L M F D M K E E I E V D P Q F I A Q L M
Rattus norvegicus	P Q K K S T V Y L Q G T I E S V C L A R Q Y L M G C L P L V L M F D M K E D I D V D P Q V I T Q L M
Pan troglodytes	P Q K K S T V Y L Q G T I E S V C L A R Q Y L M G C L P L V L M F D M K E E I E V D P Q F I A Q L M
Gallus gallus	P Q K K S T V Y L Q G T I E S V C L A R Q Y L M G C L P L V L M F D M K E E I E V E P Q F I T Q L M
Xenopus laevis	P L K K S T V Y L Q G T I D S V C L A R Q Y L M G C L P L V L M F D M K E E I E I E P Q C I T Q L M
Danio rerio	P Q H T P S L L I Q G T A D G V C L A R Q Q L M D C L P V C L M F D L K D E G E L D P R R F T Q M M
Anopheles gambiae	P I K R S Q V T I T G S I N G V Y L A R Q Q L I G S L P I A L I F D Y P E N - T V D S D E I T K L M
Drosophila melanogaster	P L K K S Q V T I S G R I D D V Y L A R Q Q L L G N L P V A L I F D F P D N - H N D A S E I M S L N
Caenorhabditis elegans	- - - - Q S I S I V G P P S G V L N V R K L L I G L S S V T V Q F D C N M M D I H Y P V Q Q L E Q E
Consensus	P q k k s t v y l q G t i X s V c l a R q y L m g c l p l v l m F D m k e X i e v d p q X i X q l m

Alignment positions 610–650:

Species	Sequence
Mus musculus	E Q L D V F I S I K P K P K Q P S K S V I V K S V E R N A L N M Y E A R K C L L G L E S S G V S I A
Homo sapiens	E Q L D V F I S I K P K P K Q P S K S V I V K S V E R N A L N M Y E A R K C L L G L E S S G V T I A
Rattus norvegicus	E Q L D V F I S I K P K P K Q P S K S V I V K S V E R N A L N M Y E A R K C L L G L E S S G V S I A
Pan troglodytes	E Q L D V F I S I K P K P K Q P S K S V I V K S V E R N A L N M Y E A R K C L L G L E S S G V T I A
Gallus gallus	E Q L D V F I S I K P K P K Q P S K S V I V K S V E R N A L N M Y E A R K C L L G L E S S G V T I A
Xenopus laevis	E Q L D V F I S I K P K P K Q P S K S V I V K S V E R N A L N M Y E A R K C L L G L D S S G V T V T
Danio rerio	Q N L G V F I S V K P K V K Q T A K S V V V K G L E R N I V N V Y E A R R L L L G L D S T E V S V S
Anopheles gambiae	L T H D V F I S V R Q K S R Q S T L C I V I K G I E K F I A N I Y E A R H Q L L K G G G A R V V A E
Drosophila melanogaster	T K Y G V Y I T L R Q K Q R Q S T L A I V V K G V E K F I D K I Y E A R Q E I L R L A T P F V K P E
Caenorhabditis elegans	R G I Q V T C K R K - - - N G D I M T I T M K S T E S K L A E V L Q S R E L L L A L P - - - - - - -
Consensus	e q l d V f i s i k p K p k q p s k s v i v K s v E r n a l n m y e a R k c l L g l X s s g V X i a

Alignment positions 660–700:

Species	Sequence
Mus musculus	T S L S P A S C P A G L A C P S L D I L A S A G L G L T G L G L L G P T T L S L N T S A T P N S L L
Homo sapiens	T S P S P A S C P A G L A C P S L D I L A S A G L G L T G L G L L G P T T L S L N T S T T P N S L L
Rattus norvegicus	T S L S P A S C P A G L A C P S L D I L A S A G L G L T G L G L L G P T T L S L N T S T T P N S L L
Pan troglodytes	T S P S P A S C P A G L A C P S L D I L A S A G L G L T G L G L L G P T T L S L N T S T T P N S L L
Gallus gallus	S N A S T V S C P V G L S C P G L D I L S S A G L G L T G L G L L G P T A L S I N T S T T P N S L L
Xenopus laevis	N - Q S T L S C P V P M N C H G L D I L A A G - L G L S G L G L L G P N T L S V N S T T A Q N S L L
Danio rerio	T - - - - K S V C E V S V M S K H S V D P L L A N N G I T G Y W L N - - - - - - - - - - - - - - -
Anopheles gambiae	I P R T Y F G P N E H P Q Q T S Q N - - - I S A L L A G P V A P P F S P - - L S P I N P L P F V G W P
Drosophila melanogaster	I P D Y Y F M P K D K D L N L A Y R T Q L T A L L A G Y V D S P K T P S L L P P S L A G G Q L T P Y A
Caenorhabditis elegans	- -
Consensus	t s X s X X s c p X g l X c p s l d i l a s a g l g l t g l g l l g P t t L s X n t s t t p n s l l

Alignment positions 710–750:

Species	Sequence
Mus musculus	N A L N T S V S P L Q S S S S S G T P S P - T L W A P P I A N T A S A T G F S T I P H L M L P S T A Q
Homo sapiens	N A L N S S V S P L Q S P S S G T P S P - T L W A P P L A N T S S A T G F S A I P H L M I P S T A Q
Rattus norvegicus	N A L N S S V S P L Q S S S S S G T P S P T T L W A S S I P N T A S A T G F S T I P H L M I P S T A Q
Pan troglodytes	N A L N S S V S P L Q S P S S S G T P S P - T L W A P P L A N T S S A T G F S A I P H L M I P S T A Q
Gallus gallus	N A L N S S V S P L Q S P S S G T P S P - A L W T T S L A N T N A T G F S A I P H L M I P S T A Q
Xenopus laevis	N A L N S S L S P L H S P S S A A P S P - - - T L W A A S L A N N A T G F S A I P H L M I P S A A Q
Danio rerio	- V L M Q Q L R L T D T G S
Anopheles gambiae	T P T S A A A A A A A V A A A A A A A S - - - - - - - - - - - L P S S D F A F S H M R G Q F Q N
Drosophila melanogaster	N N N H L L L N A N G L A T P T G V C A - - - - - - - - - - - P T Q K Y M Q L H N S F Q Q A Q N
Caenorhabditis elegans	- -
Consensus	n a l n s s v s p l q s X s s g t p s p T T l w a X X X X n t X s a t g f s X i p h l m i p s t a q

Alignment positions 760–800:

Species	Sequence
Mus musculus	A T L T N I L L S G V P T Y G H T A P S P P P G L T P V D V H I N S M Q T E G K N I S A S I N G H V
Homo sapiens	A T L T N I L L S G V P T Y G H T A P S P P P G L T P V D V H I N S M Q T E G K K I S A A L N G H A
Rattus norvegicus	A T L T N I L L S G V P T Y G H T A P S P P P G L T P V D V H I N S M Q T E G K K I S A A L N G H V
Pan troglodytes	A T L T N I L L S G V P T Y G H T A P S P P P G L T P V D V H I N S M Q T E G K K I S A A L N G H A
Gallus gallus	A T L T S I L L S G V P N Y S Q N T P S P P P G L T P V E V H V N G M Q S E S K K G S A S L N G H V
Xenopus laevis	A T L T N F L L S G V P N Y G Q N T P S P P P G L T P V D V H M N G I H S E C K K V T S A L N G H V
Danio rerio	V S I P D A V I G S L S G K P R P T P P P P P G L A V S S E D G - - - - - - - - - - - - - - - - -
Anopheles gambiae	F H V H G P G K L P T G Q H H Q L L P L S L P P G L E R T V P G G S S A G K M N H L S S P H L L L T
Drosophila melanogaster	R S M V A G G Q S N N G N Y L Q V P G A V A P P L K P P T V S P R N S C S Q N - - - - - - - - - - -
Caenorhabditis elegans	- - - P T T Y S S P D D Y D P N P V M S R P P S L T P L Q T E M A S G - - - - - - - - - - - - - - -
Consensus	a t l t X X l l s g v p X y X X X X p s p p P g l t p v X v h X n s m q X e X k k i s a X l n g h v

Mus musculus
Homo sapiens
Rattus norvegicus
Pan troglodytes
Gallus gallus
Xenopus laevis
Danio rerio
Anopheles gambiae
Drosophila melanogaster
Caenorhabditis elegans

Consensus

SAM

	1110												1120										1130										1140										1150
Mus musculus	C N L N S C F K G - - - S D L P E L F S K L G L G K Y T D V F Q Q Q E I D L Q T F L T L T D Q D L K
Homo sapiens	C N L N S S F K G - - - S D L P E L F S K L G L G K Y T D V F Q Q Q E I D L Q T F L T L T D Q D L K
Rattus norvegicus	C N L N S C F K G - - - S D L P E L F S K L G L G K Y T D V F Q Q Q E I D L Q T F L T L T D Q D L K
Pan troglodytes	C N L N S S F K G - - - S D L P E L F S K L G L G K Y T D V F Q Q Q E I D L Q T F L T L T D Q D L K
Gallus gallus	C N L N S L F K G - - - S D L P E L F S K L G L G K Y T D V F Q Q Q E I D L Q T F L T L T D Q D L K
Xenopus laevis	C N L N S S F K G - - - S D L P E L F S K L G L G K Y T D I F Q Q Q E I D L Q T F L T L T D Q D L K
Danio rerio	G R S P S P A H A - - - D D L I E L L A Q L G L E K Y I D I F Q Q Q E I D Y Q T F L T L S D E D L K
Anopheles gambiae	- - - - - - - - - - - - D V T T I L T G L G L E H Y I K N F I N G E I D M T V F Q T L T D Q D L L
Drosophila melanogaster	- - - - - - - - - - - - D I Q T L L L T S L G L E H Y I K I F V L N E I D L E V F T T L T E E N L M
Caenorhabditis elegans	L P Y N L Q W D I N Y F T D P S M V L A Q L G C S E Y M T Q L R D Q E I D M H A F L L L D E Q N L K
Consensus	c n l n s X f k g N Y F s D l p e l f s k L G l g k Y t d X f q q q E I D l q t F l t L t d q d L k

	1160												1170										1180										1190										1200
Mus musculus	E L G I T T F G A R R K M L L A I S E L S K N R R K L F E P P N - - A S C T S F L E G G A S G R L P
Homo sapiens	E L G I T T F G A R R K M L L A I S E L N K N R R K L F E S P N - - - A R T S F L E G G A S G R L P
Rattus norvegicus	E L G I T T F G A R R K M L L A I S E L S K N R R K L F E P P N T P T T C T S F L E G G V S G R L P
Pan troglodytes	E L G I T T F G A R R K M L L A I S E L N K N R R K L F E S P N - - - A R T S F L E G G A S G R L P
Gallus gallus	E L G I T T F G A R R K M L L A I S E L N K N R R K L F D P S N - - - I R A S F L E G G A S G R L P
Xenopus laevis	E L G I S T F G A R R K M L L A I S E L N K N R R K L F E P T N - - - I R A S F L E G G A S G R L P
Danio rerio	E V G V S T F G A R R K M L L A I I A D L S K K R - - - - K I P E A F V V K S G Y L E G G A S G R L P
Anopheles gambiae	N L D I K P L G A R R R I L M A I H D L S V R Q G G G L F G S S A L - - - S P S A L P S S L S R F S
Drosophila melanogaster	E L G I A A F G A R K K L L T A I H T L L A N - - E A A C S T M P S - - - S S S S Q N S S S P R F S
Caenorhabditis elegans	D I G V S T I G A R K K I H H A I L K L R D S A R L N G Y A V - - - - - - - - - - - - - - - - - - -
Consensus	e l g i X t f G A R r k m l l A I s e L X k n r r k l f X X X n X X X X r X s f l e g g a s g R l p

	1210														
Mus musculus	R Q Y H S D I A S V S G R W -
Homo sapiens	R Q Y H S D I A S V S G R W -
Rattus norvegicus	R Q Y H S D I A S V S G R W -
Pan troglodytes	R Q Y H S D I A S V S G R W -
Gallus gallus	R Q Y H S D I A S V S G R W -
Xenopus laevis	R Q Y H T D I A S V S G R W -
Danio rerio	R I M D E D V A A K S N R W -
Anopheles gambiae	G S A A P G A E R R S S S G Q
Drosophila melanogaster	G S A A P G A E R R P S N Q W
Caenorhabditis elegans	- - - - - - - - - - - - - - -
Consensus	r q y h s d i a s v s g r w X

Percent Identity Key

0-9 %		50-59 %	
10-19 %		60-69 %	
20-29 %		70-79 %	
30-39 %		80-89 %	
40-49 %		90-99 %	
		100 %	
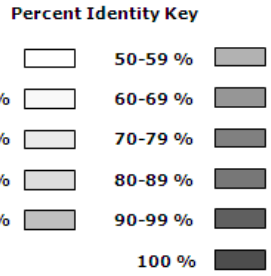
BIBLIOGRAPHY

1.	Carone FA. The pathogenesis of polycystic kidney disease. *Contrib Nephrol* 1990; **83:** 245-249.

2.	Qian Q, Harris PC, Torres VE. Treatment prospects for autosomal-dominant polycystic kidney disease. *Kidney Int* 2001; **59:** 2005-2022.

3.	Cogswell C, Price SJ, Hou X, Guay-Woodford LM*, et al.* Positional cloning of jcpk/bpk locus of the mouse. *Mamm Genome* 2003; **14:** 242-249.

4.	Mahone M, Saffman EE, Lasko PF. Localized Bicaudal-C RNA encodes a protein containing a KH domain, the RNA binding motif of FMR1. *EMBO J* 1995; **14:** 2043-2055.

5.	Tran U, Pickney LM, Ozpolat BD, Wessely O. Xenopus Bicaudal-C is required for the differentiation of the amphibian pronephros. *Dev Biol* 2007; **307:** 152-164.

6.	Igarashi P, Somlo S. Genetics and pathogenesis of polycystic kidney disease. *J Am Soc Nephrol* 2002; **13:** 2384-2398.

7.	Calvet JP. Polycystic kidney disease: primary extracellular matrix abnormality or defective cellular differentiation? *Kidney Int* 1993; **43:** 101-108.

8.	Wilson PD. Polycystic kidney disease. *N Engl J Med* 2004; **350:** 151-164.

9.	Jones C, Roper VC, Foucher I, Qian D*, et al.* Ciliary proteins link basal body polarization to planar cell polarity regulation. *Nat Genet* 2008; **40:** 69-77.

10.	Martin-Belmonte F, Mostov K. Regulation of cell polarity during epithelial morphogenesis. *Curr Opin Cell Biol* 2008; **20:** 227-234.

11.	Simons M, Walz G. Polycystic kidney disease: cell division without a c(l)ue? *Kidney Int* 2006; **70:** 854-864.

12.	Germino GG. Linking cilia to Wnts. *Nat Genet* 2005; **37:** 455-457.

13.	Torres VE. Extrarenal manifestations of autosomal dominant polycystic kidney disease. *Am J Kidney Dis* 1999; **34:** xlv-xlviii.

14.   Wilson PD. Mouse models of polycystic kidney disease. *Curr Top Dev Biol* 2008; **84:** 311-350.

15.   Rossetti S, Consugar MB, Chapman AB, Torres VE*, et al.* Comprehensive molecular diagnostics in autosomal dominant polycystic kidney disease. *J Am Soc Nephrol* 2007; **18:** 2143-2160.

16.   Deltas CC. Mutations of the human polycystic kidney disease 2 (PKD2) gene. *Hum Mutat* 2001; **18:** 13-24.

17.   Somlo S. The PKD2 gene: structure, interactions, mutations, and inactivation. *Adv Nephrol Necker Hosp* 1999; **29:** 257-275.

18.   Peters DJ, Sandkuijl LA. Genetic heterogeneity of polycystic kidney disease in Europe. *Contrib Nephrol* 1992; **97:** 128-139.

19.   Grantham JJ. Regulation of cell proliferation and fluid secretion in the progressive enlargement of renal cysts. *Contrib Nephrol* 1992; **97:** 15-22.

20.   Li X, Li HP, Amsler K, Hyink D*, et al.* PRKX, a phylogenetically and functionally distinct cAMP-dependent protein kinase, activates renal epithelial cell migration and morphogenesis. *Proc Natl Acad Sci U S A* 2002; **99:** 9260-9265.

21.   Li HP, Geng L, Burrow CR, Wilson PD. Identification of phosphorylation sites in the PKD1-encoded protein C-terminal domain. *Biochem Biophys Res Commun* 1999; **259:** 356-363.

22.   Parnell SC, Magenheimer BS, Maser RL, Rankin CA*, et al.* The polycystic kidney disease-1 protein, polycystin-1, binds and activates heterotrimeric G-proteins in vitro. *Biochem Biophys Res Commun* 1998; **251:** 625-631.

23.   Li Y, Wright JM, Qian F, Germino GG*, et al.* Polycystin 2 interacts with type I inositol 1,4,5-trisphosphate receptor to modulate intracellular Ca2+ signaling. *J Biol Chem* 2005; **280:** 41298-41306.

24.   Tsiokas L, Kim E, Arnould T, Sukhatme VP*, et al.* Homo- and heterodimeric interactions between the gene products of PKD1 and PKD2. *Proc Natl Acad Sci U S A* 1997; **94:** 6965-6970.

25.   Qian F, Germino FJ, Cai Y, Zhang X*, et al.* PKD1 interacts with PKD2 through a probable coiled-coil domain. *Nat Genet* 1997; **16:** 179-183.

26.   Hanaoka K, Qian F, Boletta A, Bhunia AK*, et al.* Co-assembly of polycystin-1 and -2 produces unique cation-permeable currents. *Nature* 2000; **408:** 990-994.

27. Koulen P, Cai Y, Geng L, Maeda Y*, et al.* Polycystin-2 is an intracellular calcium release channel. *Nat Cell Biol* 2002; **4:** 191-197.

28. Nauli SM, Alenghat FJ, Luo Y, Williams E*, et al.* Polycystins 1 and 2 mediate mechanosensation in the primary cilium of kidney cells. *Nat Genet* 2003; **33:** 129-137.

29. Onuchic LF, Furu L, Nagasawa Y, Hou X*, et al.* PKHD1, the polycystic kidney and hepatic disease 1 gene, encodes a novel large protein containing multiple immunoglobulin-like plexin-transcription-factor domains and parallel beta-helix 1 repeats. *Am J Hum Genet* 2002; **70:** 1305-1317.

30. Wang X, Gattone V, 2nd, Harris PC, Torres VE. Effectiveness of vasopressin V2 receptor antagonists OPC-31260 and OPC-41061 on polycystic kidney disease development in the PCK rat. *J Am Soc Nephrol* 2005; **16:** 846-851.

31. Bergmann C, Senderek J, Sedlacek B, Pegiazoglou I*, et al.* Spectrum of mutations in the gene for autosomal recessive polycystic kidney disease (ARPKD/PKHD1). *J Am Soc Nephrol* 2003; **14:** 76-89.

32. Bergmann C, Frank V, Kupper F, Schmidt C*, et al.* Functional analysis of PKHD1 splicing in autosomal recessive polycystic kidney disease. *J Hum Genet* 2006; **51:** 788-793.

33. Rossetti S, Torra R, Coto E, Consugar M*, et al.* A complete mutation screen of PKHD1 in autosomal-recessive polycystic kidney disease (ARPKD) pedigrees. *Kidney Int* 2003; **64:** 391-403.

34. Xiong H, Chen Y, Yi Y, Tsuchiya K*, et al.* A novel gene encoding a TIG multiple domain protein is a positional candidate for autosomal recessive polycystic kidney disease. *Genomics* 2002; **80:** 96-104.

35. Ward CJ, Hogan MC, Rossetti S, Walker D*, et al.* The gene mutated in autosomal recessive polycystic kidney disease encodes a large, receptor-like protein. *Nat Genet* 2002; **30:** 259-269.

36. McDonald RA, Avner ED. Inherited polycystic kidney disease in children. *Semin Nephrol* 1991; **11:** 632-642.

37. Alberts B, Johnson, A., Lewis, J., Raff, M., Roberts, K., Walter, P. *Molecular biology of the cell*, Fourth edn. Garland Science: New York, 2002.

38. Zhang Q, Taulman PD, Yoder BK. Cystic kidney diseases: all roads lead to the cilium. *Physiology (Bethesda)* 2004; **19:** 225-230.

39. Davenport JR, Watts AJ, Roper VC, Croyle MJ*, et al.* Disruption of intraflagellar transport in adult mice leads to obesity and slow-onset cystic kidney disease. *Curr Biol* 2007; **17:** 1586-1594.

40. Haycraft CJ, Swoboda P, Taulman PD, Thomas JH*, et al.* The C. elegans homolog of the murine cystic kidney disease gene Tg737 functions in a ciliogenic pathway and is disrupted in osm-5 mutant worms. *Development* 2001; **128:** 1493-1505.

41. Hou X, Mrug M, Yoder BK, Lefkowitz EJ*, et al.* Cystin, a novel cilia-associated protein, is disrupted in the cpk mouse model of polycystic kidney disease. *J Clin Invest* 2002; **109:** 533-540.

42. Lin F, Hiesberger T, Cordes K, Sinclair AM*, et al.* Kidney-specific inactivation of the KIF3A subunit of kinesin-II inhibits renal ciliogenesis and produces polycystic kidney disease. *Proc Natl Acad Sci U S A* 2003; **100:** 5286-5291.

43. Mahjoub MR, Trapp ML, Quarmby LM. NIMA-related kinases defective in murine models of polycystic kidney diseases localize to primary cilia and centrosomes. *J Am Soc Nephrol* 2005; **16:** 3485-3489.

44. Menezes LF, Cai Y, Nagasawa Y, Silva AM*, et al.* Polyductin, the PKHD1 gene product, comprises isoforms expressed in plasma membrane, primary cilium, and cytoplasm. *Kidney Int* 2004; **66:** 1345-1355.

45. Otto EA, Schermer B, Obara T, O'Toole JF*, et al.* Mutations in INVS encoding inversin cause nephronophthisis type 2, linking renal cystic disease to the function of primary cilia and left-right axis determination. *Nat Genet* 2003; **34:** 413-420.

46. Pathak N, Obara T, Mangos S, Liu Y*, et al.* The zebrafish fleer gene encodes an essential regulator of cilia tubulin polyglutamylation. *Mol Biol Cell* 2007; **18:** 4353-4364.

47. Pazour GJ, San Agustin JT, Follit JA, Rosenbaum JL*, et al.* Polycystin-2 localizes to kidney cilia and the ciliary level is elevated in orpk mice with polycystic kidney disease. *Curr Biol* 2002; **12:** R378-380.

48. Shalom O, Shalva N, Altschuler Y, Motro B. The mammalian Nek1 kinase is involved in primary cilium formation. *FEBS Lett* 2008; **582:** 1465-1470.

49. Siroky BJ, Ferguson WB, Fuson AL, Xie Y, *et al.* Loss of primary cilia results in deregulated and unabated apical calcium entry in ARPKD collecting duct cells. *Am J Physiol Renal Physiol* 2006; **290:** F1320-1328.

50. Sun Z, Amsterdam A, Pazour GJ, Cole DG, *et al.* A genetic screen in zebrafish identifies cilia genes as a principal cause of cystic kidney. *Development* 2004; **131:** 4085-4093.

51. Taulman PD, Haycraft CJ, Balkovetz DF, Yoder BK. Polaris, a protein involved in left-right axis patterning, localizes to basal bodies and cilia. *Mol Biol Cell* 2001; **12:** 589-599.

52. Ward CJ, Yuan D, Masyuk TV, Wang X, *et al.* Cellular and subcellular localization of the ARPKD protein; fibrocystin is expressed on primary cilia. *Hum Mol Genet* 2003; **12:** 2703-2710.

53. Yoder BK, Hou X, Guay-Woodford LM. The polycystic kidney disease proteins, polycystin-1, polycystin-2, polaris, and cystin, are co-localized in renal cilia. *J Am Soc Nephrol* 2002; **13:** 2508-2516.

54. Yoder BK, Tousson A, Millican L, Wu JH, *et al.* Polaris, a protein disrupted in orpk mutant mice, is required for assembly of renal cilium. *Am J Physiol Renal Physiol* 2002; **282:** F541-552.

55. Masyuk TV, Huang BQ, Ward CJ, Masyuk AI, *et al.* Defects in cholangiocyte fibrocystin expression and ciliary structure in the PCK rat. *Gastroenterology* 2003; **125:** 1303-1310.

56. Pan J, Wang Q, Snell WJ. Cilium-generated signaling and cilia-related disorders. *Lab Invest* 2005; **85:** 452-463.

57. Stagner EE, Bouvrette DJ, Cheng J, Bryda EC. The polycystic kidney disease-related proteins Bicc1 and SamCystin interact. *Biochem Biophys Res Commun* 2009; **383:** 16-21.

58. Watanabe D, Saijoh Y, Nonaka S, Sasaki G, *et al.* The left-right determinant Inversin is a component of node monocilia and other 9+0 cilia. *Development* 2003; **130:** 1725-1734.

59. Liu S, Lu W, Obara T, Kuida S, *et al.* A defect in a novel Nek-family kinase causes cystic kidney disease in the mouse and in zebrafish. *Development* 2002; **129:** 5839-5846.

60. Guay-Woodford LM. Murine models of polycystic kidney disease: molecular and therapeutic insights. *Am J Physiol Renal Physiol* 2003; **285:** F1034-1049.

61. Logan CY, Nusse R. The Wnt signaling pathway in development and disease. *Annu Rev Cell Dev Biol* 2004; **20:** 781-810.

62. Nusse R, Varmus HE. Many tumors induced by the mouse mammary tumor virus contain a provirus integrated in the same region of the host genome. *Cell* 1982; **31:** 99-109.

63. van Ooyen A, Nusse R. Structure and nucleotide sequence of the putative mammary oncogene int-1; proviral insertions leave the protein-encoding domain intact. *Cell* 1984; **39:** 233-240.

64. Baker NE. Molecular cloning of sequences from wingless, a segment polarity gene in Drosophila: the spatial distribution of a transcript in embryos. *EMBO J* 1987; **6:** 1765-1773.

65. Cabrera CV, Alonso MC, Johnston P, Phillips RG*, et al.* Phenocopies induced with antisense RNA identify the wingless gene. *Cell* 1987; **50:** 659-663.

66. Rijsewijk F, Schuermann M, Wagenaar E, Parren P*, et al.* The Drosophila homolog of the mouse mammary oncogene int-1 is identical to the segment polarity gene wingless. *Cell* 1987; **50:** 649-657.

67. Sharma RP, Chopra VL. Effect of the Wingless (wg1) mutation on wing and haltere development in Drosophila melanogaster. *Dev Biol* 1976; **48:** 461-465.

68. Nusslein-Volhard C, Wieschaus E. Mutations affecting segment number and polarity in Drosophila. *Nature* 1980; **287:** 795-801.

69. Wieschaus E. A combined genetic and mosaic approach to the study of oogenesis in Drosophila. *Basic Life Sci* 1980; **16:** 85-94.

70. Perrimon N, Smouse D. Multiple functions of a Drosophila homeotic gene, zeste-white 3, during segmentation and neurogenesis. *Dev Biol* 1989; **135:** 287-305.

71. Klingensmith J, Noll E, Perrimon N. The segment polarity phenotype of Drosophila involves differential tendencies toward transformation and cell death. *Dev Biol* 1989; **134:** 130-145.

72. Thorpe CJ, Schlesinger A, Carter JC, Bowerman B. Wnt signaling polarizes an early C. elegans blastomere to distinguish endoderm from mesoderm. *Cell* 1997; **90:** 695-705.

73. Eisenmann DM, Maloof JN, Simske JS, Kenyon C, *et al.* The beta-catenin homolog BAR-1 and LET-60 Ras coordinately regulate the Hox gene lin-39 during Caenorhabditis elegans vulval development. *Development* 1998; **125:** 3667-3680.

74. Herman MA, Vassilieva LL, Horvitz HR, Shaw JE, *et al.* The C. elegans gene lin-44, which controls the polarity of certain asymmetric cell divisions, encodes a Wnt protein and acts cell nonautonomously. *Cell* 1995; **83:** 101-110.

75. Shackleford GM, Shivakumar S, Shiue L, Mason J, *et al.* Two wnt genes in Caenorhabditis elegans. *Oncogene* 1993; **8:** 1857-1864.

76. Jiang LI, Sternberg PW. Interactions of EGF, Wnt and HOM-C genes specify the P12 neuroectoblast fate in C. elegans. *Development* 1998; **125:** 2337-2347.

77. Rocheleau CE, Downs WD, Lin R, Wittmann C, *et al.* Wnt signaling and an APC-related gene specify endoderm in early C. elegans embryos. *Cell* 1997; **90:** 707-716.

78. Lin R, Thompson S, Priess JR. pop-1 encodes an HMG box protein required for the specification of a mesoderm precursor in early C. elegans embryos. *Cell* 1995; **83:** 599-609.

79. Deardorff MA, Tan C, Conrad LJ, Klein PS. Frizzled-8 is expressed in the Spemann organizer and plays a role in early morphogenesis. *Development* 1998; **125:** 2687-2700.

80. McMahon AP, Moon RT. Ectopic expression of the proto-oncogene int-1 in Xenopus embryos leads to duplication of the embryonic axis. *Cell* 1989; **58:** 1075-1084.

81. Torres MA, Yang-Snyder JA, Purcell SM, DeMarais AA, *et al.* Activities of the Wnt-1 class of secreted signaling factors are antagonized by the Wnt-5A class and by a dominant negative cadherin in early Xenopus development. *J Cell Biol* 1996; **133:** 1123-1137.

82. Moon RT, Campbell RM, Christian JL, McGrew LL, *et al.* Xwnt-5A: a maternal Wnt that affects morphogenetic movements after overexpression in embryos of Xenopus laevis. *Development* 1993; **119:** 97-111.

83. Hoeflich KP, Luo J, Rubie EA, Tsao MS, *et al.* Requirement for glycogen synthase kinase-3beta in cell survival and NF-kappaB activation. *Nature* 2000; **406:** 86-90.

84. Lijam N, Paylor R, McDonald MP, Crawley JN*, et al.* Social interaction and sensorimotor gating abnormalities in mice lacking Dvl1. *Cell* 1997; **90:** 895-905.

85. Long JM, LaPorte P, Paylor R, Wynshaw-Boris A. Expanded characterization of the social interaction abnormalities in mice lacking Dvl1. *Genes Brain Behav* 2004; **3:** 51-62.

86. Zeng L, Fagotto F, Zhang T, Hsu W*, et al.* The mouse Fused locus encodes Axin, an inhibitor of the Wnt signaling pathway that regulates embryonic axis formation. *Cell* 1997; **90:** 181-192.

87. Moser AR, Shoemaker AR, Connelly CS, Clipson L*, et al.* Homozygosity for the Min allele of Apc results in disruption of mouse development prior to gastrulation. *Dev Dyn* 1995; **203:** 422-433.

88. Ishikawa TO, Tamai Y, Li Q, Oshima M*, et al.* Requirement for tumor suppressor Apc in the morphogenesis of anterior and ventral mouse embryo. *Dev Biol* 2003; **253:** 230-246.

89. Huelsken J, Vogel R, Brinkmann V, Erdmann B*, et al.* Requirement for beta-catenin in anterior-posterior axis formation in mice. *J Cell Biol* 2000; **148:** 567-578.

90. Haegel H, Larue L, Ohsugi M, Fedorov L*, et al.* Lack of beta-catenin affects mouse development at gastrulation. *Development* 1995; **121:** 3529-3537.

91. Thomas KR, Capecchi MR. Targeted disruption of the murine int-1 proto-oncogene resulting in severe abnormalities in midbrain and cerebellar development. *Nature* 1990; **346:** 847-850.

92. McMahon AP, Bradley A. The Wnt-1 (int-1) proto-oncogene is required for development of a large region of the mouse brain. *Cell* 1990; **62:** 1073-1085.

93. Takada S, Stark KL, Shea MJ, Vassileva G*, et al.* Wnt-3a regulates somite and tailbud formation in the mouse embryo. *Genes Dev* 1994; **8:** 174-189.

94. Guo N, Hawkins C, Nathans J. Frizzled6 controls hair patterning in mice. *Proc Natl Acad Sci U S A* 2004; **101:** 9277-9281.

95. Parr BA, McMahon AP. Dorsalizing signal Wnt-7a required for normal polarity of D-V and A-P axes of mouse limb. *Nature* 1995; **374:** 350-353.

96.   Ranheim EA, Kwan HC, Reya T, Wang YK, *et al.* Frizzled 9 knock-out mice have abnormal B-cell development. *Blood* 2005; **105:** 2487-2494.

97.   Stark K, Vainio S, Vassileva G, McMahon AP. Epithelial transformation of metanephric mesenchyme in the developing kidney regulated by Wnt-4. *Nature* 1994; **372:** 679-683.

98.   Kunz M, Herrmann M, Wedlich D, Gradl D. Autoregulation of canonical Wnt signaling controls midbrain development. *Dev Biol* 2004; **273:** 390-401.

99.   Koenig SF, Lattanzio R, Mansperger K, Rupp RA, *et al.* Autoregulation of XTcf-4 depends on a Lef/Tcf site on the XTcf-4 promoter. *Genesis* 2008; **46:** 81-86.

100.   Beland M, Pilon N, Houle M, Oh K, *et al.* Cdx1 autoregulation is governed by a novel Cdx1-LEF1 transcription complex. *Mol Cell Biol* 2004; **24:** 5028-5038.

101.   Martin BL, Kimelman D. Regulation of canonical Wnt signaling by Brachyury is essential for posterior mesoderm formation. *Dev Cell* 2008; **15:** 121-133.

102.   Calvo R, West J, Franklin W, Erickson P, *et al.* Altered HOX and WNT7A expression in human lung cancer. *Proc Natl Acad Sci U S A* 2000; **97:** 12776-12781.

103.   Conacci-Sorrell M, Simcha I, Ben-Yedidia T, Blechman J, *et al.* Autoregulation of E-cadherin expression by cadherin-cadherin interactions: the roles of beta-catenin signaling, Slug, and MAPK. *J Cell Biol* 2003; **163:** 847-857.

104.   Habas R, Dawid IB. Dishevelled and Wnt signaling: is the nucleus the final frontier? *J Biol* 2005; **4:** 2.

105.   Ahmed Y, Nouri A, Wieschaus E. Drosophila Apc1 and Apc2 regulate Wingless transduction throughout development. *Development* 2002; **129:** 1751-1762.

106.   Behrens J, Jerchow BA, Wurtele M, Grimm J, *et al.* Functional interaction of an axin homolog, conductin, with beta-catenin, APC, and GSK3beta. *Science* 1998; **280:** 596-599.

107.   Lewis SL, Khoo PL, Andrea De Young R, Bildsoe H, *et al.* Genetic interaction of Gsc and Dkk1 in head morphogenesis of the mouse. *Mech Dev* 2007; **124:** 157-165.

108. Onuma Y, Takahashi S, Haramoto Y, Tanegashima K, *et al.* Xnr2 and Xnr5 unprocessed proteins inhibit Wnt signaling upstream of dishevelled. *Dev Dyn* 2005; **234:** 900-910.

109. Tanaka K, Kitagawa Y, Kadowaki T. Drosophila segment polarity gene product porcupine stimulates the posttranslational N-glycosylation of wingless in the endoplasmic reticulum. *J Biol Chem* 2002; **277:** 12816-12823.

110. Herzlinger D, Qiao J, Cohen D, Ramakrishna N, *et al.* Induction of kidney epithelial morphogenesis by cells expressing Wnt-1. *Dev Biol* 1994; **166:** 815-818.

111. Davies JA, Garrod DR. Induction of early stages of kidney tubule differentiation by lithium ions. *Dev Biol* 1995; **167:** 50-60.

112. Karavanova ID, Dove LF, Resau JH, Perantoni AO. Conditioned medium from a rat ureteric bud cell line in combination with bFGF induces complete differentiation of isolated metanephric mesenchyme. *Development* 1996; **122:** 4159-4167.

113. Vukicevic S, Kopp JB, Luyten FP, Sampath TK. Induction of nephrogenic mesenchyme by osteogenic protein 1 (bone morphogenetic protein 7). *Proc Natl Acad Sci U S A* 1996; **93:** 9021-9026.

114. Carroll TJ, McMahon AP. Secreted molecules in metanephric induction. *J Am Soc Nephrol* 2000; **11 Suppl 16:** S116-119.

115. Majumdar A, Vainio S, Kispert A, McMahon J, *et al.* Wnt11 and Ret/Gdnf pathways cooperate in regulating ureteric branching during metanephric kidney development. *Development* 2003; **130:** 3175-3185.

116. Schuchardt A, D'Agati V, Pachnis V, Costantini F. Renal agenesis and hypodysplasia in ret-k- mutant mice result from defects in ureteric bud development. *Development* 1996; **122:** 1919-1929.

117. Plisov SY, Yoshino K, Dove LF, Higinbotham KG, *et al.* TGF beta 2, LIF and FGF2 cooperate to induce nephrogenesis. *Development* 2001; **128:** 1045-1057.

118. Kispert A, Vainio S, McMahon AP. Wnt-4 is a mesenchymal signal for epithelial transformation of metanephric mesenchyme in the developing kidney. *Development* 1998; **125:** 4225-4234.

119. Saadi-Kheddouci S, Berrebi D, Romagnolo B, Cluzeaud F*, et al.* Early development of polycystic kidney disease in transgenic mice expressing an activated mutant of the beta-catenin gene. *Oncogene* 2001; **20:** 5972-5981.

120. Cadigan KM, Nusse R. Wnt signaling: a common theme in animal development. *Genes Dev* 1997; **11:** 3286-3305.

121. Song DH, Sussman DJ, Seldin DC. Endogenous protein kinase CK2 participates in Wnt signaling in mammary epithelial cells. *J Biol Chem* 2000; **275:** 23790-23797.

122. Song DH, Dominguez I, Mizuno J, Kaut M*, et al.* CK2 phosphorylation of the armadillo repeat region of beta-catenin potentiates Wnt signaling. *J Biol Chem* 2003; **278:** 24018-24025.

123. Litchfield DW. Protein kinase CK2: structure, regulation and role in cellular decisions of life and death. *Biochem J* 2003; **369:** 1-15.

124. Hu J, Bae YK, Knobel KM, Barr MM. Casein kinase II and calcineurin modulate TRPP function and ciliary localization. *Mol Biol Cell* 2006; **17:** 2200-2211.

125. Park TJ, Haigo SL, Wallingford JB. Ciliogenesis defects in embryos lacking inturned or fuzzy function are associated with failure of planar cell polarity and Hedgehog signaling. *Nat Genet* 2006; **38:** 303-311.

126. Tada M, Concha ML, Heisenberg CP. Non-canonical Wnt signalling and regulation of gastrulation movements. *Semin Cell Dev Biol* 2002; **13:** 251-260.

127. Golan T, Yaniv A, Bafico A, Liu G*, et al.* The human Frizzled 6 (HFz6) acts as a negative regulator of the canonical Wnt. beta-catenin signaling cascade. *J Biol Chem* 2004; **279:** 14879-14888.

128. Medina A, Reintsch W, Steinbeisser H. Xenopus frizzled 7 can act in canonical and non-canonical Wnt signaling pathways: implications on early patterning and morphogenesis. *Mech Dev* 2000; **92:** 227-237.

129. Yamanaka H, Moriguchi T, Masuyama N, Kusakabe M*, et al.* JNK functions in the non-canonical Wnt pathway to regulate convergent extension movements in vertebrates. *EMBO Rep* 2002; **3:** 69-75.

130. Veeman MT, Axelrod JD, Moon RT. A second canon. Functions and mechanisms of beta-catenin-independent Wnt signaling. *Dev Cell* 2003; **5:** 367-377.

131. Marlow F, Topczewski J, Sepich D, Solnica-Krezel L. Zebrafish Rho kinase 2 acts downstream of Wnt11 to mediate cell polarity and effective convergence and extension movements. *Curr Biol* 2002; **12:** 876-884.

132. Wallingford JB, Fraser SE, Harland RM. Convergent extension: the molecular control of polarized cell movement during embryonic development. *Dev Cell* 2002; **2:** 695-706.

133. Boutros M, Paricio N, Strutt DI, Mlodzik M. Dishevelled activates JNK and discriminates between JNK pathways in planar polarity and wingless signaling. *Cell* 1998; **94:** 109-118.

134. Kuhl M. The WNT/calcium pathway: biochemical mediators, tools and future requirements. *Front Biosci* 2004; **9:** 967-974.

135. Miller JR, Hocking AM, Brown JD, Moon RT. Mechanism and function of signal transduction by the Wnt/beta-catenin and Wnt/Ca2+ pathways. *Oncogene* 1999; **18:** 7860-7872.

136. Ishitani T, Kishida S, Hyodo-Miura J, Ueno N*, et al.* The TAK1-NLK mitogen-activated protein kinase cascade functions in the Wnt-5a/Ca(2+) pathway to antagonize Wnt/beta-catenin signaling. *Mol Cell Biol* 2003; **23:** 131-139.

137. Westfall TA, Brimeyer R, Twedt J, Gladon J*, et al.* Wnt-5/pipetail functions in vertebrate axis formation as a negative regulator of Wnt/beta-catenin activity. *J Cell Biol* 2003; **162:** 889-898.

138. Quarmby LM, Parker JD. Cilia and the cell cycle? *J Cell Biol* 2005; **169:** 707-710.

139. Simons M, Gloy J, Ganner A, Bullerkotte A*, et al.* Inversin, the gene product mutated in nephronophthisis type II, functions as a molecular switch between Wnt signaling pathways. *Nat Genet* 2005; **37:** 537-543.

140. Kim E, Arnould T, Sellin LK, Benzing T*, et al.* The polycystic kidney disease 1 gene product modulates Wnt signaling. *J Biol Chem* 1999; **274:** 4947-4953.

141. Flaherty L, Bryda EC, Collins D, Rudofsky U*, et al.* New mouse model for polycystic kidney disease with both recessive and dominant gene effects. *Kidney Int* 1995; **47:** 552-558.

142. Saffman EE, Styhler S, Rother K, Li W, *et al.* Premature translation of oskar in oocytes lacking the RNA-binding protein bicaudal-C. *Mol Cell Biol* 1998; **18:** 4855-4862.

143. Wessely O, Tran U, Zakin L, De Robertis EM. Identification and expression of the mammalian homologue of Bicaudal-C. *Mech Dev* 2001; **101:** 267-270.

144. Eckmann CR, Kraemer B, Wickens M, Kimble J. GLD-3, a bicaudal-C homolog that inhibits FBF to control germline sex determination in C. elegans. *Dev Cell* 2002; **3:** 697-710.

145. Wessely O, De Robertis EM. The Xenopus homologue of Bicaudal-C is a localized maternal mRNA that can induce endoderm formation. *Development* 2000; **127:** 2053-2062.

146. Snee MJ, Macdonald PM. Bicaudal C and trailer hitch have similar roles in gurken mRNA localization and cytoskeletal organization. *Dev Biol* 2009; **328:** 434-444.

147. Chicoine J, Benoit P, Gamberi C, Paliouras M, *et al.* Bicaudal-C recruits CCR4-NOT deadenylase to target mRNAs and regulates oogenesis, cytoskeletal organization, and its own expression. *Dev Cell* 2007; **13:** 691-704.

148. Kugler JM, Chicoine J, Lasko P. Bicaudal-C associates with a Trailer Hitch/Me31B complex and is required for efficient Gurken secretion. *Dev Biol* 2009; **328:** 160-172.

149. Kambach C, Walke S, Young R, Avis JM, *et al.* Crystal structures of two Sm protein complexes and their implications for the assembly of the spliceosomal snRNPs. *Cell* 1999; **96:** 375-387.

150. Camasses A, Bragado-Nilsson E, Martin R, Seraphin B, *et al.* Interactions within the yeast Sm core complex: from proteins to amino acids. *Mol Cell Biol* 1998; **18:** 1956-1966.

151. Fury MG, Zhang W, Christodoulopoulos I, Zieve GW. Multiple protein: protein interactions between the snRNP common core proteins. *Exp Cell Res* 1997; **237:** 63-69.

152. Bouveret E, Rigaut G, Shevchenko A, Wilm M, *et al.* A Sm-like protein complex that participates in mRNA degradation. *EMBO J* 2000; **19:** 1661-1671.

153.   Price SJ. The genetic and molecular characterization of polycystic kidney disease-causing mouse gene *Bicc1*. Doctor of Philosophy thesis, Marshall University, Huntington, 2004.

154.   Finn RD, Mistry J, Schuster-Bockler B, Griffiths-Jones S*, et al.* Pfam: clans, web tools and services. *Nucleic Acids Res* 2006; **34:** D247-251.

155.   Pagni M, Ioannidis V, Cerutti L, Zahn-Zabal M*, et al.* MyHits: a new interactive resource for protein annotation and domain identification. *Nucleic Acids Res* 2004; **32:** W332-335.

156.   Schultz J, Ponting CP, Hofmann K, Bork P. SAM as a protein interaction domain involved in developmental regulation. *Protein Sci* 1997; **6:** 249-253.

157.   Ponting CP. SAM: a novel motif in yeast sterile and Drosophila polyhomeotic proteins. *Protein Sci* 1995; **4:** 1928-1930.

158.   Adinolfi S, Bagni C, Castiglione Morelli MA, Fraternali F*, et al.* Novel RNA-binding motif: the KH module. *Biopolymers* 1999; **51:** 153-164.

159.   Adinolfi S, Bagni C, Musco G, Gibson T*, et al.* Dissecting FMR1, the protein responsible for fragile X syndrome, in its structural and functional domains. *RNA* 1999; **5:** 1248-1258.

160.   Buckanovich RJ, Darnell RB. The neuronal RNA binding protein Nova-1 recognizes specific RNA targets in vitro and in vivo. *Mol Cell Biol* 1997; **17:** 3194-3201.

161.   Gibson TJ, Thompson JD, Heringa J. The KH domain occurs in a diverse set of RNA-binding proteins that include the antiterminator NusA and is probably involved in binding to nucleic acid. *FEBS Lett* 1993; **324:** 361-366.

162.   Khandjian EW, Corbin F, Woerly S, Rousseau F. The fragile X mental retardation protein is associated with ribosomes. *Nat Genet* 1996; **12:** 91-93.

163.   Paziewska A, Wyrwicz LS, Bujnicki JM, Bomsztyk K*, et al.* Cooperative binding of the hnRNP K three KH domains to mRNA targets. *FEBS Lett* 2004; **577:** 134-140.

164.   Bouvrette DJ, Price SJ, Bryda EC. K homology domains of the mouse polycystic kidney disease-related protein, Bicaudal-C (Bicc1), mediate RNA binding in vitro. *Nephron Exp Nephrol* 2008; **108:** e27-34.

165. Siomi H, Matunis MJ, Michael WM, Dreyfuss G. The pre-mRNA binding K protein contains a novel evolutionarily conserved motif. *Nucleic Acids Res* 1993; **21:** 1193-1198.

166. Schmidt C, Henkel B, Poschl E, Zorbas H*, et al.* Complete cDNA sequence of chicken vigilin, a novel protein with amplified and evolutionary conserved domains. *Eur J Biochem* 1992; **206:** 625-634.

167. Nielsen FC, Nielsen J, Kristensen MA, Koch G*, et al.* Cytoplasmic trafficking of IGF-II mRNA-binding protein by conserved KH domains. *J Cell Sci* 2002; **115:** 2087-2097.

168. Chmiel NH, Rio DC, Doudna JA. Distinct contributions of KH domains to substrate binding affinity of Drosophila P-element somatic inhibitor protein. *RNA* 2006; **12:** 283-291.

169. Spingola M, Armisen J, Ares M, Jr. Mer1p is a modular splicing factor whose function depends on the conserved U2 snRNP protein Snu17p. *Nucleic Acids Res* 2004; **32:** 1242-1250.

170. Burd CG, Dreyfuss G. Conserved structures and diversity of functions of RNA-binding proteins. *Science* 1994; **265:** 615-621.

171. Thanos CD, Faham S, Goodwill KE, Cascio D*, et al.* Monomeric structure of the human EphB2 sterile alpha motif domain. *J Biol Chem* 1999; **274:** 37301-37306.

172. Thanos CD, Bowie JU. p53 Family members p63 and p73 are SAM domain-containing proteins. *Protein Sci* 1999; **8:** 1708-1710.

173. Thanos CD, Goodwill KE, Bowie JU. Oligomeric structure of the human EphB2 receptor SAM domain. *Science* 1999; **283:** 833-836.

174. Jousset C, Carron C, Boureux A, Quang CT*, et al.* A domain of TEL conserved in a subset of ETS proteins defines a specific oligomerization interface essential to the mitogenic properties of the TEL-PDGFR beta oncoprotein. *EMBO J* 1997; **16:** 69-82.

175. Slupsky CM, Gentile LN, McIntosh LP. Assigning the NMR spectra of aromatic amino acids in proteins: analysis of two Ets pointed domains. *Biochem Cell Biol* 1998; **76:** 379-390.

176. Serra-Pages C, Kedersha NL, Fazikas L, Medley Q*, et al.* The LAR transmembrane protein tyrosine phosphatase and a coiled-coil LAR-interacting protein co-localize at focal adhesions. *EMBO J* 1995; **14:** 2827-2838.

177. Kaspareit-Rittinghausen J, Deerberg F, Rapp KG, Wcislo A. A new rat model for polycystic kidney disease of humans. *Transplant Proc* 1990; **22:** 2582-2583.

178. Schafer K, Gretz N, Bader M, Oberbaumer I*, et al.* Characterization of the Han:SPRD rat model for hereditary polycystic kidney disease. *Kidney Int* 1994; **46:** 134-152.

179. Brown JH, Bihoreau MT, Hoffmann S, Kranzlin B*, et al.* Missense mutation in sterile alpha motif of novel protein SamCystin is associated with polycystic kidney disease in (cy/+) rat. *J Am Soc Nephrol* 2005; **16:** 3517-3526.

180. Ramachander R, Bowie JU. SAM domains can utilize similar surfaces for the formation of polymers and closed oligomers. *J Mol Biol* 2004; **342:** 1353-1358.

181. Janaswami PM, Birkenmeier EH, Cook SA, Rowe LB*, et al.* Identification and genetic mapping of a new polycystic kidney disease on mouse chromosome 8. *Genomics* 1997; **40:** 101-107.

182. Vogler C, Homan S, Pung A, Thorpe C*, et al.* Clinical and pathologic findings in two new allelic murine models of polycystic kidney disease. *J Am Soc Nephrol* 1999; **10:** 2534-2539.

183. Upadhya P, Birkenmeier EH, Birkenmeier CS, Barker JE. Mutations in a NIMA-related kinase gene, Nek1, cause pleiotropic effects including a progressive polycystic kidney disease in mice. *Proc Natl Acad Sci U S A* 2000; **97:** 217-221.

184. Mahjoub MR, Qasim Rasi M, Quarmby LM. A NIMA-related kinase, Fa2p, localizes to a novel site in the proximal cilia of Chlamydomonas and mouse kidney cells. *Mol Biol Cell* 2004; **15:** 5172-5186.

185. Osmani SA, Ye XS. Cell cycle regulation in Aspergillus by two protein kinases. *Biochem J* 1996; **317 (Pt 3):** 633-641.

186. Feige E, Shalom O, Tsuriel S, Yissachar N*, et al.* Nek1 shares structural and functional similarities with NIMA kinase. *Biochim Biophys Acta* 2006; **1763:** 272-281.

187. Letwin K, Mizzen L, Motro B, Ben-David Y*, et al.* A mammalian dual specificity protein kinase, Nek1, is related to the NIMA cell cycle regulator and highly expressed in meiotic germ cells. *EMBO J* 1992; **11:** 3521-3531.

188. Arama E, Yanai A, Kilfin G, Bernstein A*, et al.* Murine NIMA-related kinases are expressed in patterns suggesting distinct functions in gametogenesis and a role in the nervous system. *Oncogene* 1998; **16:** 1813-1823.

189. Polci R, Peng A, Chen PL, Riley DJ*, et al.* NIMA-related protein kinase 1 is involved early in the ionizing radiation-induced DNA damage response. *Cancer Res* 2004; **64:** 8800-8803.

190. Quarmby LM, Mahjoub MR. Caught Nek-ing: cilia and centrioles. *J Cell Sci* 2005; **118:** 5161-5169.

191. Assmann EM, Alborghetti MR, Camargo ME, Kobarg J. FEZ1 dimerization and interaction with transcription regulatory proteins involves its coiled-coil region. *J Biol Chem* 2006; **281:** 9869-9881.

192. Surpili MJ, Delben TM, Kobarg J. Identification of proteins that interact with the central coiled-coil region of the human protein kinase NEK1. *Biochemistry* 2003; **42:** 15369-15376.

193. Calvet JP. Cilia in PKD--letting it all hang out. *J Am Soc Nephrol* 2002; **13:** 2614-2616.

194. Davenport JR, Yoder BK. An incredible decade for the primary cilium: a look at a once-forgotten organelle. *Am J Physiol Renal Physiol* 2005; **289:** F1159-1169.

195. Kramer-Zucker AG, Olale F, Haycraft CJ, Yoder BK*, et al.* Cilia-driven fluid flow in the zebrafish pronephros, brain and Kupffer's vesicle is required for normal organogenesis. *Development* 2005; **132:** 1907-1921.

196. Lehman JM, Michaud EJ, Schoeb TR, Aydin-Son Y*, et al.* The Oak Ridge Polycystic Kidney mouse: Modeling ciliopathies of mice and men. *Dev Dyn* 2008.

197. Liu W, Murcia NS, Duan Y, Weinbaum S*, et al.* Mechanoregulation of intracellular Ca2+ concentration is attenuated in collecting duct of monocilium-impaired orpk mice. *Am J Physiol Renal Physiol* 2005; **289:** F978-988.

198. Pazour GJ, Rosenbaum JL. Intraflagellar transport and cilia-dependent diseases. *Trends Cell Biol* 2002; **12:** 551-555.

199. Wessely O, Obara T. Fish and frogs: models for vertebrate cilia signaling. *Front Biosci* 2008; **13:** 1866-1880.

200. Mostov KE. mTOR is out of control in polycystic kidney disease. *Proc Natl Acad Sci U S A* 2006; **103:** 5247-5248.

201. Kugoh H, Kleymenova E, Walker CL. Retention of membrane-localized beta-catenin in cells lacking functional polycystin-1 and tuberin. *Mol Carcinog* 2002; **33:** 131-136.

202. Kleymenova E, Ibraghimov-Beskrovnaya O, Kugoh H, Everitt J*, et al.* Tuberin-dependent membrane localization of polycystin-1: a functional link between polycystic kidney disease and the TSC2 tumor suppressor gene. *Mol Cell* 2001; **7:** 823-832.

203. Hostetter CL, Sullivan-Brown JL, Burdine RD. Zebrafish pronephros: a model for understanding cystic kidney disease. *Dev Dyn* 2003; **228:** 514-522.

204. Igarashi P. Overview: nonmammalian organisms for studies of kidney development and disease. *J Am Soc Nephrol* 2005; **16:** 296-298.

205. Drummond IA. Kidney development and disease in the zebrafish. *J Am Soc Nephrol* 2005; **16:** 299-304.

206. Drummond IA, Majumdar A, Hentschel H, Elger M*, et al.* Early development of the zebrafish pronephros and analysis of mutations affecting pronephric function. *Development* 1998; **125:** 4655-4667.

207. Drummond IA. The zebrafish pronephros: a genetic system for studies of kidney development. *Pediatr Nephrol* 2000; **14:** 428-435.

208. Drummond I. Making a zebrafish kidney: a tale of two tubes. *Trends Cell Biol* 2003; **13:** 357-365.

209. Sigrist CJ, Cerutti L, Hulo N, Gattiker A*, et al.* PROSITE: a documented database using patterns and profiles as motif descriptors. *Brief Bioinform* 2002; **3:** 265-274.

210. Kyte J, Doolittle RF. A simple method for displaying the hydropathic character of a protein. *J Mol Biol* 1982; **157:** 105-132.

211. Thompson JD, Higgins DG, Gibson TJ. CLUSTAL W: improving the sensitivity of progressive multiple sequence alignment through sequence weighting, position-specific gap penalties and weight matrix choice. *Nucleic Acids Res* 1994; **22:** 4673-4680.

212. Chenna R, Sugawara H, Koike T, Lopez R, *et al.* Multiple sequence alignment with the Clustal series of programs. *Nucleic Acids Res* 2003; **31:** 3497-3500.

213. Clamp M, Cuff J, Searle SM, Barton GJ. The Jalview Java alignment editor. *Bioinformatics* 2004; **20:** 426-427.

214. Livak KJ, Schmittgen TD. Analysis of relative gene expression data using real-time quantitative PCR and the 2(-Delta Delta C(T)) Method. *Methods* 2001; **25:** 402-408.

215. Rozen S, Skaletsky H. Primer3 on the WWW for general users and for biologist programmers. *Methods Mol Biol* 2000; **132:** 365-386.

216. Institute of Laboratory Animal Resources CoLS, National Research Council (ed). *Guide to the care and use of laboratory animals.* National Academy Press: Washington, D.C., 1996. 140pp.

217. Westerfield M: The zebrafish book a guide for the laboratory use of zebrafish Danio (Brachydanio) rerio. In, [Eugene, OR, Institute of Neuroscience, University of Oregon, 1993

218. Altschul SF, Gish W, Miller W, Myers EW, *et al.* Basic local alignment search tool. *J Mol Biol* 1990; **215:** 403-410.

219. Gasteiger E, Gattiker A, Hoogland C, Ivanyi I, *et al.* ExPASy: The proteomics server for in-depth protein knowledge and analysis. *Nucleic Acids Res* 2003; **31:** 3784-3788.

220. de Castro E, Sigrist CJ, Gattiker A, Bulliard V, *et al.* ScanProsite: detection of PROSITE signature matches and ProRule-associated functional and structural residues in proteins. *Nucleic Acids Res* 2006; **34:** W362-365.

221. Hulo N, Bairoch A, Bulliard V, Cerutti L, *et al.* The PROSITE database. *Nucleic Acids Res* 2006; **34:** D227-230.

222. Zdobnov EM, Apweiler R. InterProScan--an integration platform for the signature-recognition methods in InterPro. *Bioinformatics* 2001; **17:** 847-848.

223. Rozen S, Skaletsky H. Primer3 on the WWW for general users and for biologist programmers. In: Krawetz S, Misener S (eds). *Bioinformatics: Methods and Protocols*, vol. 132. Humana Press: Totowa, NJ, 2000, pp 365-386.

224. Huang H, Zhang B, Hartenstein PA, Chen JN*, et al.* NXT2 is required for embryonic heart development in zebrafish. *BMC Dev Biol* 2005; **5:** 7.

225. Karlstrom RO, Tyurina OV, Kawakami A, Nishioka N*, et al.* Genetic analysis of zebrafish gli1 and gli2 reveals divergent requirements for gli genes in vertebrate development. *Development* 2003; **130:** 1549-1564.

226. Nasevicius A, Ekker SC. Effective targeted gene 'knockdown' in zebrafish. *Nat Genet* 2000; **26:** 216-220.

227. Dent JA, Polson AG, Klymkowsky MW. A whole-mount immunocytochemical analysis of the expression of the intermediate filament protein vimentin in Xenopus. *Development* 1989; **105:** 61-74.

228. Takeyasu K, Tamkun MM, Renaud KJ, Fambrough DM. Ouabain-sensitive (Na+ + K+)-ATPase activity expressed in mouse L cells by transfection with DNA encoding the alpha-subunit of an avian sodium pump. *J Biol Chem* 1988; **263:** 4347-4354.

229. Mercer EH. A scheme for section staining in electron microscopy. *J R Microsc Soc* 1963; **81:** 179-183.

230. Burns WA. *Chapter 4, "Thick Sections: Technique and Applications"*, vol. 1. John Wiley and Sons: New York, 1978, 360pp.

231. Mulder NJ, Apweiler R, Attwood TK, Bairoch A*, et al.* InterPro, progress and status in 2005. *Nucleic Acids Res* 2005; **33:** D201-205.

232. Walter BL, Parsley TB, Ehrenfeld E, Semler BL. Distinct poly(rC) binding protein KH domain determinants for poliovirus translation initiation and viral RNA replication. *J Virol* 2002; **76:** 12008-12022.

233. Buckanovich RJ, Yang YY, Darnell RB. The onconeural antigen Nova-1 is a neuron-specific RNA-binding protein, the activity of which is inhibited by paraneoplastic antibodies. *J Neurosci* 1996; **16:** 1114-1122.

234. Du Z, Fenn S, Tjhen R, James TL. Structure of a construct of a human poly(C)-binding protein containing the first and second KH domains reveals insights into its regulatory mechanisms. *J Biol Chem* 2008; **283:** 28757-28766.

235. Lin Q, Taylor SJ, Shalloway D. Specificity and determinants of Sam68 RNA binding. Implications for the biological function of K homology domains. *J Biol Chem* 1997; **272:** 27274-27280.

236. Heasman J, Wessely O, Langland R, Craig EJ, *et al.* Vegetal localization of maternal mRNAs is disrupted by VegT depletion. *Dev Biol* 2001; **240:** 377-386.

237. Siomi H, Siomi MC, Nussbaum RL, Dreyfuss G. The protein product of the fragile X gene, FMR1, has characteristics of an RNA-binding protein. *Cell* 1993; **74:** 291-298.

238. Gherzi R, Lee KY, Briata P, Wegmuller D, *et al.* A KH domain RNA binding protein, KSRP, promotes ARE-directed mRNA turnover by recruiting the degradation machinery. *Mol Cell* 2004; **14:** 571-583.

239. Lorkovic ZJ, Barta A. Genome analysis: RNA recognition motif (RRM) and K homology (KH) domain RNA-binding proteins from the flowering plant Arabidopsis thaliana. *Nucleic Acids Res* 2002; **30:** 623-635.

240. Stickney LM, Hankins JS, Miao X, Mackie GA. Function of the conserved S1 and KH domains in polynucleotide phosphorylase. *J Bacteriol* 2005; **187:** 7214-7221.

241. Linker K, Pautz A, Fechir M, Hubrich T, *et al.* Involvement of KSRP in the post-transcriptional regulation of human iNOS expression-complex interplay of KSRP with TTP and HuR. *Nucleic Acids Res* 2005; **33:** 4813-4827.

242. Rohwedel J, Kugler S, Engebrecht T, Purschke W, *et al.* Evidence for posttranscriptional regulation of the multi K homology domain protein vigilin by a small peptide encoded in the 5' leader sequence. *Cell Mol Life Sci* 2003; **60:** 1705-1715.

243. Zearfoss NR, Farley BM, Ryder SP. Post-transcriptional regulation of myelin formation. *Biochim Biophys Acta* 2008; **1779:** 486-494.

244. Bustin SA. Quantification of mRNA using real-time reverse transcription PCR (RT-PCR): trends and problems. *J Mol Endocrinol* 2002; **29:** 23-39.

245. Abramoff MD, Magelhaes, P.J., Ram, S.J. . Image Processing with ImageJ *Biophotonics International* 2004; **11:** 36-42.

246. Tajima H, Tsuchiya K, Yamada M, Kondo K, *et al.* Over-expression of GAPDH induces apoptosis in COS-7 cells transfected with cloned GAPDH cDNAs. *Neuroreport* 1999; **10:** 2029-2033.

247. Chen RW, Saunders PA, Wei H, Li Z, *et al.* Involvement of glyceraldehyde-3-phosphate dehydrogenase (GAPDH) and p53 in

neuronal apoptosis: evidence that GAPDH is upregulated by p53. *J Neurosci* 1999; **19:** 9654-9662.

248. Bauer BA, Boedges S, Cook CR, Bryda EC*, et al.* Breeding colony refinement through phenotypic and genotypic characterization of the SPRD-Pkdr1/Rrrc rat model of polycystic kidney disease. *Comp Med* 2007; **57:** 193-199.

249. Bihoreau MT, Ceccherini I, Browne J, Kranzlin B*, et al.* Location of the first genetic locus, PKDr1, controlling autosomal dominant polycystic kidney disease in Han:SPRD cy/+ rat. *Hum Mol Genet* 1997; **6:** 609-613.

250. Kaisaki PJ, Bergmann C, Brown JH, Outeda P*, et al.* Genomic organization and mutation screening of the human ortholog of Pkdr1 associated with polycystic kidney disease in the rat. *Eur J Med Genet* 2008; **51:** 325-331.

251. Jensen KB, Musunuru K, Lewis HA, Burley SK*, et al.* The tetranucleotide UCAY directs the specific recognition of RNA by the Nova K-homology 3 domain. *Proc Natl Acad Sci U S A* 2000; **97:** 5740-5745.

252. Aviv T, Lin Z, Lau S, Rendl LM*, et al.* The RNA-binding SAM domain of Smaug defines a new family of post-transcriptional regulators. *Nat Struct Biol* 2003; **10:** 614-621.

253. Johnson PE, Donaldson LW. RNA recognition by the Vts1p SAM domain. *Nat Struct Mol Biol* 2006; **13:** 177-178.

254. Ashurst JL, Chen CK, Gilbert JG, Jekosch K*, et al.* The Vertebrate Genome Annotation (Vega) database. *Nucleic Acids Res* 2005; **33:** D459-465.

255. Hubbard T, Andrews D, Caccamo M, Cameron G*, et al.* Ensembl 2005. *Nucleic Acids Res* 2005; **33:** D447-453.

256. Amores A, Force A, Yan YL, Joly L*, et al.* Zebrafish hox clusters and vertebrate genome evolution. *Science* 1998; **282:** 1711-1714.

257. Postlethwait JH, Yan YL, Gates MA, Horne S*, et al.* Vertebrate genome evolution and the zebrafish gene map. *Nat Genet* 1998; **18:** 345-349.

258. Force A, Lynch M, Pickett FB, Amores A*, et al.* Preservation of duplicate genes by complementary, degenerative mutations. *Genetics* 1999; **151:** 1531-1545.

259. McClintock JM, Kheirbek MA, Prince VE. Knockdown of duplicated zebrafish hoxb1 genes reveals distinct roles in hindbrain patterning and a novel mechanism of duplicate gene retention. *Development* 2002; **129:** 2339-2354.

260. Darby IA, Hewitson, T. (ed). In situ *hybridization protocols.* Humana Press: New Jersey, 2006.

261. Coutinho LL, Morris J, Ivarie R. Whole mount in situ detection of low abundance transcripts of the myogenic factor qmf1 and myosin heavy chain protein in quail embryos. *Biotechniques* 1992; **13:** 722-724.

262. Wilkinson DG. RNA detection using non-radioactive in situ hybridization. *Curr Opin Biotechnol* 1995; **6:** 20-23.

263. Paukert M, Sidi S, Russell C, Siba M*, et al.* A family of acid-sensing ion channels from the zebrafish: widespread expression in the central nervous system suggests a conserved role in neuronal communication. *J Biol Chem* 2004; **279:** 18783-18791.

264. Solnica-Krezel L. Pattern formation in zebrafish--fruitful liaisons between embryology and genetics. *Curr Top Dev Biol* 1999; **41:** 1-35.

265. Torres VE. New insights into polycystic kidney disease and its treatment. *Curr Opin Nephrol Hypertens* 1998; **7:** 159-169.

266. Ryder SP, Frater LA, Abramovitz DL, Goodwin EB*, et al.* RNA target specificity of the STAR/GSG domain post-transcriptional regulatory protein GLD-1. *Nat Struct Mol Biol* 2004; **11:** 20-28.

267. Git A, Standart N. The KH domains of Xenopus Vg1RBP mediate RNA binding and self-association. *RNA* 2002; **8:** 1319-1333.

268. Chen T, Damaj BB, Herrera C, Lasko P*, et al.* Self-association of the single-KH-domain family members Sam68, GRP33, GLD-1, and Qk1: role of the KH domain. *Mol Cell Biol* 1997; **17:** 5707-5718.

269. Ashley CT, Jr., Wilkinson KD, Reines D, Warren ST. FMR1 protein: conserved RNP family domains and selective RNA binding. *Science* 1993; **262:** 563-566.

270. Tamanini F, Meijer N, Verheij C, Willems PJ*, et al.* FMRP is associated to the ribosomes via RNA. *Hum Mol Genet* 1996; **5:** 809-813.

271. Feng Y, Gutekunst CA, Eberhart DE, Yi H*, et al.* Fragile X mental retardation protein: nucleocytoplasmic shuttling and association with somatodendritic ribosomes. *J Neurosci* 1997; **17:** 1539-1547.

272. De Boulle K, Verkerk AJ, Reyniers E, Vits L*, et al.* A point mutation in the FMR-1 gene associated with fragile X mental retardation. *Nat Genet* 1993; **3:** 31-35.

273. Buckanovich RJ, Posner JB, Darnell RB. Nova, the paraneoplastic Ri antigen, is homologous to an RNA-binding protein and is specifically expressed in the developing motor system. *Neuron* 1993; **11:** 657-672.

274. Musunuru K, Darnell RB. Determination and augmentation of RNA sequence specificity of the Nova K-homology domains. *Nucleic Acids Res* 2004; **32:** 4852-4861.

275. Boehning D, Moon C, Sharma S, Hurt KJ*, et al.* Carbon monoxide neurotransmission activated by CK2 phosphorylation of heme oxygenase-2. *Neuron* 2003; **40:** 129-137.

276. Charriaut-Marlangue C, Otani S, Creuzet C, Ben-Ari Y*, et al.* Rapid activation of hippocampal casein kinase II during long-term potentiation. *Proc Natl Acad Sci U S A* 1991; **88:** 10232-10236.

277. Blanquet PR. Neurotrophin-induced activation of casein kinase 2 in rat hippocampal slices. *Neuroscience* 1998; **86:** 739-749.

278. Solyakov L, Cain K, Tracey BM, Jukes R*, et al.* Regulation of casein kinase-2 (CK2) activity by inositol phosphates. *J Biol Chem* 2004; **279:** 43403-43410.

279. Bildl W, Strassmaier T, Thurm H, Andersen J*, et al.* Protein kinase CK2 is coassembled with small conductance Ca(2+)-activated K+ channels and regulates channel gating. *Neuron* 2004; **43:** 847-858.

280. Faust M, Montenarh M. Subcellular localization of protein kinase CK2. A key to its function? *Cell Tissue Res* 2000; **301:** 329-340.

281. Bachhuber T, Almaca J, Aldehni F, Mehta A*, et al.* Regulation of the epithelial Na+ channel by the protein kinase CK2. *J Biol Chem* 2008; **283:** 13225-13232.

282. Torres J, Pulido R. The tumor suppressor PTEN is phosphorylated by the protein kinase CK2 at its C terminus. Implications for PTEN stability to proteasome-mediated degradation. *J Biol Chem* 2001; **276:** 993-998.

283. Cai Y, Anyatonwu G, Okuhara D, Lee KB, *et al.* Calcium dependence of polycystin-2 channel activity is modulated by phosphorylation at Ser812. *J Biol Chem* 2004; **279:** 19987-19995.

284. Hogan PG, Chen L, Nardone J, Rao A. Transcriptional regulation by calcium, calcineurin, and NFAT. *Genes Dev* 2003; **17:** 2205-2232.

285. Staal FJ, Clevers HC. Wnt signaling in the thymus. *Curr Opin Immunol* 2003; **15:** 204-208.

286. Gustafson B, Smith U. Cytokines promote Wnt signaling and inflammation and impair the normal differentiation and lipid accumulation in 3T3-L1 preadipocytes. *J Biol Chem* 2006; **281:** 9507-9516.

287. Huelsken J, Birchmeier W. New aspects of Wnt signaling pathways in higher vertebrates. *Curr Opin Genet Dev* 2001; **11:** 547-553.

288. Li J, Mahajan A, Tsai MD. Ankyrin repeat: a unique motif mediating protein-protein interactions. *Biochemistry* 2006; **45:** 15168-15178.

289. Kim CA, Bowie JU. SAM domains: uniform structure, diversity of function. *Trends Biochem Sci* 2003; **28:** 625-628.

290. Naisbitt S, Kim E, Tu JC, Xiao B, *et al.* Shank, a novel family of postsynaptic density proteins that binds to the NMDA receptor/PSD-95/GKAP complex and cortactin. *Neuron* 1999; **23:** 569-582.

291. De Rycker M, Venkatesan RN, Wei C, Price CM. Vertebrate tankyrase domain structure and sterile alpha motif (SAM)-mediated multimerization. *Biochem J* 2003; **372:** 87-96.

292. Adato A, Michel V, Kikkawa Y, Reiners J, *et al.* Interactions in the network of Usher syndrome type 1 proteins. *Hum Mol Genet* 2005; **14:** 347-356.

293. Valverde R, Edwards L, Regan L. Structure and function of KH domains. *Febs J* 2008; **275:** 2712-2726.

294. Bouvrette DJ, Sittaramane, V., Heidel, J.R., Chandresekhar, A. and Bryda, E.C. Knockdown of Bicaudal C in Zebrafish (*Danio rerio*) Causes Cystic Kidneys: A Non-Mammalian Model of Polycystic Kidney Disease. *Comparative Medicine* 2009; **Submitted, under review**.

295. Yoder BK. Role of primary cilia in the pathogenesis of polycystic kidney disease. *J Am Soc Nephrol* 2007; **18:** 1381-1388.

296.   Kugler J-M, Chicoine J, Lasko P. Bicaudal-C Associates with a Trailer Hitch/Me31B Complex and is Required for Efficient Gurken Secretion. *Developmental Biology* 2009; **328:** 160-172.

297.   Snee MJ, Macdonald PN. Bicaudal C and Trailer hitch have similar roles in gurken mRNA localization and cytoskeletal organization. *Developmental Biology* 2009.

298.   Tran U, Zakin L, Schweickert A, Agrawal R*, et al.* 09-P030 The role of Bicaudal-C in kidney development. *Mechanisms of Development* 2009; **126:** S159-S159.

299.   Laggerbauer B, Ostareck D, Keidel EM, Ostareck-Lederer A*, et al.* Evidence that fragile X mental retardation protein is a negative regulator of translation. *Hum Mol Genet* 2001; **10:** 329-338.

300.   Li Z, Zhang Y, Ku L, Wilkinson KD*, et al.* The fragile X mental retardation protein inhibits translation via interacting with mRNA. *Nucleic Acids Res* 2001; **29:** 2276-2283.

301.   Bagni C, Mannucci L, Dotti CG, Amaldi F. Chemical stimulation of synaptosomes modulates alpha -Ca2+/calmodulin-dependent protein kinase II mRNA association to polysomes. *J Neurosci* 2000; **20:** RC76.

VITA

I was born in Bay City, MI to my parents, Greg and Jean Bouvrette. I have two siblings, an older brother Michael and a younger sister Jennifer. In high school, I began working at a restaurant and quickly moved into a supervisory position. This move initiated a long and prosperous career in restaurant management with Marriott International. While with Marriott, I lived in several states including Tennessee, Florida and West Virginia. Somewhere along the way, I decided I wanted to be a scientist, so at age 26 I went back to school to complete a B.S. in Biology. This wasn't quite enough to satisfy my craving for knowledge, however, as I went on to pursue a Master's degree in Biomedical Sciences at Marshall University in Huntington, WV. It was there that fate took its hold and introduced me to Elizabeth Bryda. The timing wasn't quite right, however, as she was planning a move to Columbia, MO. But destiny has already spoken and it wasn't long before I followed her to Columbia to pursue my Ph.D. And so you have a brief look into the last 10 years of my life. I plan to pursue a career in the biotech/pharma industry with an emphasis on regulatory affairs. Once I complete my Ph.D., I hope to return to some of the things I used to enjoy when I had free time, such as gardening, hiking with my dog and kayaking.